

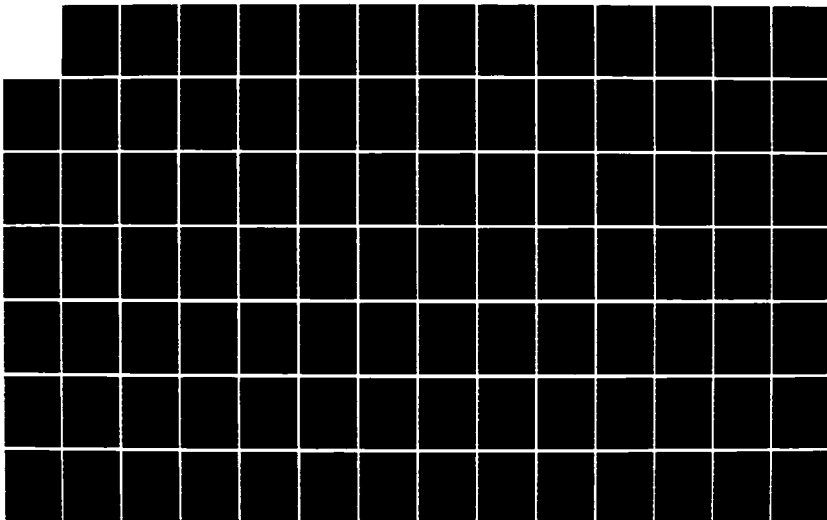
AD-A172 994

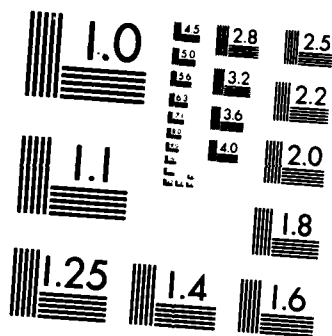
VIBRATION CONTROL OF FLEXIBLE STRUCTURE USING
PIEZOELECTRIC DEVICES AS SENSORS AND ACTUATORS(U) AIR
FORCE INST OF TECH WRIGHT-PATTERSON AFB OH H W ODAL
SEP 86 AFIT/CI/NR-86-176D F/G 9/5

1/3

UNCLASSIFIED

NL




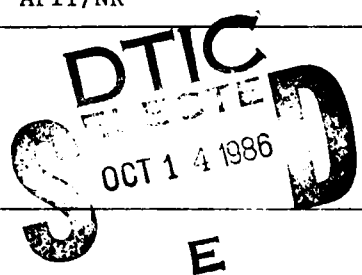


MICROCOPY RESOLUTION TEST CHART
NATIONAL BUREAU OF STANDARDS-1963-A

AD-A172 994

DTIC FILE COPY

SECURITY CLASSIFICATION OF THIS PAGE (When Data Entered)

REPORT DOCUMENTATION PAGE		READ INSTRUCTIONS BEFORE COMPLETING FORM
1. REPORT NUMBER AFIT/CI/NR 86- 176D	2. GOVT ACCESSION NO.	3. RECIPIENT'S CATALOG NUMBER
4. TITLE (and Subtitle) Vibration Control Of Flexible Structure Using Piezoelectric Devices As Sensors And Actuators		5. TYPE OF REPORT & PERIOD COVERED Thesis/DISSERTATION
		6. PERFORMING ORG. REPORT NUMBER
7. AUTHOR(s) Michael Walter Obal		8. CONTRACT OR GRANT NUMBER(s)
9. PERFORMING ORGANIZATION NAME AND ADDRESS AFIT STUDENT AT: Georgia Institute of Technology		10. PROGRAM ELEMENT, PROJECT, TASK AREA & WORK UNIT NUMBERS
11. CONTROLLING OFFICE NAME AND ADDRESS		12. REPORT DATE 1986
14. MONITORING AGENCY NAME & ADDRESS (If different from Controlling Office)		13. NUMBER OF PAGES 250
		15. SECURITY CLASS. (of this report) UNCLASS
		15a. DECLASSIFICATION/DOWNGRADING SCHEDULE
16. DISTRIBUTION STATEMENT (of this Report) APPROVED FOR PUBLIC RELEASE; DISTRIBUTION UNLIMITED		
17. DISTRIBUTION STATEMENT (of the abstract entered in Block 20, if different from Report)		
18. SUPPLEMENTARY NOTES APPROVED FOR PUBLIC RELEASE: IAW AFR 190-1		 LYNN E. WOLAVER 25641K Dean for Research and Professional Development AFIT/NR
19. KEY WORDS (Continue on reverse side if necessary and identify by block number)		 OCT 14 1986 E
20. ABSTRACT (Continue on reverse side if necessary and identify by block number) ATTACHED ...		

DD FORM 1473

JAN 73

EDITION OF 1 NOV 65 IS OBSOLETE

SECURITY CLASSIFICATION OF THIS PAGE (When Data Entered)

VIBRATION CONTROL OF FLEXIBLE STRUCTURES
USING PIEZOELECTRIC DEVICES AS
SENSORS AND ACTUATORS

A THESIS

Presented to

The Faculty of the Division of Graduate Studies

By

Michael Walter Obal

In Partial Fulfillment
of the Requirements for the Degree
Doctor of Philosophy
in the School of Aerospace Engineering

Accession For	
NTIS	<input checked="" type="checkbox"/>
DTIC	<input type="checkbox"/>
Unannounced	<input type="checkbox"/>
Justification	
By _____	
Distribution _____	
Availability Codes	
Avail and/or	
Dist	Special
A-1	



Georgia Institute of Technology

September, 1986

86 10 10 111

VIBRATION CONTROL OF FLEXIBLE STRUCTURES
USING PIEZOELECTRIC DEVICES AS
SENSORS AND ACTUATORS

Approved:

S. V. Hanagud

Sathya V. Hanagud, Chairman

James I. Craig

George A. Pierce
George A. Pierce

Date approved by Chairman: Sept 16 '86

ACKNOWLEDGEMENTS

I would like to sincerely thank my advisor, Professor Sathya V. Hanagud for his guidance, practical research orientation and confidence in me.

I would also like to thank Drs. Robert L. Forward from Hughes Research Laboratory and Charles J. Swigert from Pacific Sierra Corp. for introducing this research field to me and providing the equipment which made it possible to conduct the necessary experimental evaluations.

Dr. Murugappan Meyappa and Dr. Jonnalagadda Prasad were both extremely helpful in providing guidance and understanding in many of the technical areas covered in this research effort.

The comments by Drs. James I. Craig, George A. Pierce, Anthony J. Calise and Stephen L. Dickerson from reading the thesis were helpful and greatly appreciated.

I would like to thank Mr. John Caudell and Mr. Harald W. Meyer for their skillful assistance during the setup and execution of the experimental efforts.

I can only express the greatest gratitude to my mother Stephanie and late father Michael who unselfishly gave what they could to provide me the courage and persistence to undertake this endeavor. Furthermore, the continued support of my relations and the love and

understanding of my wife Margaret, who during this time gave me two sons Michael and Christopher, provided me with an inner strength to overcome the difficult times.

LIST OF TABLES

<u>Table</u>	<u>Title</u>	<u>Page</u>
3.1	Identified Filter Coefficients	47
3.2	Identified Baseline Stiffness, Damping and Mass Matrices for Model #1.	55
3.3	Identified Baseline Stiffness, Damping and Mass Matrices for Model #2.	56
3.4	Scaling Values to Match Baseline Experimental Results	62
3.5	Identified Dynamic Coupling Coefficients	73
3.6	Error Computation Results Between Measured And Analytical Prediction Using Identified Dynamic Coupling Coefficients	78
4.1	MACSYMA Final Results For Non Collocated Control	83
4.2	MACSYMA Final Results For Collocated Control	84
4.3	Numerical Difference Computation of Collocated And Non Collocated Feedback	99
5.1	Numerical Values For Rate Control Analysis - Model #1	114
5.2	Numerical Values For Rate Control Analysis - Model #2	124
D-1	G-1195 Piezoceramic Coefficients	216
D-2	Active Control Experiments	232
D-3	Peak Voltage at Center Tuned Frequency of 232HZ	233
D-4	Complex Eigenvalues and Real Eigenvalues Beam #3	236
D-5	Experimental Gain Values for Beam #2 Modal Control Tests	241

LIST OF ILLUSTRATIONS

<u>Figure</u>	<u>Title</u>	<u>Page</u>
2-1	Active Control Of Structures	10
2-2	Piezoceramic Unimorph Sensor	11
2-3	Simply Supported Beam With Piezoceramic Unimorph Sensor	17
2-4	Piezoceramic Unimorph Actuator	20
2-5	Actuator - DC Voltage	25
2-6	End Couples	25
2-7	Actuator Beam Element	27
2-8	Active Beam Finite Element	29
2-9	Active Element Configuration Examples	31
3-1	N Active Element Model Of A Cantilever Beam	38
3-2	Comparison Of Feedback Filter Analytical Model And Transfer Function Experimental Data - Mode 1 - Low Gain	48
3-3	Comparison Of Feedback Filter Analytical Model And Experimental Transfer Function Experimental Data - Mode 2 - Low Gain	49
3-4	Comparison Of Feedback Filter Analytical Model And Experimental Transfer Function Data - Mode 1 - High Gain	50
3-5	Comparison Of Feedback Filter Analysis Model And Experimental Transfer Function Data - Mode 2 - High Gain	51
3-6	Experimental Test Beam And Finite Element Model	53
3-7	Comparison Of The Baseline Model #1 (10 D.O.F.) And Transfer Function Experimental Data - Mode 1 - No Control	58
3-8	Comparison Of The Baseline Model #1 (10 D.O.F.) And Transfer Function Experimental Data - Mode 2 - No Control	59

<u>Figure</u>	<u>Title</u>	<u>Page</u>
3-9	Comparison Of The Baseline Model #2 (5 D.O.F.) And Transfer Function Experimental Data - Mode 1 - No Control	60
3-10	Comparison Of The Baseline Model #2 (5 D.O.F.) And Transfer Function Experimental Data - Mode 2 - No Control	61
3-11	Computer Program Flow Diagrams	70
3-12	Identification Program Evaluation	71
3-13	Comparison Of Analytical Prediction Using Identified Dynamic Coupling Coefficients With Experimental Data - Model #1 (10 D.O.F.)	74
3-14	Comparison Of Analytical Prediction Using Identified Dynamic Coupling Coefficients With Experimental Data - Model #2 (5 D.O.F.)	75
3-15	Comparison of Analytical Prediction Using Identified Dynamic Coupling Coefficients And Adjusted Center Frequency With Experimental Data - Model #1 (10 D.O.F.)	77
4-1	Collocated And Non Collocated Control Configur- ations	80
4-2	Experimental Collocated And Non Collocated Control Configuration	94
4-3	Comparison Of H_{ij} and H_{ji} - Mode 2 - No Control	95
4-4	Comparison Of H_{ij} And H_{ji} Collocated Sensor/ Actuator Mode 2 - Active Control - Low Gain	96
4-5	Comparison Of H_{ij} And H_{ji} - Non Collocated Sensor/Actuator Mode 2 - Active Control - Low Gain	97
4-6	Biorthogonal Mode Identification Experimental Configuration and Test Matrix	100
5-1	Collocated Active Rate Control	111
5-2	Baseline No Control Response Y_1	118

<u>Figure</u>	<u>Title</u>	<u>Page</u>
5-3	Active Control Input U_1	120
5-4	Active Control Output Response Y_1	121
5-5	Comparison Of The Baseline And Active Control Response	122
5-6	Two Degree Of Freedom Model	123
5-7	Baseline No Control Displacement Response - 1 sec	125
5-8	Active Control Displacement Response - 1 sec	126
5-9	Baseline No Control Displacement Response - 100 msec	127
5-10	Active Control Displacement Response - 100 msec	128
6-1	Collocated Sensor/Actuator Configuration	130
6-2	Finite Difference Model	142
6-3	Sensor Finite Difference Model	148
6-4	Free Displacement Response - No Control	155
6-5	Free Displacement Response - No Active Control	156
6-6a	Active Rate Control Voltage - Approach #1	157
6-6b	Displacement Response - Active Control Approach #1	158
6-7	Displacement Response - Active Control - Approach #2	159
6-8a	Active Lyapunov Control Voltage	160
6-8b	Displacement Response - Active Rate Control	161
6-9	Displacement Response - Active Rate Control - Full Sensor - Nodes 1 to 7	163
6-10	Displacement Response - Active Rate Control - Partial Sensor - Nodes 5-7	164
6-11	Displacement Response - Active Rate Control - Partial Sensor - Nodes 5-7, Increase in Gain	165

<u>Figure</u>	<u>Title</u>	<u>Page</u>
7-1	Typical Test Configuration	168
7-2	Baseline, Low and High Gain Comparisons	173
B-1	Actuator Element With Free Body Diagrams	193
B-2	Collocated Rate Control Example Configuration	196
D-1	Experimental Beam Mechanical Support	213
D-2	Test Beams Collocated Sensor/Actuator Locations	214
D-3	Active Feedback Filter/Control Unit	218
D-4	Typical Test Configuration Setup	219
D-5	Schematic Of The Active Feedback Filter Control Unit	222
D-6, D-7	Preamplifier Subcircuit And Equivalent Circuit	223
D-8	Bandpass Filter Section	225
D-9	Impedance Block Diagram Of Bandpass Filter Circuit Section	226
D-11	Gain vs. Freq. Phase Adjustment Circuit Section	228
D-12	Post Filter Circuit Section	230
D-13	Gain vs. Freq. Post Filter Circuit Section	230
D-14a	First Mode Transfer Function - No Active Control	234
D-14b	Second Mode Transfer Function - No Active Control	235
D-15a	Circle Fit First Mode - No Active Control	238
D-15b	Circle Fit Second Mode - No Active Control	239
D-16	Baseline, Low And High Gain Comparisons	240
D-17	Real And Imaginary Data Comparisons - Mode 1 - Control	242
D-18	Real And Imaginary Data Comparisons - Mode 2 - Control	243

TABLE OF CONTENTS

	<u>Page</u>
ACKNOWLEDGEMENTS	ii
LIST OF TABLES	iv
LIST OF ILLUSTRATIONS	v
SUMMARY	xii
Chapter	
I. INTRODUCTION AND BACKGROUND	1
1.1 Background	3
II. FINITE ELEMENT MODEL OF THE ACTIVE STRUCTURE	9
2.1 Sensing Transducer	9
2.2 Actuator Transducer	18
2.3 Analysis of Active Electronic Feedback Damping Using the Finite Element Method	24
2.4 Model of the Feedback Active Control Electronics	33
III. IDENTIFICATION OF DYNAMIC COUPLING COEFFICIENTS	36
3.1 Equations of Identification	37
3.2 Identification of Feedback Filter Electronics Parameters	41
3.3 Baseline Model Development	46
3.4 Identification of Dynamic Coupling Coefficients	57

	<u>Page</u>
3.5 Analysis Procedure and Program Verification	68
Results	
3.6 Discussion of Identification Results	72
IV. MODAL AND PARAMETER IDENTIFICATION OF STRUCTURES	79
WITH NON COLLOCATED SENSORS AND ACTUATORS	
4.1 Theoretical Development	86
4.2 Experimental Results	93
V. GAIN OPTIMIZATION OF THE ACTIVE STRUCTURE	103
5.1 Background	103
5.2 Optimal Output Limited State Feedback	107
5.3 Rate Feedback Model	110
VI. OPTIMAL CONTROL USING DISTRIBUTED SENSORS AND	129
ACTUATORS	
6.1 Analysis	129
6.2 Distributed Parameter Control	135
6.3 Finite Difference Evaluation	141
6.4 Discussion of Results	154
VII. ACTIVE CONTROL EXPERIMENTS	167
7.1 Experimental Configuration	167
7.2 Modal Control Experiments	169
7.3 Test Procedures	171
7.4 Experimental Results	172
VIII. CONCLUSIONS AND RECOMMENDATIONS	174

Page

APPENDIX

A. PIEZOELECTRIC CONSTITUTIVE EQUATIONS	177
B. FINITE ELEMENT ACTIVE BEAM MODEL	192
C. SYSTEM IDENTIFICATION OF VIBRATING STRUCTURES	206
D. ACTIVE CONTROL EXPERIMENTS	212

REFERENCES	244
------------	-----

SUMMARY

The problem of the active control of linear elastic structures using piezoceramic transducers as sensors and actuators has been investigated by a combined theoretical and experimental approach. The optimal rate feedback gain distribution of an active structure with multiple collocated sensors and actuators has been obtained by using a limited state feedback approach which resulted in an increase in system damping. To model the active structure for the optimal control problem, a finite element model has been developed. An active element consisting of a simple beam element with a bonded unimorphic piezoceramic sensors and actuators has been obtained. The model incorporates the electromechanical coupling of the transducers, bonding effects and a mathematical model for the feedback signal conditioning circuitry. The resulting discrete degrees of freedom model is in the form of a set of coupled ordinary differential equations which describe the dynamic behavior of the active structure. To obtain the unknown dynamic coupling coefficients that represent the effects of bonding and other parameters of the model accurately, parameter identification methods have been used. Modal control has also been experimentally demonstrated by conditioning the output of each individual sensor with an adjustable bandpass filter, phase shifting and gain circuits. The identification of biorthogonal modes of the resulting non self adjoint system when non collocated sensors and actuators has also been accomplished. The identified discrete

degrees of freedom model and a quadratic performance index have been used in obtaining optimal control laws. In this phase, the problem has been treated as a regulator with limited state feedback. As a next step, the optimal control problem has been solved by considering the active structure as a distributed parameter system. An optimal control law has been obtained by maximizing the decrease of the time derivative of a Lyapunov functional of a cantilever beam with a collocated sensor and actuator occupying a subdomain of the structure with rate feedback control. The developed control law has been validated by using an explicit finite difference method. The governing partial differential equations have been solved for the system subject to excitations and control.

CHAPTER I

INTRODUCTION AND BACKGROUND

In the past few years, there has been considerable research activity in the field of active and passive control of vibrations of flexible structures. One of the methods of active control of vibrations involves the placement of piezoelectric devices on a structure to sense and control dynamic strains induced by structural vibrations. The deformation of the sensing transducer results in an electric current which is conditioned by operations such as amplification and shifting of the phase of the signal. The conditioned signal is then applied to another piezoelectric, electrostrictive or magnetostrictive device placed at a selected location of the structure. This transducer acts as an actuator motor or a driver and transmits mechanical energy to the structure. Depending on the applied voltage, electromechanical coupling of the forcing transducer to the structure and its location, a certain amount of structural control of flexible structures can be achieved. The term "electronic damping" has been used to describe this method of structural control in some of the more recent literature.¹⁻⁵

This type of active control offers unique features that are not usually employed for control of structural vibrations. For example, since the dynamics of direct contact type sensors and actuators permit

a wide frequency range of control, a measure of tunability is provided for the control of structural systems that age or grow. This method also has the potential benefit of adding less mass to the system than comparable passive and active servo controller systems.

Passive systems lack narrow band tunability and active servo controllers require an inertial ground to react against. It is expected though that each particular type of vibration control device will be beneficial in different areas of operation in terms of the amplitude, control force requirements and frequency bandwidth.

The potential of using piezoceramic transducers for vibration control has been convincingly demonstrated in a variety of experiments such as jitter control of optical systems.^{2,5} Nevertheless, there are many issues which still need to be resolved before appropriate control design procedures are developed. Specifically, given a piezoelectric material, electro-mechanical coupling, the structure and the control domain, a designer should be able to obtain an optimum procedure for controlling the vibration of the given system. To meet this design goal, one must be able to obtain a measure of the system changes in damping and stiffness due to the active feedback control similar to the way the mass and stiffness properties are obtained by using other analytical techniques.

To resolve some of these issues, the research in this thesis is directed towards the following major objectives;

- (1) The first objective is to develop models for the active structure consisting of a beam structure, piezoceramic sensors, signal

conditioning systems with appropriate control laws and piezoceramic actuators. The term "active beam" or "active structure" has been used to refer to such a structure.

- (2) The second objective is to identify the dynamic characteristics of the active structure from measurements of force and acceleration of the active structure. Cases of collocated and non collocated sensors and actuators will be considered.
- (3) The third objective is to identify the system parameters from measurements of the input and output of the active structure. In particular, electromechanical dynamic coupling coefficients and structural damping, that cannot be determined otherwise, are identified.
- (4) The final objective is to develop optimal control algorithms to selected cases involving an active beam with piezoceramic sensors and actuators.

In the next section, a brief review of the field of piezoelectricity is described.

1.1. Background

Piezoelectricity was first discovered by the Curie brothers.⁶ This work led them to look at the electrification of crystals upon the application of pressure. The converse piezoelectric effect, which is the change in crystal dimensions upon the application of an electric field was first theoretically predicted by Lippman and in the same year verified by the Curies.⁶ Later investigators established the relationship between piezoelectricity and the crystalline structure of various materials.

The first practical application of the piezoelectric effect was for the development of acoustic waves in fluids. Quartz crystalline material was initially used until the development of the ferroelectric class of materials.⁶ The term ferroelectric is used to describe a material which does not have a center of symmetry or electric dipole moment above a certain temperature called the Curie temperature.⁷

The single most important factor of the ferroelectric's over other piezoelectric materials is that they have a higher electromechanical coupling. Electromechanical coupling is defined as the amount of deformation achieved per field strength applied to the piezoelectric material.

Ferroelectric materials contain both organic and inorganic compounds. The piezoceramic ferroelectric materials are used in this investigation for structural control applications.

The constitutive relationships for piezoceramic material have been discussed by a number of investigators over the years and compiled by the IEEE and the Electronic Industries and American Standards Association into standards.^{8,9} One of the most serious disadvantages of piezoceramic ferroelectric type materials with reference to this application is the sensitivity of their piezoelectric properties to changes in temperature. D. Berlincourt¹⁰ has discussed the relationship of the performance of selected piezoceramics with temperature and other environmental factors. Doping of piezoceramics with lead and other elements helps to stabilize these parameters over a wider temperature range. The lead

zirconate titanate (PZT) type piezoceramics have proven to be the most promising compounds for stable piezoelectric properties and mechanical behavior over a temperature range that includes -200 to 150 degrees C.

Organic type piezoelectric compounds such as polyvinylidene fluoride film (PVDF)¹¹ have been used for active control of structures. This type of organic ferroelectric material has the potential of providing strains of an order of magnitude greater than piezoceramics but at the cost of a much greater applied electric field. Some of the more recent applications of PVDF has been in the area of adaptive optics^{12,13} and in vibration control of structures.^{14,15}

The electrostrictive or magnetostrictive effects in some materials can perform the same function as the converse piezoelectric effect. Electrostriction is related to a material change of shape upon the application of a large electric field. Usually the change in shape is very small and until recently was considered as a second order effect. W.P. Mason¹⁶ has studied the electrostrictive effect in nonpolarized ferroelectric type ceramic of materials. According to Mason the electrostrictive effect is quite large when compared to the corresponding converse piezoelectric effect of the same polarized material. One of the advantages of electrostrictive actuators is that they do not exhibit hysteresis effect common to piezoceramic type materials.¹⁷ This feature may make electrostrictive ceramics to be more suitable as driving devices for vibration control.

Some of the applications of piezoceramics can be classified as quasistatic applications, dynamic applications with resonating piezoceramics and non resonating dynamic applications.⁷ Most of the work involving quasistatic applications is in the area of adaptive optics.^{18-25,71} Dynamic applications with resonating piezoceramics have been primarily used in creating acoustic surface and bulk waves.²⁶⁻³¹ Non resonating dynamic application are mostly in the area of transducers and only recently, non resonating dynamic applications have been in the area of active control of flexible structures. 1-5,15,32,33

Electronic Damping

One of the earliest known uses of piezoceramics to active control of structures is attributed to Olsen.¹ In this work he proposed an electronic vibration reducer consisting of a piezoelectric driver and sensor attached to a structure with a suitable feedback amplifier.

Another early example of this type of control is by Mckechnie³² who has used piezoceramic sensors in a specially built accelerometer to drive a forcing piezoceramic to reduce the resonant response of an accelerometer. His experimental results indicate a reduction in the predicted peak response by thirty percent.

The first application to the active control of a structure is due to Forward² who has investigated the vibration control of a mirror subjected to acoustical excitation of its resonances. One piezoelectric transducer has been used to sense the vibrations and its output has been conditioned by a negative feedback amplifier to drive

another spatially separated transducer. The vibration response of a single mode of the optical structure was reduced significantly.

Forward and Lui³ have also demonstrated additional applications of "electronic damping" to control resonances in gimbal torquer control loops where they reduced the peak response of a gimbal torquer loop at various modal frequencies corresponding to gimbal mechanical resonances. This was accomplished by using small piezoelectric strain transducers to provide signals into a summing junction in the torquer control loops. Forward and Swigert⁴ have applied an "electronic damping" system to reduce orthogonal bending modes in a cylindrical satellite antenna mast. The application of piezoceramic sensors and actuators to reduce the amplitude of response of two problem modes in a large composite optical bench has been reported in reference.⁵ One piezoelectric ceramic strain transducer has been used as a sensor, and ten others were wired in parallel as a combined driver in a velocity feedback loop. In a recent work, Crawley,³³ has presented a mechanics coupling type of model for a piezoceramic bonded to a small cantilever beam. The model predicts the first mode dynamic response of a beam when driven by the piezoceramic transducers.

An examination of the reported literature in the field of active control of structures with piezoceramic sensors and actuators has revealed the following. A consistent analytical model does not exist for an active structure with piezoceramic or piezoelectric sensors and actuators that occupy selected subdomain of the structure. The problem of identification of the dynamic characteristics of an active

structure from measurements of time histories of appropriate input and output has not been explored. In particular, a significant problem of practical importance is the identification of dynamic characteristics of an active structure with non collocated sensors and actuators. Procedures for the identification of system parameters such as electromechanical coupling does not exist. The problem of optimal control of structures with piezoceramic sensors and actuators has not been examined. Only the problem of "instantly optimal"⁷⁰ control of a structure with a single PVDF actuator and a conventional accelerometer sensor has been explored.¹⁵

Some of these unsolved problems discussed in the previous paragraph, have been examined in the subsequent chapters. In chapter II, the development of a finite IV a method is developed for model identification for a structure with non collocated sensors and actuators. The optimal gain distribution of multiple location control of a simple structure using rate feedback is explored by applying limited state output feedback control in chapter V. Finally, the time optimal control of a cantilever beam using a distributed piezoceramic sensor and actuator is presented in chapter VI.

CHAPTER II

FINITE ELEMENT MODEL OF THE ACTIVE STRUCTURE

In this chapter a finite element model has been developed for an active structure shown in figure 2.1 consisting of a linear isotropic elastic beam, piezoceramic sensor occupying a subdomain of the beam, with the signal conditioning and piezoceramic actuator occupying another subdomain of the beam. In the following sections, the sensor, actuator and control electronic are analyzed and the finite element model for the active structure has been developed. Previous studies have considered only a finite element model or a beam with a piezoelectric actuator^{35,36}.

2.1. Sensing Transducer

The sensing transducer consisting of a piezoceramic thin plates is assumed to be bonded to a beam structure. The basic construction of the transducer consists of a thin layer of G-1195 PZT ceramic coated with a thin nickel electrode film. In this form the piezoceramic transducer is called a unimorph. When two unimorphs are bonded together and share the common electrode between them they are called bimorphs. The polarization of the unimorph or bimorph depend on the intended application.

A idealized sketch of a section of a beam with a sensing transducer and signal conditioning circuit is shown in Figure 2.2. The piezoceramic transducer is polarized in the +z direction and

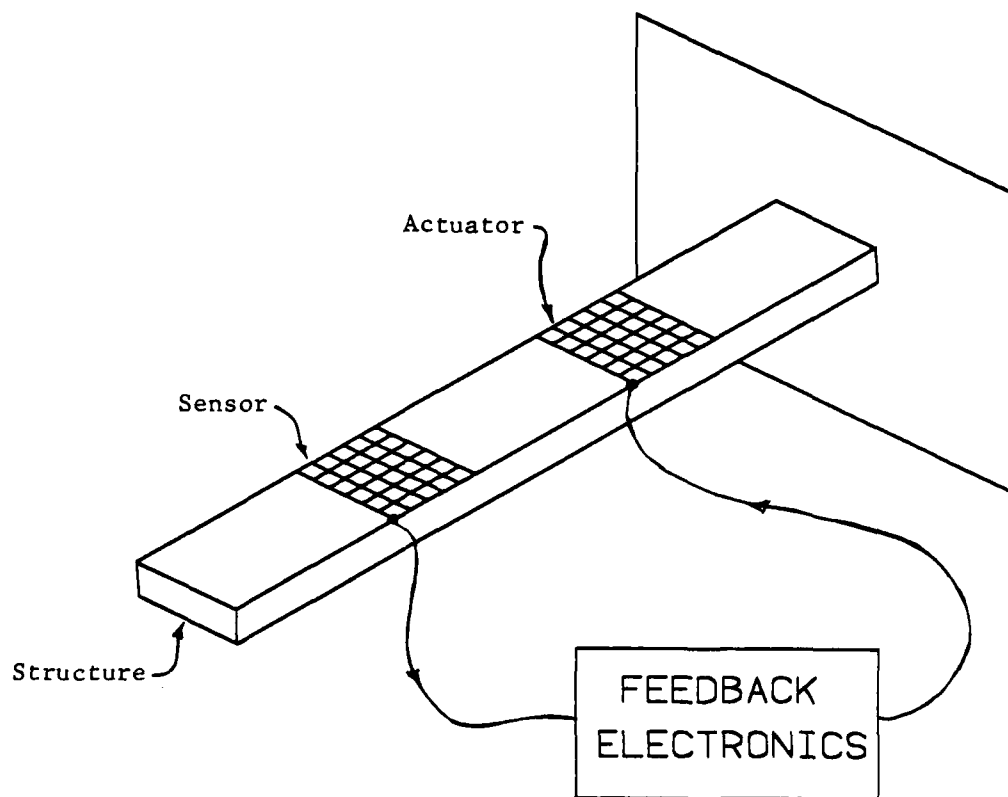


Figure 2-1 Active Control of Structures

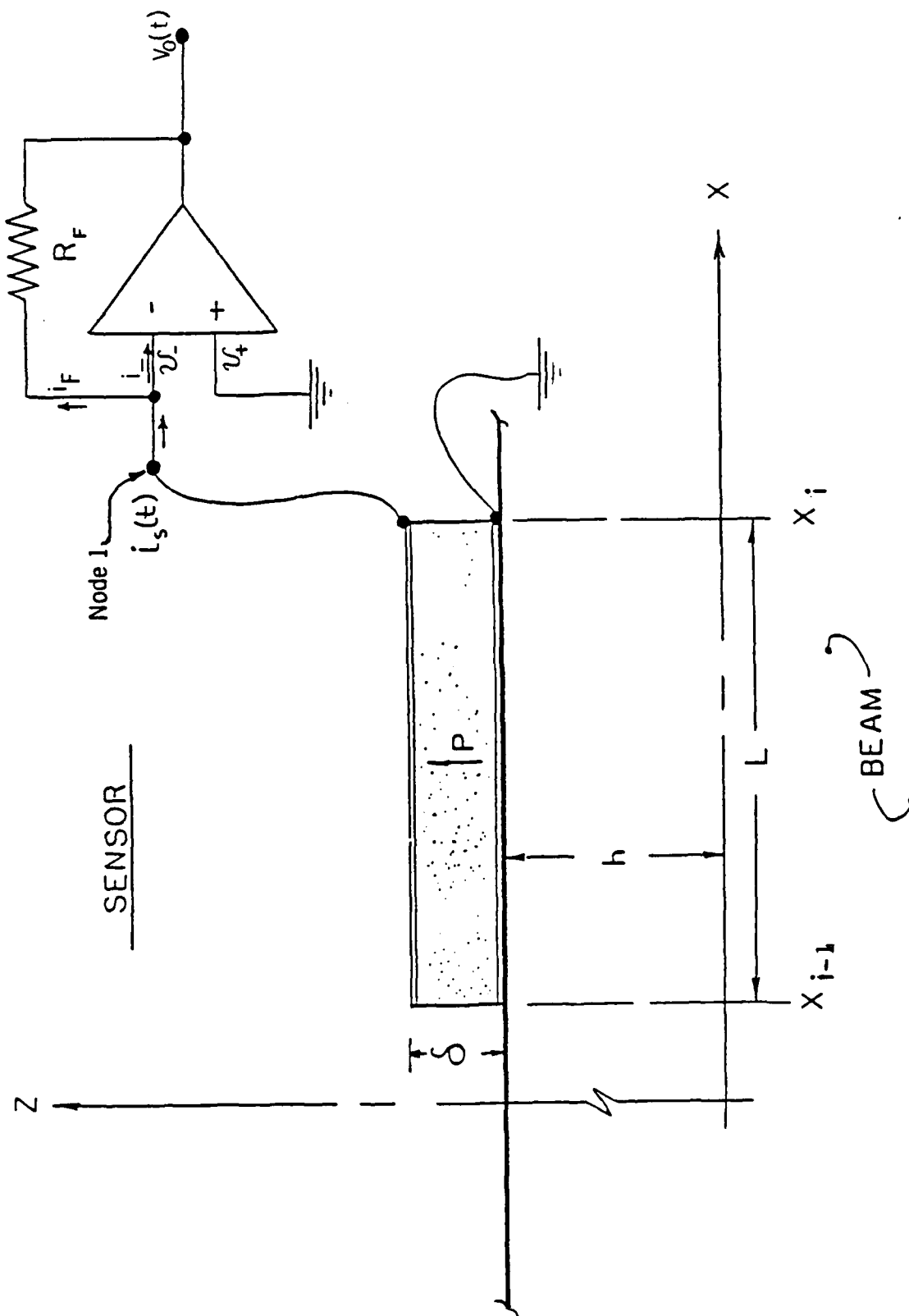


Figure 2-2 Piezoceramic Unimorph Sensor

electrically connected via two short leads a current amplifier. The following assumptions are made:

a) Initially, a perfect bond is assumed between the elastic body and the transducer. In reality there is a relative displacement due to the deformation of the bonding material. This has been initially neglected. Later, this effect is included approximately in the form of a dynamic coupling coefficient.

b) The thin film electrode surfaces add no mass or stiffness to the transducer and the transducer itself does not add any mass or stiffness to the structure to which it is bonded.

c) The capacitance of the transducer leads is considered to be negligible.

Considering a one dimensional analysis of the sensor, the following constitutive relations derived in Appendix A are approximated for $x_i < x < x_{i+1}$.

$$S_{11}(x,t) = s_{11}^E T_{11}(x,t) + d_{31} E_3(x,t) \quad (2.1)$$

$$D_3(x,t) = d_{31} T_{11}(x,t) + \epsilon_{13}^T E_3(x,t) \quad (2.2)$$

where

S_{11} = strain

T_{11} = stress

E_3 = electric field between the electrodes

D_3 = charge per unit area

s_{11}^E = elastic compliance at constant electric field

d_{31} = piezoelectric constant

ϵ_{13}^T = dielectric constant at constant stress

Notations used in eqs. (2.1) and (2.2) are based on the standards developed for piezoelectricity^{8,9}.

The sensor thickness is an order of magnitude smaller than the elastic body and the strain distribution is assumed to be constant through the sensor cross section and equal to the upper fiber strain (@ $z=h$) of the elastic beam. Therefore the strain distribution along the sensor is approximated as

$$S_{11}(x,t) = -h \frac{\partial^2 w(x,t)}{\partial x^2} \quad (2.3)$$

When the sensor is deformed, both a charge and an electric field is produced. The electric field between the two electric plates results in an electric potential at any cross section equal to

$$V_s(x_i, t) = \int_0^{\delta} E(x_i, t) dz \quad (2.4)$$

or

$$V_s(x_i, t) = \delta E(x_i, t) \quad (2.5)$$

where δ is the thickness of the sensor. Since there is no input resistance to node 1 in Figure 2.2 the following conditions arise⁶⁹,

$$V_s(t) = v_-(t) \quad (2.6)$$

$$|v_+(t) - v_-(t)| = \epsilon_v \quad (2.7)$$

for a typical commercial operational amplifier ϵ_v is of the order of 10^{-3} volt. Therefore the potential difference between the sensor electrodes is

$$V_s(t) \approx 1.0 \times 10^{-3} \text{ volt.} \quad (2.8)$$

For the transducers used, δ is approximately 2.54×10^{-4} M therefore the field between the plates is of the order of

$$E_3(t) \approx 4.0 \text{ V/M.} \quad (2.9)$$

Multiplying the field by d_{31} and ϵ_{13}^T in eqs. (2.3) and (2.4) a strain of 7.16×10^{-10} M/M and electric displacement of 6.6×10^{-8} C/M*M are obtained. These terms are negligible compared to the strain and charge produced due to the stress in the piezoceramic. Furthermore because of the negligible electric field, the sensor ideally becomes a pure current source. With this particular configuration using eq. (2.3) and solving for the stress in eq. (2.1) yields

$$T_{11}(x,t) = - \frac{h}{S_{11}E} \frac{\partial^2 w}{\partial x^2} \quad (2.10)$$

and the electric displacement in eq.(2.2) as

$$D_3(x,t) = d_{31} T_{11}(x,t) . \quad (2.11)$$

Hence the charge developed related to the sensor strain at every point given a constant width transducer is

$$D_3(x,t) = -hd_{31} c_{11}^E \frac{\partial^2 w(x,t)}{\partial x^2} \quad (2.12)$$

where $c_{11}^E = 1/s_{11}^E$ is now the elastic modulus of the piezoceramic material measured at constant field conditions. The input sensor current $i_s(t)$ is dependent on the rate of charge developed

$$di_s(t) = \dot{D}_3(t) dx dy. \quad (2.13)$$

For a constant width plate the current is

$$i_s(t) = w_d \int_0^L \dot{D}_3 dx \quad (2.14)$$

where w_d is the width and L is the plate length.

The charge D_3 in general, is a function of x and time. Eqs. (2.12) and (2.14) are combined to yield

$$i_s = -w_d h d_{31} c_{11}^E \int_{x_{i-1}}^{x_i} \frac{\partial^2 \dot{w}}{\partial x^2} (x,t) dx. \quad (2.15)$$

Using Kirchhoff's current law for node 1 in Figure 2.2

$$i_s = i_F + i_- \quad (2.16)$$

furthermore, for the circuit shown in Figure 2.2

$$V_o(t) = -R_F i_F(t) \quad (2.17)$$

and since for an ideal op amp (34)

$$i_- = 0 \quad (2.18)$$

the output voltage $V_o(t)$ becomes

$$V_o(t) = -R_F i_s(t). \quad (2.19)$$

The final result is obtained by combining eqs. (2.17) and (2.21)

$$V_o(t) = K_s \int_{x_{i-1}}^{x_i} \frac{\partial^2 \dot{w}}{\partial x^2} (x,t) dx \quad (2.20)$$

where

$$K_s = w_d h d_{31} c_{11}^E R_F.$$

Equation (2.22) represents the electromechanical equation for the sensor perfectly bonded to an elastic beam. It provides the voltage output of the sensor as a function of the strain distribution.

Limitation of the Distributed Sensor Model

Consider a unimorph piezoceramic sensor bonded along the entire length of a simply supported beam as shown in Figure 2.3 where h is the distance from the neutral axis to the upper beam surface. The motion of the beam under conditions of free vibrations is approximated by

$$w(x,t) = \sum_{n=1}^{\infty} A_n \sin \frac{n\pi x}{L} \sin \Omega_n t. \quad (2.21)$$

By considering only the first term of the series

$$n=1: \quad \frac{\partial^2 \dot{w}}{\partial x^2} = - \left(\frac{\pi}{L} \right)^2 \Omega_1 A_1 \sin \frac{\pi x}{L} \cos \Omega_1 t. \quad (2.22)$$

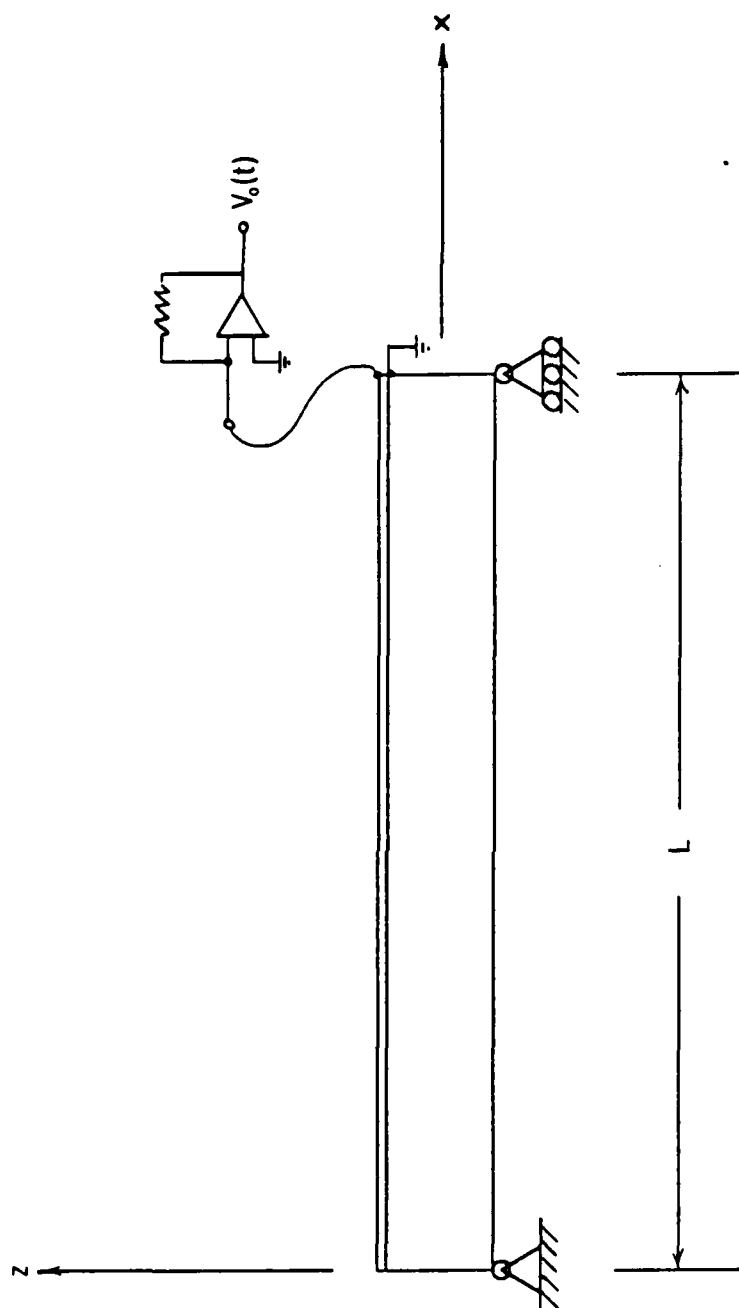


Figure 2-3 Simply Supported Beam With Piezoceramic Unimorph Sensor

From eqs. (2.20) and (2.22)

$$n=1: V_o(t) = 2K_s \frac{\pi}{L} \Omega_1 A_1 \cos \Omega_1 t \quad . \quad (2.23)$$

For the second term of the series gives

$$n = 2: V_o(t) = 0 \quad . \quad (2.24)$$

Under pure second mode excitation, ideally half of the sensor would be under compression and half of it would be under tension resulting in a zero output voltage. Therefore the limitations of the sensing model is that the highest frequency for control is limited to that below the modal density which results in a nodal line within the domain of the sensor.

2.2. Actuator Transducer

In a previous study³⁵, a finite element model for a beam with an electrostrictive transducer has been derived using an energy approach. The electrostrictive transducer behaves similarly to the piezoelectric transducer with a driver with an applied voltage. In this thesis a model is derived using a force equilibrium approach (Appendix B) and agrees with the previous work.

The piezoceramic actuator configuration is basically the same as a sensor except that in this case a relatively high voltage of the order of 100 to 120 volt(RMS) can be applied to the piezoceramic plates. When a high voltage is applied, the converse piezoelectric effect occurs which results in a deformation of the piezoceramic material. A particular unimorph can be polarized such that a positive electric field results in an elongation in the directions perpendicular to the

polarization vector with a simultaneous contraction in directions parallel to the polarization vector. A negative voltage would result in the opposite responses.

When an actuator transducer is bonded to an elastic structure it is constrained and as an electric field is applied the actuator tends to elongate or contract the resulting body.

A composite structure consisting of an elastic beam and two piezoceramic actuators is shown in figure 2.4. The two unimorph actuators bonded to the top and bottom of a thin beam and wired in such a manner that when a voltage is applied to the transducers the bottom actuator expands and the top actuator contracts. To analyze this sandwich construction, an inverted form of the constitutive equations 2.1 and 2.2 are (Appendix A)

$$T_{11}(x,t) = c_{11}^D S_{11}(x,t) - H_{31} D_3(x,t) \quad (2.25)$$

$$E_3(x,t) = - H_{31} S_{11}(x,t) + \frac{1}{\epsilon_{33}^S} D_3(x,t) \quad (2.26)$$

where

S_{11} = Strain

T_{11} = Stress

D_3 = Charge per unit area

c_{11}^D = Elastic modulus with the piezoceramic circuit open

ϵ_{33}^S = Dielectric constant at constant strain

$H_{31} = e_{31}/\epsilon_{11}$

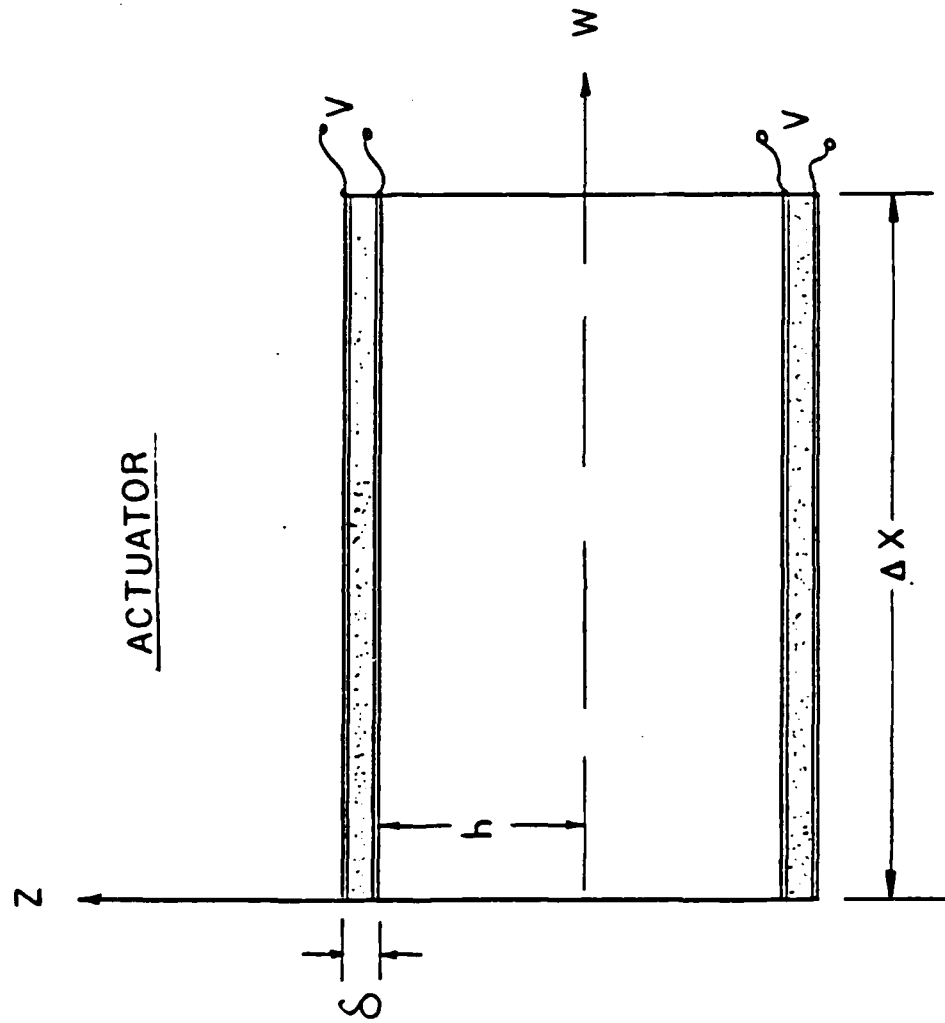


Figure 2-4 Piezoceramic Unimorph Actuator

E_3 = Electric Field.

Since the drivers are fully covered with electrodes the electric field E_3 produced between the plates for a given potential applied can be considered only dependent on time.

Because of the direction of polarization E_3 is assumed to be much greater than E_1 and E_2 . Since $E_3 \gg E_1$ and $E_3 \gg E_2$, assuming $E_1 = E_2 = 0$,

$$E_3 = \frac{\partial V_D}{\partial z} \quad (2.27)$$

or

$$V_D(t) = E_3(t)\delta \quad (2.28)$$

where δ is the separation between the electrode plates.

The potential applied across the plates of the top unimorph is then equal to

$$V_D(t) = \int_h^{h+\delta} E_3(t) dz = \int_h^{h+\delta} (-H_{31}S_{11} + 1/\epsilon_{33}^S D_3) dz \quad (2.29)$$

Furthermore when pure bending is assumed,

$$S_{11}(x,t) = -z \frac{\partial^2 w}{\partial x^2}(x,t) \quad (2.30)$$

and the piezoceramic is a dielectric material that is polarized in the z direction, the charge within the body is governed by (Appendix A)

$$\frac{\partial D_3}{\partial z} = 0 \quad \therefore D_3(x, y, t) \quad (2.31)$$

Using conditions given by eqs. (2.30) and (2.31)

$$V_D(t) = -H_{31} \left(h\delta + \frac{\delta^2}{2} \right) \frac{\partial^2 w}{\partial x^2} + \frac{D_3 \delta}{\epsilon_{33}^s} \quad (2.32)$$

Solving for D_3 for a constant unit width actuator in eq.(2.32) gives

$$D_3(x, t) = \frac{\epsilon_{33}^s}{\delta} V_D(t) + \frac{H_{31} \epsilon_{33}^s}{\delta} \left(h\delta + \frac{\delta^2}{2} \right) \frac{\partial^2 w}{\partial x^2} (x, t). \quad (2.33)$$

Equation (2.33) is simplified to

$$D_3(x, t) = \frac{\epsilon_{33}^s}{\delta} V_D(t) + e_{31} h \frac{\partial^2 w}{\partial x^2} (x, t) \quad (2.34)$$

since $\delta \ll h$ and $H_{31} = e_{31}/\epsilon_{11}^s$ and it is assumed that piezoceramic used $\epsilon_{33}^s = \epsilon_{11}^s$. This assumption is valid for PZT type ceramics. Substituting eq. (2.34) into eq. (2.25) yields

$$T_{11} = - \left(c_{11}^D h + \frac{e_{31}^2 h^2}{\epsilon_{11}^s} \right) \frac{\partial^2 w}{\partial x^2} - \frac{e_{31}}{\delta} V_D(t) \quad (2.35)$$

and since

$$\frac{e_{31}^2}{\epsilon_{11}^s c_{11}^D} \approx .012$$

eq. (2.37) can be approximated by

$$T_{11} = - c_{11}^D h \frac{\partial^2 w}{\partial x^2} - \frac{e_{31}}{\delta} V_D(t) \quad \left\{ \begin{array}{l} h < z < h + \delta \\ -(h + \delta) < z < -h. \end{array} \right. \quad (2.36)$$

Given two unimorph actuators wired as previously mentioned, the moment for at any cross section of the beam of unit thickness is given as

$$M(x,t) = - \int_{-h}^h E z^2 \frac{\partial^2 w}{\partial x^2} dz + \int_{-(h+\delta)}^{-h} T_{11} z dz + \int_h^{h+\delta} T_{11} z dz \quad (2.37)$$

$$M(x,t) = EI \frac{\partial^2 w}{\partial x^2} - 2 \int_h^{h+\delta} (c_{11}^D z^2 \frac{\partial^2 w}{\partial x^2} + \frac{e_{31} z}{\delta} V_D(t)) dz . \quad (2.38)$$

Neglecting terms that are multiplied by δ and δ^2 the final result is

$$M(x,t) = EI \frac{\partial^2 w}{\partial x^2} (x,t) - 2\bar{e}_{31} h V_D(t) \quad (2.39)$$

where \bar{e}_{31} is equal to e_{31} times the width of the actuator.

If only one surface has an actuator the moment equation is

$$M(x,t) = EI \frac{\partial^2 w}{\partial x^2} (x,t) - K_D V_D(t) \quad (2.40)$$

where

$$K_D = \bar{e}_{31} h .$$

From eq. (2.40) certain observations are made. As a voltage is applied to the piezoceramic unimorph it is equivalent to adding opposing couples at the ends of the section whose sign is dependent on the sign of the applied potential to the plates^{35,36}.

Consider a structure as shown in figure 2.5, with no external forces. For an applied DC voltage V_D to the actuators eq. (2.40) becomes

$$K_D V_D = EI \frac{\partial^2 w}{\partial x^2}. \quad (2.41)$$

Integrating eq. (2.41) twice and solving for the unknown constants using the boundary conditions at $x = 0$ and $x = \pm L$ gives

$$w = \frac{K_D V_D}{EI} \frac{x^2}{2}. \quad (2.42)$$

For the same structure without unimorph piezoceramic layers and loaded as shown in figure 2.6, the resulting expression for displacement is

$$w = \frac{M_0 x^2}{2EI}. \quad (2.43)$$

A comparison eqs. (2.42) and (2.43) further supports the observation that a piezoceramic unimorph driver produces equivalent point or concentrated external moments proportional to the voltage applied.

2.3. Analysis of Active Electronic Feedback Damping Using the Finite Element Method

A finite element approximation of the coupled sensor, actuator and structure is developed in this section. In previous studies, finite element models for such an active structural dynamic system have not been developed. To accomplish this a beam with only a piezoceramic unimorph actuator is considered first. Later an element consisting of a collocated sensor and actuator transducer is examined.

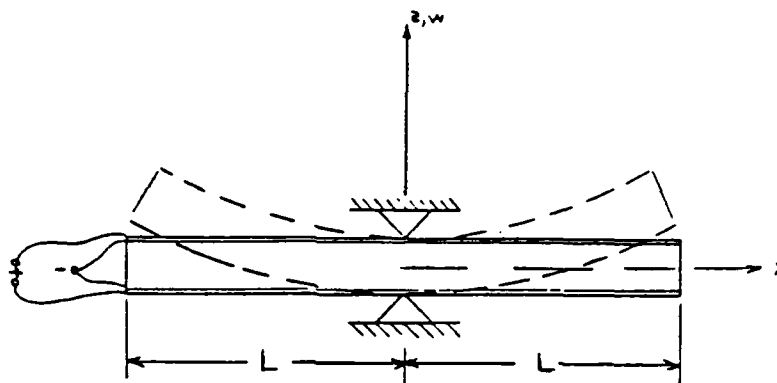


Figure 2-5 Actuator - DC Voltage

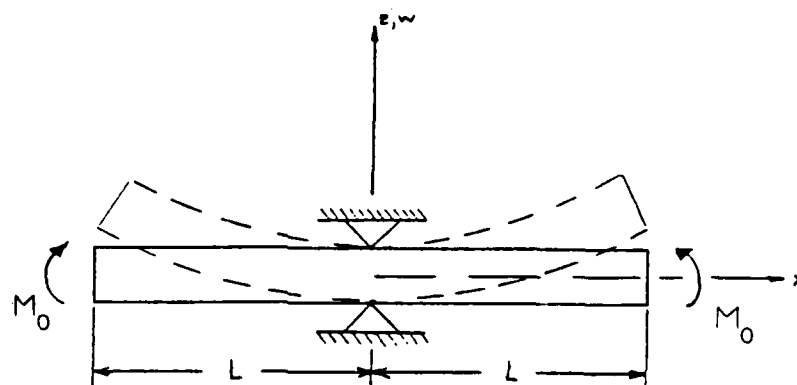


Figure 2-6 End Couples

The beam drawn in figure 2.7 is analyzed in Appendix B. Equation (B-17) from this Appendix is the resultant beam element matrix equation neglecting the elastic stiffness contribution of the actuator

$$\begin{Bmatrix} V_{i-1} \\ M_{i-1} + K_D V_D \\ V_i \\ M_i - K_D V_D \end{Bmatrix}^e = \frac{EI}{L^3} \begin{bmatrix} 12 & & & \\ -6L & 4L^2 & \text{sym.} & \\ -12 & 6 & 12 & \\ -6L & 2L^2 & 6L & 4L^2 \end{bmatrix} \begin{Bmatrix} w_{i-1} \\ \theta_{i-1} \\ w_i \\ \theta_i \end{Bmatrix}^e \quad (2.44)$$

[K_e]

where K_D is the piezoceramic actuator coupling coefficient and V_D is the applied voltage to the actuator electrodes. As noted in eq. (2.41), the contribution of an applied DC voltage to the actuator is equivalent to the application of two equal and opposite couples at the element nodes.

If an AC voltage is applied to the actuators then the applied moments would be dynamic in nature and the response of the FEM model could be determined given the mass matrix of the system.

For a system considering only the mass of the structure and not the transducers, the resulting equation of motion could be written as

$$[M] \begin{Bmatrix} \ddot{w}_{i-1} \\ \ddot{\theta}_{i-1} \\ \ddot{w}_i \\ \ddot{\theta}_i \end{Bmatrix} + [K] \begin{Bmatrix} w_{i-1} \\ \theta_{i-1} \\ w_i \\ \theta_i \end{Bmatrix} = \begin{Bmatrix} V_{i-1}(t) \\ M_{i-1}(t) + K_D V_D(t) \\ V_i(t) \\ M_i(t) - K_D V_D(t) \end{Bmatrix} \quad (2.45)$$

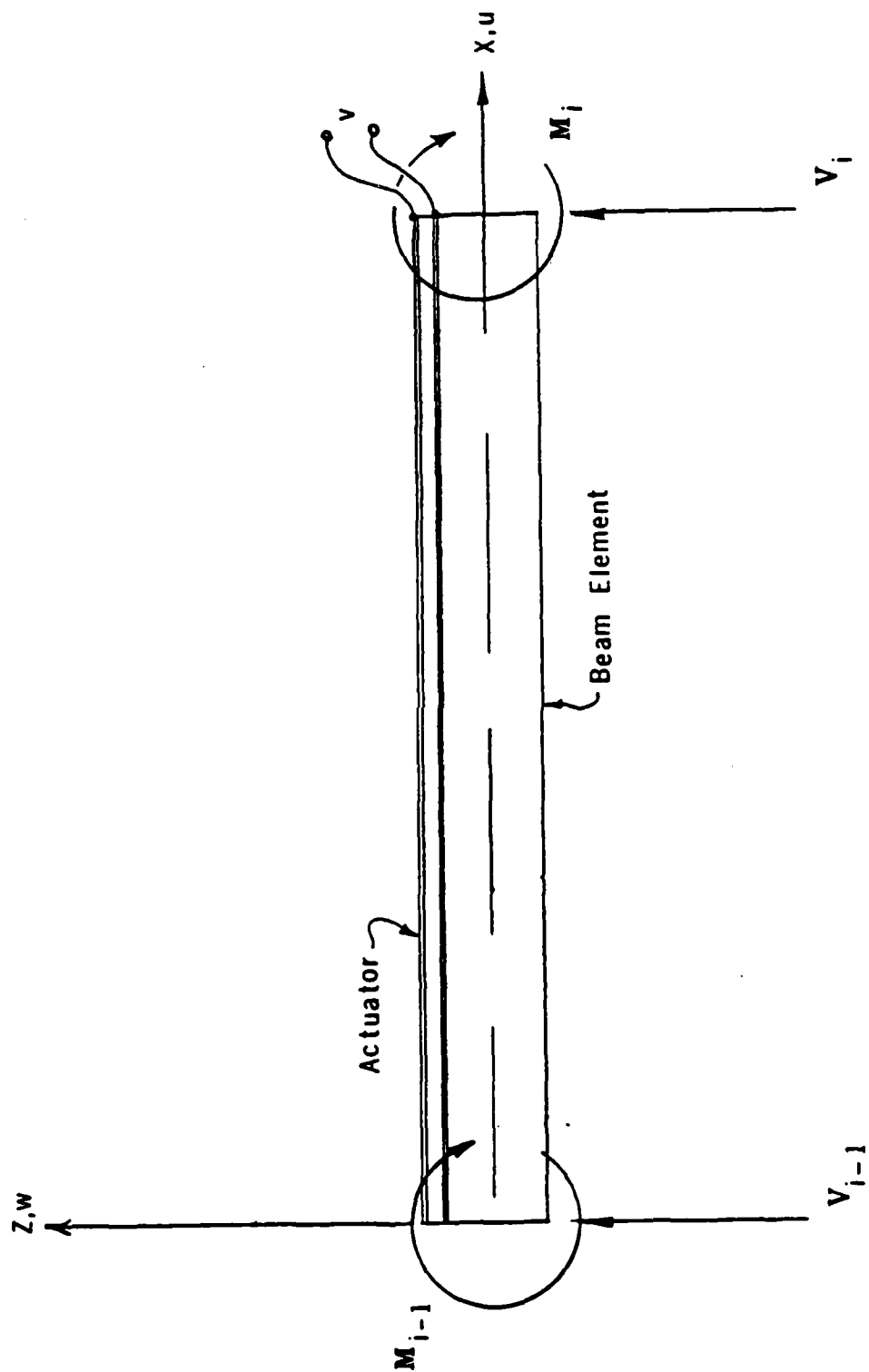


Figure 2-7 Actuator Beam Element

In reference 35, the same element eq. (2.44) is obtained by using the method of weighted residuals. When the ratio of the thickness of the actuator to the beam is much greater as in reference 35, the contribution to stiffness and mass of the transducer must also be considered.

The structure shown in figure 2.8 is considered. A transducer is bonded to the upper surface as a sensor; similarly, the transducer bonded to the bottom surface is an actuator. The output voltage from the sensor is increased in gain by a constant amount and supplied to the actuator. Depending on either the orientation of the polarity vectors of the unimorphs or the sign of the feedback voltage, the sign of the couples at the element nodes is determined. With no other type of conditioning of the sensor signal voltage supplied to the actuator is equal to

$$V_D(t) = V_S(t) = GK_S \int_{x_{i-1}}^{x_i} \frac{\partial^2 \dot{w}}{\partial x^2}(x,t) dx \quad (2.46)$$

where K_S represents the sensor coupling coefficient of eq.(2.20), and x_{i-1} and x_i are the locations of the element node points. If it is assumed that the applied voltage to the actuator is slowly varying such that the inertial effects of the beam can be ignored. The resulting beam equation (Appendix B) for a collocated sensor actuator is written as

$$\begin{Bmatrix} V_{i-1} \\ M_{i-1} \\ V_i \\ M_i \end{Bmatrix} = \frac{EI}{L^3} [K_e] \begin{Bmatrix} w_{i-1} \\ \theta_{i-1} \\ w_i \\ \theta_i \end{Bmatrix} + K_D K_S \underbrace{\begin{bmatrix} 0 & & & \\ 0 & 1 & \text{Sym.} & \\ 0 & 0 & 0 & \\ 0 & -1 & 0 & 1 \end{bmatrix}}_{[C_{ED}]} \begin{Bmatrix} \dot{w}_{i-1} \\ \dot{\theta}_{i-1} \\ \dot{w}_i \\ \dot{\theta}_i \end{Bmatrix} \quad (2.47)$$

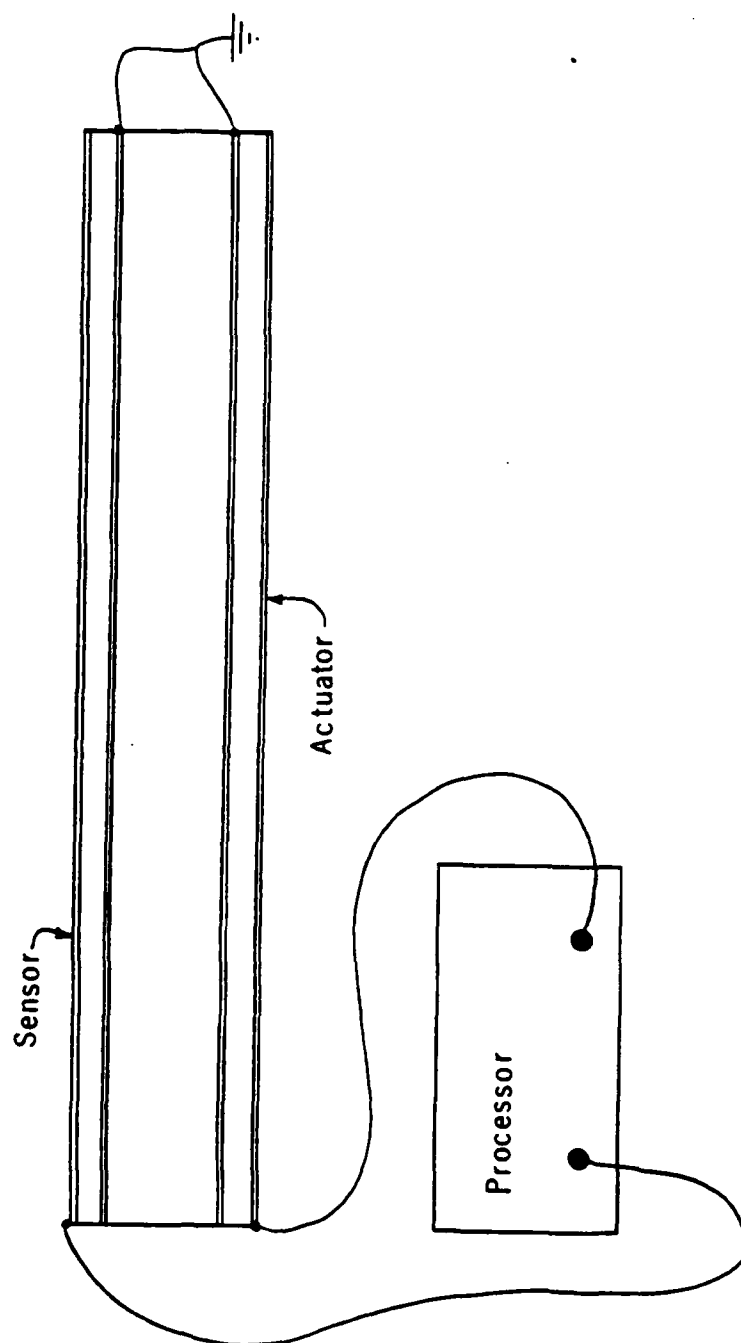


Figure 2-8 Active Beam Finite Element

The element matrix $[C_{ED}]$ is multiplied by the velocity of the element displacements and rotations. As such, it is considered as an equivalent viscous damping contribution to the element. This matrix can be called the "electronic damping" matrix.

A four element approximation of a cantilever beam with various sensor and actuator configurations is shown in figure 2.9. By adding the additional assumption that a sensor can only supply a feedback voltage to an individual actuator, the corresponding global system $[C_{ED}]$ matrices for each case is shown. Case B of figure 2.9 indicates that for non collocated sensors and actuators that the $[C_{ED}]$ is no longer symmetric.

For the configurations shown in figure 2.9 the total inertia matrix for the complete structure is

$$[M] = \sum_{s=1}^4 [A_s]^T [M_s] [A_s] . \quad (2.48)$$

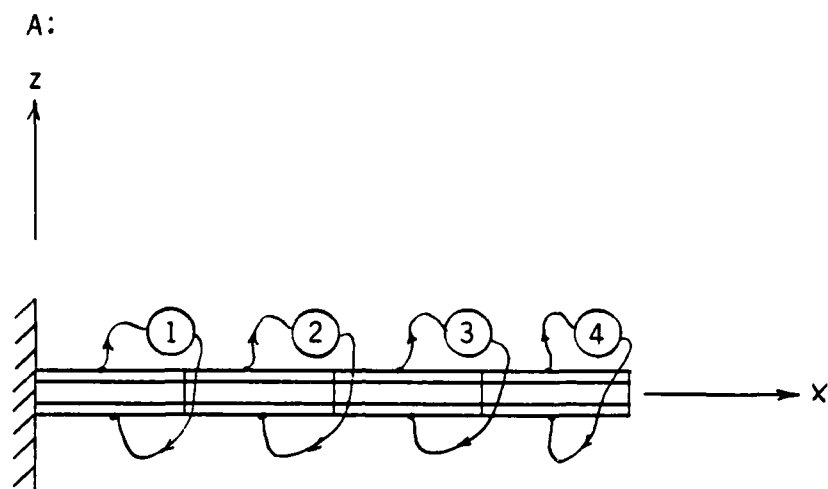
where $[A]_s$ is a rectangular matrix that is used to assemble the element mass matrices into a mass matrix of the entire structure.

Similarly,

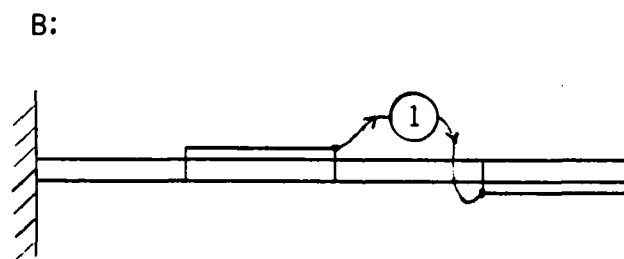
$$[K] = \sum_{s=1}^4 [A_s]^T [K_s] [A_s] \quad (2.49)$$

is the assembled system stiffness matrix.

Depending on the global location of the sensor/actuator active elements, the system electronic damping matrix is also assembled as



$$C_{ED} = \frac{K_S K_D}{L^3} \begin{bmatrix} 0 & & & & & & \\ 0 & 2 & & & & & \\ 0 & 0 & 0 & & & & \\ 0 & -1 & 0 & 2 & & & \\ 0 & 0 & 0 & 0 & 0 & & \\ 0 & 0 & 0 & -1 & 0 & 2 & \\ 0 & 0 & 0 & 0 & 0 & 0 & \\ 0 & 0 & 0 & 0 & -1 & 0 & 1 \end{bmatrix} \quad \text{Sym}$$



$$C_{ED} = \frac{K_S K_D}{L^3} \left[\begin{array}{ccc|ccc} & & & & & \\ & & & & & \\ & & & & & \\ \hline 0 & 0 & 0 & 0 & & \\ 0 & 1 & 0 & -1 & & \\ 0 & 0 & 0 & 0 & & \\ 0 & -1 & 0 & 1 & & \\ \hline & & & & & \end{array} \right] \begin{array}{l} [0] \\ [0] \\ [0] \\ [0] \end{array}$$

Figure 2-9 Active Element Configuration Examples

$$[C_{ED}] = \sum_{s=1}^4 [B_s]^T [C_{ED}] [B_s] \quad (2.50)$$

where $[B_s]$ is a rectangular matrix coordinating the location of the sensors and their respective actuators.

The vector of all the non conservative joint forces for the system with electronic damping is written as

$$\{F_i\} = \sum_{s=1}^4 [A_s]^T \{\bar{F}_s\} - \sum_{s=1}^4 [B_s]^T [C_{ED}] [B_s] \begin{Bmatrix} \dot{w}_i \\ \dot{\theta}_i \end{Bmatrix} \quad (2.51)$$

The equation of motion for the complete structure is

$$[M] \begin{Bmatrix} \ddot{w}_i \\ \ddot{\theta}_i \end{Bmatrix} + [K] \begin{Bmatrix} w_i \\ \theta_i \end{Bmatrix} = \{F_i\} \quad (2.52)$$

where the non conservative nodal forces are defined by eq.(2.51). Combining eqs. (2.51) and (2.52) and excluding all viscous type forces from the non conservative force vector gives

$$[M] \begin{Bmatrix} \ddot{w}_i \\ \ddot{\theta}_i \end{Bmatrix} + [C] \begin{Bmatrix} \dot{w}_i \\ \dot{\theta}_i \end{Bmatrix} + [C_{ED}] \begin{Bmatrix} \dot{w}_i \\ \dot{\theta}_i \end{Bmatrix} + [K] \begin{Bmatrix} w_i \\ \theta_i \end{Bmatrix} = \{F_i\} \quad (2.53)$$

where the internal damping matrix $[C]$ is defined as

$$[C] = \sum_{s=1}^4 [A_s]^T [C] [A_s] \quad (2.54)$$

The contribution of the electronic damping matrix in eq.(2.53) is directly related to the internal system viscous damping matrix for rate feedback between the sensor and actuator (no filtering).

It will be shown later that when signal conditioning is used to selectively increase the damping for a particular mode that for other than a special case, the feedback will add to both the stiffness and damping of the system.

2.4. Model of the Feedback Active Control Electronics

A specific type of signal conditioning electronics is now examined. Schematic drawings for the prototype electronics are shown in Appendix D. From the results presented in appendix D the final model of the active control filter unit was determined to be

$$\ddot{V}_{D_i} + (\omega_f/Q) \dot{V}_{D_i} + \omega_f^2 V_{D_i} = \frac{G\omega_f}{Q} V_{S_i} \quad (2.55)$$

where ω_f is the filter center frequency
 Q is the filter bandwidth
 G is the gain
 V_{D_i} is the voltage to the actuator
 V_{S_i} is the voltage from the preamplifier.

For r sensors and actuators eq.(2.55) can be written in the following matrix form.

$$[I]\{\ddot{V}_D\} + [a]\{\dot{V}_D\} + [b]\{V_D\} = \left[\frac{G_i\omega_{fi}}{Q_i} \right] \{\dot{V}_S\} \quad (2.56)$$

where $[a] = [\omega/Q_i]$

$$[b] = [\omega_f^2]$$

Solving the integral of Equation (2.20) for a particular sensor element yields

$$V_{S_i}(t) = V_o(t) = K_s[\dot{\theta}_i - \dot{\theta}_{i-1}] \quad (2.57)$$

Combining equations (2.57) with (2.56) gives

$$[I]\{\ddot{V}_D\} + [a]\{\dot{V}_D\} + [b]\{V_D\} = [\bar{K}_s][T_s]\{\ddot{q}_i\} \quad (2.58)$$

where

$$\{q_i\} = \begin{Bmatrix} w_i \\ \theta_i \end{Bmatrix}$$

$[T_s]$ is the sensor location matrix containing 1's, -1's and 0's ($r \times 2n$)

and

$$[\bar{K}_s] = \begin{bmatrix} \frac{G_i \omega_{fi}}{Q_i} & K_{si} \end{bmatrix} \quad (r \times r)$$

For the structural system excited by only actuators the matrix equations are written as

$$[M]\{\ddot{q}_i\} + [C]\{\dot{q}_i\} + [K]\{q_i\} = \{F_{ED}\} \quad (2.59)$$

The actuator force vector contains only nonzero moment terms and can be expanded to yield

$$\{F_{ED}\} = [T_D][\bar{K}_D]\{V_D\} \quad (2.60)$$

where $[T_D]$ is the actuator location matrix matrix containing 1's , -1's and 0's ($2n \times r$) and $[\bar{K}_D]$ is a diagonal matrix of the actuator coupling coefficients.

Combining equations 2.56, 2.59 and 2.60 yields

$$[I]\{\ddot{V}_D\} + [a] \{\dot{V}_D\} + [b]\{V_D\} = [K_s][T_s] \{q_i\} \quad (2.61)$$

$$[M] \{\ddot{q}_i\} + [C] \{\dot{q}_i\} + [K] \{q_i\} = [T_D][\bar{K}_D]\{V_D\} \quad (2.62)$$

Eqs. (2.61) and (2.62) represent the coupled pairs of differential equations modelling the active structure conditioned with a modal feedback filter system. Previous work⁴³ has developed a similar set of equations for control of a plane grid structure using accelerometers sensors and electrodynamic shaker actuators.

CHAPTER III

IDENTIFICATION OF DYNAMIC COUPLING COEFFICIENTS

In the previous chapter a finite element model has been developed for the closed system consisting of an Euler-Bernoulli beam, sensors, signal conditioning subsystem and actuators. This model, with discrete degrees of freedom will be used to develop optimal control strategies. In order to implement analytically developed optimal control algorithms, it is necessary to establish the model parameters accurately. Identification procedures are used to estimate the model parameters. The identification is necessary because of the approximation of the structure by a system of discrete degrees of freedom, assumption of the bonding effects of the transducer to the structure by coupling coefficients, idealization of the signal conditioning system by a second order equation and the unknown damping parameters.

There has been a significant amount of reported research work in the field of the identification of benign structural dynamic systems or open loop systems that do not have feedback effects⁶⁵. However, there is no reported research work in the field of identification of an active structural dynamic system or closed loop structural dynamic system with feedback. In the following sections, the development of procedures to identify parameters of the model for closed loop systems and the application of the procedure to selected beam systems with measurements are discussed.

3.1. Equations of Identification

A system shown in Figure 3.1 is considered. This system was been approximated by n finite elements each with a unique sensor/actuator pair bonded to it with its own individual signal conditioning system or feedback control processor.

Equations (2.61) and (2.62) in Chapter II form a coupled pair of equations describing the overall feedback control system. The Fourier transform of Eq. (2.61) yields

$$[-\omega^2[M] + j\omega[C] + [K]]\{q(\omega)\} = \{F_e(\omega)\} + \{F_c(\omega)\} \quad (3.1)$$

where as before

$$\{q(\omega)\} = \begin{Bmatrix} w_i(\omega) \\ \theta_i(\omega) \end{Bmatrix} \quad (3.2)$$

$\{F_c\}$ = Active actuator control moment vector

$\{F_e\}$ = External applied forces and moments

The Fourier transform of eq (2.56) yields

$$[c_i - a_i\omega^2 + j\omega b_i]V_{Di}(\omega) = j\omega V_{Si}(\omega) \quad (3.3)$$

where,

$$a_i = Q/G\omega_f, \quad b_i = 1/G, \quad c_i = Q\omega_f/G \quad (3.4)$$

Taking a slightly different approach than Chapter II, the control force vector $\{F_c(\omega)\}$ when expanded has the following form

$$\{F_c(\omega)\} = [0 \ (M_1 - M_2) \ 0 \ (M_2 - M_3) \ \dots \ (M_{n-1} - M_n) \ 0 \ M_n]^T \quad (3.5)$$

Solving for $V_{Di}(\omega)$ in eq. 3.3 the applied moment at an actuator element node is

$$M_i(\omega) = \bar{K}_{Di} \left[\frac{j\omega}{(c_i - a_i\omega^2) + j\omega b_i} \right] V_{Si}(\omega) \quad (3.6)$$

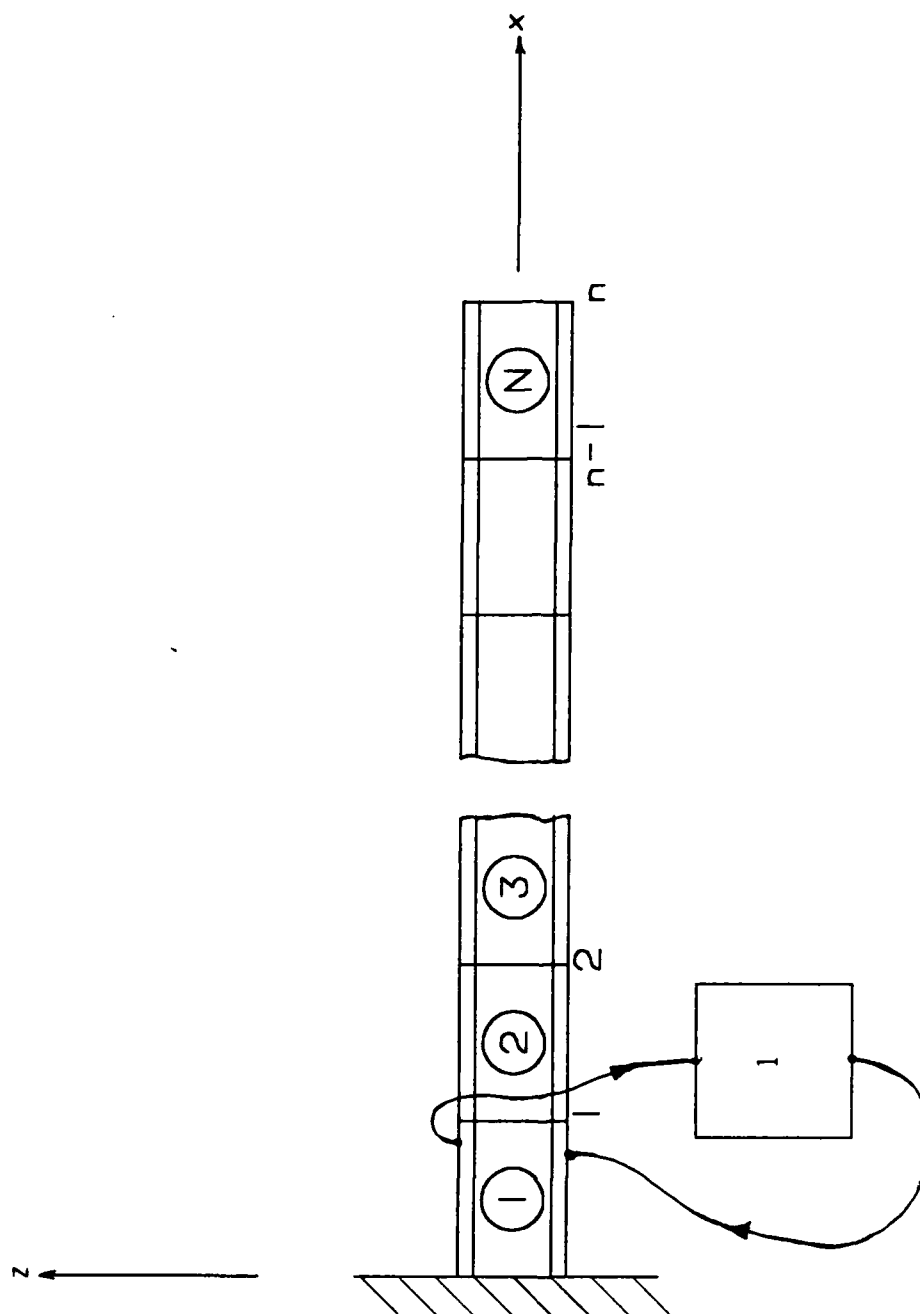


Figure 3-1 N Active Element Model Of A Cantilever Beam

Using eq. (3.6) and the fourier transform of the sensor eq. (2.20) in Chapter II yields,

$$M_i(\omega) = \bar{K}_{D_i} \left[\frac{-\omega^2}{(c_i - a_i \omega^2) + j\omega b_i} \right] [\theta(x_i) - \theta(x_{i-1})] \quad (3.7)$$

where,

$$\bar{K}_{D_i} = K_{s_i} K_{D_i} \quad (3.8)$$

By using a notation

$$h_{f_i}(\omega) = \bar{K}_{D_i} \left[\frac{-\omega^2}{(c_i - a_i \omega^2) + j\omega b_i} \right] \quad (3.9)$$

Therefore

$$M_i(\omega) = h_{f_i}(\omega) [\theta(x_i) - \theta(x_{i-1})] \quad (3.10)$$

Equation (3.5) is rewritten as follows

$$\{F_c(\omega)\} = [0 \ M_1 \ 0 \ M_2 \ \dots \ M_n]^T - [0 \ M_2 \ 0 \ M_3 \ \dots \ M_n \ 0 \ 0]^T \quad (3.11)$$

By using eq. (3.9) the first vector component is equal to

$$[0 \ M_1 \ 0 \ M_2 \ \dots \ M_n]^T = \begin{bmatrix} 0 & 0 & 0 & & & 0 \\ 0 & h_{f_1} & 0 & 0 & & \\ 0 & 0 & 0 & 0 & & \\ \vdots & -h_{f_2} & 0 & h_{f_2} & & \\ \vdots & \vdots & & & & \\ 0 & 0 & & & & h_{f_2} \end{bmatrix} \{q_i\} \quad (3.12)$$

and the second component is equal to

$$[0 \ M_1 \ 0 \ M_2 \dots M_n \ 0 \ 0]^T = \begin{bmatrix} 0 & 0 & 0 & 0 \\ 0 & h_{f2} & 0 & -h_{f2} \\ \cdot & 0 & 0 & 0 \\ \cdot & & & h_{f3} \\ 0 & & & \end{bmatrix} \{q_i\} \quad (3.13)$$

Combining eqs. (3.12) and (3.13) yields

$$\{F_c(\omega)\} = [H_2(\omega)] \{q(\omega)\} \quad (3.14)$$

where

$$[H_2(\omega)] = \begin{bmatrix} 0 & 0 & 0 & 0 \\ 0 & h_{f1} + h_{f2} & 0 & -h_{f2} \\ \cdot & 0 & 0 & 0 \\ \cdot & -h_{f2} & 0 & h_{f2} + h_{f3} & 0 & -h_{f3} \\ \cdot & \cdot & & 0 & & \\ & & & -h_{f3} & & \end{bmatrix} \quad (3.15)$$

Combining eqs. (3.1) and (3.14) further yields

$$[[K] - \omega^2[M] + j\omega[C] - [H_2(\omega)]]\{q(\omega)\} = \{F_e(\omega)\} \quad (3.16)$$

By denoting

$$[H_3(\omega)] = [[K] - \omega^2[M] + j\omega[C] - [H_2(\omega)]]^{-1} \quad (3.17)$$

the following equation is obtained

$$\{q(\omega)\} = [H_3(\omega)]\{F_e(\omega)\} \quad (3.18)$$

3.2. Identification of Feedback Filter Electronics Parameters

Parameters a_i , b_i , c_i of eq. (3.4) can be calculated from a knowledge of the circuits of the signal conditioning system. However, the actual values used for active control were determined from experiments which measured $V_{S_i}(t)$ and $V_{D_i}(t)$ and applied a least square identification procedure to the real and imaginary spectral data. The admittance function of equation (3.4) is

$$Z_i(\omega) = \frac{V_{S_i}(\omega)}{V_{D_i}(\omega)} = b_i + j(a_i\omega - c_i/\omega) \quad (3.19)$$

Expanding eq. (3.19) into real and imaginary parts yields

$$Z_{Ri}(\omega) = b_i \quad (3.20)$$

$$Z_{Ii}(\omega) = a_i\omega - c_i/\omega \quad (3.21)$$

The real and imaginary spectral data was obtained by computing the transfer function between the wideband random sensor voltage signal and high voltage output signal. The uncorrelated noise can be reduced by computing the transfer function by dividing the autospectrum of the input voltage by the cross spectrum between the input and output voltage.

For n data samples, the following matrix relation can be written for a particular feedback system.

$$\{Z\} = \begin{Bmatrix} Z_R(\omega_1) \\ \vdots \\ Z_R(\omega_n) \\ Z_I(\omega_1) \\ \vdots \\ Z_I(\omega_n) \end{Bmatrix} = \begin{bmatrix} 0 & +1 & 0 \\ \vdots & \vdots & \vdots \\ 0 & +1 & 0 \\ \omega_1 & 0 & -1/\omega_1 \\ \vdots & \vdots & \vdots \\ \omega_n & 0 & -1/\omega_n \end{bmatrix} \begin{Bmatrix} a \\ b \\ c \end{Bmatrix} = \begin{bmatrix} C_1 \\ C_2 \end{bmatrix} \begin{Bmatrix} a \\ b \\ c \end{Bmatrix}$$

or

$$\begin{Bmatrix} Z_R \\ Z_I \end{Bmatrix} = \begin{bmatrix} C_1 \\ \text{---} \\ C_2 \end{bmatrix} \{Y\} \quad (3.22)$$

where

$$\{Y\} = \begin{Bmatrix} a \\ b \\ c \end{Bmatrix} \quad (3.23)$$

From exact values of a_i, b_i and c_i , equation (3.19) is exactly satisfied.

For other values of a_i, b_i and c_i an error matrix is defined as

$$\{e\} = \{Z\} - [c]\{\gamma\} \quad (3.24)$$

and a square measure of the error is

$$J = \{e\}^T \{e\} \quad (3.25)$$

Minimizing J with respect to each unknown parameter leads to the identification of the parameters a_i , b_i and c_i . Each sensor/actuator control system requires n independent identification computations.

Equating the partial derivative of eq. (2.25) with respect to γ to zero yields

$$\frac{\partial e^T}{\partial \gamma} e + e^T \frac{\partial e}{\partial \gamma} = 0 \quad (3.26)$$

or

$$2 \frac{\partial e^T}{\partial \gamma} e = 0 \quad (3.27)$$

Using Eq. (3.24) and eq. (3.27) solving for γ yields

$$\{\gamma\} = [[C]^T [C]]^{-1} [C]^T \{Z\} \quad (3.28)$$

Partitioning the matrices of eq. (3.28) yields

$$\{\gamma\} = [C_1^T C_1 + C_2^T C_2]^{-1} \{C_1^T Z_R + C_2^T Z_I\} \quad (3.29)$$

with the matrix inverse equal to

$$[C_1^T C_1 + C_2^T C_2]^{-1} = \begin{bmatrix} \frac{\beta}{\alpha\beta - n^2} & 0 & \frac{n}{\alpha\beta - n^2} \\ 0 & 1/n & 0 \\ \frac{n}{\alpha\beta - n^2} & 0 & \frac{\alpha}{\alpha\beta - n^2} \end{bmatrix} \quad (3.30)$$

where

$$\beta = \sum_{i=1}^n 1/\omega_i^2 \quad (3.31)$$

$$\alpha = \sum_{i=1}^n \omega_i^2 \quad (3.32)$$

$n \equiv$ number of samples

Also

$$C_1^T Z_R = \begin{Bmatrix} 0 \\ d_2 \\ 0 \end{Bmatrix} \quad (3.33)$$

and

$$C_2^T Z_I = \begin{Bmatrix} d_1 \\ 0 \\ d_3 \end{Bmatrix} \quad (3.34)$$

where

$$d_1 = \sum_{i=1}^n \omega_i Z_{Ii} \quad (3.35)$$

$$d_2 = + \sum_{i=1}^n Z_{Ri} \quad (3.36)$$

$$d_3 = - \sum_{i=1}^n Z_{Ii}/\omega_i \quad (3.37)$$

Using these relationships eq. (3.29) is written as

$$\{Y\} = \begin{Bmatrix} a \\ b \\ c \end{Bmatrix} = \begin{bmatrix} \frac{\beta}{\alpha\beta - n^2} & 0 & \frac{n}{\alpha\beta - n^2} \\ 0 & 1/n & 0 \\ \frac{n}{\alpha\beta - n^2} & 0 & \frac{\alpha}{\alpha\beta - n^2} \end{bmatrix} \begin{Bmatrix} d_1 \\ d_2 \\ d_3 \end{Bmatrix} \quad (3.38)$$

Solving for the unknown parameters gives

$$a = \frac{(d_1\beta + d_3h)}{\alpha\beta - n^2} \quad (3.39)$$

$$b = d_2/n \quad (3.40)$$

$$c = \frac{nd_1 + d_3\alpha}{\alpha\beta - n^2} \quad (3.41)$$

Using the relations described in eq. (3.4) the final results are

$$G = 1/b \text{ gain} \quad (3.42)$$

$$\omega_f = \sqrt{c/a} \text{ center frequency}$$

$$Q = \frac{1}{b}\sqrt{ac} \text{ filter bandwidth.}$$

A computer program has been written to compute the feedback system gain, center frequency and Q from experimental admittance data.

The procedure for identifying the feedback filter control coefficients (a_i, b_i and c_i) is as follows. A wideband 1.0 volt rms signal was sent thru a 1×10^6 ohm resistor into the input of each control unit. This produced 1×10^{-6} amp wideband input into the preamplifier. With the gain set at 1×10^6 the output voltage was expected to be 1.0Vrms. The transfer function was taken between the input voltage and the output voltage with the control units set for the different control experiments. The frequency, real and imaginary spectral components were saved and processed by the identification scheme for different selected bandwidths about the filter center frequencies. As a comparison to the identification scheme, the center frequency and damping (Q) for a single degree of freedom model curve fit using the Genrad complex estimation routine 51 was used. The identification results using both methods are listed in table 3.1.

Figures 3.2 to 3.5 are analytical functions using equation (3.7) and the identified values from the least squares method over the actual experimental wideband transfer function data. The fit for the first mode is better than the second mode. The high gain second mode fit was the poorest (figure 3.5).

3.3. Baseline Model Development

Equation (3.28) represents the model of the structure that is controlled by using piezoceramic sensors and actuators and a particular feedback control system. The approximately known feedback control system coefficients (a_i, b_i , and c_i) are first individually identified for a particular experimental setting. All that remains to be identified then

Table 3.1 Identified Filter Coefficients

Least Squares Identification

Mode	Q	G	Freq.(Hz)	a	b	c
(Low Gain)						
1	16.787	.962	58.84	5.722E-02	1.040	6.453E+03
2	15.887	.814	368.09	8.439E-03	1.229	4.514E+04
(High Gain)						
1	14.756	3.664	61.22	1.047E-02	.273	1.549E+03
2	14.800	1.633	379.70	3.800E-03	.612	2.162E+04

Genrad Poly. Fit

(Low Gain)						
1	15.437	.845	59.10	4.809E-02	1.157	6.630E+03
2	15.625	.794	369.72	8.467E-03	1.259	4.569E+04
(High Gain)						
1	14.505	3.566	61.37	1.055E-02	.280	1.569E+03
2	15.461	1.669	382.76	3.852E-03	.599	2.228E+04

Notes: $a = Q/(G \cdot \omega)$, $b = 1.0/G$, $c = \omega^2 \cdot a$

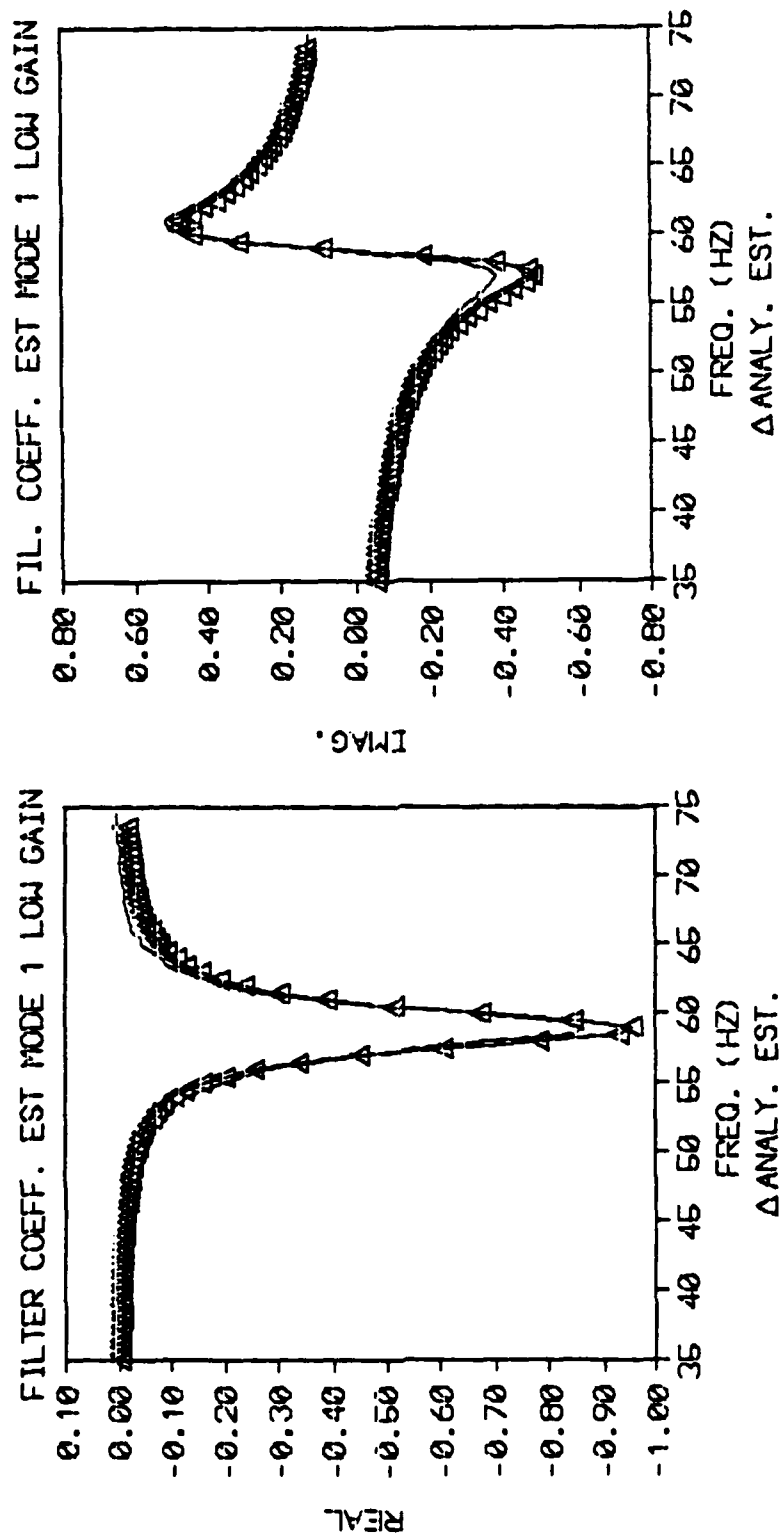


Figure 3-2 Comparison of Feedback Filter Analytical Model And Transfer Function Experimental Data - Mode 1 Low Gain

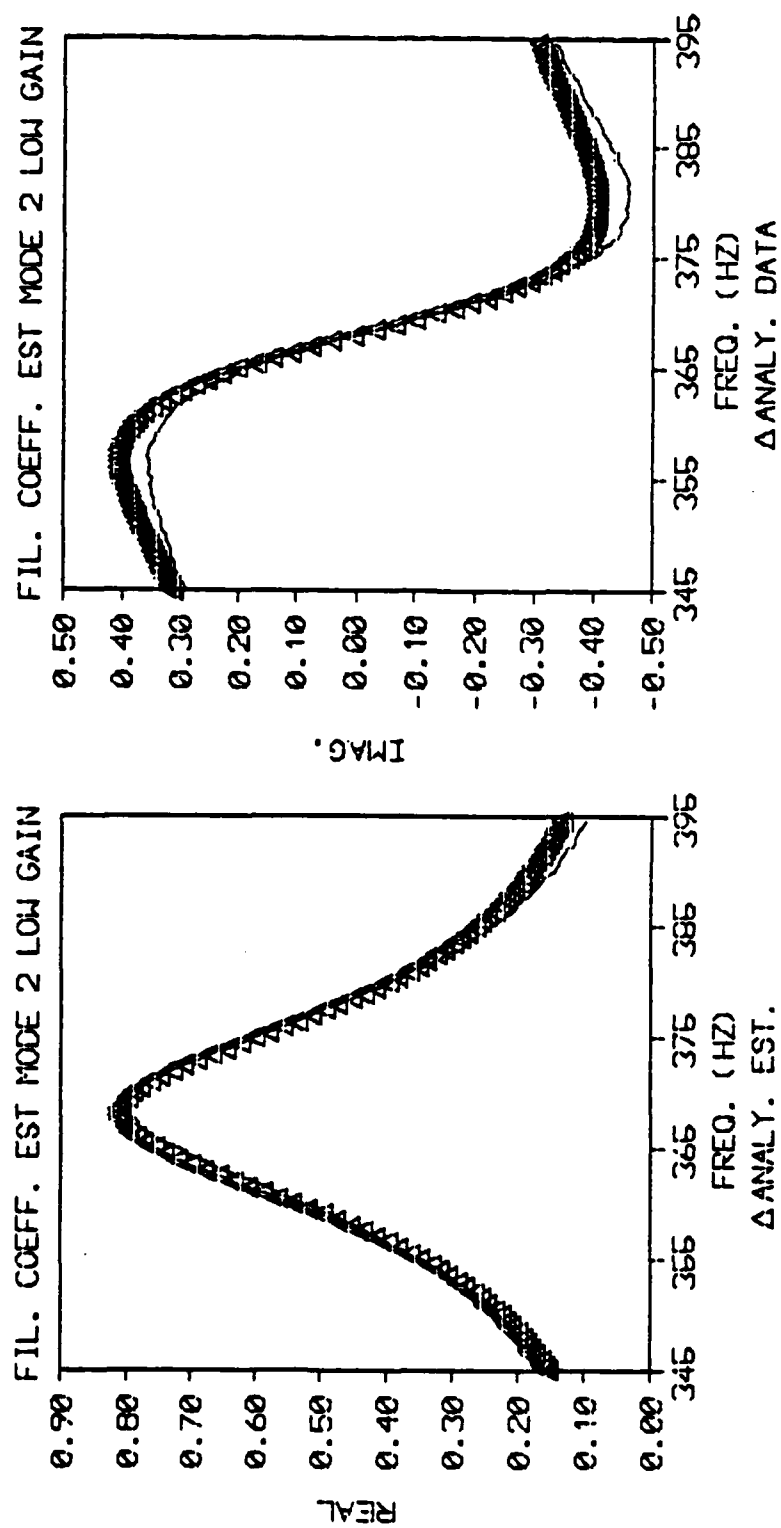


Figure 3-3 Comparison of Feedback Filter Analytical Model and Experimental Transfer Function Experimental Data Mode 2 - Low Gain

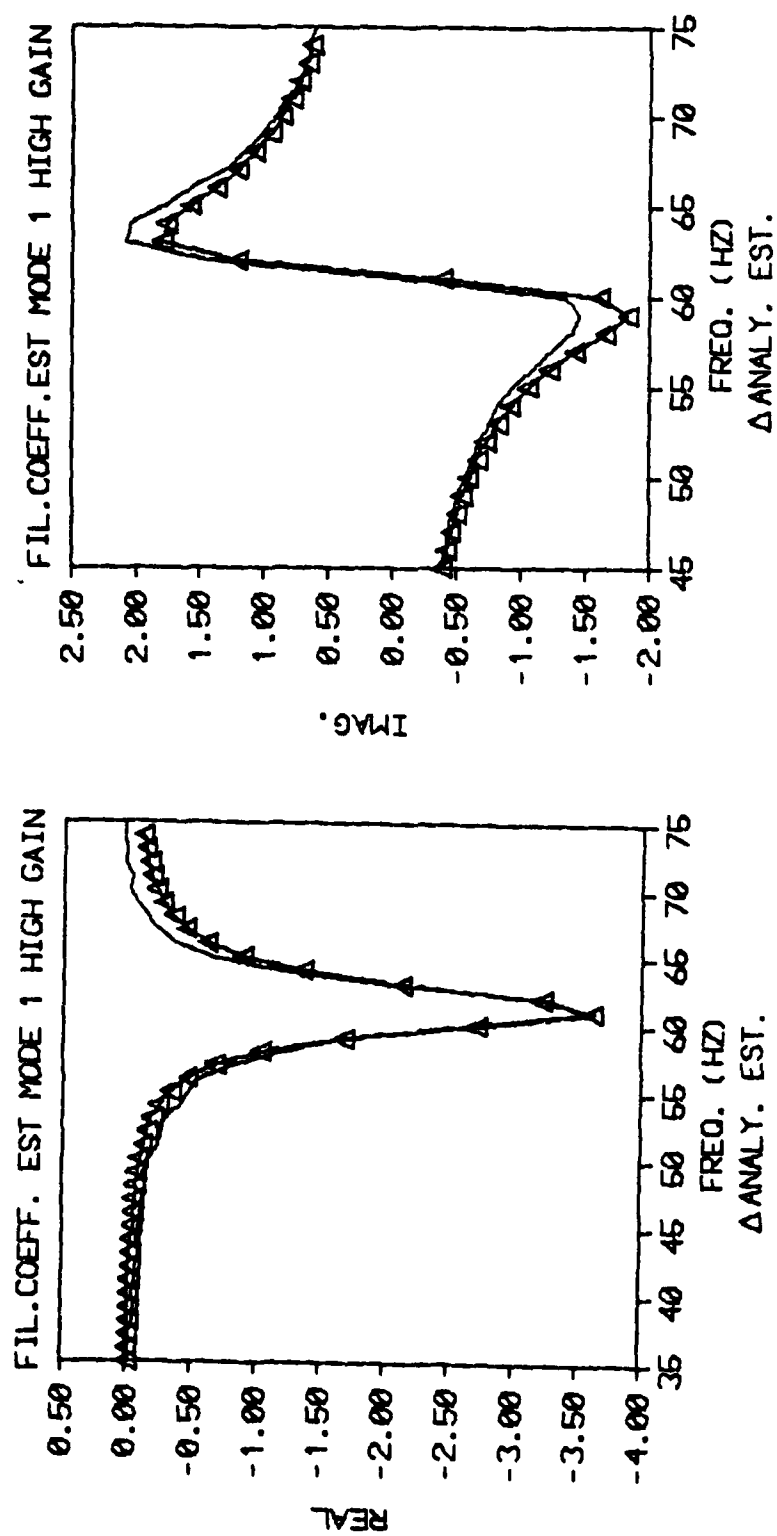


Figure 3-4. Comparison of Feedback Filter Analytical Model
And Experimental Transfer Function Data
Mode 1 - High Gain

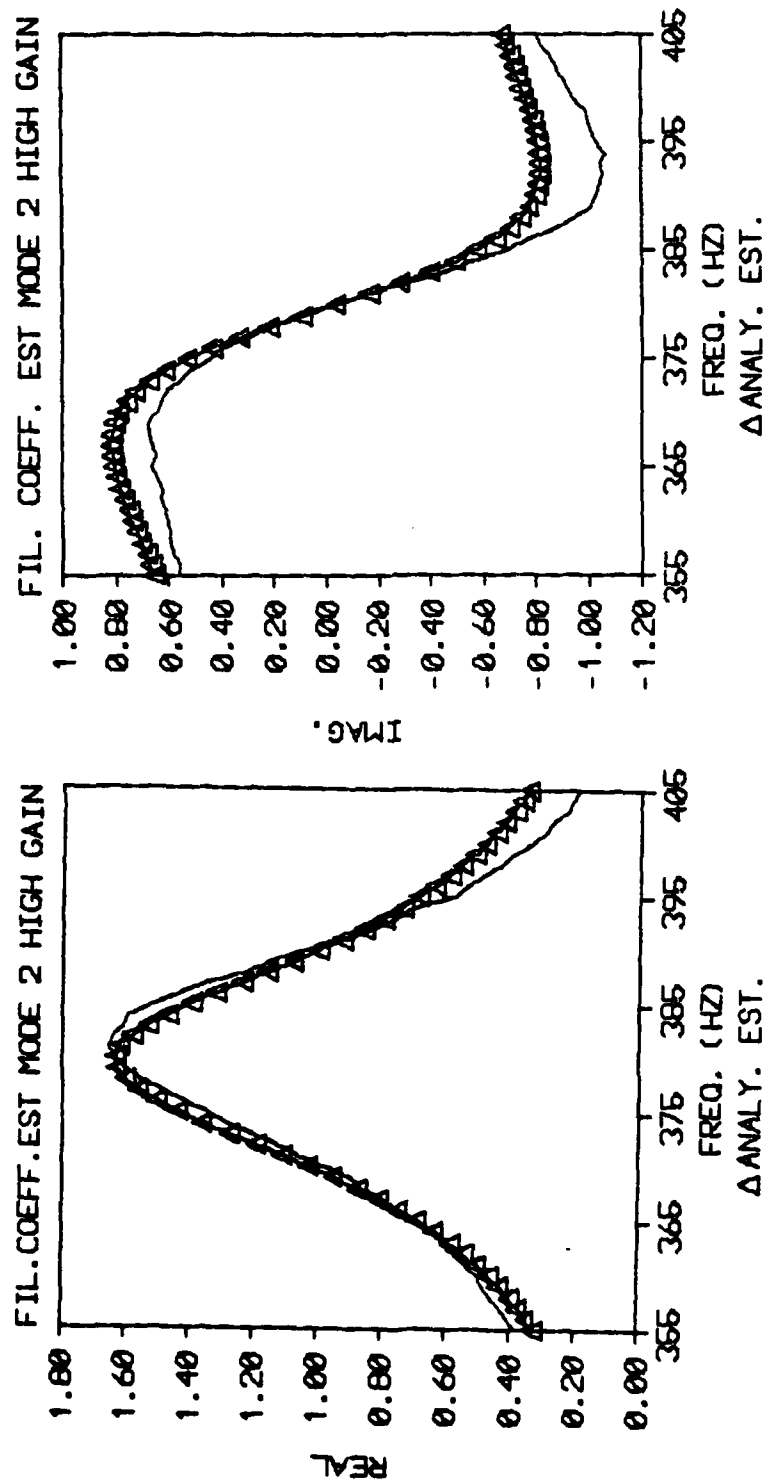


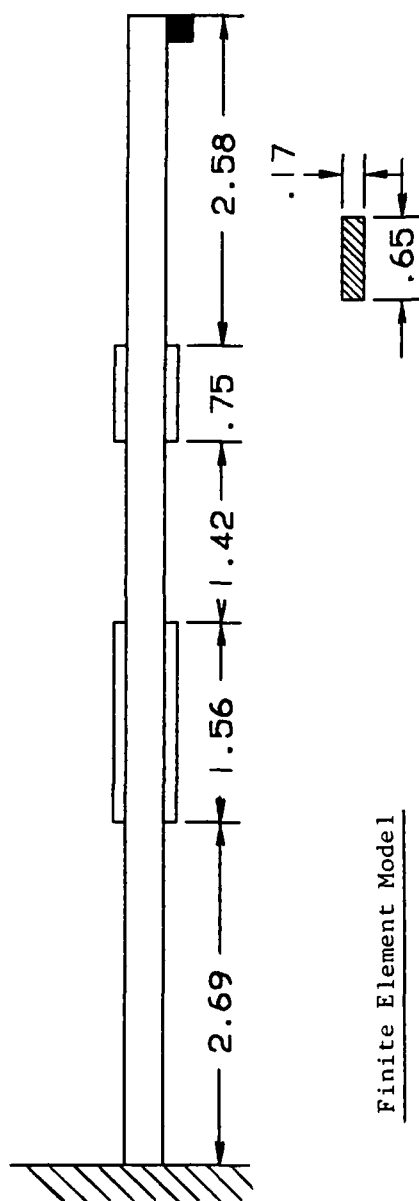
Figure 3-5 Comparison of Feedback Filter Analysis
 Model and Experimental Transfer Function Data
 Mode 2 - High Gain

is the dynamic coupling coefficients defined in eqs. (3.1) and (3.3) and the mass stiffness and damping matrices of the baseline non controlled system.

To obtain the mass, stiffness and damping matrices of the baseline system an identification scheme appropriate for structural systems with non proportional damping⁴⁵ was used. A brief outline of the procedure used is presented in Appendix C.

The baseline matrix identification system requires a full set of eigenvalues and eigenvector data as well as some a priori mass, stiffness or damping data. From this information the identification scheme is used to identify the remaining unknown matrix coefficients. Two discrete models were selected for the cantilever beam shown in figure 3.6. Model #1 consisted of five translation and five rotational degrees of freedom and model #2 consisted of five translational degrees of freedom. The two models were identical except for reduction of the rotational degrees of freedom in model #2. Model #1 represents the coupling of the transducer in the structure more accurately because of the retention of the rotational degrees of freedom but has the limitation of the difficulty of obtaining rotational eigenvector data experimentally. Model #2 uses Guyan condensation⁶⁶ to eliminate the rotational degrees of freedom and therefore is expected to increase the overall identification error. However the requirement of using only translational eigenvector data which are more accurately and easily measured justifies the investigation of using such a model. The mass

Experiment Beam



Finite Element Model

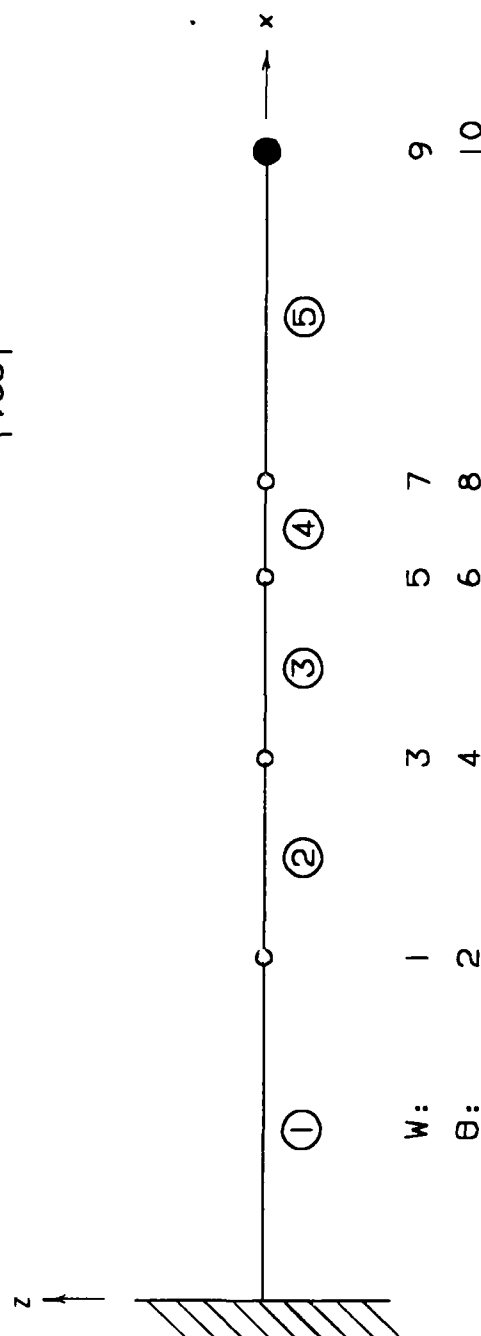


Figure 3-6 Experimental Test Beam and Finite Element Model

stiffness and damping matrices for model #1 are identified using the following information:

- a) selected mass elements from a STRUDL⁶⁷ finite element model
- b) experimental eigenvalues and damping for modes 1 to 5 (Appendix D)
- c) experimental translational eigenvector data for modes 1 and 2
- d) the analytical eigenvalue data for modes 6 to 10 with an estimated .005 damping value for these modes
- e) analytical translational eigenvector data for modes 3 to 10
- f) analytical rotational eigenvector data for all the modes.

For model #2 the following has been used:

- a) selected mass elements from the finite element model
- b) experimental eigenvalue and damping for mode 1 to 5 (Appendix D)
- c) experimental translational eigenvector data for mode 1 and 2 (Appendix D)
- d) analytical translational eigenvector data for mode 3 to 5

The identified mass, damping and stiffness matrices are listed in tables 3.2 and 3.3.

To verify the accuracy of the identification of the baseline matrices a computer program has been developed to compute the transfer function matrix of either the 5 or 10 of models. The analytically generated transfer function matrix results were compared to baseline non controlled experimental results. The identification scheme⁴⁵ can

Table 3.2 Identified Baseline Stiffness, Damping, and Mass Matrices
For Model #1.

(LOWER TRIANGLE)

STIFFNESS MATRIX

.1043E+05							
-.5710E+04	.1098E+05						
-.8738E+04	.8345E+04	.1898E+05					
-.6958E+04	.4027E+04	-.2148E+03	.1398E+05				
-.2321E+04	-.1831E+04	-.1488E+05	.7700E+04	.6888E+05			
.2257E+04	-.1040E+04	-.6262E+04	.1463E+04	-.1427E+05	.1815E+05		
.3391E+04	.1908E+03	.4220E+04	-.1169E+04	-.6031E+05	.2219E+05		
.6422E+05							
-.2810E+03	.6290E+03	.2871E+04	.1318E+04	-.2253E+05	.3808E+04		
.2013E+05	.1652E+05						
-.5077E+03	.2286E+03	-.7976E+03	.8871E+03	.4635E+04	-.1253E+04		
-.6046E+04	.1193E+04	.2223E+04					
-.2772E+03	.4862E+03	-.5310E+03	.5983E+03	.2199E+04	-.5963E+03		
-.4338E+04	.2142E+04	.2674E+04	.4277E+04				

DAMPING MATRIX.

.2787E-02							
-.3751E-03	.1822E-02						
-.1301E-02	.1216E-02	.3377E-02					
-.4191E-03	.7339E-04	-.6964E-05	.1238E-02				
-.2700E-04	-.5177E-03	-.2136E-02	.5314E-03	.5440E-02			
.1951E-03	-.9349E-04	-.3872E-03	-.2444E-03	-.8060E-04	.8791E-03		
-.8227E-05	.4497E-06	.5284E-03	-.1334E-03	-.3792E-02	.4142E-03		
.4836E-02							
-.7331E-04	-.4845E-04	.1929E-03	.2390E-03	-.7764E-03	-.2174E-03		
.4771E-03	.1208E-02						
.5578E-04	.5208E-04	-.1709E-04	.5662E-04	.5084E-03	-.3209E-04		
-.1041E-02	.1281E-03	.7587E-03					
-.1492E-04	.1352E-03	-.1479E-03	-.1527E-04	.5153E-03	.1254E-05		
-.8123E-03	.1886E-04	.4809E-03	.7362E-03				

MASS MATRIX

.4497E-04							
.7122E-05	.6332E-05						
.4962E-05	-.2143E-05	.3163E-04					
.2045E-05	-.6569E-06	.6267E-06	.1840E-05				
.5562E-06	-.2560E-06	.5783E-05	-.1772E-05	.2311E-04			
.1737E-07	-.1180E-06	.1750E-05	-.6884E-06	.2230E-05	.9130E-06		
.3080E-05	.5255E-06	.1336E-05	.3735E-07	.4409E-05	-.4061E-06		
.3839E-04							
-.8535E-06	-.8135E-07	-.8801E-07	.1357E-06	.7087E-07	-.1992E-06		
-.1018E-04	.5064E-05						
-.1114E-05	-.1047E-06	-.1127E-06	-.1637E-06	.1754E-05	.9116E-07		
.1195E-04	-.6727E-05	.4287E-04					
.2521E-06	.8915E-07	-.4543E-08	.2174E-07	.6386E-06	-.2405E-08		
.6743E-05	-.3733E-05	.1110E-04	.5017E-05				

TABLE 3.3 Identified Baseline Stiffness, Damping and Mass
Matrices for Model #2

STIFFNESS MATRIX

.6051E+04					
-.5227E+04	.7623E+04				
-.4608E+03	-.5286E+04	.1468E+05			
.3063E+04	.8083E+03	-.1157E+05	.1167E+05		
-.5584E+03	.1088E+02	.1858E+04	-.2124E+04	.4465E+03	

DAMPING MATRIX

.2715E-02					
-.1433E-02	.2241E-02				
-.5987E-03	-.7677E-03	.3768E-02			
.9774E-03	-.4103E-03	-.3073E-02	.4042E-02		
-.1325E-03	.7586E-04	.3727E-03	-.6770E-03	.3467E-03	

MASS MATRIX

.5127E-04					
-.1418E-04	.3923E-04				
-.1045E-04	.2311E-05	.5055E-04			
.2018E-04	-.5171E-05	-.4475E-04	.9477E-04		
-.3630E-05	.3583E-05	-.2714E-05	.1040E-04	.2214E-04	

only identify the mass, damping and stiffness matrices to within a scalar. Therefore the analytical and experimental transfer functions differed slightly. The identified matrices were scaled to match the experiment data at one frequency location (380 Hz). Comparison of the real and imaginary parts of the transfer function data of the experimental and baseline models for modes 1 and 2 is presented in figures 3.7 to 3.10. In table 3.4 the scaling values have been listed.

Both models adequately identified the first two modes of the structure. The greatest variance between the models and the experimental baseline results occurred in the real part of the first mode.

3.4. Identification of Dynamic Coupling Coefficients

The coupling coefficients and the sensor/actuator parameters are contained in \bar{K}_{D_i} as defined by eq. (3.8). This constant when expanded yields

$$\bar{K}_{D_i} = \xi_s \xi_d (w_s^h d_{31} c_{11}^E R_F e_{31} w_d^h) \quad (3.43)$$

with units defined as

$$[C \text{ OHM}][NM/V] = NM \text{ sec or in lb. sec.}$$

Let $\xi = \xi_s \xi_d$ represent the dynamic coupling of a particular pair of collocated sensor/actuator to the elastic beam.

It is assumed that the following transfer function matrices are available,

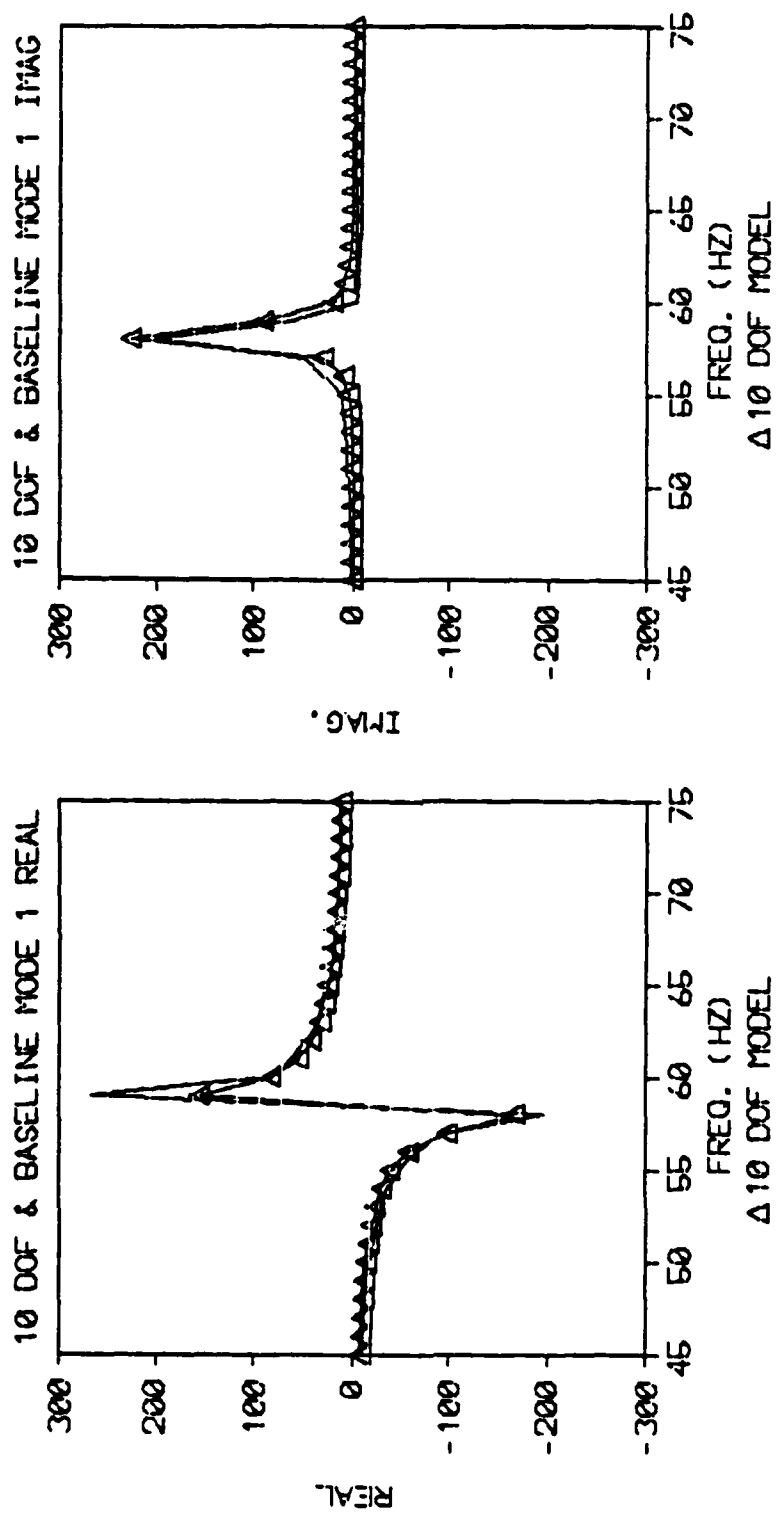


Figure 3-7 Comparison of the Baseline Model #1 (10 D.O.F.) and Transfer Function
Experimental Data - Mode 1 No Control

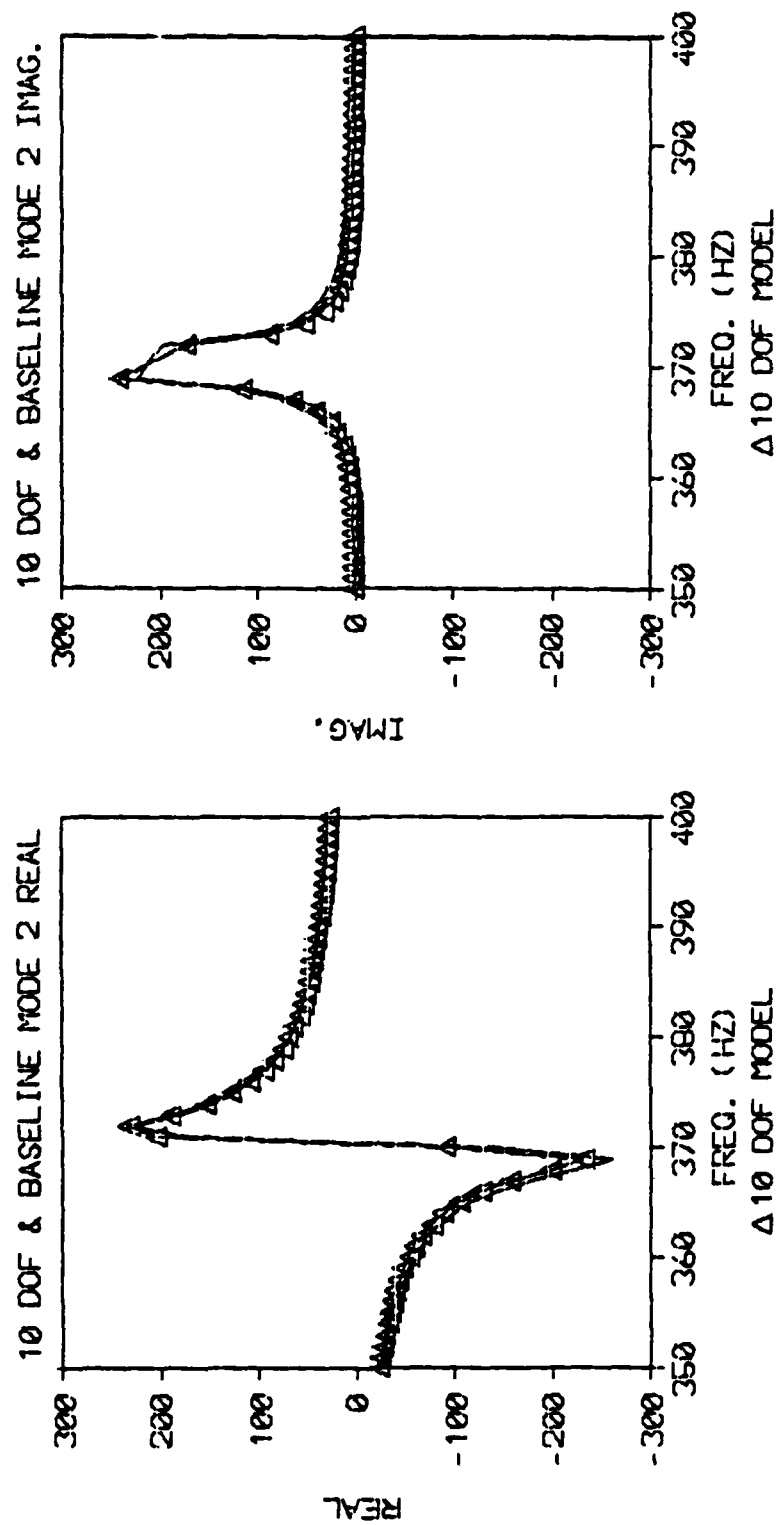


Figure 3-8 Comparison of The Baseline Model #1 (10 D.O.F.) And Transfer Function Experimental Data - Mode 2 - No Control

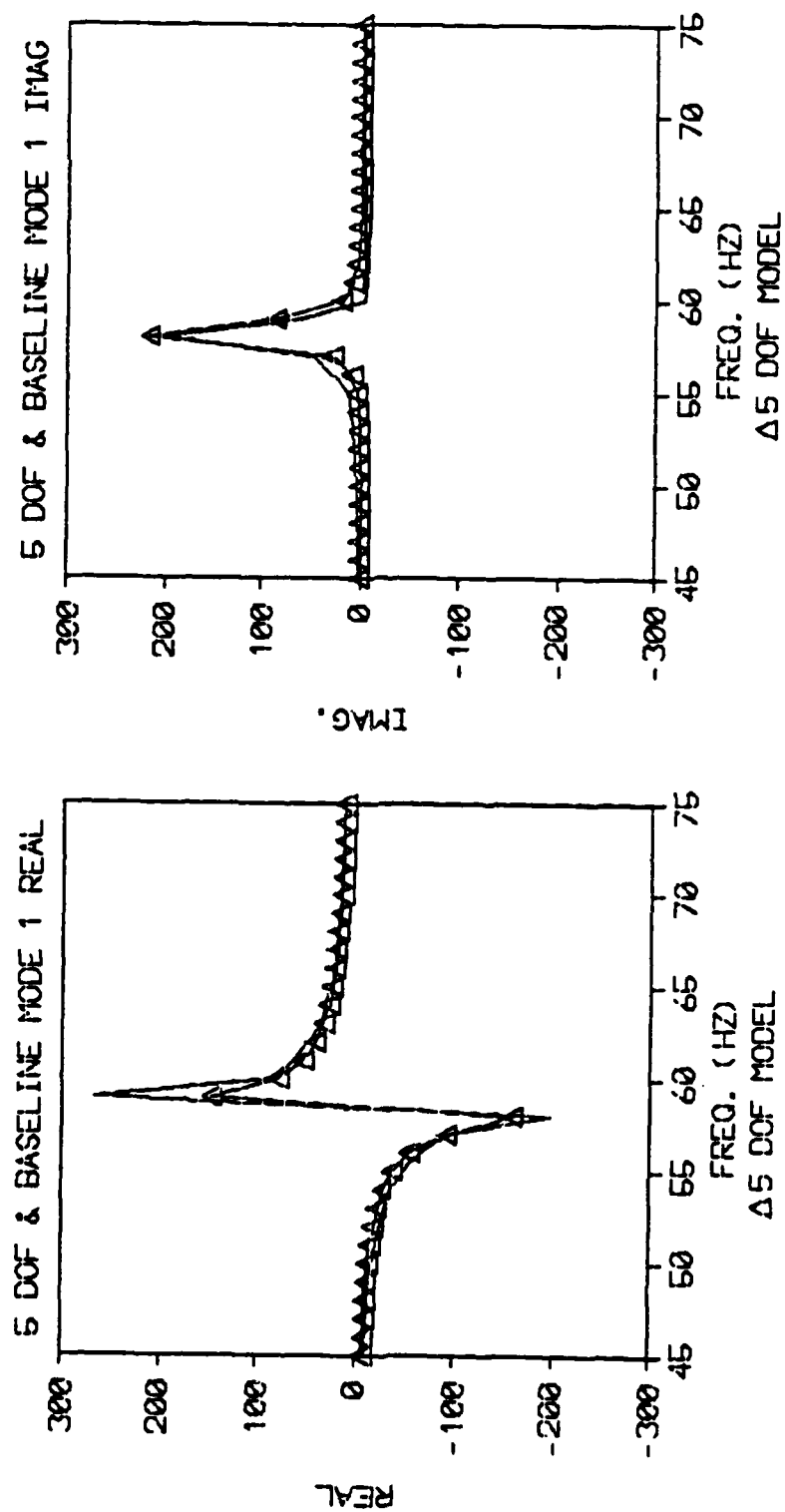


Figure 3-9 Comparison of The Baseline Model #2 (5 D.O.F.) And Transfer Function Experimental Data - Mode 1 - No Control

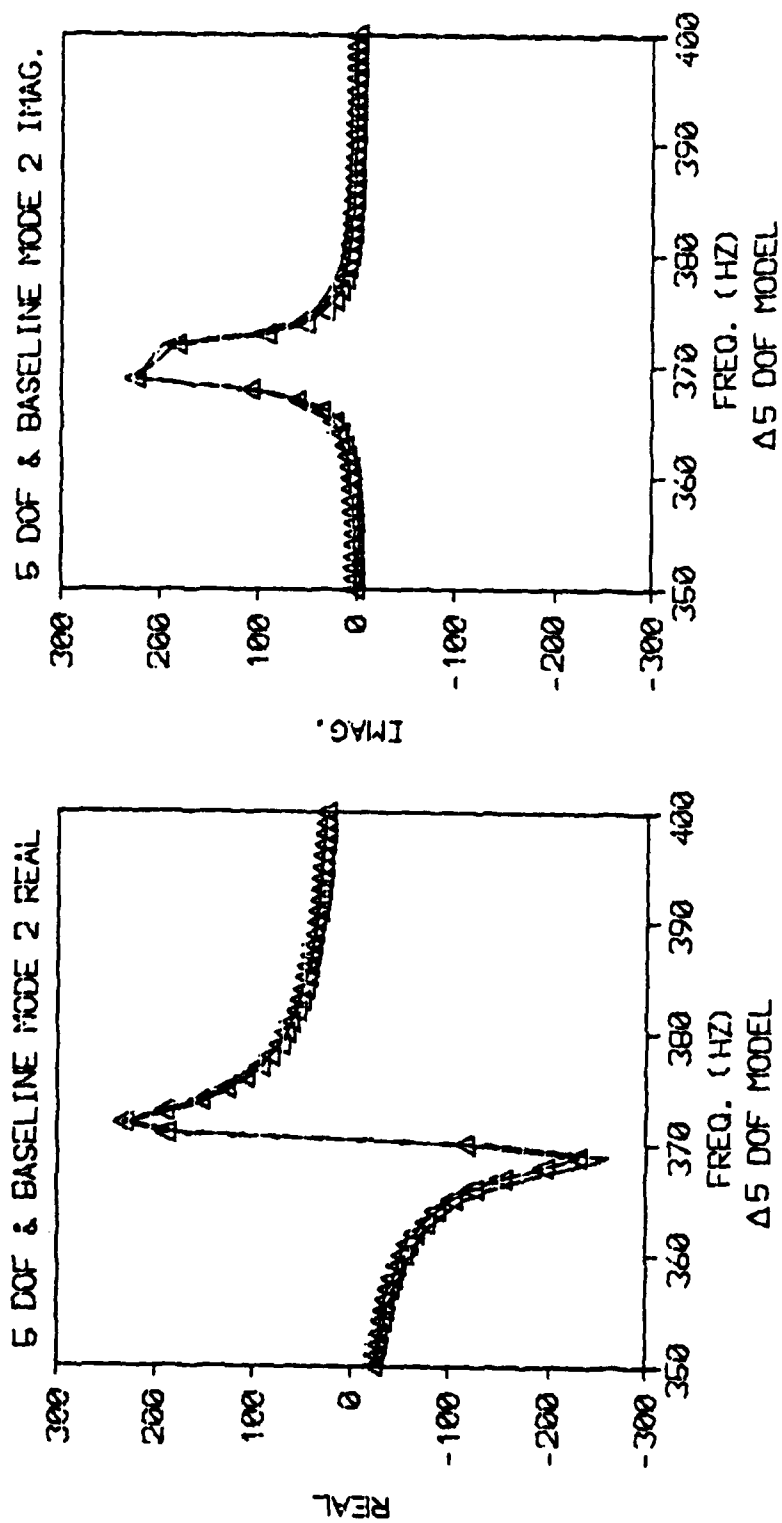


Figure 3-10 Comparison of the Baseline Model #2 (5 D.O.F.) And Transfer Function Experimental Data - Mode 2 - No Control

Table 3.4. Scaling Values to Match Baseline Experimental Results

MODEL #	VALUE
1	1.5307
2	.975

Note: Experimental and Analytical Results matched at 380 Hz.
in magnitude.

$[H_{ex}(\omega)]$ experimental data

$[H_3(\omega)]$ analytical prediction.

An objective function is defined as the difference between the experimental and identified analytical prediction and is written as follows:

$$J = \int_{\omega_1}^{\omega_2} \sum_{k=1}^n |H_{ex_1}^k(\omega) - H_{3_1}^k(\omega)|^2 d\omega + \int_{\omega_2}^{\omega_3} \sum_{k=1}^n |H_{ex_2}^k(\omega) - H_{3_2}^k(\omega)|^2 d\omega + \dots \quad (3.44)$$

where for selected frequency bands the error is defined as

$$|e_k| = |H_{ex}^k(\omega)_{ij} - H_3^k(\omega)_{ij}|$$

is squared and summed over all the transfer functions available. Minimization of the objective function is then done with respect to the unknown parameters and the parameters identified using a modified Marquardt approach⁷⁶.

For a structure with a single collocated sensor/driver pair eq. (3.44) reduces to

$$J = \int_{\omega_1}^{\omega_2} \sum_{k=1}^n |H_{ex}^k(\omega) - H_3^k(\omega)|^2 d\omega \quad (3.45)$$

Using eq. (3.42), eq. (3.43) can be rewritten as

$$J \approx \sum_{i=1}^{NPTS} W_i^{12} \sum_{k=1}^{N \text{ FUNCTIONS}} [e_k^* e_k] \quad (3.46)$$

where W_i^{12} is the appropriate weighting matrix factors for the integration and NPTS are the number of points used for the integration, and * denotes the complex conjugate.

To identify the unknown parameters (dynamic coupling coefficients) the objective functions defined in eqs.(3.42)and(3.45)are minimized with respect to these parameters.

Briefly, suppose that $\bar{\alpha}$ is a vector which makes the objective function $J(\bar{\alpha})$ a minimum. Let $\bar{\alpha}^i$ be the estimate of $\bar{\alpha}$ after the i th iteration. As shown in reference 78 ideally the $i+1$ iteration should be

$$\bar{\alpha}^{i+1} = \bar{\alpha}^i - \rho[R_i] q_i \quad (3.47)$$

where ρ is the step size, R_i is a positive definite matrix and q_i is the gradient vector of the objective function. When Matrix R_i is positive definite the direction of the next iteration is acceptable⁷⁸ (i.e., improves the minimization). When R_i is the identity matrix the method is referred to as the steepest descent. To improve the iteration method an approximation of the objective function at the minimum can be used. An approximation of the objective functions behavior at a minimum is achieved by a second order Taylor series expansion of the objective function about the i^{th} iteration value. Equating the derivative of the second order expansion with respect of the unknown parameters to zero yields

$$\bar{\alpha}^{i+1} = \bar{\alpha}^i - H_i^{-1} q_i \quad (3.48)$$

where H_i is the Hessian Matrix.

As mentioned in reference 76 various methods have been developed to solve the iterative scheme defined by equation (3.48). The particular method used for the identification of the dynamic coupling coefficient was the modified Marquardt method.⁷⁶ Two particular features of this method are that an approximate Hessian matrix is used and iterative step size is modified prior to each iteration. The method required close estimates of the dynamic coupling coefficients for successful convergence. This was not a problem since the range of the dynamic coupling coefficient was between zero (unbonded) to one (perfectly bonded).

The first and second order derivative necessary for the method were computed as follows. Taking the derivative of eq. (3.46) yields

$$\frac{\partial J}{\partial \xi} \approx -2 \sum_{i=1}^{NPTS} w_i^{12} \sum_{k=1}^N \operatorname{Re} \left(e_k^* \frac{\partial H_3^k}{\partial \xi} \right) \quad (3.49)$$

where from Eq. (3.17)

$$[H_3(\omega)] = [[K] - \omega^2[M] + j\omega[c] - [H_2(\omega)]]^{-1} \quad (3.50)$$

where $[H_2(\omega)]$ is the contribution of the signal conditioning system.

From the following identity

$$[A]^{-1} [A] = [I] \quad (3.51)$$

if

$$\frac{\partial}{\partial \xi} [A]^{-1} [A] = [0] \quad (3.52)$$

$$\frac{\partial}{\partial \xi} [A]^{-1} = - [A]^{-1} \left[\frac{\partial}{\partial \xi} [A] \right] [A]^{-1} \quad (3.53)$$

Since the only unknown parameter is ξ from eqs. (3.46) and (3.50)

$$\frac{\partial}{\partial \xi} [H_3] = - [H_3] \left[\frac{\partial}{\partial \xi} H_2 \right] [H_3] \quad (3.54)$$

or

$$\frac{\partial}{\partial \xi} [H_3] = [H_3] \left[\frac{\partial}{\partial \xi} H_2 \right] [H_3] \quad (3.55)$$

From eq. (3.9) and the definition of \bar{K}_{D1} any particular non zero element of H_2 is

$$h_{f_{ij}}(\omega) = \frac{\xi(w_s h d_{31} c_{11}^E R_F)(e_{31} w_d h)(-\omega^2)}{(c_i - a_i \omega^2) + j\omega b_i} \quad (3.56)$$

Therefore

$$\frac{\partial}{\partial \xi} [H_2] = \begin{bmatrix} 1 \\ 1 \end{bmatrix} [H_2(\omega)] \quad (3.57)$$

Eq. (3.55) becomes

$$\frac{\partial}{\partial \xi} [H_3] = [H_3] \left[\frac{1}{\xi} H_2 \right] [H_3] \quad (3.58)$$

By setting

$$[B] = [H_3] \left[\frac{1}{\xi} H_2 \right] [H_3] \quad (3.59)$$

Eq. (3.49) yields

$$\frac{\partial J}{\partial \xi} \approx 2 \sum_{i=1}^{NPTS} w_i^{12} \sum_{k=1}^N \operatorname{Re}(e_i^* B_i^k) \quad (3.60)$$

When more than one collocated sensor/driver pair is used the objective function becomes

$$J = \sum_{i=1}^{NPTS} w_i^{12} \sum_{h=1}^N |e_i|^2 + \sum_{i=1}^{NPTS} w_i^{34} \sum_{k=1}^N |e_i|^2 + \dots \quad (3.61)$$

Then for each unknown coupling parameter

$$\frac{\partial J}{\partial \xi_i} = -2 \sum_{i=1}^{NPTS} w_i^{12} \sum_{k=1}^N \operatorname{Re}(e_i^{k*} \frac{\partial H_3^k}{\partial \xi_i}) - 2 \sum_{i=1}^{NPTS} w_i^{34} \sum_{k=1}^N \operatorname{Re}(e_i^{k*} \frac{\partial H_3^k}{\partial \xi_i}) + \quad (3.62)$$

or using eqs. (3.47) to (3.49)

$$\frac{\partial J}{\partial \xi} = 2 \sum_{i=1}^{NPTS} w_i^{12} \sum_{k=1}^N \operatorname{Re}(e_i^{k*} B_i^k) + 2 \sum_{i=1}^{NPTS} w_i^{34} \sum_{k=1}^N \operatorname{Re}(e_i^{k*} B_i^k) + \quad (3.63)$$

where

$$[B_i] = [H_3] \left[\frac{1}{\xi_i} H_2 \right] [H_3] \quad (3.64)$$

For the Hessian matrix (eq. 3.48) the approximation of the second derivative of the objective function J is.

$$\frac{\partial^2 J}{\partial \xi_m \partial \xi_n} \approx \sum_{i=1}^{NPTS} W_i^{12} \sum_{k=1}^N \frac{\partial}{\partial \xi_n} \left[\frac{\partial e_i^k}{\partial \xi_m} e_i^k + e_i^{k*} \frac{\partial e_i^k}{\partial \xi_n} \right] + \dots \quad (3.65)$$

or

$$\frac{\partial^2 J}{\partial \xi_m \partial \xi_n} \approx 2 \sum_{i=1}^{NPTS} W_i^{12} \sum_{k=1}^N \left(\frac{\partial e_i^{k*}}{\partial \xi_m} \frac{\partial e_i^k}{\partial \xi_n} + \frac{\partial e_i^{k*}}{\partial \xi_n} \frac{\partial e_i^k}{\partial \xi_m} \right) + \dots \quad (3.66)$$

It can be shown that eq. (3.66) reduces to

$$\frac{\partial^2 J}{\partial \xi_m \partial \xi_n} = 2 \sum_{i=1}^{NPTS} W_i^{12} \sum_{k=1}^N \operatorname{Re} \left(\frac{\partial H_3^k}{\partial \xi_m} \right) \left(\frac{\partial H_3^k}{\partial \xi_n} \right) + \operatorname{Im} \left(\frac{\partial H_3^k}{\partial \xi_n} \right) \operatorname{Im} \left(\frac{\partial H_3^k}{\partial \xi_m} \right) \quad (3.67)$$

for example, for two sensor/driver pairs

$$\frac{\partial^2 J}{\partial \xi_m \partial \xi_n} \approx \begin{bmatrix} \frac{\partial^2 J}{\partial \xi_1^2} & \frac{\partial^2 J}{\partial \xi_1 \partial \xi_2} \\ \frac{\partial^2 J}{\partial \xi_1 \partial \xi_2} & \frac{\partial^2 J}{\partial \xi_2^2} \end{bmatrix} \quad (3.68)$$

3.5. Analysis Procedure and Program Verification Results

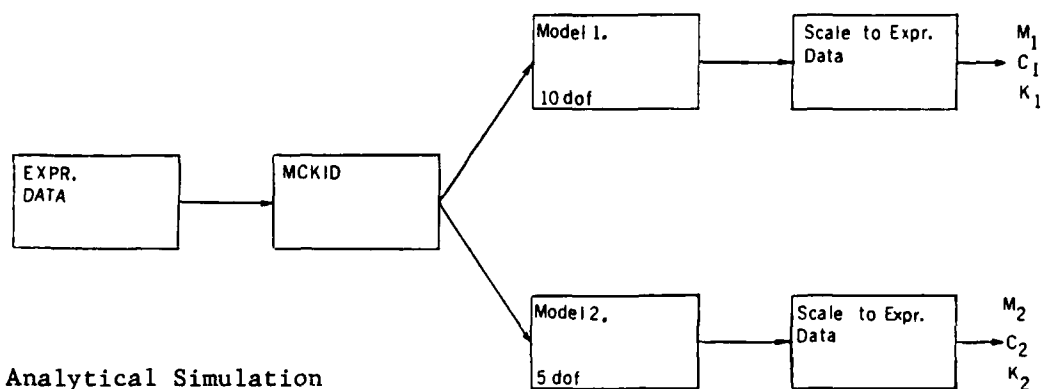
A computer program (EDMFPL.FOR) has been developed combining the analytical model of the system and the multiple sensor/driver

identification scheme. The inputs to the program includes of the particular model's mass, stiffness and damping matrices, frequency bandwidths and transfer function element locations of interest, feedback control filter identified parameters, sensor/actuator locations, weighting matrix for the numerical integration and measured transfer function data corresponding to the locations of interest. For model #2 (5 dof), the FEM condensation matrix has also been provided. In figure 3.11 data flow diagrams for the various programs have been illustrated. Prior to identifying actual dynamic coupling coefficients the routine has been tested by using analytical generated results from a simulation program (EDAT2.FOR).

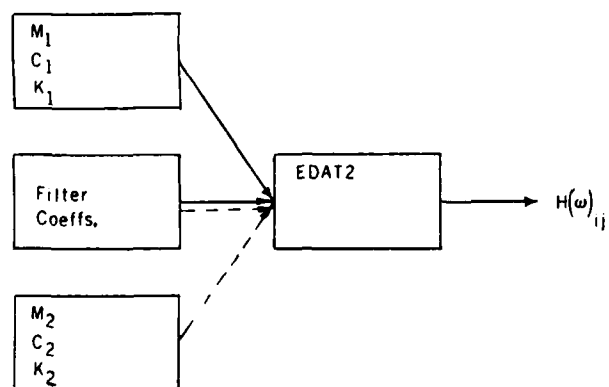
Estimated dynamic coupling and feedback control (a_i , b_i and c_i) filter coefficients for mode 1 and 2 control have been used to generated a set of transfer function data. These tests were conducted using only a single transfer function which was the tip translational element ie, H_{99} (model #1) or H_{55} (model #2). In figures 3.12 the identified results around the first and second mode for the test #1 are presented. The routine usually identified the unknown parameters exactly within 10 iterations.

Two set of experiments have been conducted on a cantilevered test beam as shown in figure 3.6. Actual details of the experiments are discussed in the Appendix D. In both experiments the control of the first and second modes of the beam subjected to impact loading have been discussed. The identified feedback control filter settings for both series of tests was previously presented in table 3.1.

Baseline Matrix Development



Analytical Simulation



Dynamic Coupling Coefficient Development

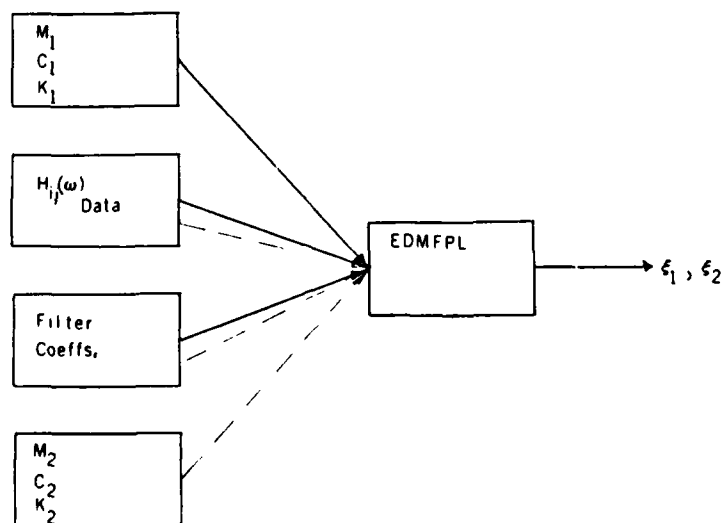
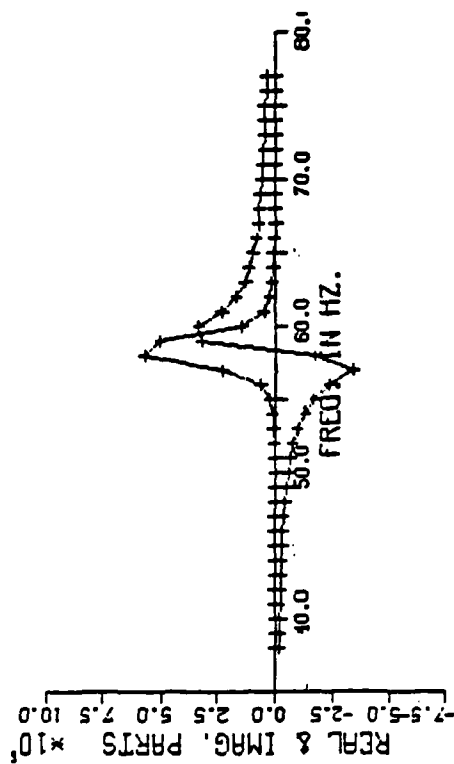
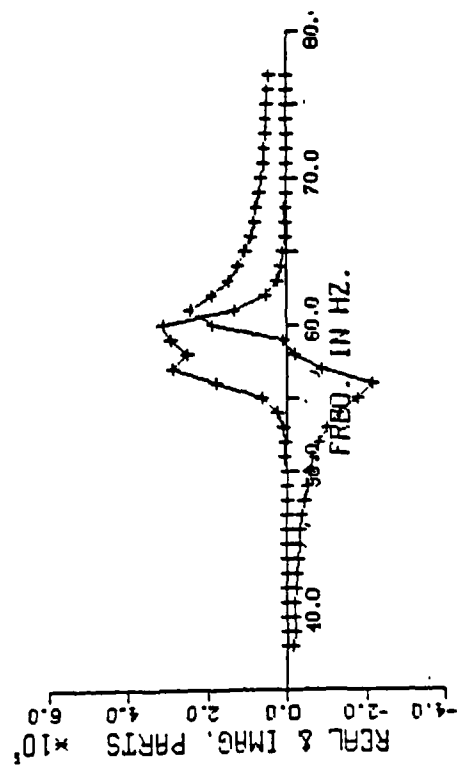


Figure 3-11 Computer Program Flow Diagrams

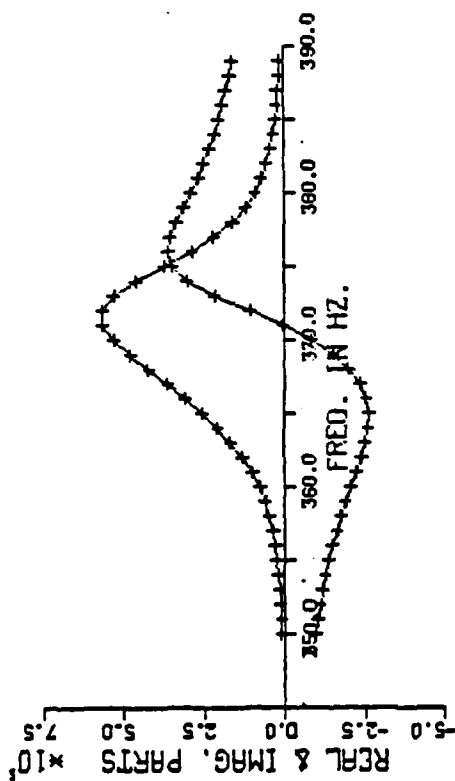
$f = 58.3\text{Hz}$, $Q = 17.0$
 Gain = 1.0
 $\xi_1 = -.20$



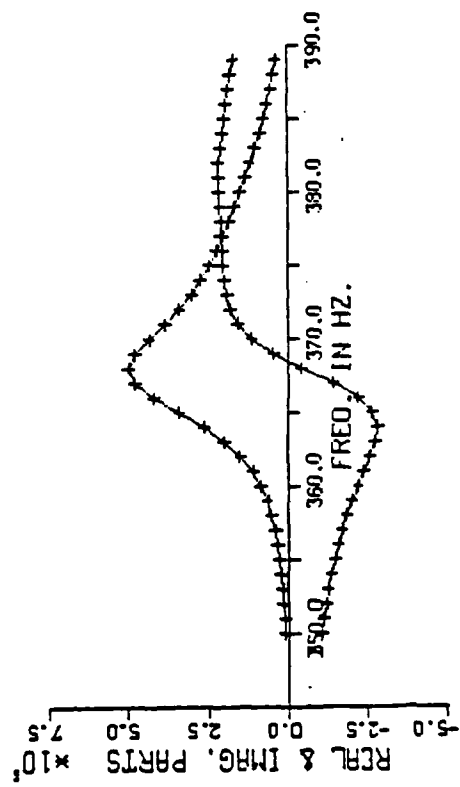
$f = 58.84\text{Hz}$, $Q = 14.756$
 Gain = 3.664
 $\xi_1 = -.20$



$f = 370.0\text{Hz}$, $Q = 16.0$
 Gain = 1.0
 $\xi_2 = -.10$



$f = 368.09\text{Hz}$, $Q = 14.80$
 Gain = 1.633
 $\xi_2 = -.10$



In table 3.5 the identified dynamic coupling coefficients for the different tests are listed and reflex the changes in the coupling of the collocated sensor/actuator pair. For a perfect bonding condition the coupling would have a maximum value of 1.00.

Figures 3.13 to 3.14 represents the quality of the matching of the model with the identified dynamic coupling factor plotted over the actual data for both models.

3.6. Discussion of Identification Results

From the final identified dynamic coupling coefficients presented in table 3.5 various observations were made. The collocated sensor and actuator pair with its filter tuned to the first mode was twice the area in size as the pair used to the control the second mode and the dynamic coupling coefficients reflect this. Also, the dynamic coupling coefficients did not change substantially as a function of feedback gain. The lower order model (5 dof.) results using condensation to remove the rotational degrees of freedom differed in magnitude from the 10 dof. model but approximately followed the same trends.

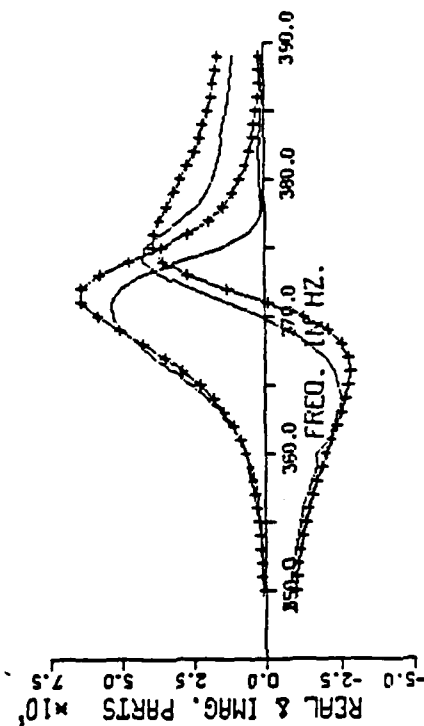
The identification scheme^{75,76} using the objective function and its derivatives as defined in eqs.(3.42),(3.61) and (3.65) was used to identify the dynamic coupling coefficients separately to determine if there was any interaction between the first two widely spaced modes. As expected, the identification results did not change.

Table 3.5 Identified Dynamic Coupling Coefficients

Model #1	ξ_1	ξ_2	J
Low Gain	.1827	.1026	.5604E+12
High Gain	.2205	.1030	.3910E+12
Model #2			
Low Gain	.2348	.0648	.5170E+12
High Gain	.3201	.0712	.4410E+12

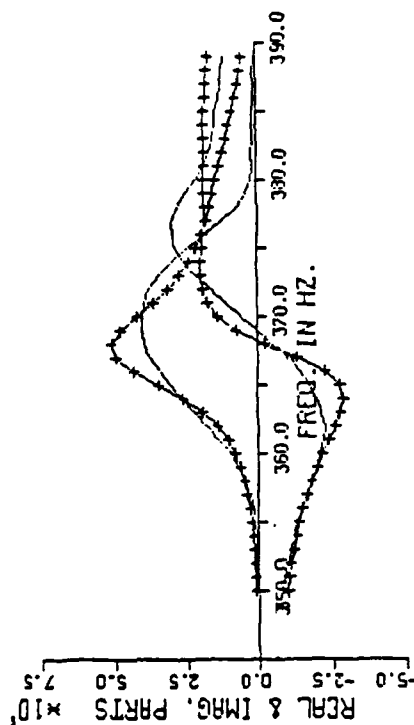
(.814)

Mode 2



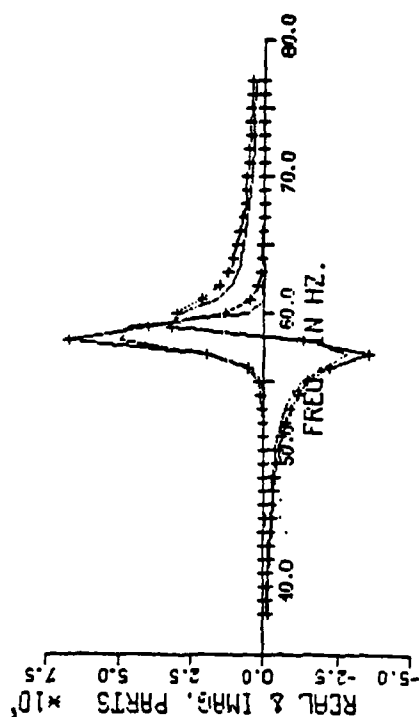
(1.633)

Mode 2



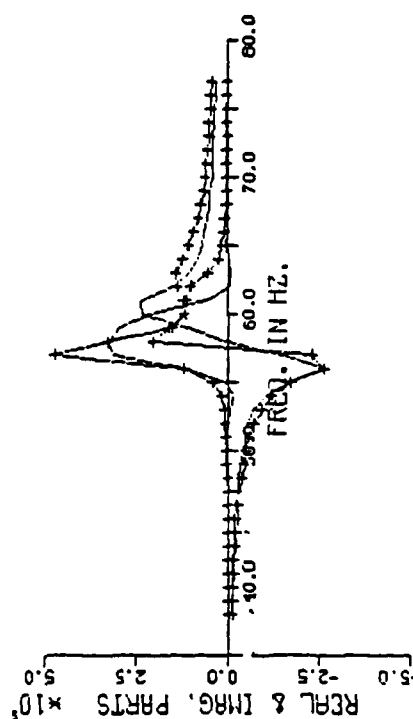
(.962)

Low Gain
Mode 1



(3.664)

High Gain
Mode 1



Gain = ()

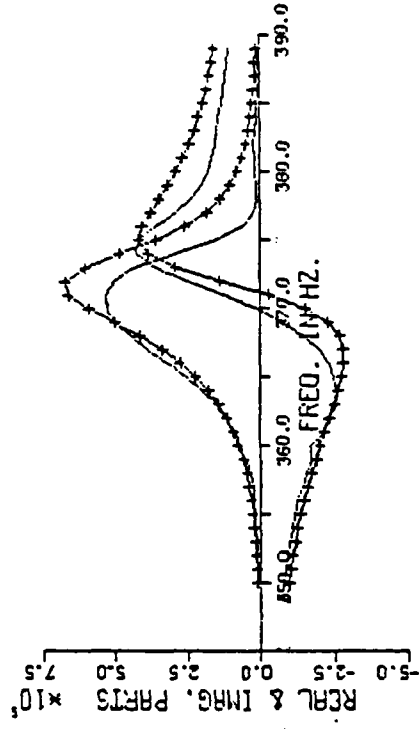
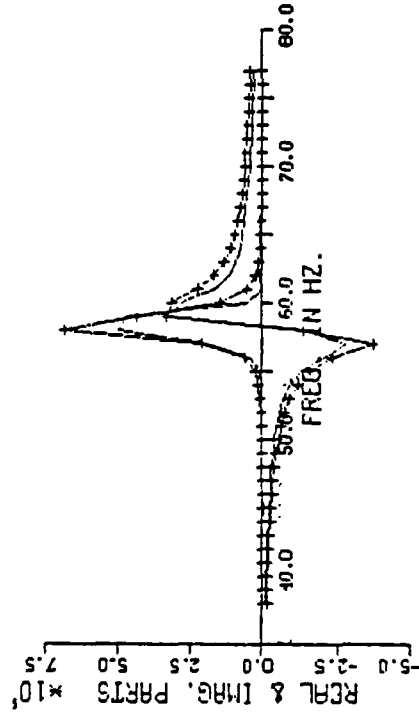
Figure 3-13 Comparison of Analytical Prediction Using Identified Dynamic Coupling Coefficients With Experimental Data - Model #1 (10 D.O.F.)

Low Gain
Mode #1

(.967)

Mode #2

(.814)

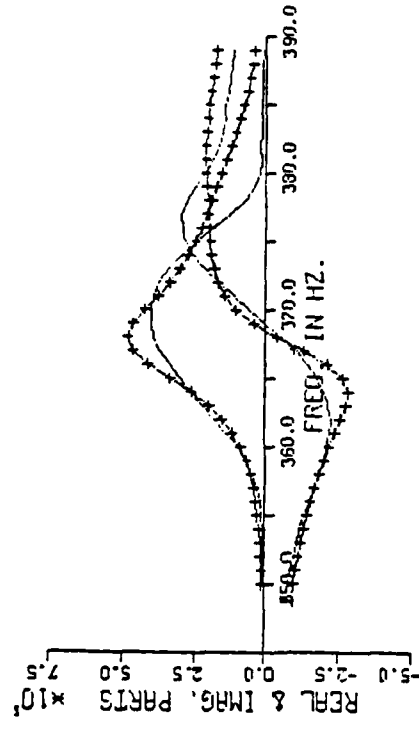
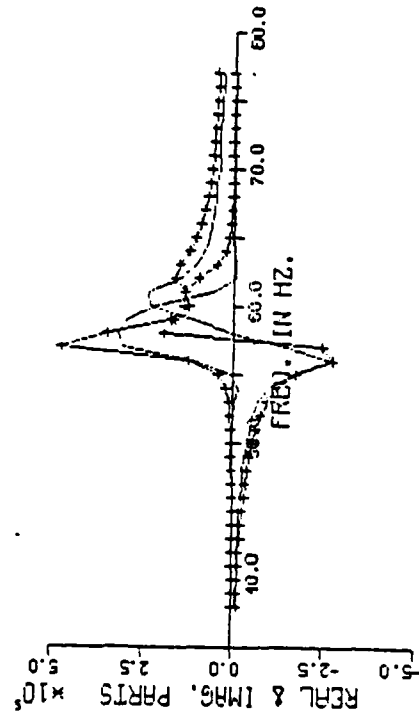


High Gain
Mode #1

(3.664)

Mode #2

(1.633)



Gain=()

Figure 3-14 Comparison of Analytical Prediction Using Identified Dynamic

An improvement was obtained by varying the filter center frequency. The identified results for the high gain tests with the center frequency selected at 59.0 Hz and 375.0 Hz is shown in figure 3.15. The results were sensitive to errors in the center frequency which therefore should be a key parameter to be varied in the identification. The predicted dynamic coupling coefficients were changed by 16 to 20%.

To obtain an additional measure of the accuracy of the identification system, the square root of the error squared divided by the maximum magnitude within a selected frequency band was computed. The error is defined as the difference between the experimental and analytical predicted transfer function given the identified dynamic coupling coefficient (eq. 3.42). The results of these computations are presented in table 3.6. The first mode low gain results were the best and the second mode results were the poorest.

The limitations of the identification procedure were primarily due to:

- a) Identification of the single dynamic coupling coefficient per mode.
- b) Damping estimates and mode shape rotational coefficients of the baseline model.
- c) Single degree of freedom model of the feedback filter electronics.

f: 59.0HZ
 Q: 14.756
 G: 3.664
 ξ_1 : -.18904

f: 375.0 HZ
 Q: 14.800
 G: 1.633
 ξ_2 : -.12534

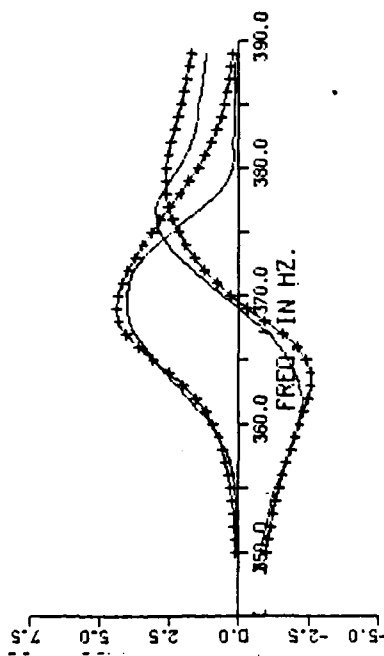
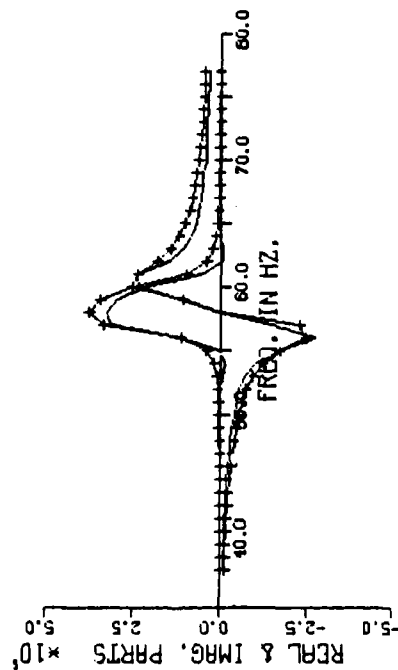


Figure 3-15 Comparison of Analytical Prediction Using Identified Dynamic Coupling Coefficients And Adjusted Center Frequency With Experimental Data - Model #1 (10 D.O.F.)

Table 3.6 Error Computation Results Between Measured and Analytical Prediction Using Identified Dynamic Coupling Coefficients

	Mode 1 (50-60 Hz)	Mode 2 (360-379 Hz.)
Low Gain	.470	1.14
High Gain	.987	1.10

Note: Value reflects error summed over the bandwidth divided by the maximum magnitude within the frequency band.

CHAPTER IV

MODAL AND PARAMETER IDENTIFICATION OF STRUCTURES WITH NON COLLOCATED SENSORS AND ACTUATORS

In Chapter III, a parameter identification scheme has been developed for an active structure with collocated sensors and actuators. In this chapter, the case of non collocated sensors and actuators has been considered. Two active structures shown in figure 4.1 is considered. Case A is an idealized structure with the sensor/actuator pairs non collocated and case B is the corresponding system with collocated sensors and actuators. It is assumed that the translational degrees of freedom have been removed by using an appropriate condensation technique. Furthermore, it is assumed that only external moments are applied. For the purpose of illustration, coupled differential equations for the structure and the control electronics are written for a system with four degrees of freedom.

Non collocated:

$$\begin{bmatrix} M_{11} & M_{12} & 0 & 0 \\ M_{21} & M_{22} & 0 & 0 \\ K_s & -K_s & a_{11} & 0 \\ 0 & -K_s & 0 & a_{22} \end{bmatrix} \begin{Bmatrix} \ddot{\theta}_1 \\ \ddot{\theta}_2 \\ \ddot{V}_1 \\ \ddot{V}_2 \end{Bmatrix} + \begin{bmatrix} C_{11} & C_{12} & 0 & 0 \\ C_{21} & C_{22} & 0 & 0 \\ 0 & 0 & b_{11} & 0 \\ 0 & 0 & 0 & b_{22} \end{bmatrix} \begin{Bmatrix} \dot{\theta}_1 \\ \dot{\theta}_2 \\ \dot{V}_1 \\ \dot{V}_2 \end{Bmatrix}$$

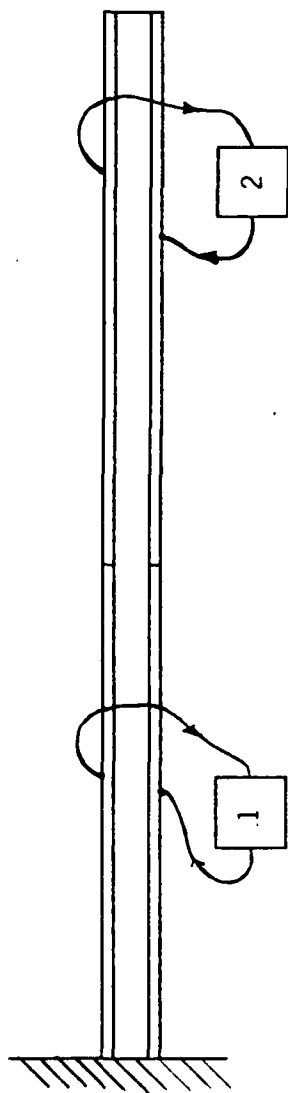
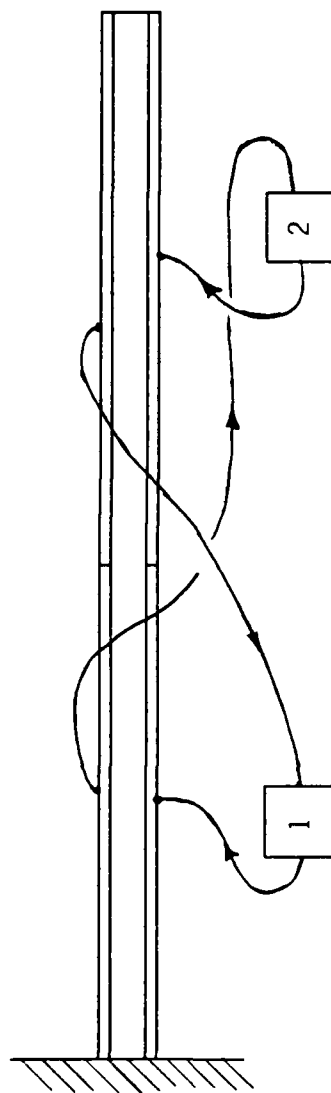
Collocated ControlNon-Collocated Control

Figure 4-1 Collocated And Non-Collocated Control Configurations

$$+ \begin{bmatrix} K_{11} & K_{12} & -K_D & K_D \\ K_{21} & K_{22} & 0 & -K_D \\ 0 & 0 & d_{11} & 0 \\ 0 & 0 & 0 & d_{22} \end{bmatrix} \begin{Bmatrix} \theta_1 \\ \theta_2 \\ \dot{V}_1 \\ \dot{V}_2 \end{Bmatrix} = \begin{Bmatrix} M_1 \\ M_2 \\ 0 \\ 0 \end{Bmatrix} \quad (4.1)$$

Collocated:

$$\begin{bmatrix} M_{11} & M_{12} & 0 & 0 \\ M_{21} & M_{22} & 0 & 0 \\ -K_s & 0 & a_{11} & 0 \\ K_s & -K_s & 0 & a_{22} \end{bmatrix} \begin{Bmatrix} \ddot{\theta}_1 \\ \ddot{\theta}_2 \\ \ddot{V}_1 \\ \ddot{V}_2 \end{Bmatrix} + \begin{bmatrix} C_{11} & C_{12} & 0 & 0 \\ C_{21} & C_{22} & 0 & 0 \\ 0 & 0 & b_{11} & 0 \\ 0 & 0 & 0 & b_{22} \end{bmatrix} \begin{Bmatrix} \dot{\theta}_1 \\ \dot{\theta}_2 \\ \dot{V}_1 \\ \dot{V}_2 \end{Bmatrix} + \begin{bmatrix} K_{11} & K_{12} & -K_D & K_D \\ K_{21} & K_{22} & 0 & -K_D \\ 0 & 0 & d_{11} & 0 \\ 0 & 0 & 0 & d_{22} \end{bmatrix} \begin{Bmatrix} \theta_1 \\ \theta_2 \\ \dot{V}_1 \\ \dot{V}_2 \end{Bmatrix} = \begin{Bmatrix} M_1 \\ M_2 \\ 0 \\ 0 \end{Bmatrix} \quad (4.2)$$

By denoting

$$\alpha_{ij} = -\omega^2 M_{ij} + j\omega C_{ij} + K_{ij} \quad (4.3)$$

$$\beta_{ij} = \omega^2 a_{ij} + j\omega b_{ij} + d_{ij} \quad (4.4)$$

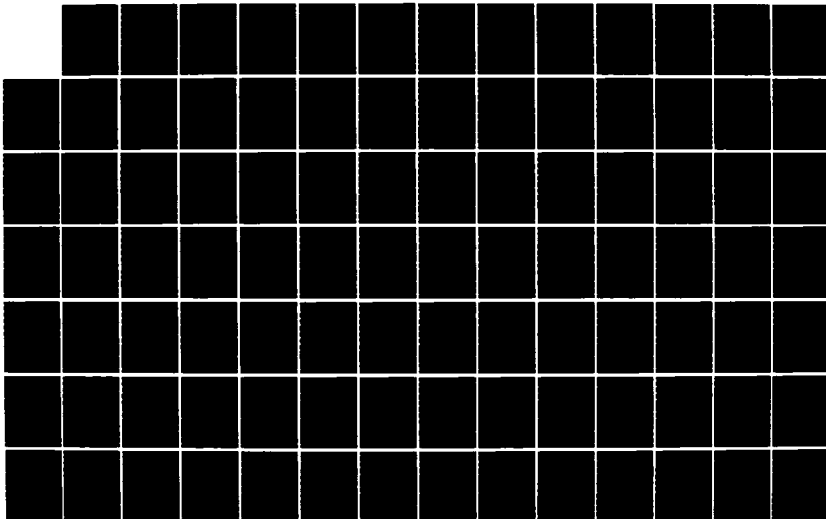
AD-A172 994

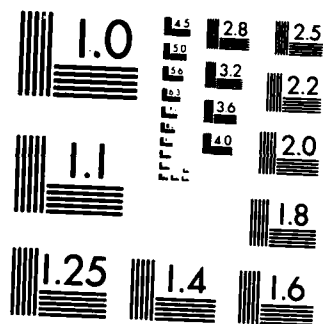
VIBRATION CONTROL OF FLEXIBLE STRUCTURE USING
PIEZOELECTRIC DEVICES AS SENSORS AND ACTUATORS(U) AIR
FORCE INST OF TECH WRIGHT-PATTERSON AFB OH M W OBAL
SEP 86 AFIT/CI/NR-86-176D F/G 9/5

2/3

UNCLASSIFIED

NL





MICROCOPY RESOLUTION TEST CHART
NATIONAL BUREAU OF STANDARDS-1963-A

and fourier transforms of eqs. (4.1) and (4.2) yield

Non collocated:

$$\begin{bmatrix} \alpha_{11} & \alpha_{12} & -K_D & K_D \\ \alpha_{21} & \alpha_{22} & 0 & -K_D \\ \bar{K}_S & -\bar{K}_S & \beta_{11} & 0 \\ 0 & -\bar{K}_S & 0 & \beta_{22} \end{bmatrix} \begin{Bmatrix} \theta_1(\omega) \\ \theta_2(\omega) \\ V_1(\omega) \\ V_2(\omega) \end{Bmatrix} = \begin{Bmatrix} M_1(\omega) \\ M_2(\omega) \\ 0 \\ 0 \end{Bmatrix} \quad (4.5)$$

Collocated

(4.6)

$$\begin{bmatrix} \alpha_{11} & \alpha_{12} & -K_D & K_D \\ \alpha_{21} & \alpha_{22} & 0 & -K_D \\ -\bar{K}_S & 0 & \beta_{11} & 0 \\ \bar{K}_S & -\bar{K}_S & 0 & \beta_{22} \end{bmatrix} \begin{Bmatrix} \theta_1(\omega) \\ \theta_2(\omega) \\ V_1(\omega) \\ V_2(\omega) \end{Bmatrix} = \begin{Bmatrix} M_1(\omega) \\ M_2(\omega) \\ 0 \\ 0 \end{Bmatrix}$$

where

$$\bar{K}_S = -\omega^2 K_S \quad .$$

These matrices were inverted by using the MACSYMA program and the results for the two cases are shown in Tables 4.1 and 4.2. The upper left quadrant of each of the resultant matrices represents the measurable transfer function elements. From Table 4.1 it is observed

Table 4.1 MACSYMA FINAL RESULTS FOR
NON COLLOCATED CONTROL

$$\frac{1}{\text{Det}} \begin{bmatrix} \alpha_{22}\beta_{11}\beta_{12} - \kappa_0\tilde{\kappa}_S\beta_{11} & -\alpha_{21}\beta_{11}\beta_{22} + \kappa_0\tilde{\kappa}_S(\beta_{22} - \beta_{11}) & \kappa_0(\alpha_{22}\beta_{22} - \kappa_0\kappa_S) & -\kappa_0\beta_{11}(\alpha_{22} - \alpha_{12}) + \kappa_0^2\tilde{\kappa}_S \\ -\alpha_{21}\beta_{11}\beta_{22} & \alpha_{11}\beta_{11}\beta_{22} + \kappa_0\tilde{\kappa}_S\beta_{22} & -\alpha_{21}\kappa_0\beta_{22} & \kappa_0\beta_{11}(\alpha_{21} + \alpha_{11}) + \kappa_0^2\tilde{\kappa}_S \\ -\tilde{\kappa}_S\beta_{22}(\alpha_{22} + \alpha_{21}) + \kappa_0\tilde{\kappa}_S^2 & \tilde{\kappa}_S\beta_{22}(\alpha_{21} + \alpha_{22}) + \kappa_0\tilde{\kappa}_S^2 & \alpha_{11}(\alpha_{22}\beta_{22} - \kappa_0\kappa_S) - \alpha_{12}^2\beta_{22}\alpha_{21}\kappa_0\tilde{\kappa}_S & \kappa_0\tilde{\kappa}_S(\alpha_{22} + \alpha_{21}) + \kappa_0\tilde{\kappa}_S(\alpha_{22} + \alpha_{21}) \\ -\alpha_{21}\kappa_0\tilde{\kappa}_S & \alpha_{11}\tilde{\kappa}_S\beta_{11} + \kappa_0\tilde{\kappa}_S^2 & -\tilde{\kappa}_S\kappa_0\alpha_{21} & \alpha_{11}\alpha_{22}\beta_{11} - \alpha_{12}^2\beta_{11} + \kappa_0\tilde{\kappa}_S(\alpha_{22} + \alpha_{21}) \end{bmatrix}$$

$$\begin{bmatrix} \theta_1 \\ \theta_2 \\ v_1 \\ v_2 \end{bmatrix} = \begin{bmatrix} H_{11} & H_{12} & H_{13} & H_{14} \\ H_{21} & H_{22} & H_{23} & H_{24} \\ H_{31} & H_{32} & H_{33} & H_{34} \\ H_{41} & H_{42} & H_{43} & H_{44} \end{bmatrix} \begin{bmatrix} M_1 \\ M_2 \\ 0 \\ 0 \end{bmatrix}$$

$H_{12} \neq H_{21}$

$$\text{Det} = [\alpha_{11}\beta_{11}(\alpha_{22}\beta_{22} - \kappa_0\kappa_S) - \kappa_0\kappa_S(-\alpha_{22}\beta_{22} - \alpha_{21}\beta_{22} + \kappa_S\kappa_0) - \alpha_{21}^2\beta_{11}\beta_{22} - \alpha_{21}\kappa_0\kappa_S\beta_{11}]$$

Table 4.2 MACSYMA FINAL RESULTS FOR
COLLOCATED CONTROL

$$\frac{1}{\text{Det}} \begin{bmatrix} \frac{a_{22}\beta_{11} - k_0 k_S \beta_{11}}{-a_{12}\beta_{11}\beta_{22} - k_0 k_S \beta_{11}} & \frac{-a_{12}\beta_{11}\beta_{22} - k_0 k_S \beta_{11}}{a_{11}\beta_{11}\beta_{12} - k_0 k_S(\beta_{22} + \beta_{11})} & k_0(a_{22}\beta_{22} - k_S k_0) & -k_0 k_S(a_{22} + a_{12}) \\ \frac{-a_{12}\beta_{11}\beta_{22} - k_0 k_S \beta_{11}}{a_{22}k_S \beta_{22} - k_0 k_S^2} & \frac{a_{11}\beta_{11}\beta_{12} - k_0 k_S(\beta_{22} + \beta_{11})}{-a_{21}k_S \beta_{22} - k_0 k_S^2} & -k_0(a_{12}\beta_{22} + k_S k_0) & k_0(a_{21}\beta_{11} + a_{11}\beta_{11} - k_S k_0) \\ -k_S \beta_{11}(a_{22} + a_{21}) & k_S(a_{21}\beta_{11} + a_{11}\beta_{11} - k_S k_0) & a_{11}(a_{22}\beta_{22} - k_0 k_S) - a_{21}(a_{21}\beta_{22} + k_0 k_S) + k_0 k_S - (-a_{22} - a_{21}) & -k_0 k_S(a_{22} + a_{21}) \\ & & & a_{11}a_{22}\beta_{11} - a_{21}\beta_{11} - k_S k_0 a_{22} \end{bmatrix}$$

$$\begin{bmatrix} \theta_1 \\ \theta_2 \\ v_1 \\ v_2 \end{bmatrix} = \begin{bmatrix} H_{11} & H_{12} & H_{13} & H_{14} \\ H_{21} & H_{22} & H_{23} & H_{24} \\ H_{31} & H_{32} & H_{33} & H_{34} \\ H_{41} & H_{42} & H_{43} & H_{44} \end{bmatrix} \begin{bmatrix} M_1 \\ M_2 \\ 0 \\ 0 \end{bmatrix} \quad H_{12} = H_{21}$$

$$\text{Det} = [a_{11}(a_{22}\beta_{11}\beta_{22} - k_0 k_S \beta_{11}) + a_{12}(-a_{12}\beta_{11}\beta_{22} - k_S k_0 \beta_{11}) - k_S k_0(a_{22}\beta_{22} - k_S) - k_0 k_S(a_{22}\beta_{11} + a_{12})]$$

$$\text{NOTE:} \quad \{o\} = \begin{bmatrix} H_{11} & H_{12} \\ H_{21} & H_{22} \end{bmatrix} \begin{bmatrix} M_1 \\ M_2 \end{bmatrix} \quad \{v\} = \begin{bmatrix} H_{31} & H_{32} \\ H_{41} & H_{42} \end{bmatrix} \begin{bmatrix} M_1 \\ M_2 \end{bmatrix}$$

that the the upper left quadrant is no longer symmetric and reciprocity between the off diagonal elements is no longer maintained.

If the system contains a non symmetrical transfer function matrix an equivalent linear model of the system using mass stiffness and damping matrices will have non symmetric matrices⁴⁴. Such a system is non self adjoint and orthogonality of the eigenvectors is not maintained. The eigenvectors of such a system and the eigenvectors of the transpose of the system are orthogonal to each other and form a biorthogonal set. In addition to making the system no longer self adjoint, non collocation of sensors and actuators results in compounding the control stability problems associated with the control of flexible structures^{47,73}. One example of the difficulties in designing an optimal control regulator using a quadratic performance index with non collocated sensors and drivers has been discussed by Cannon⁵². A control law for a flexible robot manipulator arm with a tip position sensor and a root torquer has been developed with the objective of reducing the final position placement of the end of the arm.

Modal identification of a structural dynamic system with non symmetrical matrices from the measurement of time histories of applied forces and accelerations at selected locations requires a method to post process experimental transfer function data and extract the biorthogonal eigenvector parameters.

Such a method has been developed by Potter⁵³. The modal analysis algorithms currently used to extract modal data from appropriate transfer functions impose the assumption of symmetric system matrices⁵¹

Structures are rarely modelled as non self adjoint systems⁴⁶. A popular approach to solving these type of problems is to expand the unsymmetrical matrix into a symmetric and antisymmetric matrix. The use of a non self adjoint analysis has been used by Hablani⁵⁰. This analysis yields uncoupled pairs of first order equations containing adjoint eigenvectors.

The intent of the efforts here are to use the developments by Potter⁵³ and identify the modes of a non symmetric active system with active feedback control from the measurement of the time histories of the applied input and system response output. The following is a slightly simplified theoretical presentation than that presented by Potter and serves to enhance the overall discussion of the final results.

4-1. Theoretical Development

The equivalent linear system is given by⁷³

$$[M]_s \{\ddot{q}_i\} + [C]_s \{\dot{q}_i\} + [K_s] \{q_i\} = \{F_i\} \quad (4.7)$$

where all the matrices are considered general real matrices.

By denoting

$$\{y_i\} = \begin{Bmatrix} \{\dot{q}_i\} \\ \{q_i\} \end{Bmatrix}, \quad \{Z_i\} = \begin{Bmatrix} \{0\} \\ \{F_i\} \end{Bmatrix}$$

the system equations are written as

$$[A]\{\dot{y}_i\} + [B]\{y_i\} = \{z_i\} \quad (4.8)$$

where

$$[A] = \begin{bmatrix} [0] & [M]_s \\ [M]_s & [C]_s \end{bmatrix}, \quad [B] = \begin{bmatrix} -[M]_s & [0] \\ [0] & [K]_s \end{bmatrix} \quad (4.9)$$

By assuming eq.

$$\{y_i\} = \{Y\} e^{\lambda t}$$

Eq. (4.8) becomes

$$[[B] + \lambda[A]] \{Y\} = \{0\} \quad (4.10)$$

for the no excitation case.

By solving

$$\det |B + \lambda A| = 0$$

2n complex roots and λ_r (eigenvalue) a corresponding eigenvector ψ^r are determined. Therefore

$$[[B] + \lambda_r[A]]\{\psi^r\} = \{0\} \quad (4.11)$$

where

$$\{\psi^r\} = \begin{Bmatrix} \lambda_r \phi^r \\ \phi^r \end{Bmatrix} \quad .$$

Since $[B]$ and $[A]$ are non symmetric it is shown⁴⁶ that eq. (4.11) can also be written as

$$[[B] + \lambda_p[A]]^T \{r^p\} = \{0\} \quad (4.12)$$

Using eqs. (4.11) and (4.12) the biorthogonal relationships are

$$\{r^p\}^T [A] \{\psi^r\} = 0 \quad (4.13)$$

$$\{r^p\}^T [B] \{\psi^r\} = 0 \quad .$$

From the following external forces

$$\{Z_i(t)\} = \{Z_i\} e^{j\omega t} \quad (4.14)$$

and a solution of the form

$$\{Z_i(t)\} = \{Z_i\} e^{j\omega t} \quad (4.15)$$

and the additional assumption that either type of eigenvalue can provide a solution of the form

$$\{Y_i\} = \sum_{r=1}^{2n} \alpha_r \psi^r \quad (4.16)$$

it can be shown that

$$\{Y_i(t)\} = \sum_{r=1}^{2n} \frac{\{r^r\}^T \{Z_i\} \{\psi^r\}}{(j\omega - \lambda_r)} \quad (4.17)$$

with

$$[r]^T [B] [\psi] = [\Lambda]$$

where $[\Lambda]$ is the diagonal matrix of the eigenvalues, then

$$\lambda_r = \xi_r \omega_r \pm j\omega \sqrt{1 - \xi_r^2}$$

then

$$[r]^T [A] [\psi] = [I] \quad .$$

By substituting for Y_i and Z_i in eq. (4.17)

$$\begin{Bmatrix} j\omega \{q_i\} \\ \{q_i\} \end{Bmatrix} = \frac{\sum_{r=1}^{2n} \{r^r\}^T \begin{Bmatrix} \{0\} \\ \{f_i\} \end{Bmatrix} \{\psi^r\}}{(j\omega - \lambda_r)} \quad (4.18)$$

An expansion of eq. (4.18) yields

$$\{q_i\} = \sum_{r=1}^{2n} \frac{\{r^r\}^T \{f_i\} \{\psi^r\}}{(j\omega - \lambda_r)} \quad (4.19)$$

For force input at k and displacement response at i

$$H_{ik} = \sum_{r=1}^{2n} \frac{\Gamma_k^r \psi_i^k}{j\omega - \lambda_r} \quad (4.20)$$

If $A_{ik}^r = \Gamma_k^r \psi_i^r$ represents the residues at λ_r eq. (4.20) becomes

$$H_{ik} = \sum_{r=1}^n \frac{A_{ik}^r}{j\omega + \xi_r \omega_r - j\omega_r \sqrt{1 - \xi_r^2}} + \sum_{r=1}^n \frac{A_{ik}^{r*}}{j\omega + \xi_r \omega_r + j\omega_r \sqrt{1 - \xi_r^2}} \quad (4.21)$$

In order to identify the eigenvectors and the adjoint eigenvectors, it is necessary to identify λ_r and A_{ik} from the measured data in the

time domain. It is assumed that the following transfer function matrix is determined from measurement of input and output time history at selected locations

$$[H] = \begin{bmatrix} H_{11} & \cdot & \cdot & \cdot & \cdot & H_{1n} \\ \cdot & & & & & \cdot \\ \cdot & & & & & \cdot \\ \cdot & & & & & \cdot \\ H_{n1} & \cdot & \cdot & \cdot & \cdot & H_{nn} \end{bmatrix} \quad (4.22)$$

An expansion of the terms of eq. (4.22) yields

$$[H] = \begin{bmatrix} \frac{A_{11}^1}{j\omega - \lambda_1} + \dots + \frac{A_{11}^n}{j\omega - \lambda_n} & \dots & \frac{A_{1n}^1}{j\omega - \lambda_1} + \dots + \frac{A_{1n}^n}{j\omega - \lambda_n} \\ \vdots & & \vdots \\ \frac{A_{n1}^1}{j\omega - \lambda_1} + \dots + \frac{A_{n1}^n}{j\omega - \lambda_n} & \dots & \frac{A_{nn}^1}{j\omega - \lambda_1} + \dots + \frac{A_{nn}^n}{j\omega - \lambda_n} \end{bmatrix} \quad (4.23)$$

In this equation, the complex conjugate terms have not been retained and each residue is now replaced by its biorthogonal pair

$$[H] = \begin{bmatrix} \frac{\Gamma_{11}^1 \psi_1^1}{j\omega - \lambda_1} + \dots + \frac{\Gamma_{11}^n \psi_1^n}{j\omega - \lambda_n} & \dots & \frac{\Gamma_{n1}^1 \psi_1^1}{j\omega - \lambda_1} + \dots + \frac{\Gamma_{n1}^n \psi_1^n}{j\omega - \lambda_n} \\ \vdots & & \vdots \\ \frac{\Gamma_{1n}^1 \psi_n^1}{j\omega - \lambda_1} + \dots + \frac{\Gamma_{1n}^n \psi_n^n}{j\omega - \lambda_n} & \dots & \frac{\Gamma_{nn}^1 \psi_n^1}{j\omega - \lambda_1} + \dots + \frac{\Gamma_{nn}^n \psi_n^n}{j\omega - \lambda_n} \end{bmatrix} \quad (4.24)$$

or when separated into components

$$[H] = [H]^{(1)} + [H]^{(2)} + \dots + [H]^{(n)}$$

For example

$$[H]^1 = \begin{bmatrix} \frac{\Gamma_1^1 \psi_1^1}{j\omega - \lambda_1} & \dots & \frac{\Gamma_n^1 \psi_1^1}{j\omega - \lambda_1} \\ \vdots & & \vdots \\ \frac{\Gamma_1^1 \psi_n^1}{j\omega - \lambda_1} & \dots & \frac{\Gamma_n^1 \psi_n^1}{j\omega - \lambda_1} \end{bmatrix} \quad (4.25)$$

In terms of the residues, eq. (4.25) becomes

$$[H]^{(1)} = \frac{1}{j\omega - \lambda_1} \begin{bmatrix} A_{11}^1 & \dots & A_{1n}^1 \\ \vdots & & \vdots \\ A_{n1}^1 & \dots & A_{nn}^1 \end{bmatrix} \quad (4.26)$$

For each eigenvector the same result occurs

$$\psi^1 = \begin{Bmatrix} A_{11}^1/A_{n1}^1 \\ \vdots \\ 1 \end{Bmatrix}, \quad \psi^2 = \begin{Bmatrix} A_{11}^2/A_{n1}^2 \\ \vdots \\ 1 \end{Bmatrix} \dots \psi^n = \begin{Bmatrix} A_{11}^n/A_{n1}^1 \\ \vdots \\ 1 \end{Bmatrix} \quad (4.29)$$

To obtain the other eigenvectors, let

$$\Gamma_n^1 = 1 \text{ therefore } A_{1n}^1 = \psi_1^1 \text{ and}$$

$$\Gamma^1 = [A_{11}^1/A_{1n}^1 \quad A_{12}^1/A_{1n}^1 \quad \dots \quad 1]$$

or

$$r^1 = [A_{21}^1/A_{2n}^1 \quad A_{22}^1/A_{2n}^1 \quad \dots \quad 1]$$

For n modes then

(4.30)

$$r^1 = [A_{11}^1/A_{1n}^1 \quad A_{12}^1/A_{1n}^1 \quad \dots \quad 1]$$

$$r^2 = [A_{11}^2/A_{1n}^2 \quad A_{12}^2/A_{1n}^2 \quad \dots \quad 1]$$

\vdots

$$r^n = [A_{11}^n/A_{1n}^n \quad A_{12}^n/A_{1n}^n \quad \dots \quad 1]$$

With the relationships established in eqs. (4.29) and (4.30), the biorthogonal eigenvector coefficients can be identified by normalizing the row and columns respectably.

From eqs. (4.29) and (4.30) it can also be shown that obtaining a full set of residues experimentally is not necessary. Given the residues of the lower triangle of the transfer function matrix for a given mode, the upper half values can be computed from

$$A_{ik}^r = (A_{ii}^r \quad A_{kk}^r)/A_{ki}^r \quad (4.31)$$

or

$$A_{ij}^r = (A_{i\ell}^r/A_{mj})/A_{m\ell} \quad \ell \neq j, m \neq i \quad (4.32)$$

and ℓ, m cannot be such that an upper half value is chosen prematurely.

4.2 Experimental Results

A cantilever beam shown in Figure 4.2 represents a structure with a single pair of collocated sensor and actuator and a single pair of non collocated sensor and actuator. The feedback signal is conditioned to correspond to the second mode frequency.

The transfer function data taken at the two reciprocal locations noted on Figure 4.2 with feedback control are shown in Figure 4.3. From this data the difference between the transfer function is very slight. To avoid any shift in second mode frequency from a repositioning of the accelerometer, small masses were used. Results for the beam subjected to low gain control using a collocated sensor and actuator are shown in Figure 4.4. The difference between the two transfer functions was more than expected indicating that factors such as transducer misalignment and incomplete bonding may be present. Figure 4.5 is the transfer function data for the non collocated control case shown in figure 4.2 at the same gain level. The greater reduction in the second mode response at the same gain is because the actuator is now twice the size. Nevertheless the difference between the transfer function results is greater.

To obtain a numerical estimate of the difference between reciprocal transfer functions (H_{ij} , H_{ji}) The difference between the real and imaginary components was defined as

$$e = |H_{ij}(\omega) - H_{ji}(\omega)| \quad (4.33)$$

or

$$e = |x_{ij}(\omega) - x_{ji}(\omega) + j(y_{ij}(\omega) - y_{ji}(\omega))| \quad (4.34)$$

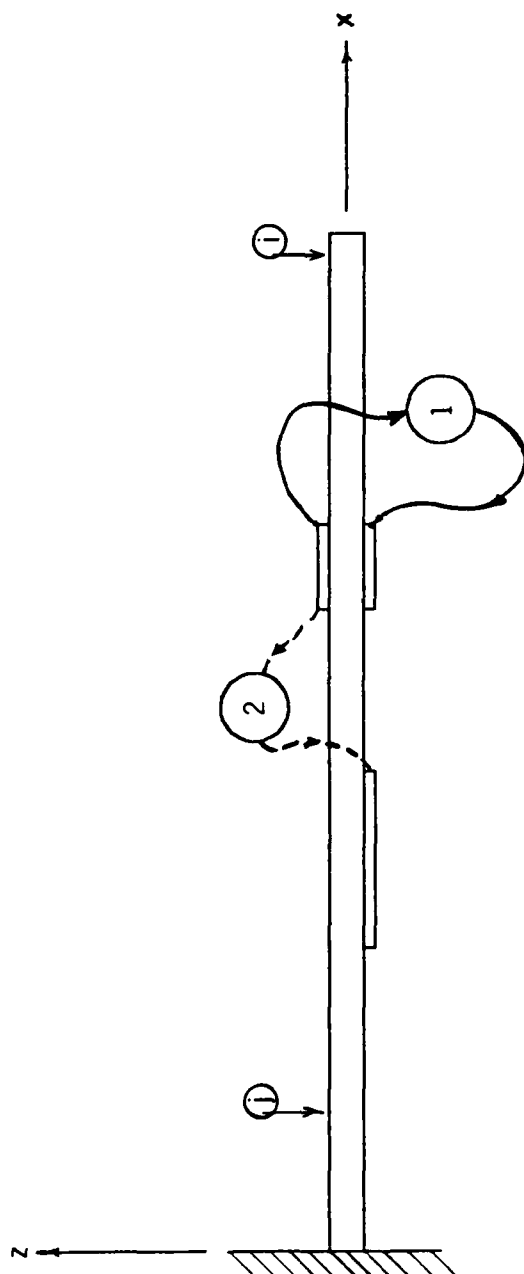


Figure 4-2 Experimental Collocated And Non-Collocated Control Configuration

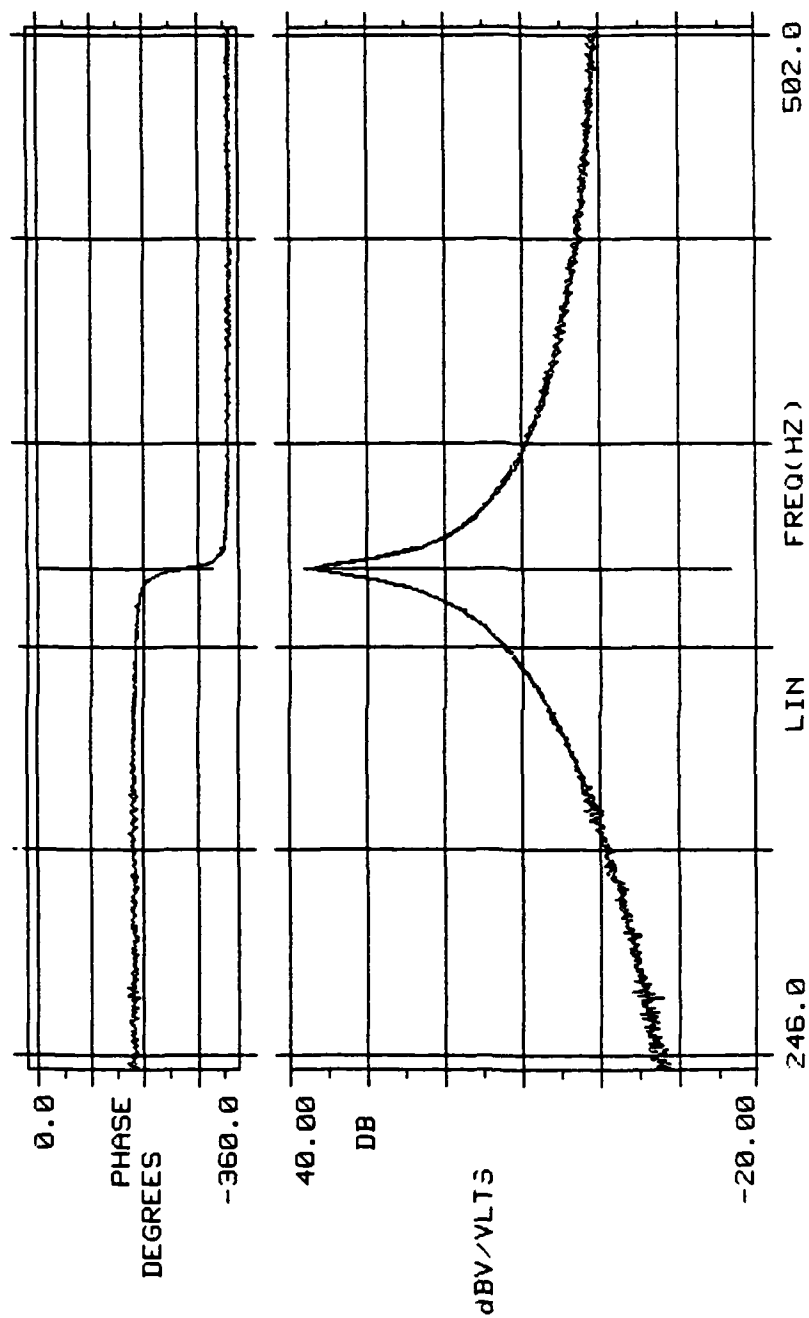


Figure 4-3 Comparison of Hij And Hji - Mode 2 - No Control

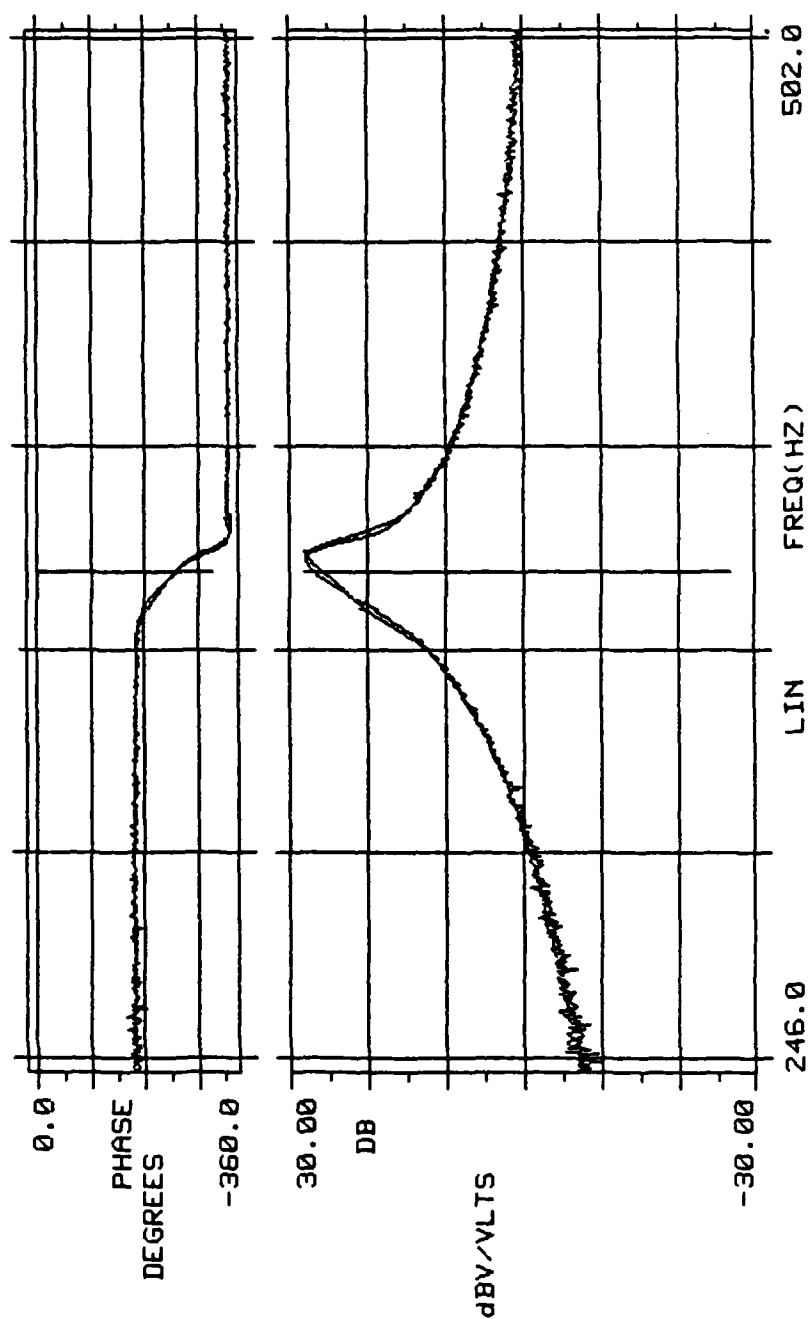


Figure 4-4 Comparison of Hij And Hji Collocated Sensor/Actuator
Mode 2 - Active Control - Low Gain

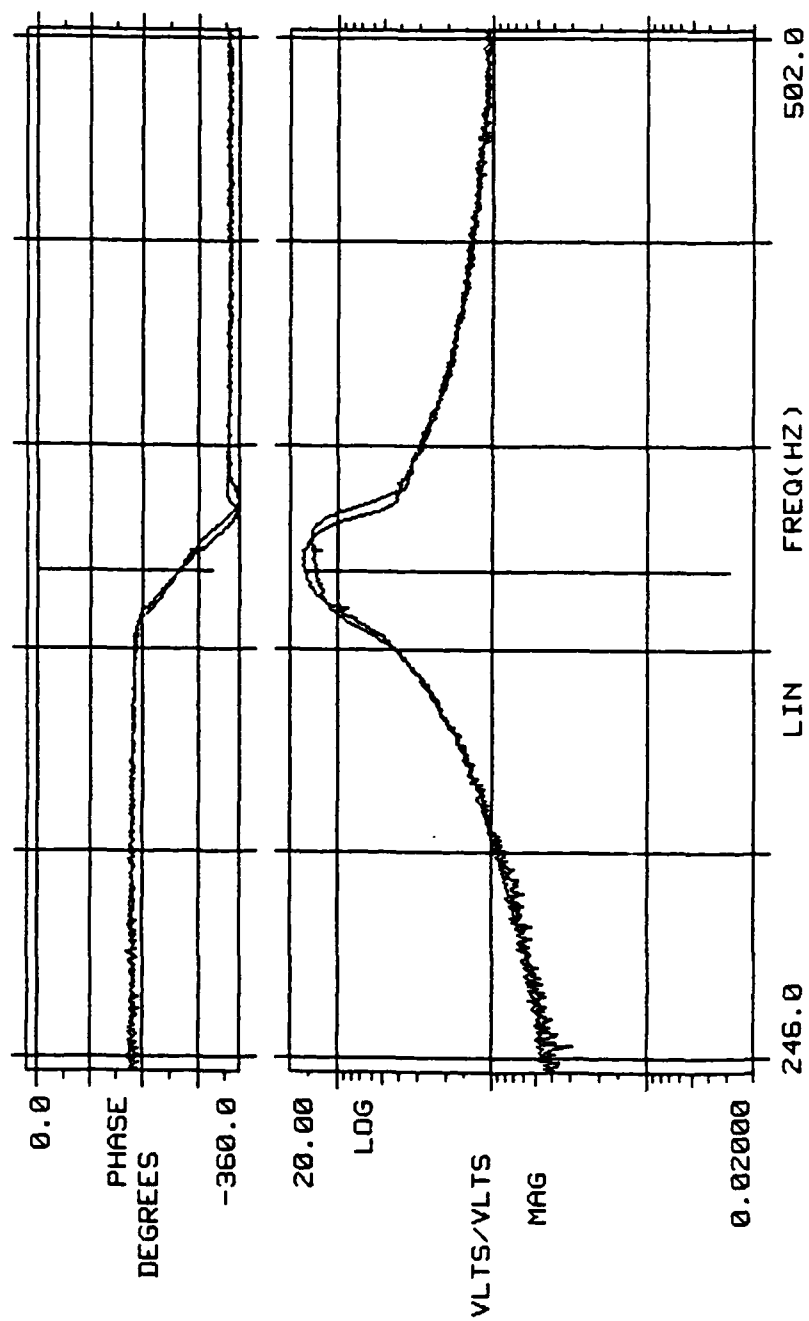


Figure 4-5 Comparison of Hij And Hji - Non-Collocated Sensor/Actuator
Mode 2 - Active Control - Low Gain

where x_{ij} and y_{ij} are the real and imaginary part of H_{ij} .

Therefore the normalized difference is

$$\xi_B = \frac{\sum_{\omega_1}^{\omega_2} e^* e}{\Delta \epsilon_{NC}} \quad (4.35)$$

where $\Delta \epsilon_{NC}$ is the sum of the difference results for the no control case.

The results are listed in Table 4.3. The numerical results support the above observations.

Shown in Figure 4.6 is another beam with the feedback filter centered at the second bending mode frequency using a single sensor and single actuator. Also shown in the figure are the transfer functions measurement locations necessary to obtain the lower triangle of the transfer function matrix. Using the residues computed from these transfer functions the residues for the remaining elements of the full transfer function matrix have been computed by using a post processor. The post processor consists of expanding eq.(4.31) as follows:

For each mode r ,

$$A_{ik} = \frac{(U_{ii}^r + jV_{ii}^r)(U_{kk}^r + jV_{kk}^r)}{(U_{ki}^r + jV_{ki}^r)} \quad (4.36)$$

where U_{ij} is the real part and V_{ij} is the imaginary part. Expanding eq. (4.36) yields for a given mode

Table 4-3 Numerical Difference Computation of Collocated
and Non Collocated Feedback

Experiment	Error
No Feedback	1.0
Collocated	1.42
Non Collocated	2.10

Note: 60 data samples (360 - 390 Hz.)

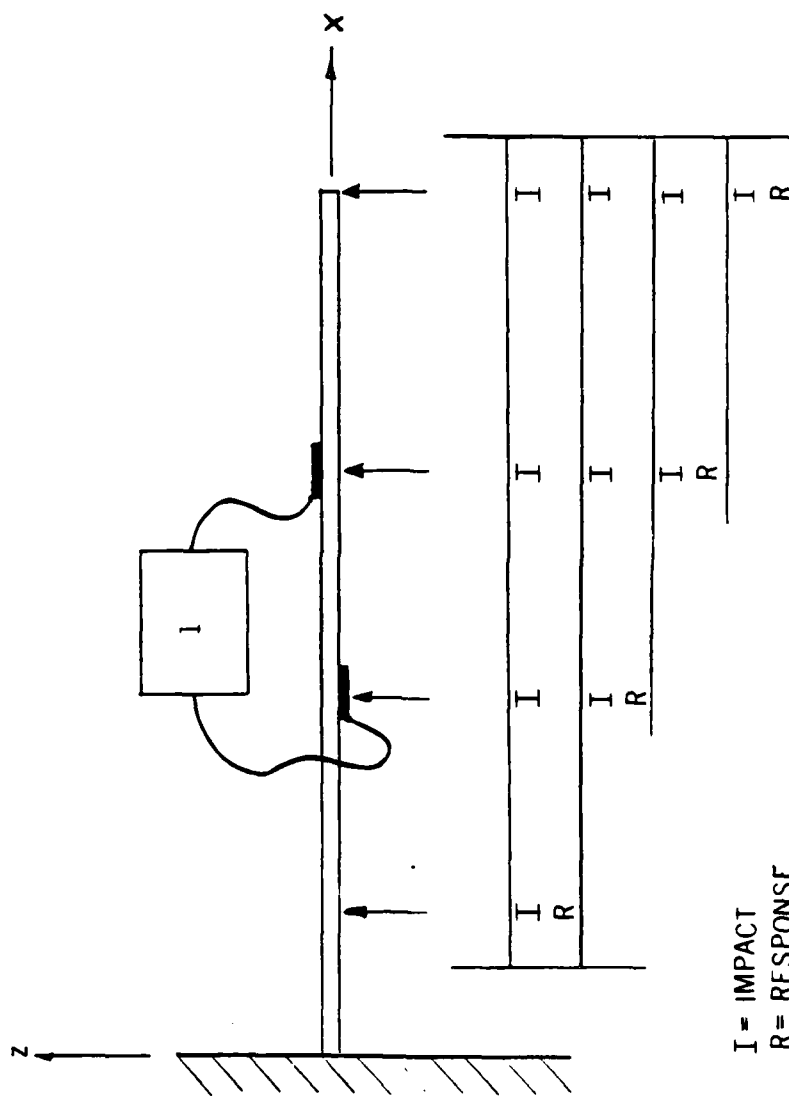


Figure 4-6 Biorthogonal Mode Identification Experimental Configuration And Test Matrix

$$\operatorname{Re}(A_{ik}) = \frac{U_{ii}U_{kk}U_{ki} + V_{ki}V_{ii}U_{kk} + V_{ki}U_{ii}V_{kk} - V_{ii}V_{kk}U_{ki}}{U_{ki}^2 + V_{ki}^2} \quad (4.37)$$

$$\operatorname{Im}(A_{ik}) = \frac{V_{ii}U_{kk}U_{ki} + U_{ii}V_{kk}U_{ki} + U_{ii}U_{kk}V_{ki} + V_{ii}V_{kk}V_{ki}}{U_{ki}^2 + V_{ki}^2} \quad (4.38)$$

The same post processor computed and normalized the left and right eigenvectors according to eqs. (4.29) and (4.30) with and without feedback. The coefficients of the second left and right eigenvectors were used to compute a variance given as

$$\sum_{i=1}^n \sum_{j=1}^n |\psi_{ij} - r_{ji}|^2 = \varepsilon \quad (4.39)$$

to provide a relative measure of the degree of biorthogonality for the different cases. If the eigenvectors are orthogonal, then ε will be very small. For example, a four degree of freedom finite element model of the beam with no control gave a ε of $.206 \times 10^{-3}$. Experimental results when no control is applied yielded a value of .124. This number can be considered an equivalent measure of the noise of the experimental measurement as well as the residue estimation and eigenvector coefficient identification. For the case of non collocated control, the experimental results were

$$\{\psi^2\} = \begin{Bmatrix} .648 \\ .513 \\ -.800 \\ 1.0 \end{Bmatrix} \quad \{\Gamma^2\}^T = \begin{Bmatrix} .694 \\ .427 \\ -.762 \\ 1.00 \end{Bmatrix}$$

with a computed ε of .472.

Though preliminary in nature these results demonstrate the modification of the active structure's modal behavior.

CHAPTER V

GAIN OPTIMIZATION OF THE ACTIVE STRUCTURE

In this chapter, an application of optimal control theory for active damping of the structural dynamic system consisting of multiple collocated piezoceramic sensors and actuators is discussed. The control objective is to bring the active structure from a perturbed initial state to the origin in an optimal fashion.

5.1. Background

To apply the concepts of optimal control to the active structure a brief review is presented of a method of obtaining optimal feedback gains of a system described in state space with full state and limited state output feedback applied. A detail description of this method for full state feedback is provided for a in a variety of texts on modern control theory ^{54,58,61,78}.

Consider a constant coefficient system defined as

$$\dot{x}(t) = Ax(t) + Bu(t) \quad (5.1)$$

with

$$x(t_0) = x_0 \quad (5.2)$$

where t_0 is the initial time. To optimize the control of such a system, a quadratic performance can be written as⁷⁸

$$J = \frac{1}{2} \int_{t_0}^{t_f} (x^T Q x + u^T R u) dt \quad (5.3)$$

where Q is an arbitrary positive semidefinite matrix and R is an arbitrary positive definite matrix.

Let the functional L be defined as

$$L(x, \dot{x}, u) = \frac{1}{2} \int_{t_0}^{t_f} [(x^T Q x + u^T R u) + \lambda^T (-\dot{x} + Ax + Bu)] dt \quad (5.4)$$

where λ is a vector of lagrange multipliers. Equation (5.4) can be rewritten as

$$L(x, \dot{x}, u) = \frac{1}{2} \int_{t_0}^{t_f} (H(x, u) - \lambda^T \dot{x}) dt \quad (5.5)$$

where

$$H(x, u) = \frac{1}{2} [x^T Q x + u^T R u + \lambda^T (Ax + Bu)]. \quad (5.6)$$

Setting the first variation of L to zero yields

$$\delta L = 0 = \frac{\partial L}{\partial x} \delta x + \frac{\partial L}{\partial \dot{x}} \delta \dot{x} + \frac{\partial L}{\partial u} \delta u. \quad (5.7)$$

Using Equations (5.5), (5.6) and (5.7) gives

$$\delta L = \int_{t_0}^{t_f} \left(\frac{\partial H}{\partial x} \delta x + \frac{\partial P}{\partial u} \delta u - \lambda^T \delta \dot{x} \right) dt = 0. \quad (5.8)$$

Integrating the second part of Equation (5.8) by parts yields

$$\int_{t_0}^{t_f} \lambda^T \delta \dot{x} = \lambda^T \delta x \Big|_{t_0}^{t_f} - \int_{t_0}^{t_f} \dot{\lambda}^T \delta x \, dt \quad (5.9)$$

The first term is zero if $\delta x(t_0) = 0$ and $\lambda(t_f)$ is chosen to be zero.

Combining Equations (5.8) and (5.9) yields

$$\delta L = \int_{t_0}^{t_f} \left[\left(\frac{\partial H}{\partial x} + \dot{\lambda}^T \right) \delta x + \left(\frac{\partial H}{\partial u} \right) \delta u \right] dt = 0. \quad (5.10)$$

Equation (5.10) can be simplified when $\lambda(t)$ is chosen such that

$$\frac{\partial H}{\partial x} = -\dot{\lambda}^T, \quad \lambda(t_f) = 0 \quad (5.11)$$

Then

$$\delta L = \int \frac{\partial H}{\partial u} \delta u \, dt$$

For arbitrary δu we are led to the necessary condition.

$$\frac{\partial H}{\partial u} = 0. \quad (5.12)$$

Using Equations (5.6), equation (5.11) and (5.12) become

$$\dot{\lambda}^T = -Qx - A^T x \quad (5.13)$$

$$u = -R^{-1}B^T \lambda \quad (5.14)$$

Equations (5.1), (5.2), (5.13) and (5.14) are the necessary conditions for optimality.

Selecting a solution in the form

$$\lambda(t) = P(t) x(t). \quad (5.15)$$

Then differentiating equation (5.15) and substituting the results in equation (5.13) along with Equation (5.1) and (5.14) yields the Ricatti equation

$$\dot{P} = -PA + PBR^{-1}B^TP - Q - A^TP, \quad P(t_f) = 0 \quad (5.16)$$

follows from the choice of $\lambda(t_f) = 0$.

It can be shown that $P(t, t_f)$, $t < t_f$, is stable backwards in time.

Therefore,

$$\lim_{t \rightarrow \infty} \dot{P}(t, t_f) = \dot{P}(t) = 0 \quad (5.17)$$

With Equation (5.17), equation (5.16) becomes the algebraic Ricatti equation for full state feedback.

$$PA + A^T P - PBR^{-1}B^TP - Q = 0 \quad (5.18)$$

The corresponding optimal control in state feedback form is

$$u = -R^{-1}B^T\bar{P}x \quad (5.19)$$

where \bar{P} is the positive definite solution of equation (5.18).

Uniqueness is guaranteed if the pair (A,B) is controllable, are closed loop stability is guaranteed if the pair (A,C) is observable, where C is any matrix such that $Q = C^TC$.

5.2 Optimal Output Feedback

Now consider the situation where perhaps all of the state cannot be measured and the control vector is proportional to the output vector. Such a system can be defined as

$$\dot{x} = Ax + Bu \quad x \in R^n \quad (5.20)$$

$$y = Cx \quad y \in R^m \quad (5.21)$$

$$u = -Gy \quad (5.22)$$

where matrices A,B,C and G are constant coefficient matrices and the initial state is unknown, but assumed to have zero mean with a variance

$$E\{x_0 x_0^T\} = X_0 \quad (5.23)$$

Optimization of such a problem has been formulated by Levine and Athans⁵⁹ and later by Mendel.⁶⁰ An algorithm has also been developed by Moerder and Calise⁶³ to solve the problem with an objective

function defined as

$$J = E_{x_0} \left\{ \int_0^{\infty} (x^T Q x + u^T R u) dt \right\} + \gamma(G) \quad (5.24)$$

where $\gamma(G)$ allows for a penalty to be placed on certain element of the gain matrix. Using Equations (5.12) and (5.22), equation (5.20) becomes

$$\dot{x} = [A - BGC]x \quad (5.25)$$

whose solution can be of the form

$$x(t) = [\exp(A - BGC)t]x_0 \quad (5.26)$$

Let

$$\phi(t,0) = \exp(A - BGC)t \quad (5.27)$$

equation (5.24) becomes

$$J = E \{ x_0^T K x_0 \} + \gamma(G) \quad (5.28)$$

where

$$K = \int_0^{\infty} \phi^T (Q + C^T G^T R G C) \phi dt \quad (5.29)$$

when Equations (5.27) and (5.22) are substituted into Equation (5.24).

Furthermore equation (5.28) can be written as⁶³

$$J = \text{tr}(K X_0) + \gamma(G) \quad (5.30)$$

where tr denotes the trace of the matrix and the matrix K satisfies.

$$(A - BGC)^T K + K(A - BGC) + Q - C^T G^T RGC = 0 \quad (5.31)$$

To obtain the optimal feedback gain matrix a lagrangian is defined in reference 60 as

$$\begin{aligned} L(G, K, \lambda) = & \gamma(G) + \text{tr} K X_0 - \text{tr} [(A - BGC)^T K \\ & + K(A - BGC) + Q - C^T G^T RGC] \lambda^T. \end{aligned} \quad (5.32)$$

Taking the partial derivative of the lagrangian with respect to each variable yields

$$-B^T K \lambda C^T + RGC \lambda C^T + \frac{1}{2} \gamma_G(G) = 0 \quad (5.33)$$

$$(A - BGC) \lambda + \lambda (A - BGC)^T + X_0 = 0 \quad (5.34)$$

$$(A - BGC)^T K + K(A - BGC) + Q - C^T G^T RGC = 0 \quad (5.35)$$

where $\gamma_G(G)$ is the gradient of $\gamma(G)$.

This result obtained by Moerder and Calise was solved using a sequential numerical algorithm. The algorithm has the added feature that certain elements in the gain matrix can be penalized to reduce their influence on the system. This feature is of particular importance in the active control of structures represented by finite elements. In the next section, the optimal gains are determined using this algorithm for a simple structural system subjected to active rate feedback control using piezoceramic sensors and actuators.

5.3 Rate Feedback Model

The active structure shown in figure 5.1 consists of two collocated pairs of piezoceramic sensors and actuators. The output from each sensor was only multiplied by a gain and applied to its corresponding actuator.

The following assumptions are made for this analysis:

- a) The closed loop system is stabilizable by output feedback.
- b) The piezoceramic sensors and actuators do not contribute mass or stiffness to the structure.
- c) The piezoceramic actuators have no internal dynamic characteristics (actuator dynamics).

The governing equations of the active system were transformed into the limited state feedback equations (5.20) to (5.22). The structural was modelled as

$$[M] \begin{Bmatrix} \ddot{\theta}_1 \\ \vdots \\ \ddot{\theta}_5 \end{Bmatrix} + [C] \begin{Bmatrix} \dot{\theta}_1 \\ \vdots \\ \dot{\theta}_5 \end{Bmatrix} + [K] \begin{Bmatrix} \theta_1 \\ \vdots \\ \theta_5 \end{Bmatrix} = \begin{Bmatrix} M_1 \\ \vdots \\ M_5 \end{Bmatrix} \quad (5.36)$$

where the translation d.o.f.'s have been eliminated by a condensation procedure and the vector $\{M_i\}$ represents only active feedback control moments. When control network #1 and #2 of figure 5.1 condition the sensor signal in a rate feedback manner for only first two modes, the output voltage to the actuator is

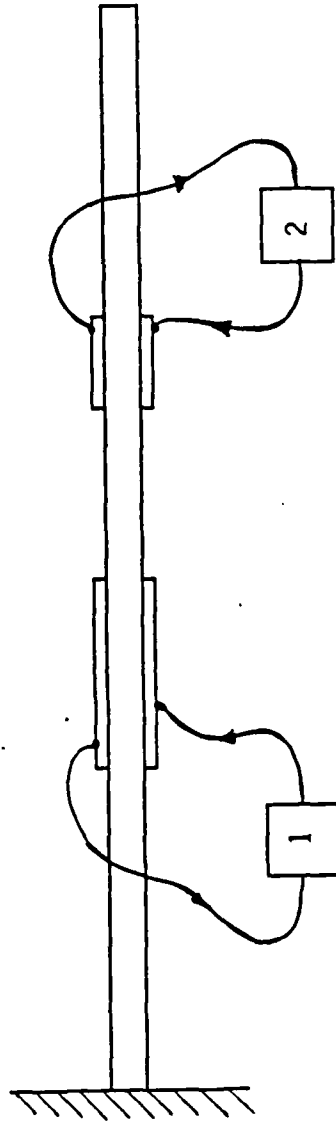


Figure 5-1 Collocated Active Rate Control

$$\begin{Bmatrix} V_1 \\ V_2 \end{Bmatrix} = \begin{bmatrix} g_{11} & 0 \\ 0 & g_{22} \end{bmatrix} \begin{bmatrix} -K_s & K_s & 0 & 0 & 0 \\ 0 & 0 & -K_s & K_s & 0 \end{bmatrix} \begin{Bmatrix} \dot{\theta}_1 \\ \dot{\theta}_5 \end{Bmatrix} \quad (5.37)$$

where K_s represents the sensor piezoceramic and dynamic coupling coefficients. The control moment vector for the actuators becomes

$$\{M_i\} = \begin{bmatrix} -K_D & K_D & 0 & 0 & 0 \\ 0 & 0 & -K_D & K_D & 0 \end{bmatrix}^T \begin{Bmatrix} V_1 \\ V_2 \end{Bmatrix} \quad (5.38)$$

Combining Equations (5.37) and (5.38) yields

$$\{M_i\} = [K_D] [G] [K_s] \{\dot{\theta}_i\} \quad (5.39)$$

Substituting Equation (5.39) into (5.36) and multiplying both sides by the inverse of the mass matrix yields

$$\{\ddot{\theta}_i\} = -[M]^{-1}[C] \{\dot{\theta}_i\} - [M]^{-1}[K]\{\theta_i\} + [M]^{-1}[K_D][G][K_D] \{\dot{\theta}_i\} \quad (5.40)$$

Let the following state variables be defined as

$$\{x\}^T = \{x_1 \dots x_{10}\} = \{\theta_1 \dots \theta_5, \dot{\theta}_1 \dots \dot{\theta}_5\} \quad (5.41)$$

Equation (5.40) can now be rewritten in state space form as

$$\{\dot{x}_i\} = \begin{bmatrix} [0] & [I] \\ -[M]^{-1}[K] & -[M]^{-1}[C] \end{bmatrix} \{x_i\} + [B] \{u\} \quad (5.42)$$

where

$$[B] = \begin{bmatrix} [0] \\ [M_i]^{-1} [K_D] \end{bmatrix}$$

and

$$\begin{Bmatrix} y_1 \\ y_2 \end{Bmatrix} = \begin{bmatrix} [0] & [K_S] \end{bmatrix} \{x_i\} \quad (5.43)$$

$$\begin{Bmatrix} u_1 \\ u_2 \end{Bmatrix} = -[G] \begin{Bmatrix} y_1 \\ y_2 \end{Bmatrix} \quad (5.44)$$

The mass, stiffness and damping coefficients have been obtained from the identified model of the selected beam (Model #1), shown in figure 5.1. The sensor/actuator coefficients were from previous presented results. Perfect dynamic coupling has been assumed and Table 5.1 lists the values of the matrices A,B and C.

Optimization Results

The procedure for using the algorithm is as follows:

- a) The numerical values for the A,B,C,Q and R matrices provided as input data to the program.
- b) The program requests initial gain matrix and penalty values.
- c) The program computes the open loop eigenvalues which provide a check on the input data.
- d) If no initial gain matrix is given the program estimates one.

Table 5.1 Numerical Values for Rate Control Analysis
Model #1.

[A] =	0.0	0.0	0.0	0.0	0.0		
	0.0	0.0	0.0	0.0	0.0		
	0.0	0.0	0.0	0.0	0.0		
	0.0	0.0	0.0	0.0	0.0		
	0.0	0.0	0.0	0.0	0.0		
	-2.334E+07	3.465E+07	-1.938E+07	2.734E+06	1.097E+06		
	5.653E+07	-1.204E+08	1.180E+08	-4.236E+07	-4.915E+06		
	-3.016E+07	1.190E+08	-2.429E+08	1.656E+08	-1.290E+07		
	-4.608E+06	-1.090E+07	1.425E+08	-1.799E+08	5.264E+07		
	6.401D+06	-6.459E+06	-9.703E+07	1.772E+08	-7.933E+07		
	1.0	0.0	0.0	0.0	0.0		
	0.0	1.0	0.0	0.0	0.0		
	0.0	0.0	1.0	0.0	0.0		
	0.0	0.0	0.0	1.0	0.0		
	0.0	0.0	0.0	0.0	1.0		
	-2.442E+01	1.405E+01	1.241	-8.169	-1.856		
	2.422E+01	-4.755E+01	1.919E+01	-1.528	2.264		
	5.013	2.173E+01	-6.656E+01	3.201E+01	4.129		
	3.169	4.390	2.619E+01	-5.146E+01	1.349E+01		
	-5.384	7.757	-2.545	3.750E+01	-4.332E+01		
[B] =	0.0	0.0					
	0.0	0.0					
	0.0	0.0					
	0.0	0.0					
	0.0	0.0					
	-1.503E+03	-3.937E+03					
	7.544E+03	2.087E+04					
	-1.475E+04	-4.326E+04					
	1.006E+04	3.130E+04					
	-8.576E+04	-2.738E+04					
[C] =	0.0	0.0	0.0	0.0	0.0	-4.074E+02	4.074E+02
	0.0	0.0	0.0	0.0	0.0	0.0	0.0
	0.0	0.0					
	-4.074E+02	4.074E+02					

e) The iteration procedure begins and the attempts to obtain an optimal solution.

f) After a particular solution is obtained, interactive analysis is possible.

Using previously identified structural and sensor/actuator coefficients gave the following open loop natural frequencies and damping values

Rad/sec	Damping
367.9	.0090
2329.8	.0039
6534.5	.0039
12918.1	.0023
20752.1	.0023

The R matrix was an identity matrix and the Q matrix was defined as

$$Q = \begin{bmatrix} 0 & 0 & 0 & 0 & 0 & 1 & 1 & 1 & 1 & 0 \\ 0 & 0 & 0 & 0 & 0 & 1 & 1 & 1 & 1 & 1 \end{bmatrix}$$

penalizing all the angular velocities equally and giving no penalty to the angular displacements. With a null initial gain matrix the resultant optimal gain matrix is

Gain Matrix

2.419D-03 -2.570D-04
 -2.290D-04 1.515D-03

with a performance index of .900D+06 and natural frequencies and damping values of

<u>Rad/sec</u>	<u>Damping</u>	<u>Increase over</u> <u>Open Loop (%)</u>
367.0	.0090	0
2330.0	.0046	18
6535.6	.0089	228
12916.5	.0276	1200
split	over damped	

When the Q matrix was an identity matrix almost identical gain and eigenvalue results were obtained. The optimal gain distribution increased the damping of the higher modes compared to the lower modes. This was expected since the contribution to the objective function by the higher modes is greater because for velocity, each displacement variable modal contribution is multiplied by its corresponding resonant frequency. When the off diagonal terms of the gain matrix are penalized in $\gamma(G)$, the resulting optimal gain obtained was

Gain Matrix

2.500D-03	-2.530D-07
-7.600D-07	1.740D-03

with a slightly higher performance index of .9013D+06 with the following resultant natural frequencies and damping values.

<u>Rad/sec</u>	<u>Damping</u>
367.9	.0091
2330.2	.0047
6535.6	.0085
12917.7	.0268
split	over damped

These results did not differ much from the results obtained from not penalizing the off diagonal gain terms in the gain matrix.

To show the effect of the optimal gain distribution, the state equations Equations (5.20-5.22) were solved using a Runge Kutta technique for the open and closed loop control configurations. The system angular rate state variables were given a unit angular rate initial condition and the time histories of system response obtained.

The output response $y_1(t)$ in volts from the sensor in control loop #1 of the baseline no control configuration for 50 msec is shown in Figure 5.2. The response signal content contains the contributions of the five modes of the structure with their respective

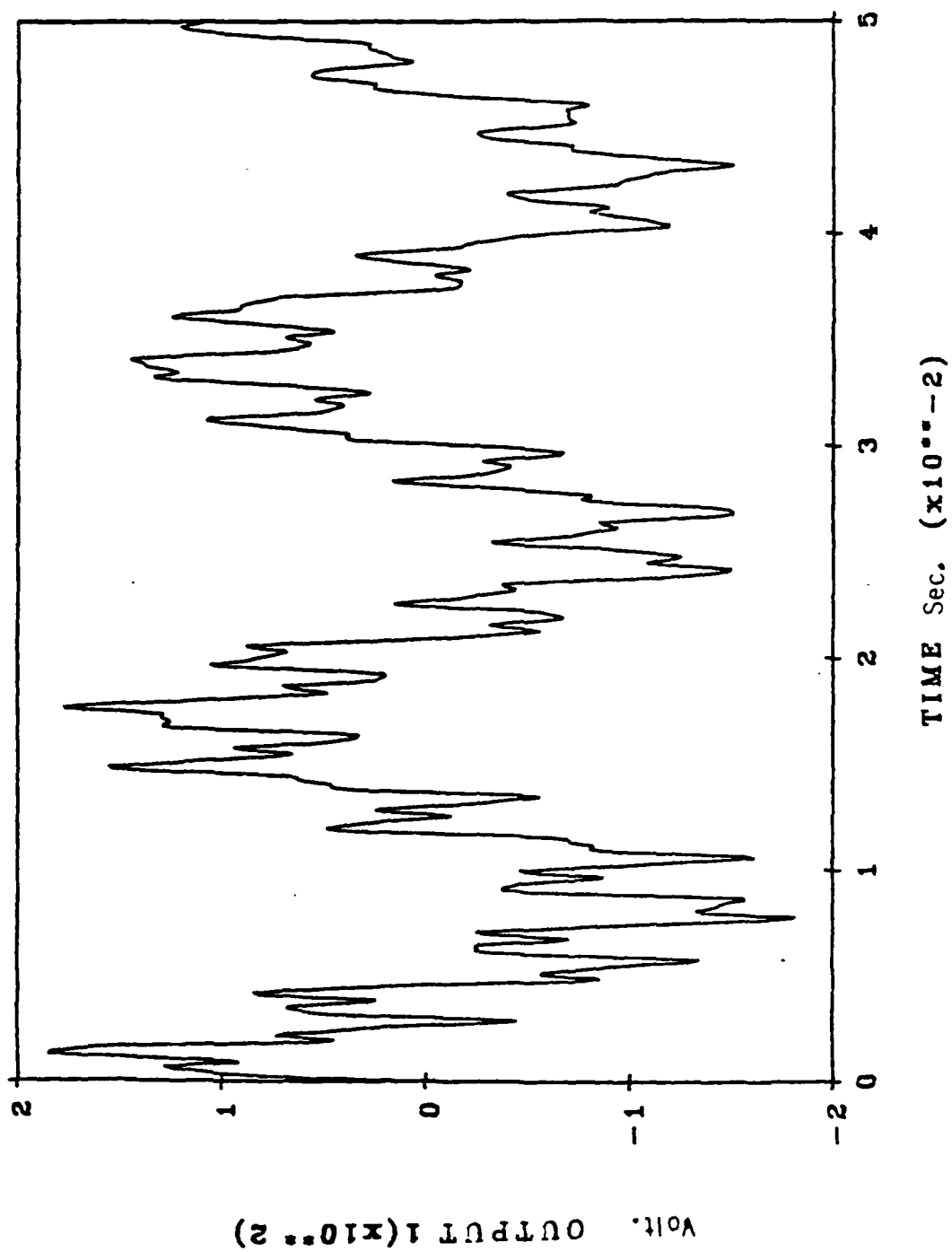


Figure 5.2 Baseline No Control Response Y₁

damping values. When active rate control is initiated for the same set of initial conditions, the control voltage to the actuator u_1 is shown in Figure 5.3. Comparison of Figures 5.3 to 5.4 demonstrates that the control signal is the exact inverse of the sensor signal and scaled appropriately.

Since the optimal gain distribution shown previously increases the damping of the higher modes for the system, the predominant signal response due to the first two modes does not change. In Figure 5.5 the baseline and active control output signals from control loop #1 for the first 20 msec are superimposed. The observed smoothing of the output signal during active control is due to the increase in the damping of the higher modes.

The active structure (Model #2) shown in Figure 5.6 was also analyzed using the limited state feedback approach. As before the output voltage is

$$\begin{Bmatrix} V_1 \\ V_2 \end{Bmatrix} = \begin{bmatrix} g_{11} & 0 \\ 0 & g_{22} \end{bmatrix} \begin{bmatrix} K_s & 0 \\ -K_s & K_s \end{bmatrix} \begin{Bmatrix} \dot{\theta}_1 \\ \dot{\theta}_2 \end{Bmatrix} \quad (5.45)$$

and the control moment vector

$$\{M_i\}_{ext} = \begin{bmatrix} K_D & -K_D \\ 0 & K_D \end{bmatrix}^T \begin{Bmatrix} V_1 \\ V_2 \end{Bmatrix}. \quad (5.46)$$

The system equation retaining only the rotational degrees of

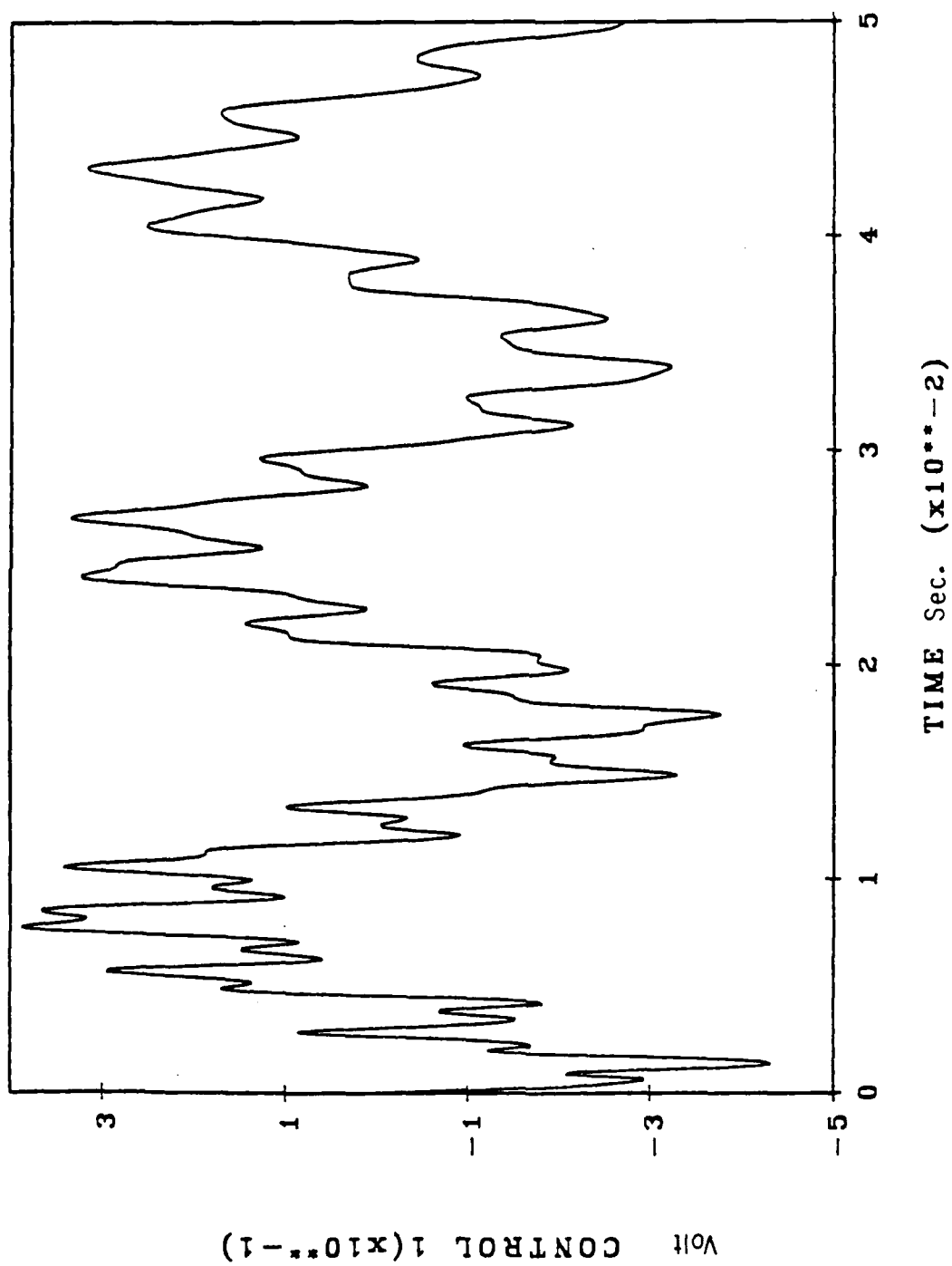


Figure 5.3 Active Control Input U1

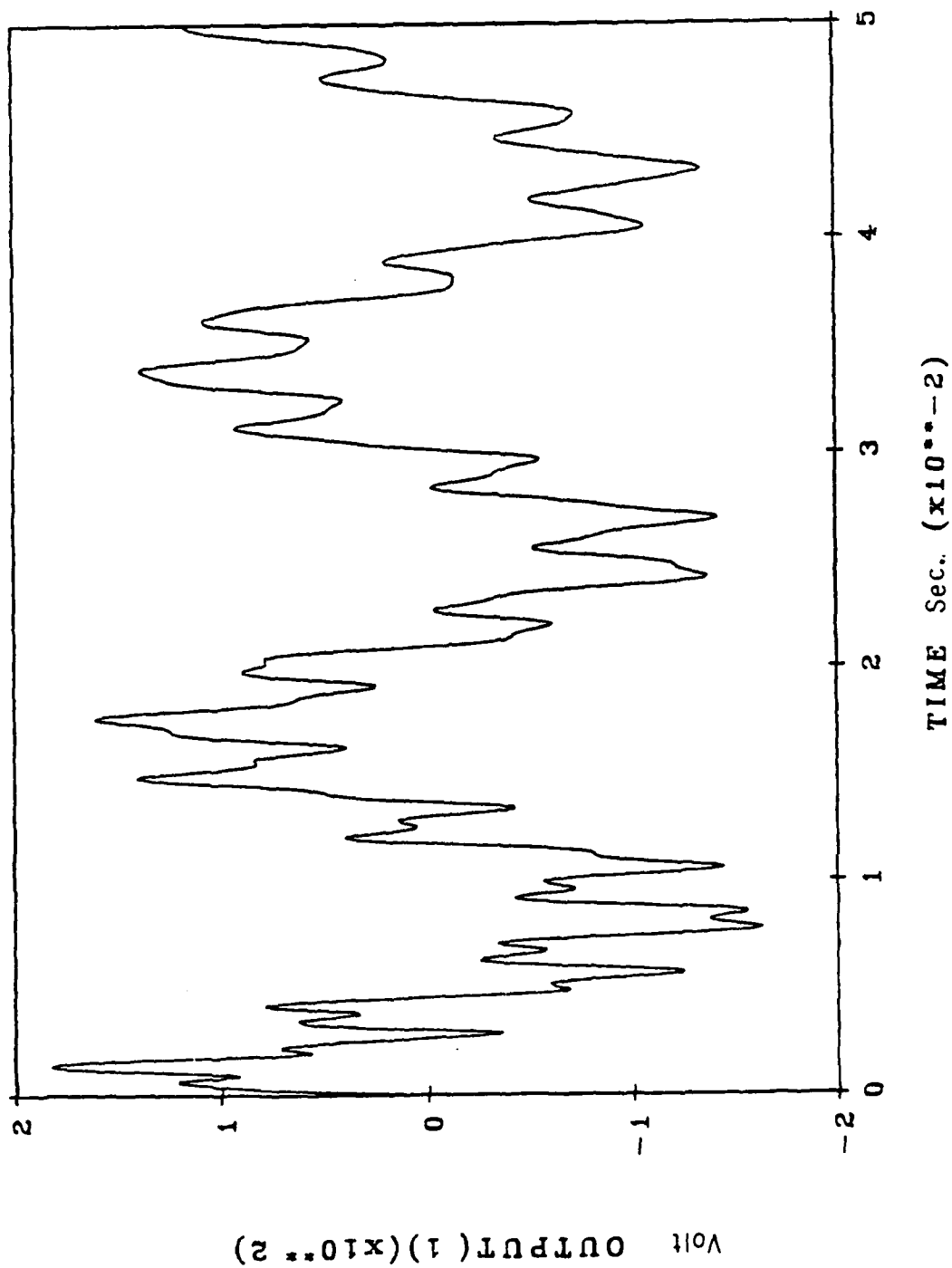


Figure 5.4 Active Control Output Response Y1

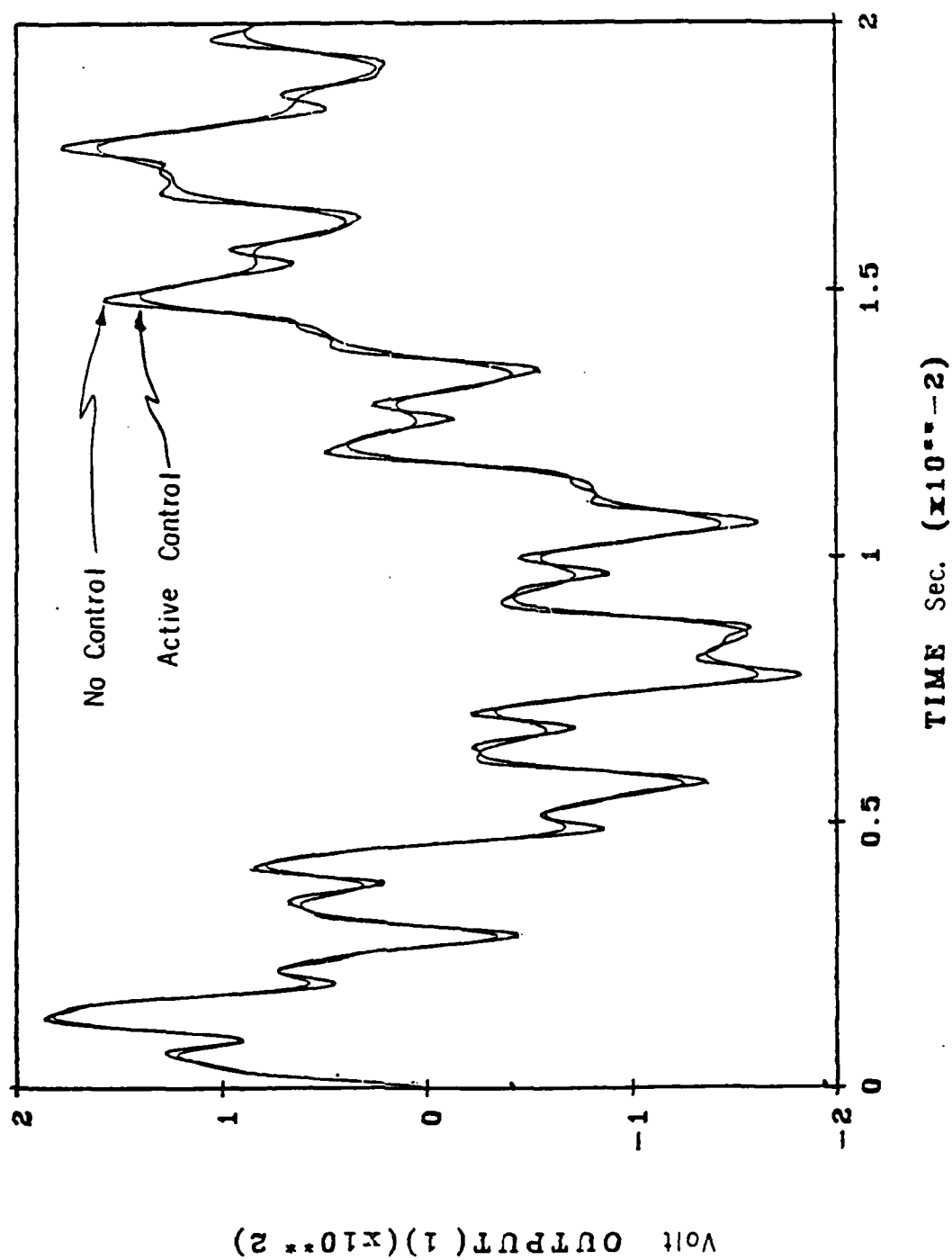
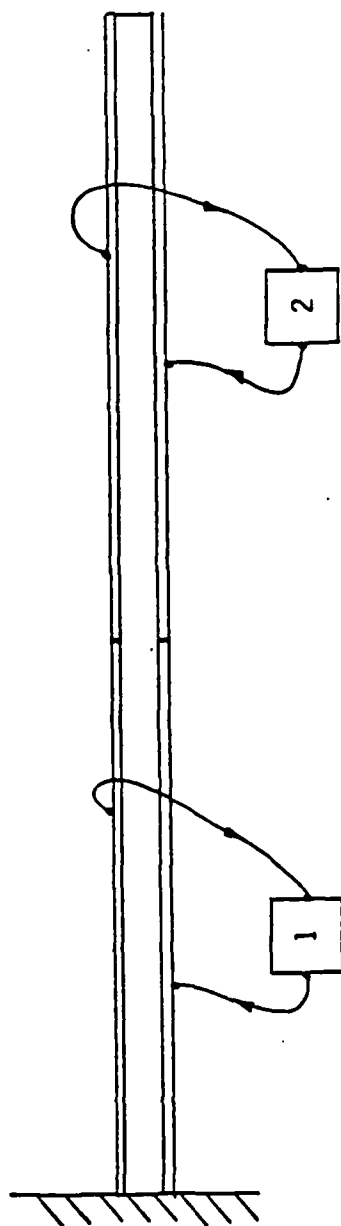


Figure 5.5 Comparison of the Baseline and Active Control



$$Q = \begin{bmatrix} 0 & 0 & 1 & 10 \end{bmatrix}$$

Figure 5.6 Two Degree of Freedom Model

freedom is

$$\ddot{\theta}_i = -[M]^{-1}[C]\{\dot{\theta}\} - [M]^{-1}[K]\{\theta_i\} + [M]^{-1}[K_D][G][K_S]\{\dot{\theta}_i\} \quad (5.47)$$

and the state variable chosen were

$$\{x\}^T = \{\theta_1, \theta_2, \dot{\theta}_1, \dot{\theta}_2\}. \quad (5.48)$$

Equations (5.45) to (5.48) are rewritten in a state space form and the optimal gain matrix with off diagonal element penalized is

$$G = \begin{bmatrix} 6.957 \text{ D-03} & 1.697 \text{ D-04} \\ 2.239 \text{ D-05} & 5.778 \text{ D-03} \end{bmatrix}$$

when the Q matrix is defined as

$$Q = \begin{bmatrix} 0 & & & \\ & 0 & & \\ & & 1 & \\ & & & 10 \end{bmatrix}$$

and matrices A, B and C are given in Table 5.2.

The resultant system baseline and changes in modal damping values are

<u>Rad/sec</u>	<u>Damping Baseline</u>	<u>Damping at Optimal Gain</u>
448.	.0015	.005
4284.	.002	.033

Figures 5.7 through 5.10 indicate the first mode and the second mode response attenuation. The results were similar to model #1.

Table 5.2 Numerical Values for Rate Control Analysis
Model #2.

$$[A] = \begin{bmatrix} 0.0 & 0.0 & 1.0 & 0.0 \\ 0.0 & 0.0 & 1.0 & 0.0 \\ -4.420E+06 & 3.453E+06 & -5.014 & 3.003 \\ 1.703E+07 & -1.414E+07 & 1.481E+01 & -1.347E+01 \end{bmatrix}$$

$$[B] = \begin{bmatrix} 0.0 & 0.0 \\ 0.0 & 0.0 \\ 5.370 & -2.143E+01 \\ -1.606E+01 & 8.774E+01 \end{bmatrix}$$

$$[C] = \begin{bmatrix} 0.0 & 0.0 & 4.074E+02 & 0.0 \\ 0.0 & 0.0 & -4.074E+02 & -4.074E+02 \end{bmatrix}$$

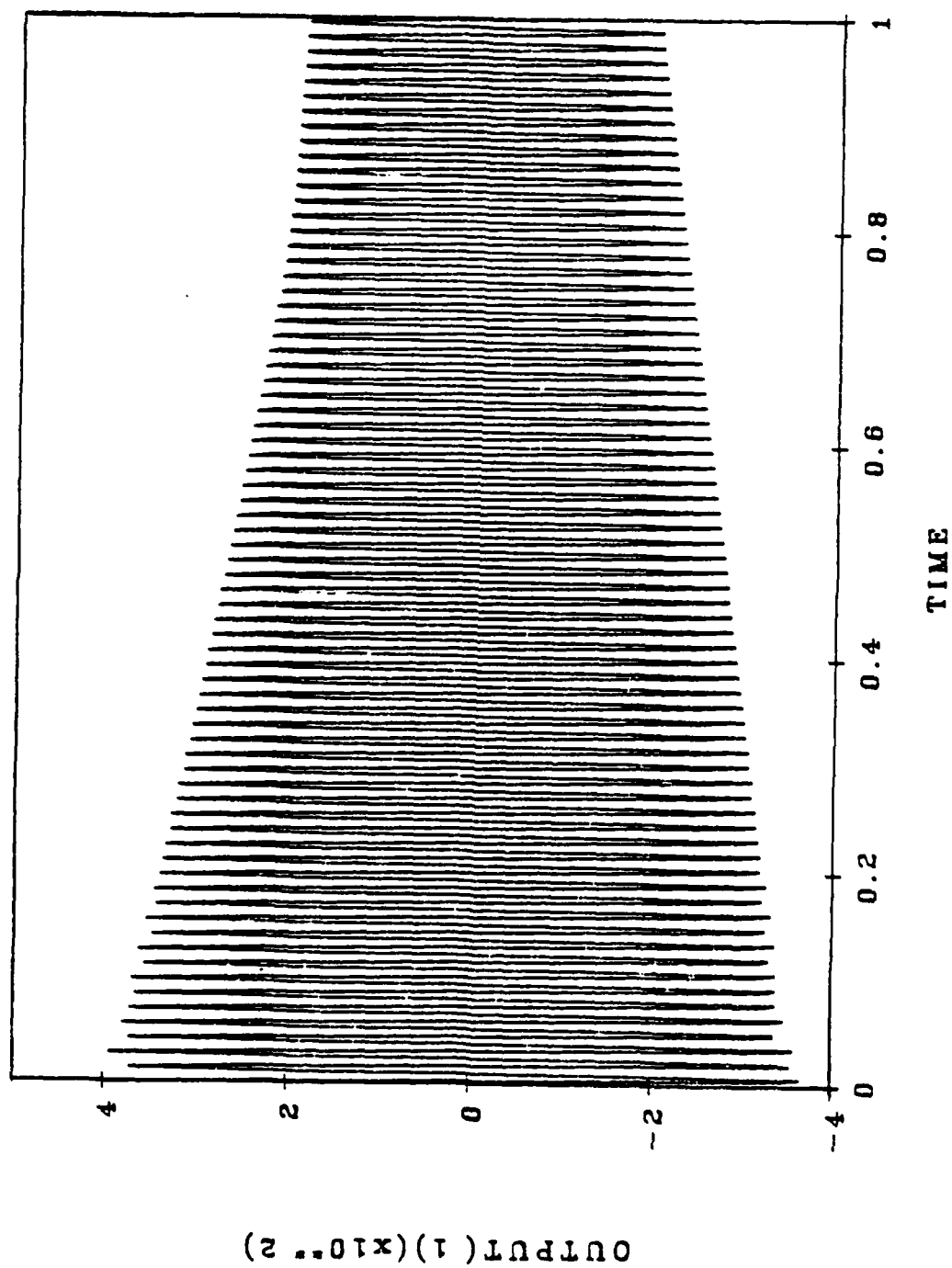


Figure 5.7 Baseline No Control Displacement Response 1 sec.

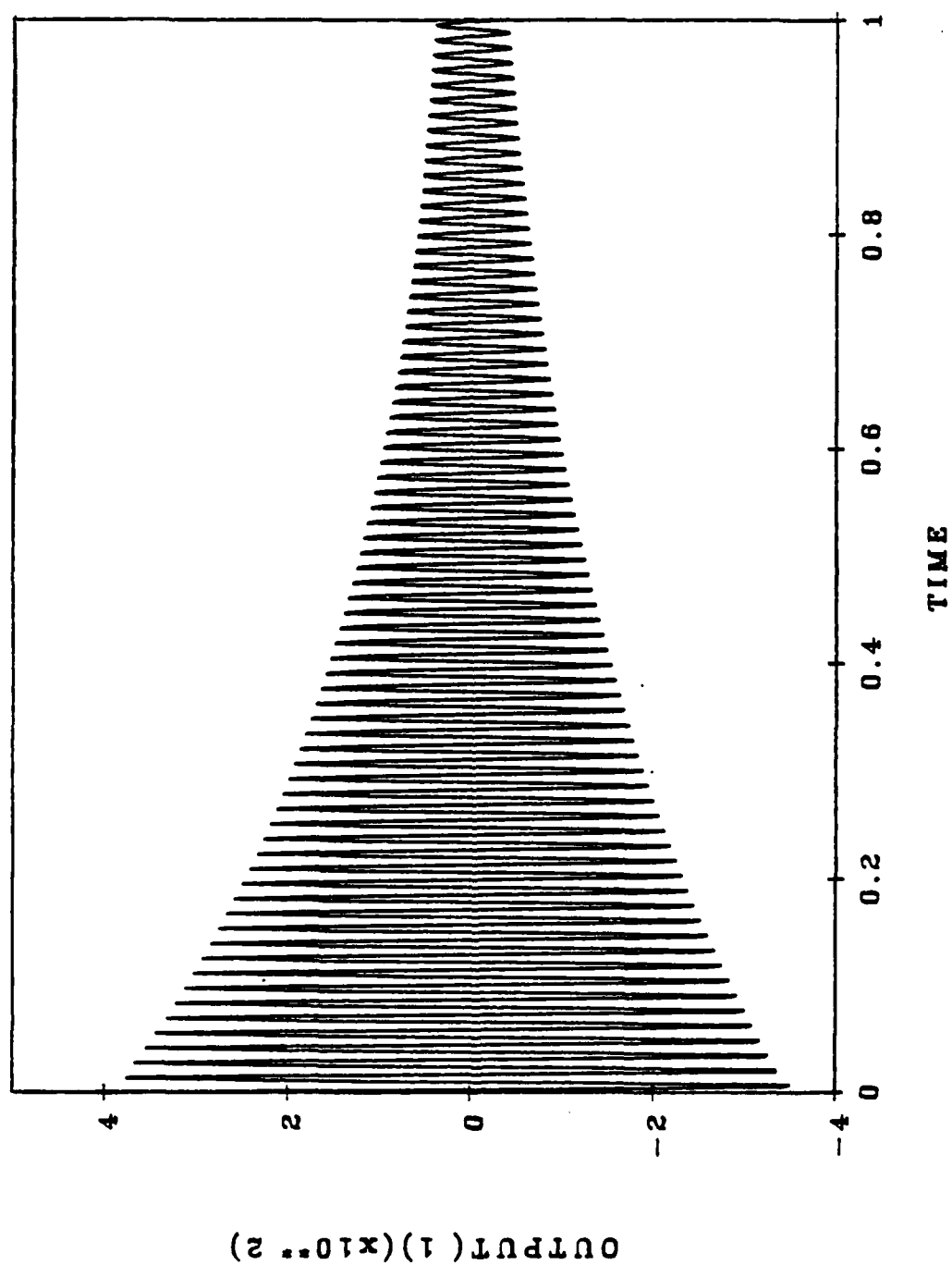


Figure 5.8 Active Control Displacement Response 1 sec.

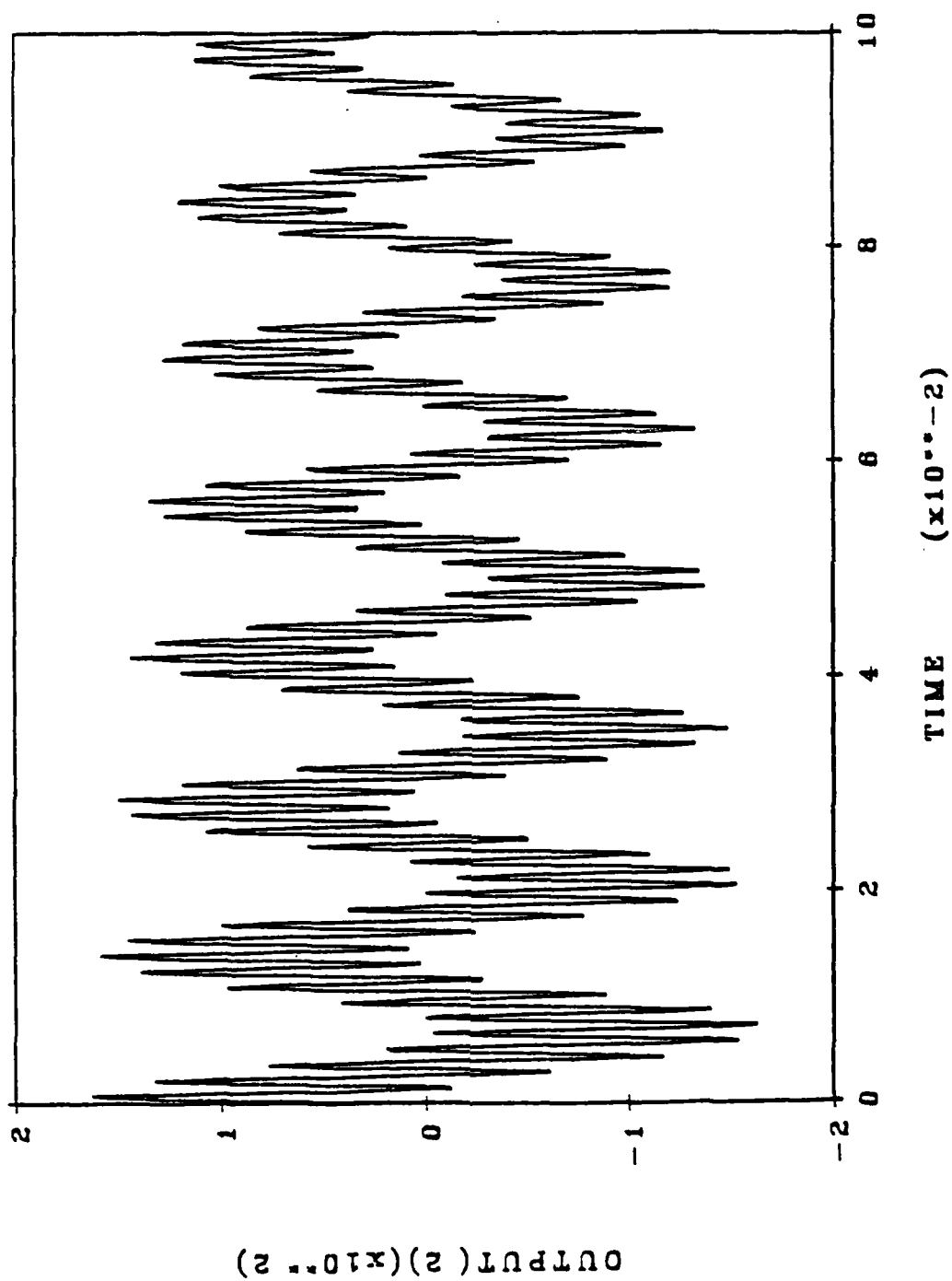


Figure 5.9 Baseline No Control Displacement Response 100 msec.

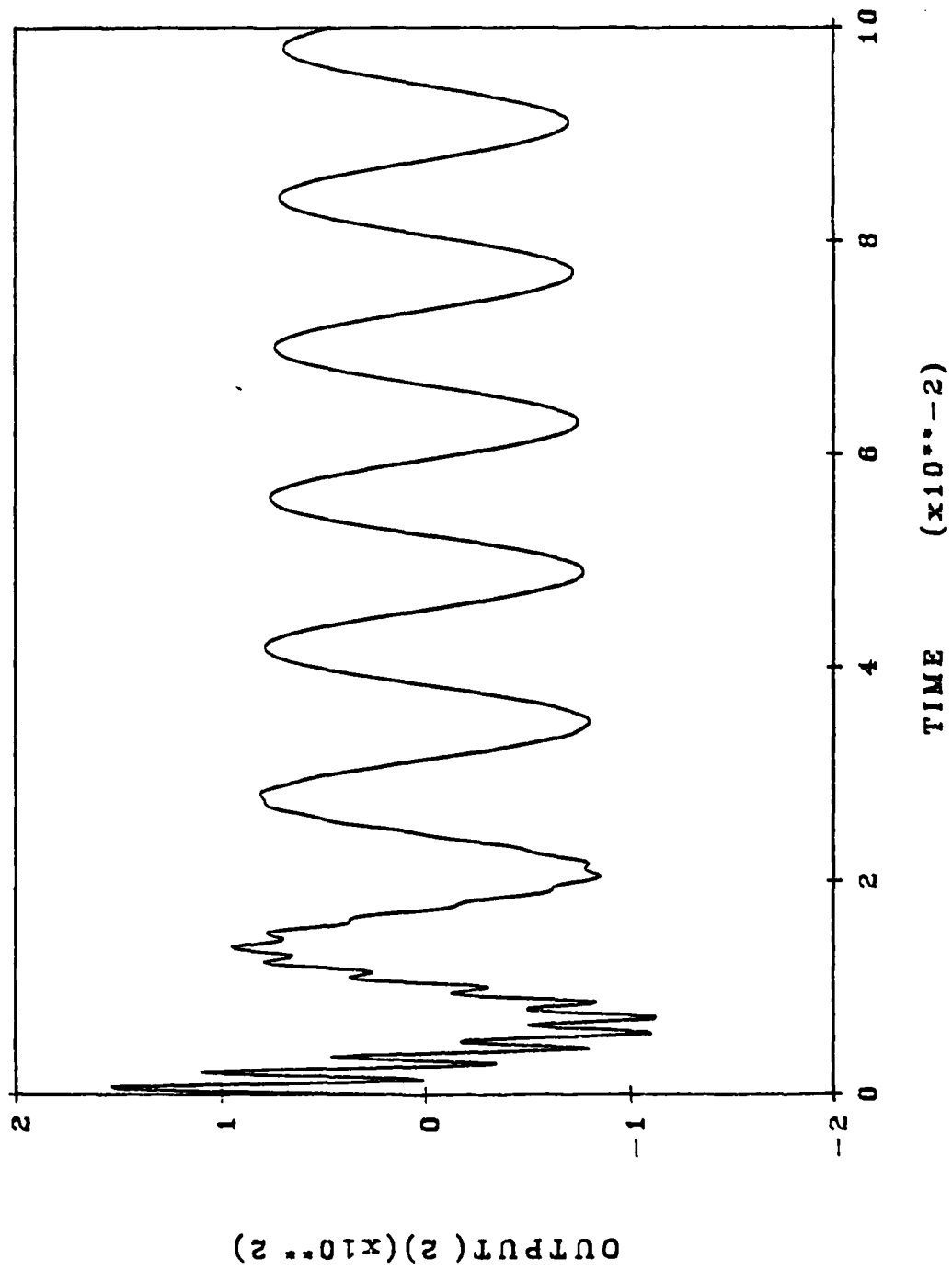


Figure 5.10 Active Control Displacement Response 100 msec.

CHAPTER VI

OPTIMAL CONTROL USING DISTRIBUTED SENSORS AND ACTUATORS

In a recently reported work Bailey and Hubbard¹⁵ have developed an optimal control algorithm for a system consisting of a cantilever beam with a point sensor and a distributed actuator. The actuator was a unimorph piezoelectric transducer made out of polyvinylidene fluoride polymer (PVF) and covered the entire upper surface of the beam.

The objective of this chapter is to extend the work of Bailey and Hubbard¹⁵ to explore control strategies by using distributed piezoceramic unimorph transducers as both sensors and actuators.

6.1. Analysis

The structure shown in Figure 6.1, consists of a cantilever beam of length L , with constants E, I and ρ . Subdomains of the beam are covered by pairs of bonded collocated piezoceramic unimorph transducers polarized in the z direction. The transducer on the upper surface is used as a sensor. When conditioned by a zero impedance amplifier it was shown in chapter II, eq.(2.22) that the output voltage for a constant width sensor is

$$V_s = K_s \int_{x_i}^{x_j} \frac{\partial^2 \dot{w}}{\partial x^2}(x, t) dx \quad x_i < x < x_j \quad (6.1)$$

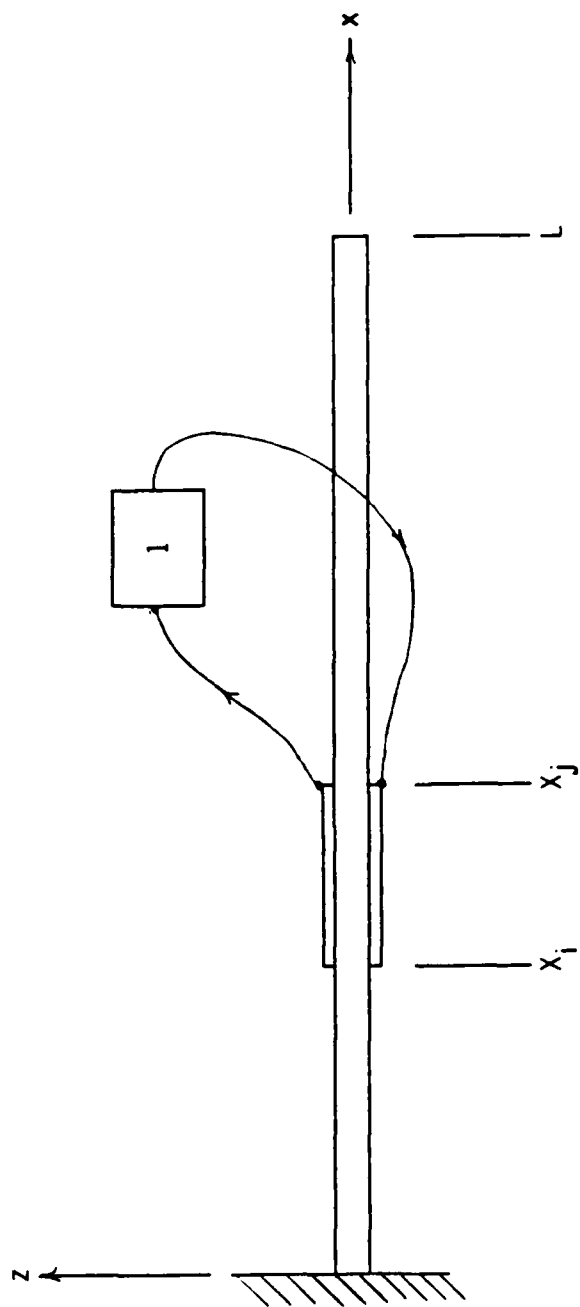


Figure 6-1 Collocated Sensor/Actuator Configuration

where K_s represents the sensor coefficient. The transducer on the lower surface is used as an actuator. As shown in chapter II, eq. (2.43), the moment induced by the actuator at any point within its domain is

$$M(x,t) = EI \frac{\partial^2 w}{\partial x^2}(x,t) - K_D V_D(t) \quad x_i < x < x_j \quad (6.2)$$

where as before K_D represents the actuator material and dynamic coupling coefficients and $V_D(t)$ is the applied voltage to the transducer electrodes. When the sensor output is amplified and applied to the actuator without any filtering (rate feedback) $V_D(t)$ is

$$V_D(t) = G V_s(t) \quad (6.3)$$

where G represents the gain.

From eqs. (6.1), (6.2) and (6.3) the applied control moment becomes for $x_i < x < x_j$

$$M(x,t) = EI \frac{\partial^2 w}{\partial x^2}(x,t) - K_D G K_s \left(\left. \frac{\partial \dot{w}}{\partial x} \right|_{x=x_j} - \left. \frac{\partial \dot{w}}{\partial x} \right|_{x=x_i} \right) \quad (6.4)$$

As previously discussed in Chapter II, the distributed piezoceramic actuators can be modelled as external point couples applied at the ends of the domain x_i , x_j . Using the conventional Bernoulli-Euler beam analysis and assuming that the transducers add neither mass or stiffness to the beam the governing differential equation for the portion of the beam with the collocated transducers is

$$\frac{\partial^2}{\partial x^2} \left[EI \frac{\partial^2 w}{\partial x^2} (x, t) - K_D G K_s \left(\frac{\partial \dot{w}}{\partial x} \Big|_{x=x_j} - \frac{\partial \dot{w}}{\partial x} \Big|_{x=x_i} \right) \right] + \rho A \frac{\partial^2 w}{\partial t^2} = 0 \quad (6.5)$$

for $x_i < x < x_j$.

As noted in Chapter II, the sensor output is approximated by the difference of the angular velocities at the transducer ends, and is not a function of x . Therefore in eq. (6.5), the second spatial derivative makes this contribution vanish within the domain $x_i < x < x_j$. Nevertheless, the control moments are present in the moment equilibrium equations at the transducers's boundaries (ie., $x = x_i$ and $x = x_j$).

Let the domain of the beam be subdivided into three subdomains defined as follows.

$$w_1: 0 < x < x_i$$

$$w_2: x_i < x < x_j$$

$$w_3: x_j < x < L$$

The governing differential equation and boundary conditions for each subdomain are as follows

$$EI \frac{\partial^4 w_1}{\partial x^4} + \rho A \frac{\partial^2 w_1}{\partial t^2} = 0 \quad 0 < x < x_i \quad (6.6)$$

$$\text{at } x = 0, w_1 = \frac{\partial w_1}{\partial x} = 0$$

$$\text{at } x = x_i, w_1 = w_2$$

$$\frac{\partial w_1}{\partial x} = \frac{\partial w_2}{\partial x}$$

$$\frac{\partial^2 w_1}{\partial x^2} = \frac{\partial^2 w_2}{\partial x^2} - \bar{K} \left[\frac{\partial \dot{w}_2}{\partial x}(x_j, t) - \frac{\partial \dot{w}_2}{\partial x}(x_i, t) \right]$$

$$\frac{\partial^3 w_1}{\partial x^3} = \frac{\partial^3 w_2}{\partial x^3}$$

and

$$EI \frac{\partial^4 w_2}{\partial x^4} + \rho A \frac{\partial^2 w_2}{\partial t^2} = 0 \quad x_i < x < x_j$$

$$\text{at } x = x_j, w_2 = w_3$$

$$\frac{\partial w_2}{\partial x} = \frac{\partial w_3}{\partial x} \quad (6.7)$$

$$\frac{\partial^2 w_2}{\partial x^2} = \frac{\partial^2 w_3}{\partial x^2} + \bar{K} \left[\frac{\partial \dot{w}_2}{\partial x}(x_j, t) - \frac{\partial \dot{w}_2}{\partial x}(x_i, t) \right]$$

$$\frac{\partial^3 w_2}{\partial x^3} = \frac{\partial^3 w_3}{\partial x^3}$$

and

$$EI \frac{\partial^4 w_3}{\partial x^4} + \rho A \frac{\partial^2 w_3}{\partial t^2} = 0 \quad x_j < x < L \quad (6.8)$$

$$\text{at } x = L, \frac{\partial^2 w_3}{\partial x^2} = 0$$

$$\frac{\partial^3 w_3}{\partial x^3} = 0$$

where

$$\bar{K} = (K_D G K_S) / EI$$

Equations (6.6) through (6.8) represent the governing differential equation and appropriate boundary conditions for the structure in figure 6.1.

Equivalent Formulation

The problem of the active beam with piezoceramic sensors and actuators can also be formulated as follows.

$$\frac{\partial^2}{\partial x^2} \left(EI \frac{\partial^2 w}{\partial x^2} \right) + \rho A \frac{\partial^2 w}{\partial t^2} = \sum_{i=1}^n \delta(x-x_i) M_i(t) + \sum_{j=1}^n \delta(x-x_j) M_j(t) \quad (6.9)$$

where $M_i(t)$, $M_j(t)$ are the externally applied points control moments due to the piezoceramic actuators. From eqs. (6.2) and (6.4) these point moments are applied at the transducer boundaries as

$$M_i = K_D G K_S \left(\left. \frac{\partial w}{\partial x} \right|_{x=x_j} - \left. \frac{\partial w}{\partial x} \right|_{x=x_i} \right)$$

$$M_j = -K_D G K_s \left(\frac{\partial \dot{w}}{\partial x} \Big|_{x=x_j} - \frac{\partial \dot{w}}{\partial x} \Big|_{x=x_i} \right)$$

Then the expression for the bending moment at any point in the beam is

$$M(x,t) = EI \frac{\partial^2 w}{\partial x^2} \quad (6.10)$$

with the following boundary conditions

$$x = 0 \quad w = 0$$

$$\frac{\partial w}{\partial x} = 0$$

$$\text{at } x = L \quad \frac{\partial^2 w}{\partial x^2} = 0$$

$$\frac{\partial^3 w}{\partial x^3} = 0$$

and the strain energy of any point of the beam is

$$U = \frac{1}{2} \int_0^L EI \left(\frac{\partial^2 w}{\partial x^2} \right)^2 dx \quad (6.11)$$

The resultant effects of the piezoceramic actuators are treated as externally applied moments.

6.2. Distributed Parameter Control

To derive a control algorithm for the system, Lyapunov's second method⁶¹ was used. This method is based on the principle that if a system has an asymptotically stable equilibrium state, the stored energy

within system when displaced decays with increasing time until it assumes a minimum value . A direct relationship can also be shown between Lyapunov's second method and the generalized quadratic performance indices used in designing optimal control systems⁵⁴.

A functional is chosen which is the sum of the strain and kinetic energies of the free response motion of the beam⁷⁰.

$$F = \frac{1}{2} \int_0^L \left[EI \left(\frac{\partial^2 w}{\partial x^2} \right)^2 + \rho A \left(\frac{\partial w}{\partial t} \right)^2 \right] dx \quad (6.12)$$

and for the system described yields,

$$\begin{aligned} F = & \frac{1}{2} \int_0^{x_i} \left[EI \left(\frac{\partial^2 w_1}{\partial x^2} \right)^2 + \rho A \left(\frac{\partial w_1}{\partial t} \right)^2 \right] dx \\ & + \frac{1}{2} \int_{x_i}^{x_j} \left[EI \left(\frac{\partial^2 w_2}{\partial x^2} \right)^2 + \rho A \left(\frac{\partial w_2}{\partial t} \right)^2 \right] dx \\ & + \frac{1}{2} \int_{x_j}^L \left[EI \left(\frac{\partial^2 w_3}{\partial x^2} \right)^2 + \rho A \left(\frac{\partial w_3}{\partial t} \right)^2 \right] dx \end{aligned} \quad (6.13)$$

Using this functional, the objective will be to bring the system to equilibrium from a disturbed state in a minimum amount of time. Alternately, as discussed by Komkov⁷⁰, the objective will be to obtain a control actuating force which in this case is a control couple pair that has the characteristic of decreasing the total energy at a maximum rate for each time interval under consideration. Such a

control couple would be labeled "instantly optimal" by Komkov.

Therefore, maximization

of $\left(-\frac{\partial F}{\partial t}\right)$ is what is required.

The first derivative of eq. (6.13) is

$$\begin{aligned} \frac{\partial F}{\partial t} = & \int_0^{x_i} \left[EI \left(\frac{\partial^2 w_1}{\partial x^2} \right) \left(\frac{\partial^3 w_1}{\partial x^2 \partial t} \right) + \rho A \left(\frac{\partial w_1}{\partial t} \right) \left(\frac{\partial^2 w_1}{\partial t^2} \right) \right] dx \\ & + \int_{x_i}^{x_j} \left[EI \left(\frac{\partial^2 w_2}{\partial x^2} \right) \left(\frac{\partial^3 w_2}{\partial x^2 \partial t} \right) + \rho A \left(\frac{\partial w_2}{\partial t} \right) \left(\frac{\partial^2 w_2}{\partial t^2} \right) \right] dx \\ & + \int_{x_j}^L \left[EI \left(\frac{\partial^2 w_3}{\partial x^2} \right) \left(\frac{\partial^3 w_3}{\partial x^2 \partial t} \right) + \rho A \left(\frac{\partial w_3}{\partial t} \right) \left(\frac{\partial^2 w_3}{\partial t^2} \right) \right] dx \end{aligned} \quad (6.14)$$

Substituting eqs. (6.6), (6.8), and (6.10) into (6.14) yields

$$\begin{aligned} \frac{\partial F}{\partial t} = & EI \left[\int_0^{x_i} \left[\left(\frac{\partial^2 w_1}{\partial x^2} \right) \left(\frac{\partial^3 w_1}{\partial x^2 \partial t} \right) - \left(\frac{\partial w_1}{\partial t} \right) \left(\frac{\partial^4 w_1}{\partial x^4} \right) \right] dx \right. \\ & + \int_{x_i}^{x_j} \left[\left(\frac{\partial^2 w_2}{\partial x^2} \right) \left(\frac{\partial^3 w_2}{\partial x^2 \partial t} \right) - \left(\frac{\partial w_2}{\partial t} \right) \left(\frac{\partial^4 w_2}{\partial x^4} \right) \right] dx \end{aligned} \quad (6.15)$$

$$+ \int_{x_j}^L \left[\left(\frac{\partial^2 w_3}{\partial x^2} \right) \left(\frac{\partial^3 w_3}{\partial x^2 \partial t} \right) - \left(\frac{\partial w_3}{\partial t} \right) \left(\frac{\partial^4 w_3}{\partial x^4} \right) \right] dx$$

Integrating the second part of each integral twice yields

$$\frac{\partial F}{\partial t} = EI \left[\int_0^{x_i} \left(\frac{\partial^2 w_1}{\partial x^2} \right) \left(\frac{\partial^3 w_1}{\partial x^2 \partial t} \right) dx - \left(\frac{\partial w_1}{\partial t} \right) \left(\frac{\partial^3 w_1}{\partial x^3} \right) \right]_0^{x_i} \quad (6.15b)$$

$$+ \left(\frac{\partial^2 w_1}{\partial x \partial t} \right) \left(\frac{\partial^2 w_1}{\partial x^2} \right) \Big|_0^{x_i} - \int_0^{x_i} \left(\frac{\partial^2 w_1}{\partial x^2} \right) \left(\frac{\partial^3 w_1}{\partial x^2 \partial t} \right) dx$$

$$+ EI \left[\int_{x_i}^{x_j} \dots \right] + EI \left[\int_{x_j}^L \dots \right]$$

The integral in the brackets cancel yielding

$$\begin{aligned} \frac{\partial F}{\partial t} = EI & \left[\left(\frac{\partial w_1}{\partial t} \right) \left(\frac{\partial^3 w_1}{\partial x^3} \right) \right]_0^{x_i} + \left(\frac{\partial^2 w_1}{\partial x \partial t} \right) \left(\frac{\partial^3 w_1}{\partial x^2} \right) \Big|_0^{x_i} \\ & - \left(\frac{\partial w_2}{\partial t} \right) \left(\frac{\partial^3 w_2}{\partial x^3} \right) \Big|_{x_i}^{x_j} \end{aligned}$$

$$\begin{aligned}
& + \left(\frac{\partial^2 w_2}{\partial x \partial t} \right) \left(\frac{\partial^2 w_2}{\partial x^2} \right) \Big|_{x_i}^{x_j} - \left(\frac{\partial w_3}{\partial t} \right) \left(\frac{\partial^3 w_3}{\partial x^3} \right) \Big|_{x_j}^L \\
& + \left(\frac{\partial^2 w_3}{\partial x \partial t} \right) \left(\frac{\partial^2 w_3}{\partial x^2} \right) \Big|_{x_j}^L \quad (6.15c)
\end{aligned}$$

$$\frac{\partial F}{\partial t} = EI \left[\left(\frac{\partial^2 w_1}{\partial t \partial x} \right) \left(\frac{\partial^2 w_1}{\partial x^2} \right) + \left(\frac{\partial^2 w_2}{\partial t \partial x} \right) \left(\frac{\partial^2 w_2}{\partial x^2} \right) \right] \quad (6.16)$$

$$- \left(\frac{\partial^2 w_2}{\partial t \partial x} \right) \left(\frac{\partial^2 w_2}{\partial x^2} \right) - \left(\frac{\partial^2 w_3}{\partial t \partial x} \right) \left(\frac{\partial^2 w_3}{\partial x^2} \right) \Big]$$

Equation (6.16) can be further simplified using the moment boundary conditions at x_i and x_j giving

$$\frac{\partial F}{\partial t} = EI \left[\left(\frac{\partial^2 w_1}{\partial t \partial x} \right) \left(\frac{\partial^2 w_1}{\partial x^2} - \bar{K} \left(\frac{\partial^2 \dot{w}_2}{\partial x} - \frac{\partial^2 \dot{w}_2}{\partial x} \right) \right) \right] \quad (6.17)$$

$$- \left(\frac{\partial^2 w_2}{\partial t \partial x} \right) \left(\frac{\partial^2 w_2}{\partial x^2} \right) - \left(\frac{\partial^2 w_3}{\partial t \partial x} \right) \left(\frac{\partial^2 w_3}{\partial x^2} \right)$$

$$+ \left(\frac{\partial^2 w_2}{\partial t \partial x} \right) \left(\frac{\partial^2 w_3}{\partial x^2} + \bar{K} \left(\frac{\partial^2 \dot{w}_2}{\partial x} - \frac{\partial^2 \dot{w}_2}{\partial x} \right) \right) \Big]$$

Finally using the following boundary conditions at

$$x = x_i$$

$$\frac{\partial w_1}{\partial x} = \frac{\partial w_2}{\partial x}$$

$$\frac{\partial^2 w_1}{\partial x \partial t} = \frac{\partial^2 w_2}{\partial x \partial t}$$

and at

$$x = x_j$$

$$\frac{\partial w_2}{\partial x} = \frac{\partial w_3}{\partial x}$$

$$\frac{\partial^2 w_2}{\partial x \partial t} = \frac{\partial^2 w_3}{\partial x \partial t}$$

Equation (6.17) reduces to

$$\frac{\partial F}{\partial t} = K_D G K_S [\dot{\theta}(x_j, t) - \dot{\theta}(x_i, t)]^2 \quad (6.18)$$

where

$$\dot{\theta} = \frac{\partial^2 w}{\partial x \partial t}$$

Equation 6.18 represents the time derivative of F given the feedback voltage as

$$V_D(t) = G K_S [\dot{\theta}(x_j, t) - \dot{\theta}(x_i, t)] \quad (6.19)$$

where the difference in the angular velocity between the two nodes can either be negative or positive. For negative feedback the gain value G is set negative and eq. (6.19) is now equal to

$$V_D(t) = -GK_s[\dot{\theta}(x_j, t) - \dot{\theta}(x_i, t)] \quad (6.20)$$

To maximize $-(\partial F / \partial t)$ the control moments at x_i and x_j can be such that a maximum value is always applied opposite to the motion. This is done by setting $V_D(t)$ to

$$V_D(t) = -GK_s \text{sgn}[\dot{\theta}(x_j, t) - \dot{\theta}(x_i, t)] \quad (6.21)$$

where the $\text{sgn}(\)$ is either +1 or -1 depending on the sign of the difference in the brackets. Eq. (6.21) will be referred to as Lyapunov control and when eq. (6.20) is used it will be referred to as rate control.

This result is similar to the one obtain in reference 15, however there is no need to approximate the control law by using a linear velocity measurement as was done in reference 15 since it is directly measured by the piezoceramic sensor. Secondly, the derivation has been extended to sensors and actuators occupying a subdomain of the beam rather than the complete region.

6.3 Finite Difference Evaluation

To evaluate the performance the optimal control laws discussed in the previous section an explicit numerical finite difference technique⁵⁵ was used. Consider the structure shown in Figure 6.2, consisting of a distributed piezoceramic sensor on top and an actuator on the bottom. It is assumed that the transducers add neither mass nor stiffness to the structure.

The following analysis consists of two parts: open loop which considers only the beam with no active control and closed loop control.

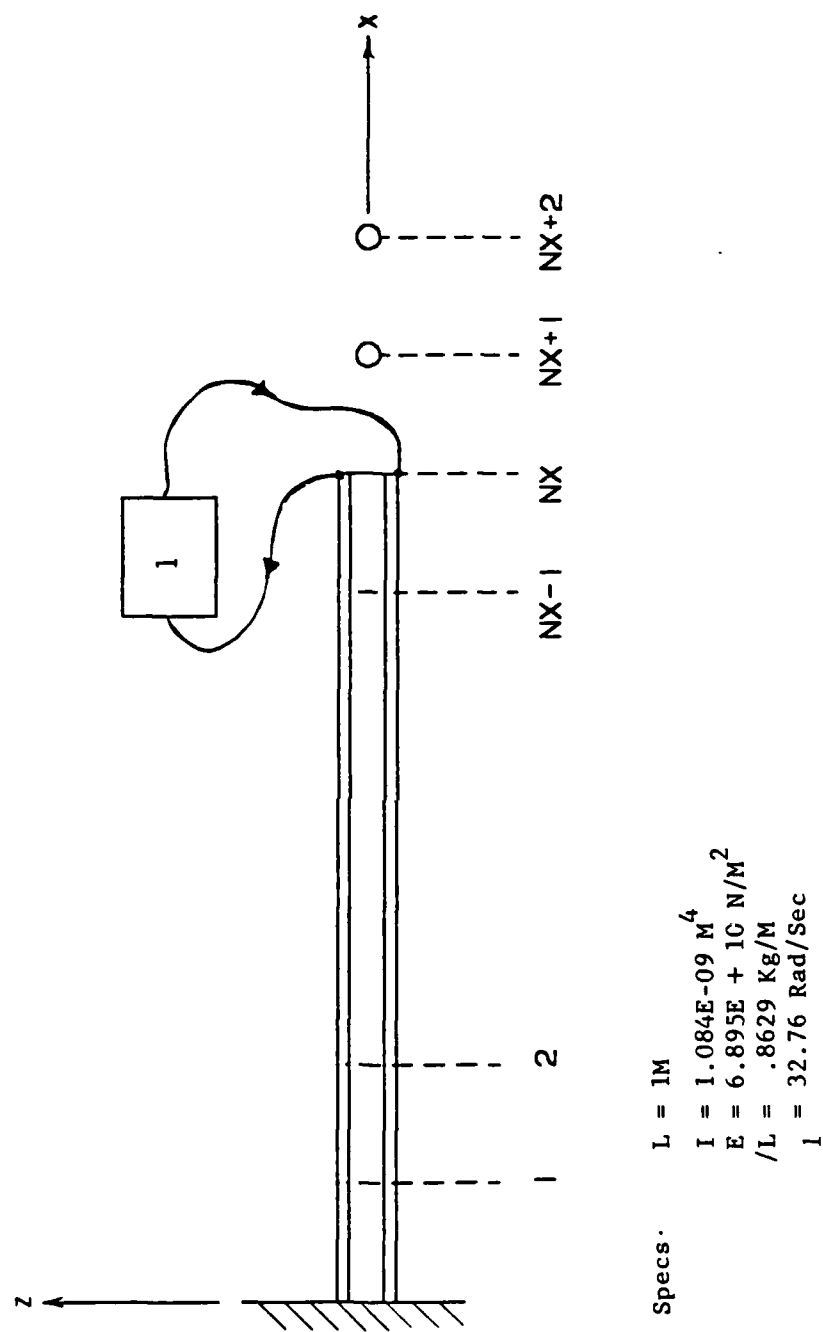


Figure 6-2 Finite Difference Model

In the open loop control the beam is given an initial velocity distribution and only internal viscous damping of the beam is modelled. In the closed loop control, active control is applied to the structure given initial velocity conditions. The output from the sensor is amplified and used to excite the actuator. Two approaches for modelling closed loop control have been examined.

Open Loop Model - No Active Control

The dynamic behavior of the elastic structure without active control is modelled as

$$\frac{\partial w}{\partial t} = v \quad (6.22)$$

$$\frac{\partial v}{\partial t} + \frac{c}{m} v = - \frac{1}{m} \frac{\partial^2 M}{\partial x^2} \quad (6.23)$$

$$\frac{\partial M}{\partial t} = EI \frac{\partial^2 v}{\partial x^2} \quad (6.24)$$

where w is the displacement, v is the velocity, M the moment and c is the viscous damping coefficient. The boundary conditions for the cantilever beam are

$$w(0,t) = 0, \quad \frac{\partial^2 w}{\partial x^2}(L,t) = 0$$

$$\frac{\partial w}{\partial x}(0,t) = 0, \quad \frac{\partial^3 w}{\partial x^3}(L,t) = 0$$

The beam has been discretized as shown in figure (6.2) for the development of the finite difference equations. The nodes $NX + 1$ and

$NX + 2$ are additional fictitious nodes necessary for computing the shear and moment boundary conditions at the end of the beam.

Finite differencing approximation of eqs. (6.22) to (6.24) are for node $I=2$ to NX considering the $n+1$ and n time step

$$(w^{n+1}(I) - w^n(I))/\Delta t = v^n(I) \quad (6.25)$$

$$\frac{v^{n+1}(I) - v^n(I)}{\Delta t} + \frac{c}{m} v^n(I) = - \frac{1}{m} \left[\frac{M^n(I+1) - 2M^n(I) + M^n(I-1)}{\Delta x^2} \right] \quad (6.26)$$

$$\frac{M^{n+1}(I) - M^n(I)}{\Delta t} = \frac{EI}{\Delta x^2} \left[v^{n+1}(I+1) - 2v^{n+1}(I) + v^{n+1}(I-1) \right] \quad (6.27)$$

For node 1 the following finite difference equation are applied

$$\begin{aligned} w^n(1) &= 0 \\ w^{n+1}(1) &= 0 \\ v^n(1) &= 0 \\ v^{n+1}(1) &= 0 \\ M^n(1) &= \frac{2EI}{\Delta x^2} w^n(2) \\ M^{n+1}(1) &= \frac{2EI}{\Delta x^2} w^{n+1}(2) \end{aligned} \quad (6.28)$$

To compute the moments from eq. (6.27) requires that the velocity of the additional fictitious points be known from the boundary conditions at $x=L$ (node NX). The finite difference equations can be

written as

$$w^{n+1}(NX+1) - 2w^{n+1}(NX) + w^{n+1}(NX-1) = 0 \quad (6.29)$$

$$M^{n+1}(NX+1) - M^{n+1}(NX) = 0 \quad (6.30)$$

Equation (6.30) can be expanded in terms of displacements and combined with (6.29) to form the matrix eq.

$$\begin{bmatrix} 1 & -3 \\ 0 & 1 \end{bmatrix} \begin{bmatrix} w^{n+1}(NX+2) \\ w^{n+1}(NX+1) \end{bmatrix} = \begin{bmatrix} -3 & 1 \\ 2 & -1 \end{bmatrix} \begin{bmatrix} w^{n+1}(NX) \\ w^{n+1}(NX-1) \end{bmatrix} \quad (6.31)$$

Solving for the displacement of the two fictitious points yields

$$w^{n+1}(NX+1) = 2w^{n+1}(NX) - w^{n+1}(NX-1) \quad (6.32)$$

$$w^{n+1}(NX+2) = 3w^{n+1}(NX) - 2w^{n+1}(NX+1) \quad (6.33)$$

The velocity at $NX+1$ can now be determined from

$$v^{n+1}(NX+1) = 1/\Delta t (w^{n+1}(NX+1) - w^n(NX+1)) \quad (6.34)$$

From eq. (6.26) the velocity for the $n+1$ time step is

$$v^{n+1}(I) = v^n(I) - \frac{\Delta t c}{m} v^n(I) - \frac{\Delta t}{m \Delta x^2} [M^n(I+1) - 2M^n(I) + M^n(I-1)] \quad (6.35)$$

and the moment from eq. (6.27)

$$M^{n+1}(I) = M^n(I) + \frac{\Delta t E I}{\Delta x^2} [v^{n+1}(I+1) - 2v^{n+1}(I) + v^{n+1}(I-1)] \quad (6.36)$$

The displacement can be computed for the $n+1$ time step from eq.

(6.25)

$$w^{n+1}(I) = w^n(I) + \Delta t v^n(I) \quad (6.37)$$

Finally, the following shear boundary condition is used to compute the velocity at the $n + 1$ time step for the NX node

$$M^{n+1}(NX+1) = M^{n+1}(NX-1) \quad (6.38)$$

To obtain only the first mode response of the beam the following velocity initial condition was chosen for the structure.

For node 1

$$v^n(1) = 0 \quad (6.39)$$

and for nodes 2 to NX

$$v^n(I) = AR[(.36705)[\sin\beta_1 x - \sinh\beta_1 x] - (.5)[\cos\beta_1 x - \cosh\beta_1 x]] \quad (6.40)$$

where AR is the desired maximum velocity at node NX (tip) and $\beta_1 = 1.8751$ for a cantilever beam of length one for the first mode. Given this velocity distribution the beam response contained only the first mode contribution.

The computation sequence was as follows:

- a) Initial conditions eqs. (6.39) and (6.40) are solved for time step 1 for nodes $I = 1$ to NX .
- b) For $I=2, NX$ velocity from eq. (6.35) and the displacement from eq. (6.37) are computed. Note, the moment for $I = 1$ to $NX + 1$ is zero for the initial time step.
- c) The displacement for the fictitious nodes and are computed from eqs. (6.32) and (6.33).
- d) For nodes $I = 2, NX$ the moment for time step $n + 1$ is obtained from eq. (6.36)

- e) The next time step is incremented and the procedure steps (b) to (e) are repeated.

Closed Loop Analysis

Two finite difference approximations have been examined to model the closed loop feedback response of the system under free vibration with a first mode velocity initial condition (eq. 6.39 and 6.40). For each approach, two different control laws eqs. (6.19) and (6.21) have been evaluated. The sensor output was described previously as

$$V_s(t) = K_s \left. \frac{\partial v}{\partial x} \right|_{x_i}^{x_j} \quad (6.41)$$

where $V_s(t)$ is the output voltage of the sensor and K_s is the sensor coupling coefficients.

First the sensor is assumed to cover a portion of a beam and is discretized as shown in figure 6.3. The sensor output is proportional to the difference in the angular velocity at its end points provided no nodal lines exist within its domain of the modal frequency of interest. The voltage output of the sensor can be approximated in a finite difference manner as

$$V_s^{n+1}(q) \approx \frac{[v^{n+1}(q+1) - v^{n+1}(q-1)]}{2\Delta x} - \frac{[v^{n+1}(p+1) - v^{n+1}(p-1)]}{2\Delta x} \quad (6.42)$$

where p and q are the beginning and end nodes of the sensor. When the sensor covers the entire surface of the cantilever beam the following additional condition is necessary at the node $p = 1$

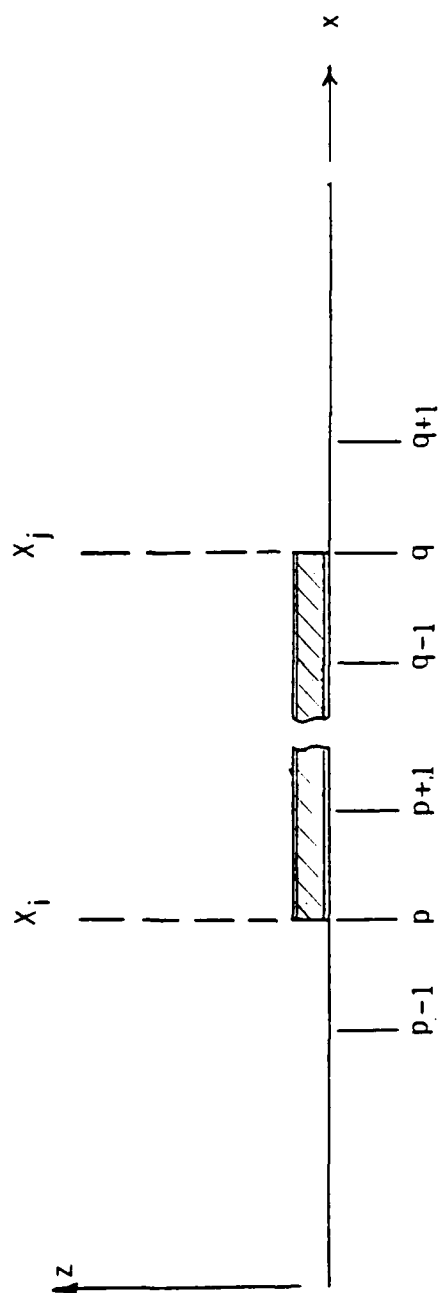


Figure 6-3 Sensor Finite Difference Model

$$v^{n+1}(p+1) - v^{n+1}(p-1) = 0 \quad (6.43)$$

The first method of solution (approach #1) for the active structure covered entirely by a piezoceramic sensor and actuator is as follows. The output sensor signal is conditioned by a controller (rate or Lyapunov) and fed back into the system to the beam tip as

$$M^{n+1}(NX, t) = K_D V_D(t) \quad (6.44)$$

In terms of finite difference eq. (5.44) can be approximated as

$$w^{n+1}(NX+1) - 2w^{n+1}(NX) + w^{n+1}(NX-1) = \frac{\Delta x^2 K_D V_D(t)}{EI} \quad (6.45)$$

with

$$M^{n+1}(NX+1) - M^{n+1}(NX) = 0 \quad (6.46)$$

form the shear condition at node NX. Combining eqs. (6.45) and (6.46) expended in term of displacements and solving for $w(NX+1)$ and $w(NX+2)$ yields

$$w^{n+1}(NX+1) = 2w^{n+1}(NX) - w^{n+1}(NX-1) + \frac{\Delta x^2}{EI} K_D V_D(t) \quad (6.47)$$

$$w^{n+1}(NX+2) = 3w^{n+1}(NX) - 2w^{n+1}(NX-1) + \frac{3\Delta x^3}{EI} K_D V_D(t) \quad (6.48)$$

In approach #1 the control was implemented through the displacement and velocity computations for the fictitious nodes $NX + 1$ and $NX + 2$. A more direct method (approach #2) is possible by using eq. (6.24) at node NX with active control. From eq. (6.2), eq. (6.24)

becomes

$$\frac{\partial M}{\partial t}(NX, t) = EI \frac{\partial^2 v}{\partial x^2}(NX, t) + K_D \dot{V}_D(t) \quad (6.49)$$

Approximated eq. (6.49) in finite difference yields

$$\begin{aligned} M^{n+1}(NX) = M^n(NX) + \frac{\Delta t EI}{\Delta x^2} [v^{n+1}(NX+1) - 2v^{n+1}(NX) \\ + v^{n+1}(NX-1)] + \Delta t K_D \frac{[V_D^{n+1} - V_D^n]}{\Delta t} \end{aligned} \quad (6.50)$$

Since,

$$V_D(t) = K_S V_S(t) \quad (6.51)$$

eq. (6.50) becomes

$$\begin{aligned} M^{n+1}(NX) = M^n(NX) + \frac{\Delta t EI}{\Delta x^2} [v^{n+1}(NX+1) - 2v^{n+1}(NX) + v^{n+1}(NX+1)] \\ + K_D K_S [V_S^{n+1} - V_S^n] \end{aligned} \quad (6.52)$$

For rate control for approach #1 and #2,

$$V_D = -K_S V_S(t) \quad (6.53)$$

The Lyapunov controller for approach #1 was

$$V_D = K_S \operatorname{sgn}(V_S) \text{ where } \operatorname{sgn}(V_S) = \begin{cases} 1.0, V_S < 0 \\ 0.0, V_S = 0 \\ -1.0, V_S > 0 \end{cases} \quad (6.54)$$

The Lyapunov controller for approach #2 was not pursued since it is a discontinuous function. Because of this limitation, approach #1 was used for comparison between the performance of the rate and Lyapunov control laws.

The computational sequence was as previously except that approach #1, step C now uses eqs. (6.47) and (6.48) and either eqs. (6.53) or (6.54) for control. For approach #2 step d, for $I = NX$ eq. (6.52) is used and eq. (6.53) for control.

Stability Analysis

To compute the desired response of the finite difference model of the active structure, a time step must be selected which insures numerical stability. To obtain a proper time step, a Von Neumann⁵⁵ stability analysis was used for the open loop control which in turn served as an upper limit to empirically find the proper time step for the closed loop control model.

The two coupled finite difference eqs. (6.26) and (6.27) can be written as

$$v_i^{n+1} = v_i^n - \frac{\Delta t}{M\Delta x^2} (M_{i+1}^n - 2M_i^n + M_{i-1}^n) \quad (6.55)$$

$$M_{i+1}^{n+1} = M_i^n - \frac{\Delta t EI}{\Delta x^2} (v_i^{n+1} - 2v_i^{n+1} + v_{i-1}^{n+1}) \quad (6.56)$$

where the subscript (i) represents the spatial node and the superscript (n) represents the time increment. The fourier component at each node is defined as

$$v_i^n = v^n e^{j\theta i} \quad (6.57)$$

$$M_i^n = M^n e^{j\theta i}$$

$$v_{i\pm 1}^{n+1} = v^{n+1} e^{j\theta(i\pm 1)}$$

$$M_{i\pm 1}^{n+1} = M^{n+1} e^{j\theta(i\pm 1)}$$

Using the relations given in eq. (6.57) , eqs. (6.55) and (6.56) become

$$v^{n+1} = v^n - \frac{\Delta t}{M\Delta x^2} M^n [e^{j\theta} - 2 + e^{-j\theta}] \quad (6.58)$$

$$M^{n+1} = M^n - \frac{\Delta t}{\Delta x^2} EI v^{n+1} [e^{j\theta} - 2 + e^{-j\theta}] \quad (6.59)$$

further by defining

$$p = 4 \sin^2 \theta / 2$$

Equations (6.58) and (6.59) can be further simplified and written in matrix form as

$$\begin{Bmatrix} v^{n+1} \\ M^{n+1} \end{Bmatrix} = \begin{bmatrix} 1 & \frac{\Delta t p}{M\Delta x^2} \\ -\frac{\Delta t EI p}{\Delta x^2 M} & 1 - \left(\frac{\Delta t}{\Delta x^2} \right)^2 \frac{EI}{M} p^2 \end{bmatrix} \quad (6.60)$$

The eigenvalues of the matrix given in eq. (6.60) can be obtained by solving the following determinant

$$\det \begin{vmatrix} 1 - \lambda & \frac{\Delta t p}{M\Delta x^2} p \\ -\frac{\Delta t EI p}{\Delta x^2 M} & \left(1 - \left(\frac{\Delta t}{\Delta x^2} \right)^2 \frac{EI}{M} p^2 \right) - \lambda \end{vmatrix} = 0 \quad (6.61)$$

The resulting quadratic equation becomes

$$\lambda^2 - \lambda(2 - A^*) + 1 = 0 \quad (6.62)$$

where

$$A^* = \left(\frac{\Delta t}{\Delta x} \right)^2 \frac{EI p^2}{M} \quad (6.63)$$

The roots of equation (6.62) are

$$\lambda = \frac{(2 - A^*)}{2} \pm \frac{1}{2} \sqrt{(2 - A^*)^2 - 4} \quad (6.64)$$

In order for the numerical computations to be stable the errors generated must not grow. It can be shown that this condition is satisfied when if

$$\lambda = 1 \text{ when } (2 - A^*)^2 = 4 \quad (6.65)$$

$$\lambda < 1 \text{ when } (2 - A^*)^2 < 4 \quad (6.66)$$

$$\lambda > 1 \text{ when } (2 - A^*)^2 > 4 \quad (6.67)$$

Using eqs. (6.63) and (6.65) or (6.66) the time increment can be directly computed given the spatial mesh size from

$$\Delta t \leq \frac{\beta_i^2 \Delta x^2}{2\omega_i} \quad (6.68)$$

where

ω_i is the highest natural frequency of interest,

β_i is the coefficient for the highest eigenvalue which is dependent on the boundary condition,

$P=1$ for the maximum value.

Closed loop stability was evaluated empirically and was an order of magnitude smaller than the open loop time step.

6.4 Discussion of Results

Optimal Control

A seven node model of the beam shown in figure 6.2 was used for evaluation of the different models and control laws.

To check on the accuracy of the active structure model for the first mode response the beam was given the first mode profile initial condition velocity with a maximum tip velocity of 1.0 m/sec and allowed to oscillate with no control. Figure 6.4 is a plot of the tip displacement versus time for this test. The first natural frequency of the model was approximately 5.2 Hz which is the theoretical natural frequency for the structure.

Figure 6.5 is the tip displacement response given the same initial condition of the beam with internal viscous value (c) of .002. Figures 6.6a and 6.6b are the feedback actuator signal and the tip displacement respectively using approach #1 for a feedback gain of .036. Figure 6.7 is the tip displacement using approach #2 for the same feedback gain and initial condition. Figures 6.6b and 6.7 are in close agreement.

Figures 6.8a and 6.8b are the same results employing the Lyapunov controller. The controller required a scaling value of the sensor maximum output for the given initial velocity condition. The Lyapunov controller was disengaged when the sensor output was less than node separation distance times the maximum initial tip velocity. Comparison

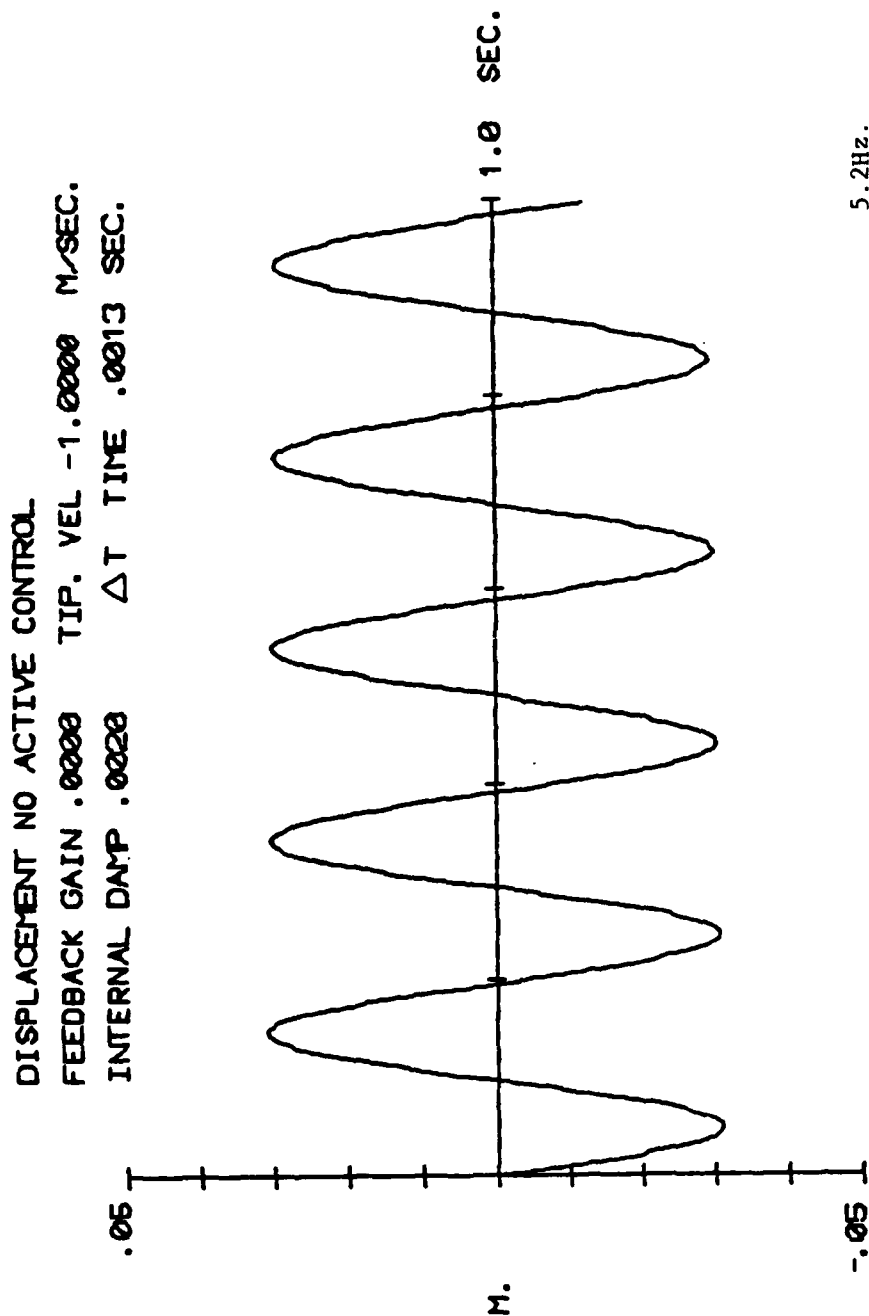


Figure 6-4 Free Displacement Response - No Control

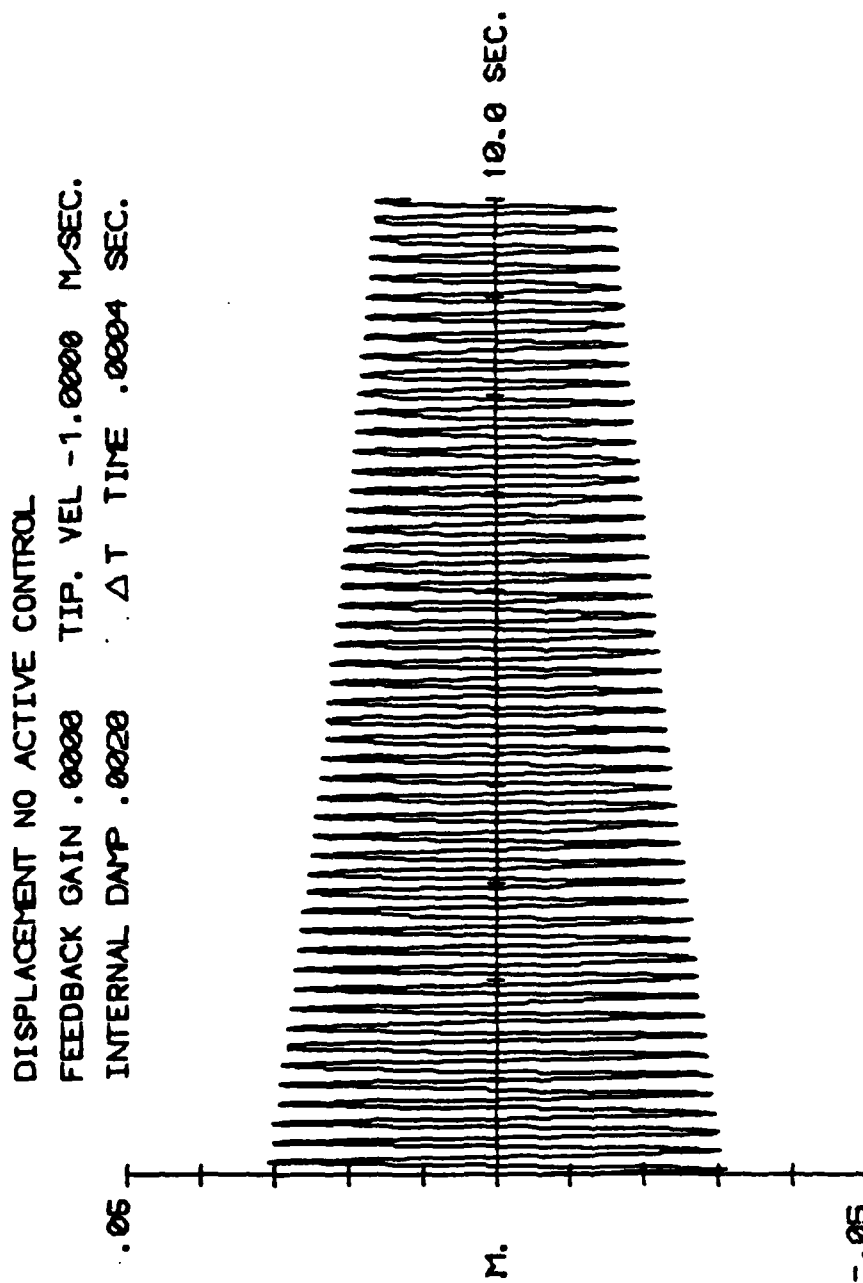


Figure 6-5 Free Displacement Response - No Active Control

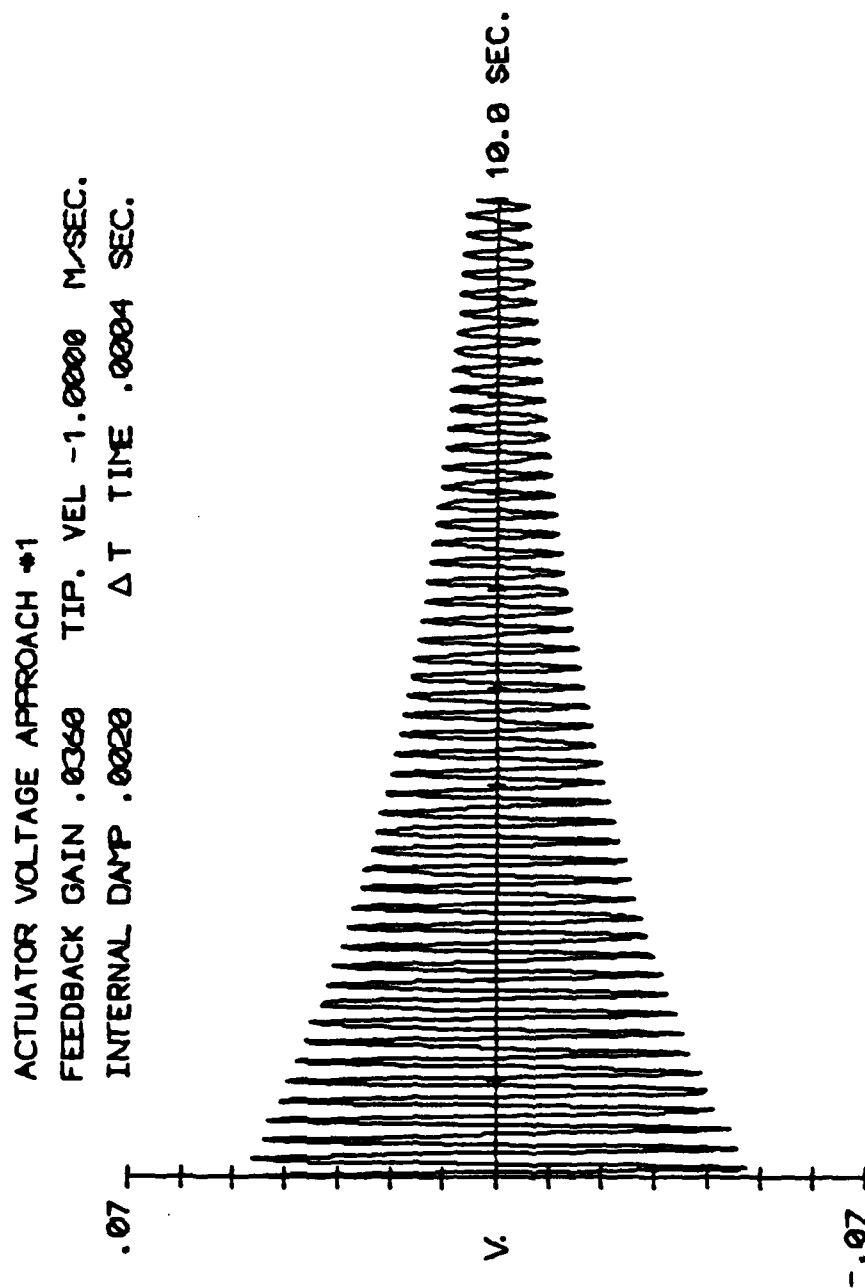


Figure 6-6a Active Rate Control Voltage - Approach #1

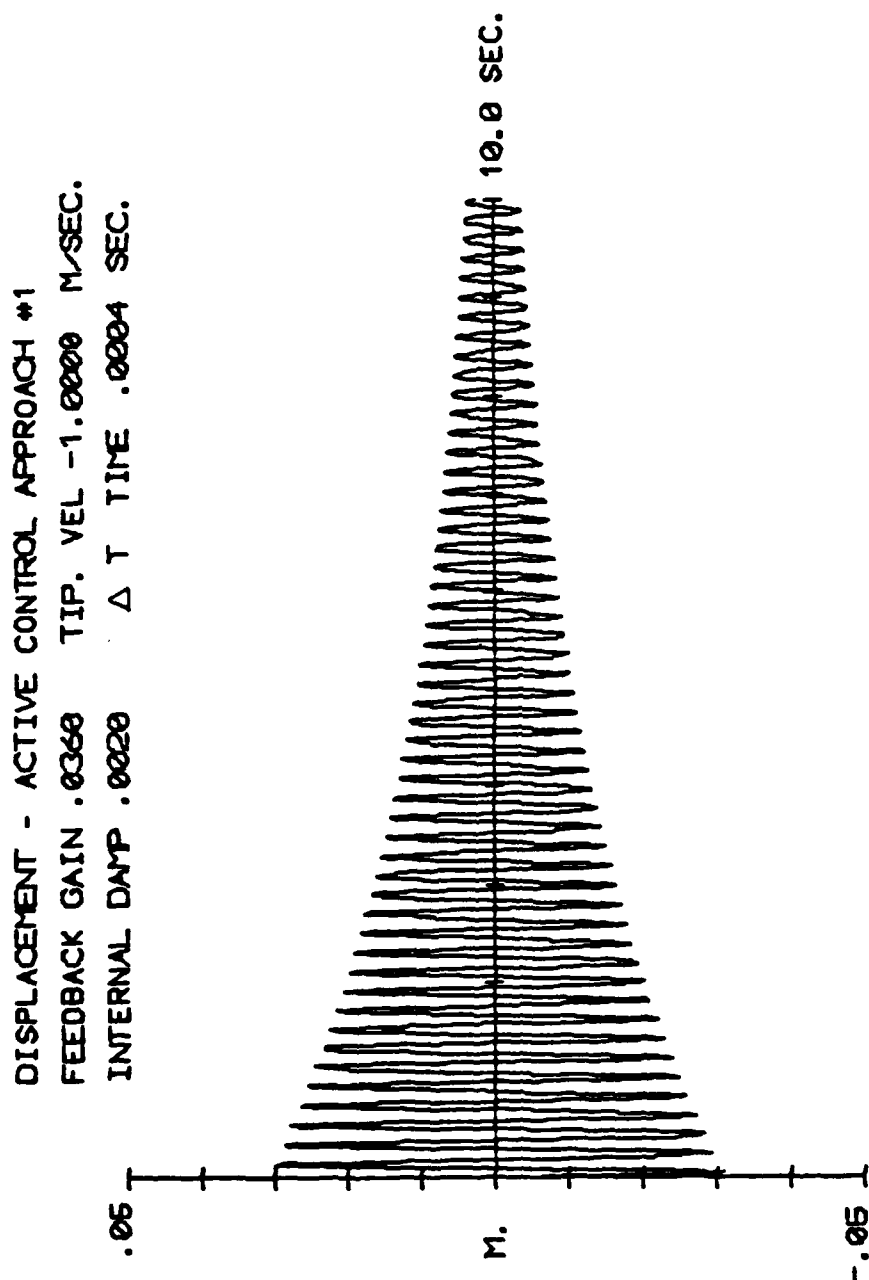


Figure 6-6b. Displacement Response - Active Control Approach #1

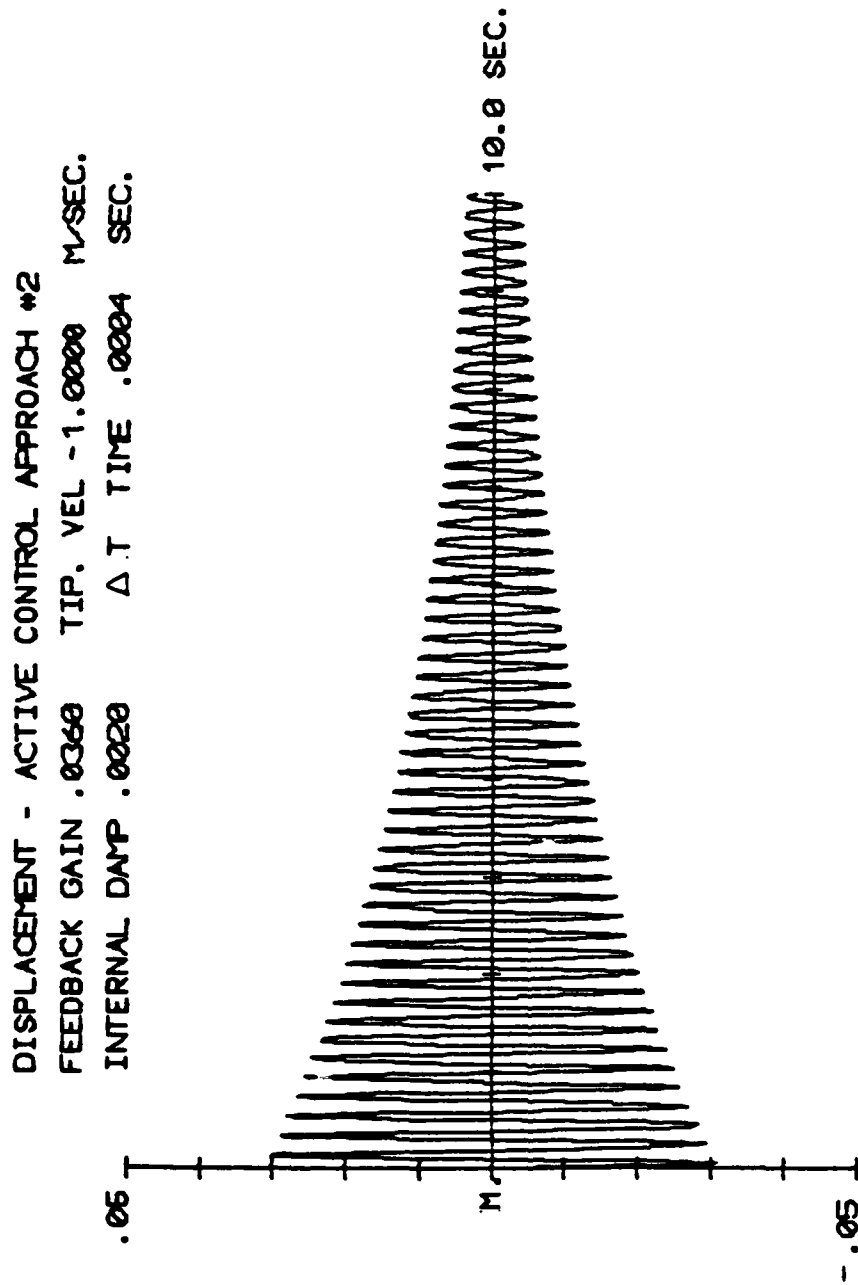


Figure 6-7 Displacement Response - Active Control - Approach #2

ACTUATOR VOLTAGE LYAPUNOV ACTIVE CONTROL
FEEDBACK GAIN .0360 TIP. VEL -1.0000 M/SEC.
INTERNAL DAMP .0020 ΔT TIME .0004 SEC.

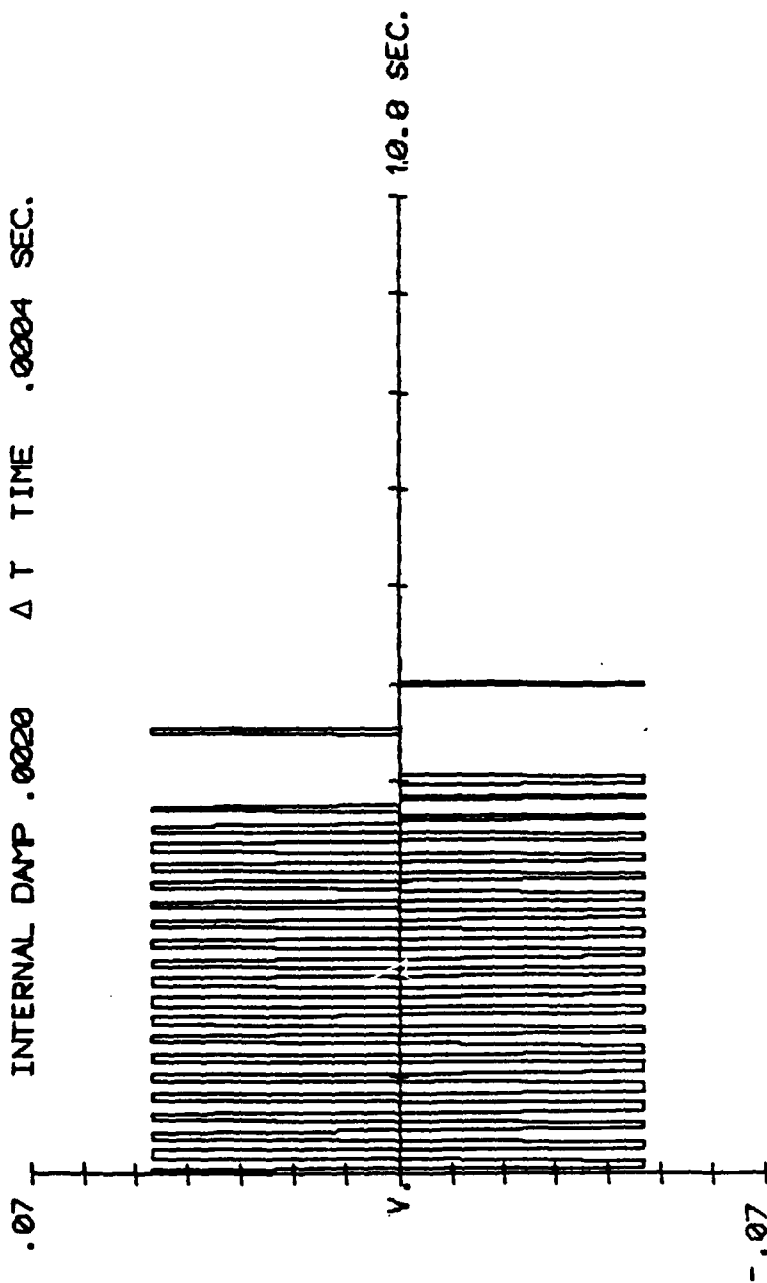


Figure 6-8a Active Lyapunov Control Voltage

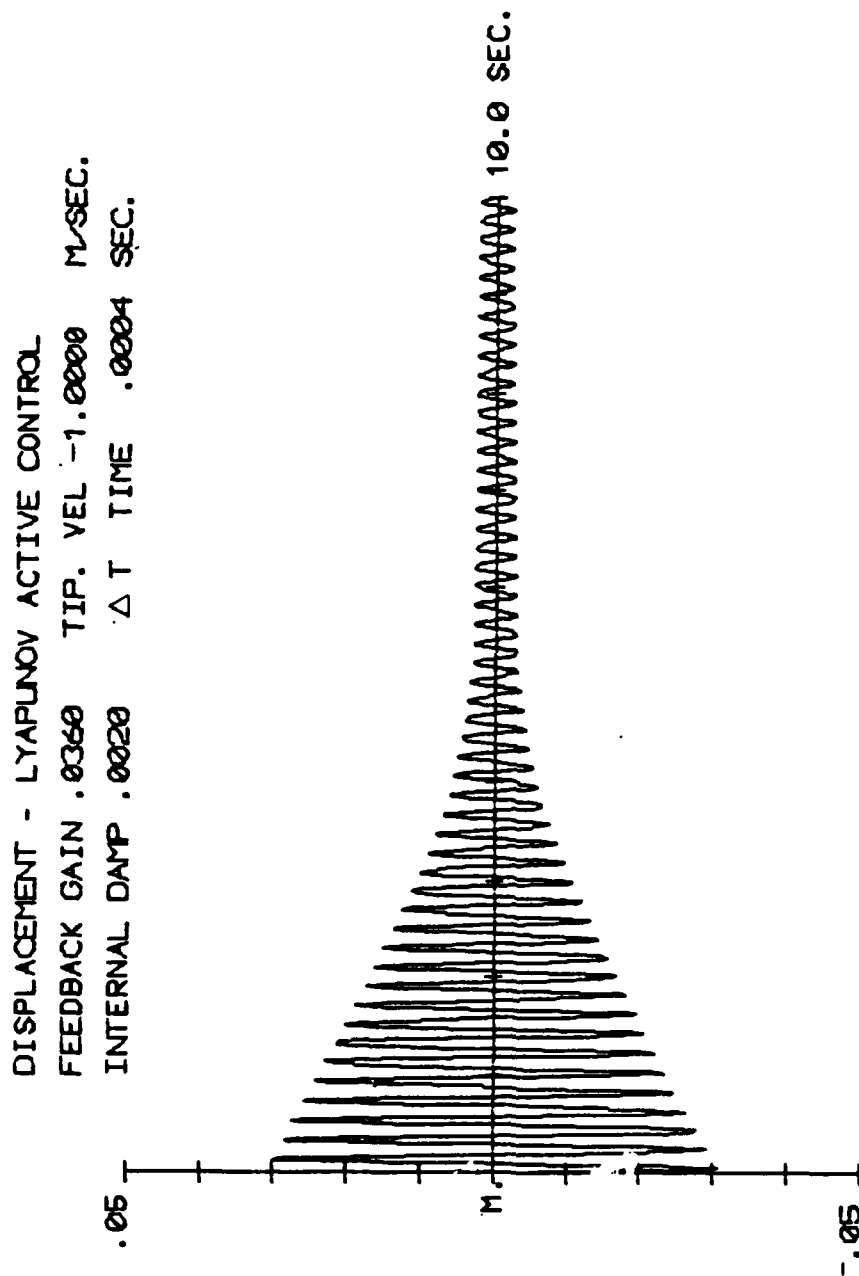


Figure 6-8b Displacement Response - Active Lyapunov Control

of figures 6.6b and 6.8b demonstrates the enhanced control performance of the Lyapunov controller using piezoceramic sensors and actuators.

Sensor Size Evaluation

Either type of feedback control is directly proportional to the input sensor signal. As the sensor size is decreased, the sensor output is reduced since the difference between the angular rate at the two end nodes decrease as the nodes approach each other. This can be demonstrated using approach #2 to evaluate various sensor sizes.

Figure 6.9 is the tip displacement of the rate feedback control using a .2 gain level with a sensor covering the entire upper surface. Using the same feedback gain level, the sensor was decrease 72% in size which resulted in a decrease in control performance as shown in figure 6.10. Figure 6.11 demonstrates that control can performance can be reclaimed by increasing the feedback gain by a factor of 18.5.

As mentioned in Chapter II, the sensor signal will degrade for frequencies at which there exist standing nodal line within its subdomain. As the sensor size is decreased, the bandwidth of the measured input to the control system is increased but at a cost of a decrease in the signal to noise of the input current signal. This is usually not a problem, though, since with the proper signal conditioning electronics the sensitivity of the piezoceramic dynamic strain gages is very high⁴².

Actuator Size Evaluation

A similar difficulty arises in the actuator. As noted before, the piezoceramic actuator is modelled as a system with dynamic opposing

DISP. APPR. #2 SENSOR 5-7
 FEEDBACK GAIN 3.7000 TIP. VEL -1.0000 M/SEC.
 INTERNAL DAMP .0020 DELTA TIME .00004 SEC.

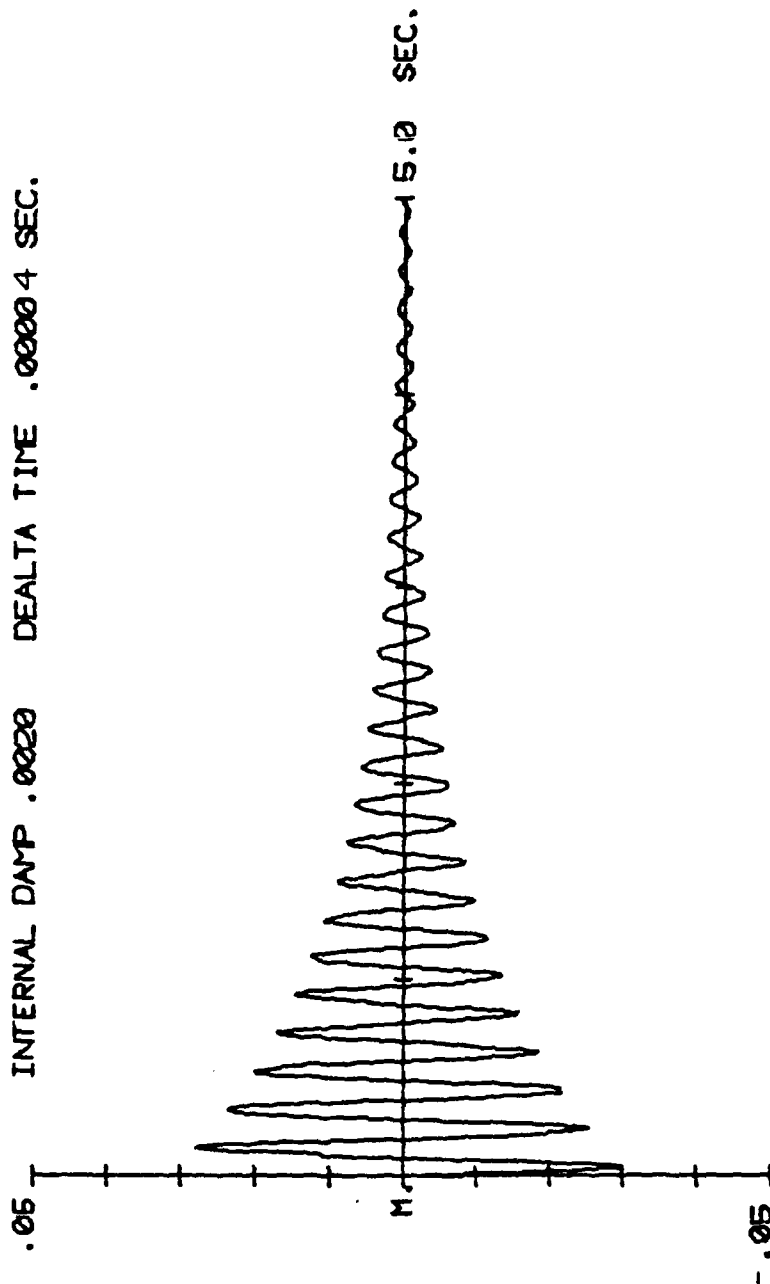


Figure 6-9 Displacement Response - Active Rate Control - Full Sensor - Nodes 1 to 7

DISP. APPR. #2 SENSOR 5-7
 FEEDBACK GAIN .2000 TIP. VEL -1.0000 M/SEC.
 INTERNAL DAMP .0020 Δ T. TIME .0004 SEC.

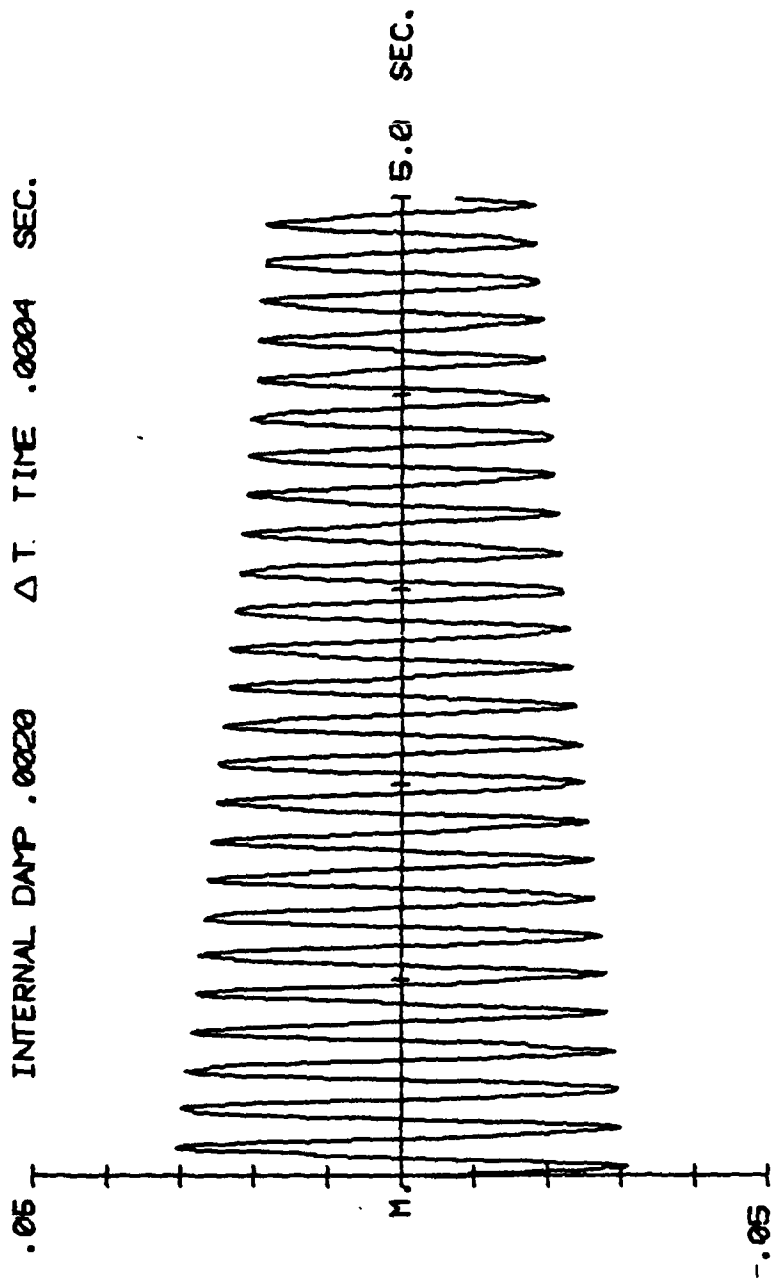


Figure 6-10 Displacement Response - Active Rate Control - Partial Sensor - Nodes 5-7

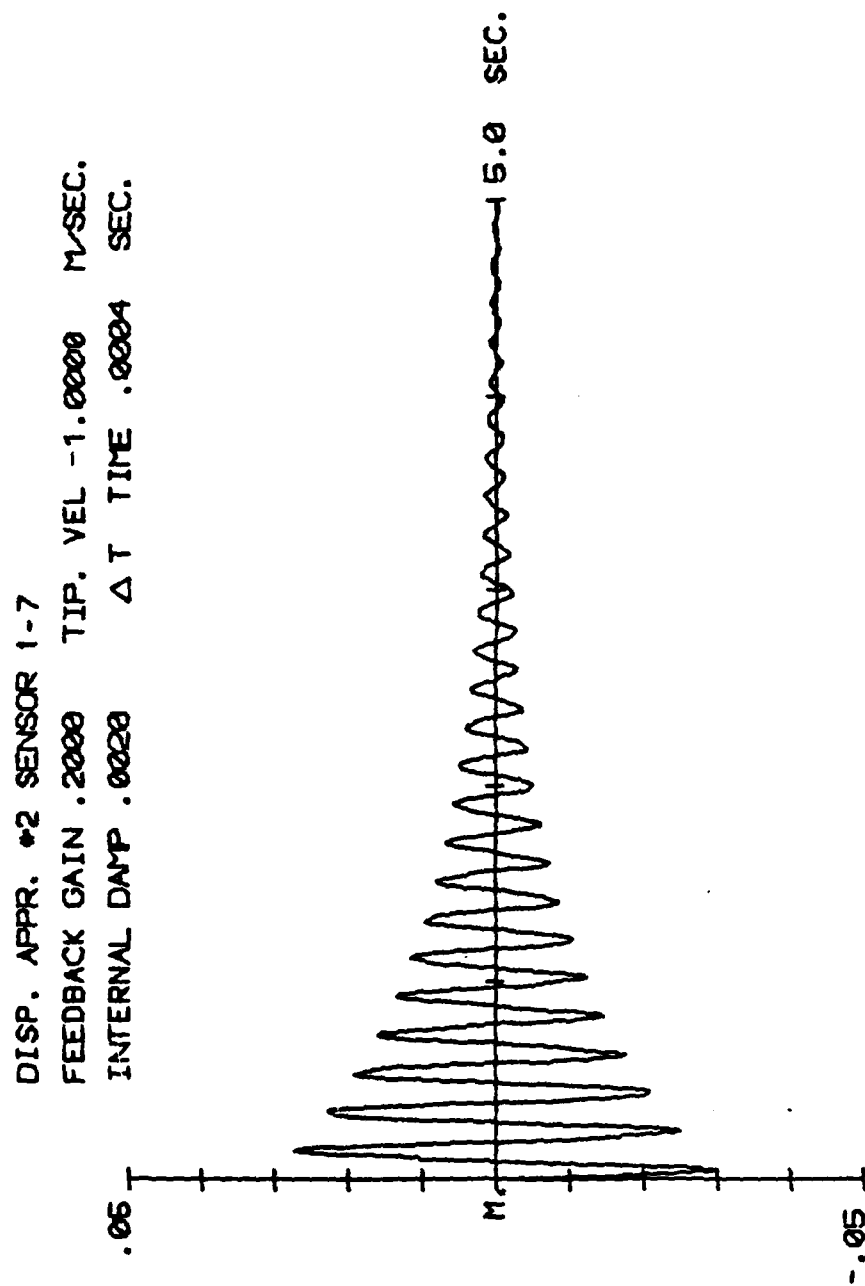


Figure 6-11 Displacement Response - Active Rate Control - Partial Sensor
 Nodes 5-7, Increase In Gain

couples at its boundaries. Should a transducer attempt to control a mode such that it results in at least one node line existing within its subdomain, a degradation of performance would result because of the phase difference due to the spatial distance between the two dynamic couples. To eliminate this problem requires proper conditioning of the control voltage to remove the signal contributions above the control bandwidth of the system.

Incorporation of the feedback filter electronic differential equation discussed in Chapter II into the finite difference scheme was attempted. Stability difficulties were encountered which were primarily due to the second order differentiation of the control signal. Finite difference evaluations were conducted on a model that contained an actuator which occupied a subdomain of the beam. Stability difficulties were again encountered. The primary suspected problem was the inability to adequately model the point nodal moments in the domain of the beam.

CHAPTER VII

ACTIVE CONTROL EXPERIMENTS

Throughout out this research effort, a variety of active control or "electronic damping" experiments were undertaken. The experiments consisted primarily of investigating the behavior and performance of the individual unimorph transducers or analysis of the behavior of an active structural system. The experiments were inherently flexible due to the adjustability of the feedback control electronics, to explore both rate and modal feedback system stability and performance issues.

7.1. Experimental Configuration

A typical test configuration is shown in figure 7.1. A test structure was chosen and unimorph transducers bonded to select locations. In all cases a cantilever beam was the test structure. Depending on the desired test, transducers served as either sensors or actuators. The output of a sensor was conditioned by the feedback electronics which in turn supplied a high voltage control signal to an actuator. For the tests conducted in this research one sensor controlled an individual actuator. It is possible to control more than one actuator with a single sensor but unfortunately the prototype electronics were electrically unstable in this type of configuration.

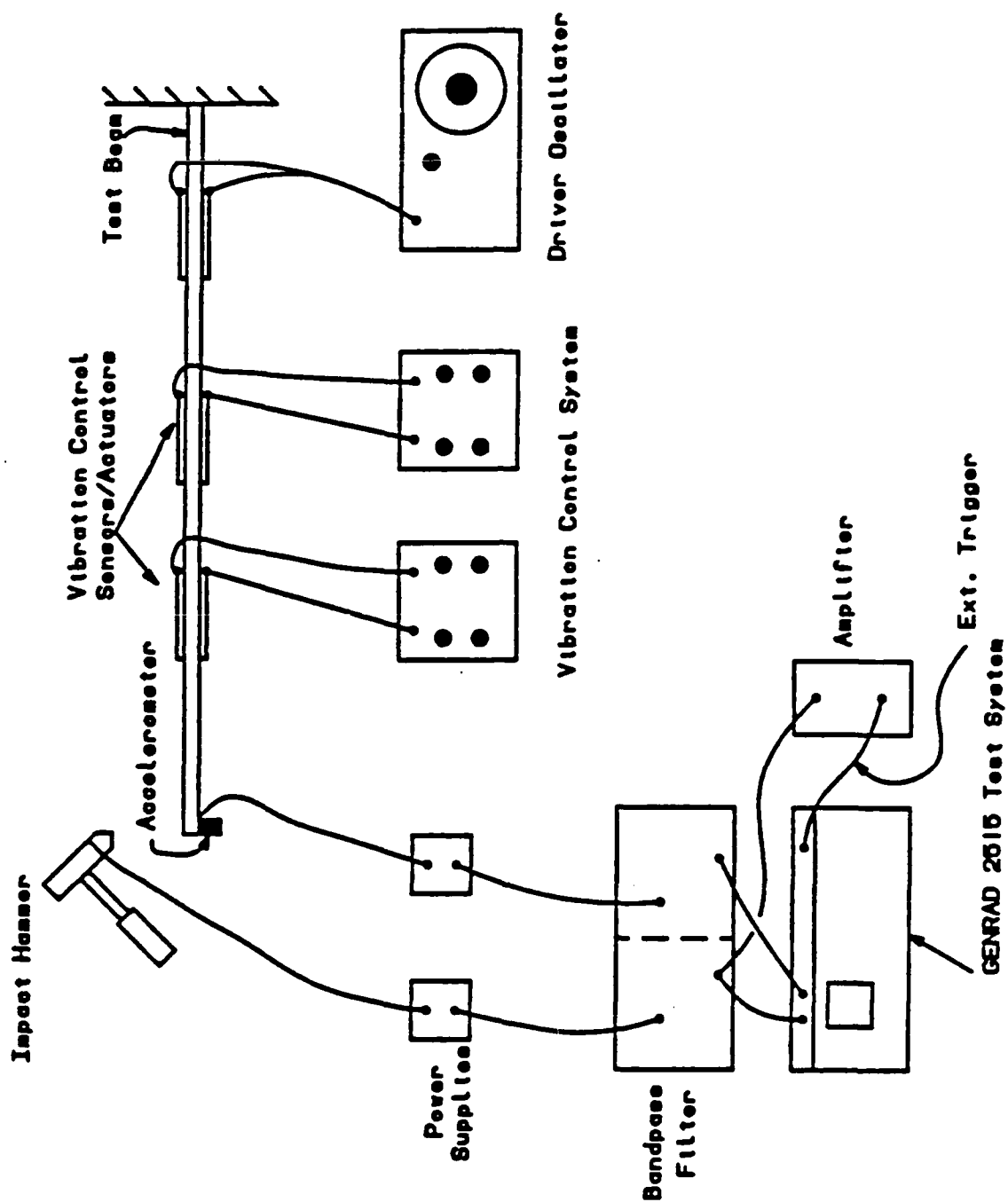


Figure 7-1 Typical Test Configuration Setup

The feedback electronics were specifically designed to be used with piezoceramic transducers. Each unit basically consisted of a preamplifier, filter and high power output section. The preamplifier converted the current output of the sensor to a voltage signal which was conditioned by a bandpass filter whose center frequency and Q were adjustable. The conditioned signal's phase could also be adjusted. Finally the low voltage signal was amplified and applied to an actuator. Details of the different experimental configurations and the feedback control electronics is provided for in appendix D.

7.2. Modal Control Experiments

The experimental setup provided an ideal platform to examine some of the problems associated with the application of modern control theory to flexible structures. A major difficulty when this is attempted is that flexible structures are distributed parameter systems. According to Balas³⁸ the fundamental problem of feedback control of flexible systems is meeting the requirement of precise control of a large dimensional system with a much smaller dimensional controller. The approach used by most investigators reduces to the problem of modal control³⁹. Modal control as defined by Simon⁴⁰ as a method of control which changes the eigenvalues and eigenvectors of the system matrix to achieve desired control objectives.

When only a limited number of modes of the infinite number of modes of the actual structure are controlled observation spillover

usually occurs. Observer spillover^{40,41} results when a finite dimensional controller attempts to control an infinite dimension system such as an active structure. At some stage the sensors of the system will sense the modes of the system that are not accounted in the analysis (residual). This will lead to system instabilities observed when the narrow bandpass filters are bypassed. Control spillover occurs when in the process of controlling the desired modes the uncontrolled modes are excited.

According to Balas³⁸ control spillover only causes a degradation of system control performance while the observer spillover can make the system go unstable. Meirovitch⁵⁷ has shown that even a small amount of structural damping in the uncontrolled modes has the potential to eliminate the instability caused by observer spillover.

The use of the active control feedback with narrow bandpass filters reduces the effect of the residual modes on the control system. Since piezoceramic unimorph sensors are sensitive to very small dynamic strains⁴² they tend to be overly affected by modes outside of the control bandwidth and thus required the bandpass filters.

Examples of theoretically and experimental results in modal space control are presented by Meirovitch³⁹, Hallauer^{43,44} just to name a few. In these works, modal space control has been accomplished by using fewer sensors and actuators than control modes and employing narrow band filters similar to the ones used in these experiments.

To initiate rate control the bandpass filter could be bypassed. When this was done experimentally, as expected, the control feedback

system went unstable. Therefore, all the experiments used the bandpass filters. Since the filters only had a Q of 20 instabilities would occur if the current to voltage gain was increased passed 10^7 .

To measure and reduce the dynamic response data a 16 channel Computer Aided Test System (Genrad Model 2515) was used. This system had spectral, frequency response and modal analysis capabilities.

7.3. Test Procedures

The primary form of testing used to evaluate the modal control performance was impact response transfer function analysis. The test procedure followed consisted primarily of measuring the structure's response from a stationary accelerometer while impacting the structure with a force gage hammer at selected locations.

From this data changes in the system's eigenvalues and eigenvectors could be extracted using the various methods provided for by the SDRC Modal Plus software⁵¹. Prior to evaluating the system's response due to impact excitation, the center frequency of the active control electronic had to be tuned. Setting the center frequency at measured frequencies of the structure did not provide maximum modal control and an iterative procedure was required to optimize the tuning of the filters. When the gain was changed the filters required retuning to maintain maximum performance.

7.4. Experimental Results

Figure 7.2 is typical of the data obtained during the experimental investigation. Shown in the figure is multimode control of the first and second bending modes of a cantilever beam at two different gain levels using two collocated pairs of piezoceramic sensor and actuators. The low gain results are at the lowest gain settings of the feedback electronics. Both high Q resonant peaks are reduced with the relative change greater in the higher mode. As the gain is increased to just below the point at which the system goes unstable the peaks are further reduced. At this level the first mode is also beginning to split. Appendix D provides the actual numerical data for these particular results.

The results from initial tests conducted on a steel beam (Beam #1 appendix D) were used primarily in a preliminary study of identifying the changes in the damping matrix of a discrete model of the test cantilever beam. These results are detailed in reference 77 and the change of selected damping matrix elements were determined to be proportional to the gain for both single and multimode control.

The next series of tests examined collocated and non collocated control of a aluminum beam (Beam #2 appendix D) and these results were discussed in chapter IV. The last series of tests were conducted on the smallest test structure (Beam #3, appendix D) to identify the dynamic coupling coefficients of the unimorph transducers. The results of these efforts is presented in chapter III.

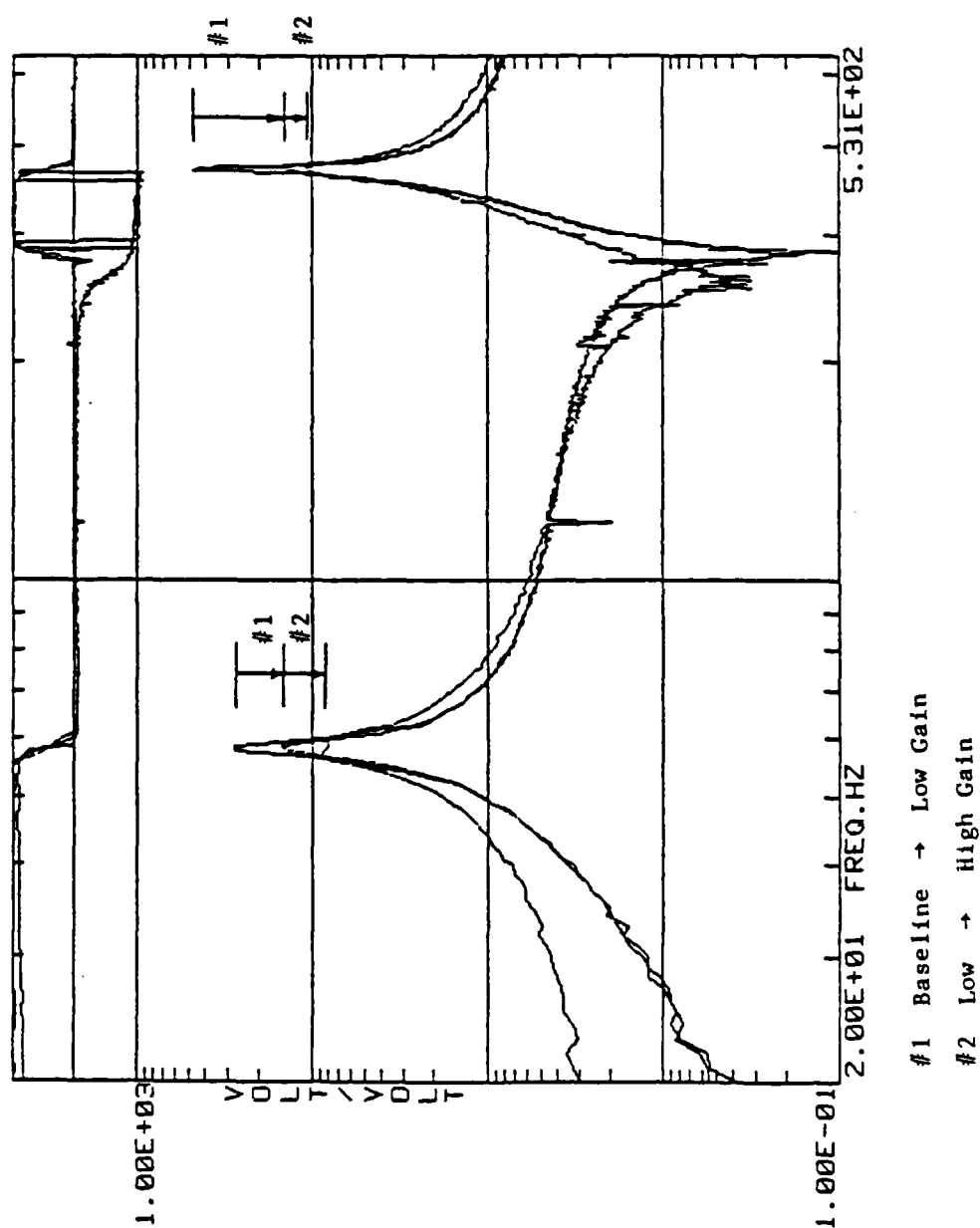


Figure 7-2 Baseline, Low And High Gain Comparisons

CHAPTER VIII.

CONCLUSIONS AND RECOMMENDATIONS

The potential of using piezoceramic transducers for active control of structures has been demonstrated in the past by a variety of experiments. Based on the results of these efforts the objective of this research has been to understand how the use of piezoceramic sensors and actuators can actively control a flexible structure by developing suitable models and conducting experimental investigations.

A finite element model of the active structure was developed from the basic piezoceramic constitutive equations for a beam element with a piezoceramic unimorph sensor and actuator bonded to it. From this model the current output of the piezoceramic sensor was determined to be proportional to the integral of the strain rate over the element length. The effect of the actuator was approximated by a pair of opposing couples applied at the element modal points which were proportional to the applied actuator voltage. Furthermore, it was also established that no collocated sensing and actuating transducers resulted in a non self adjoint system.

Using a frequency formulation of the coupled differential equations of the active structure, experimental data and least squares type of identification routines, the identification of the dynamic coupling coefficients for a cantilever beam subjected to multimode

control was accomplished. Improvement in the values of the identified coefficients is possible based on the accuracy of the baseline and active control feedback electronics models.

A study was undertaken to examine the changes in the active structure's modes when controlled with non collocated transducers. Experimental results verified the non self adjointness of the system due to non collocated control and a procedure was developed to identify the biorthogonal eigenvectors from experimental residue data. Preliminary verification of the modal post processing routine was accomplished using experimental data.

A model of a collocated piezoceramic sensor and actuator occupying a subdomain of a cantilever was developed and by a minimization of a selected quadratic functional an optimal control law was derived. This control law was evaluated for an active structure consisting of a sensor and actuator occupying the whole domain of the beam using a finite difference approach. The results of the analysis indicated that a step Lyapunov optimal control law surpassed a rate control law in reducing the response of the beam in the shortest time. Also, a study was undertaken to evaluate the control performance of the system when the sensors occupy a subdomain of the structure. Results of this study indicated that through the sensor output decreases with sensor size, control can be regained with an increase in feedback gain.

Control optimization of an active structure using a limited output state feedback control was investigated using piezoceramic

sensors and actuators. A discrete model of a cantilever structure with multimode control was formulated in state space and the output feedback control gain matrix optimized. The results indicated that at the optimum gain distribution the negative real part of the eigenvalues is increased.

The following recommendations are presented for additional research into the area of the active control of structures:

a) An extension of the finite element active beam element to structures of higher order such as plates and shallow shells should be undertaken. This will permit greater flexibility in modelling structures such as membrane optics or large dish antenna type structures.

b) Enhancement of the dynamic coupling results should be explored by using an enhanced structure and electronic feedback models and identification procedures.

c) Additional experimental work should be performed on non collocated control from both a system stability point of view as well as identification of biorthogonal modal description of the controlled response of simple structures.

d) The use of a higher order control compensator incorporating narrow band filtering characteristics should be evaluated for optimum pole placement and gain distribution for multimode control of structure using a limited state feedback approach.

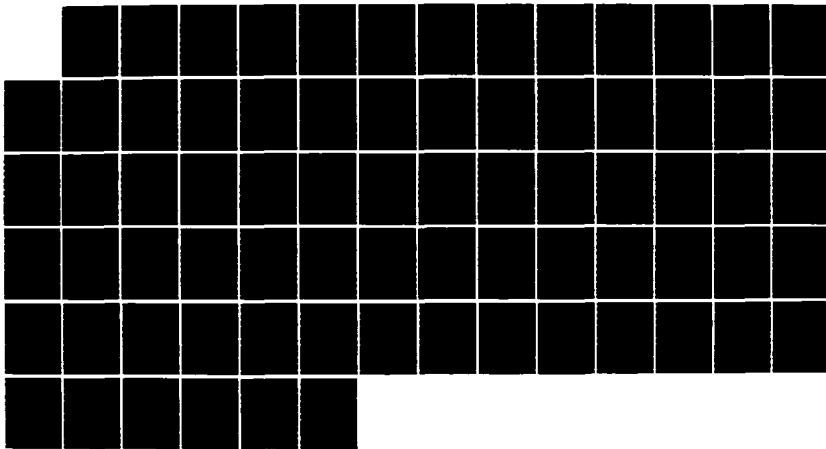
AD-A172 994

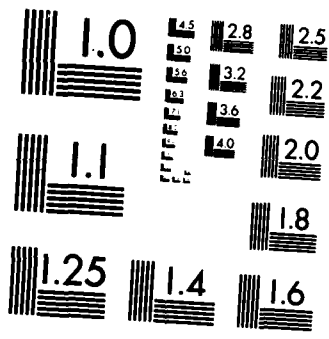
VIBRATION CONTROL OF FLEXIBLE STRUCTURE USING
PIEZOELECTRIC DEVICES AS SENSORS AND ACTUATORS(U) AIR
FORCE INST OF TECH WRIGHT-PATTERSON AFB OH M M OBAL
SEP 86 AFIT/CI/NR-86-176D F/G 9/5

3/3

UNCLASSIFIED

NL





MICROCOPY RESOLUTION TEST CHART
NATIONAL BUREAU OF STANDARDS 1963-A

APPENDIX A

Piezoelectric Constitutive Equations

Derivation of the piezoceramic constitutive equations has been done by many investigators^{8,62,64 & 74} but is repeated here for completeness. The approach commonly used and followed here is:

a) Derivation of Poynting equation from Maxwell's electromagnetic theory which is an electromagnetic statement of the principle of the conservation of energy⁴⁹.

b) Using a modified form of Poynting equation to develop the first law of thermodynamics for a piezoelectric medium^{8,27,49}.

c) Combining this law with crystallography of piezoceramic materials to construct a set of constitutive equations for piezoceramic transducers^{8,62}.

Derivation of Poynting Equation.

Maxwell's equations in MKS Units are:

$$\nabla \times \vec{H} = \vec{D} + \vec{J} \quad (\text{Ampere's Circuital Law}) \quad (\text{A-1})$$

$$\nabla \times \vec{E} = -\vec{B} \quad (\text{Faraday's Law}) \quad (\text{A-2})$$

$$\nabla \cdot \vec{B} = 0 \quad (\text{Gauss's Law for Magnetic Field}) \quad (\text{A-3})$$

$$\nabla \cdot \vec{D} = \rho_e \quad (\text{Gauss's Law for Elect. Field}) \quad (\text{A-4})$$

with

$$\vec{D} = \epsilon_0 \vec{E} + \vec{P} \quad (\text{A-5})$$

$$\vec{H} = \mu_0 \vec{B} - \vec{M} \quad (A-6)$$

where

UNITS

ρ_e = charge density	[C/M]
E = electric field intensity*	[N/C], [V/M]
H = magnetic field intensity*	[A/M]
J = current density	[A/M ²], [C/S M ²]
D = electric flux density*	[C/M ²]
B = magnetic flux density*	[N S/C M]
P = polarized vector	[C/M ²]
M = magnetized vector	[A/M]
ϵ_0 = permittivity of a vacuum	
μ_0 = magnetic constant	

and * signifies a vector field. The polarized vector is a measure of the electric dipole per unit volume and the magnetized vector is a measure of the magnetic dipole per unit volume.

Using the vector identity

$$\nabla \cdot (\vec{A} \times \vec{B}) = \vec{B} \cdot \nabla \times \vec{A} - \vec{A} \cdot \nabla \times \vec{B} \quad (A-7)$$

and equations (A-1) and (A-2), the differential form of Poynting's equation is derived as follows

$$\nabla \cdot (\vec{E} \times \vec{H}) = \vec{H} \cdot (\nabla \times \vec{E}) - \vec{E} \cdot (\nabla \times \vec{H}) \quad (A-8)$$

$$\nabla \cdot (\vec{E} \times \vec{H}) = -\vec{H} \cdot \vec{B} - \vec{E} \cdot (\vec{J} \times \vec{D}) \quad (A-9)$$

therefore

$$-\nabla \cdot (\vec{E} \times \vec{H}) = \vec{E} \cdot \vec{J} + (\vec{E} \cdot \vec{D} + \vec{H} \cdot \vec{B}) \quad (\text{A-10})$$

The integral form of equation (A-10) is obtained by integration over a volume v bounded by the closed surface s .

$$-\int_V \nabla \cdot (\vec{E} \times \vec{H}) dV = \int_V \vec{E} \cdot \vec{J} dV + \int_V (\vec{E} \cdot \vec{D} + \vec{H} \cdot \vec{B}) dV \quad (\text{A-11})$$

Using the divergence theorem

$$\int_V \nabla \cdot \vec{A} dV = \oint_S \vec{A} \cdot \vec{n} da \quad (\text{A-12})$$

for the left side of equation (A-11) yields

$$\oint_S (\vec{E} \times \vec{H}) \cdot \vec{n} da = \int_V \vec{E} \cdot \vec{J} dV + \int_V (\vec{E} \cdot \vec{D} + \vec{H} \cdot \vec{B}) dV \quad (\text{A-13})$$

Letting

$$\vec{h} = \vec{E} \times \vec{H} \quad (\text{A-14})$$

and

$$U_e = (\vec{E} \cdot \vec{D} + \vec{H} \cdot \vec{B})$$

equation (A-13) is rewritten as

$$\frac{\partial}{\partial t} \int_V U_e dV = - \oint_S \vec{n} \cdot \vec{h} dS - \int_V \vec{E} \cdot \vec{J} dV \quad (\text{A-15})$$

Equation (A-15) is the integral form of Poynting's theorem and with units $[N \text{ M/S}] = [J/S] = [\text{WATTS}]$. This theorem is a power theorem representing the electromagnetic statement of the principle of the conservation of energy. Each part of equation (A-15) is defined as:

$$\left[\begin{array}{l} \text{Rate of change} \\ \text{of energy} \\ \text{stored in} \\ \text{the volume} \end{array} \right] = \left[\begin{array}{l} \text{Net inward power} \\ \text{flow through a} \\ \text{closed surface} \end{array} \right] + \left[\begin{array}{l} \text{Power imparted to} \\ \text{charges in the} \\ \text{volume enclosed by the} \\ \text{surface (Joule heat)} \end{array} \right]$$

This theorem is also expressed in a different format using vector and scalar potentials A [Weber/Meter] and γ [Volt]. The vector field A and a scalar field are defined from the knowledge of J and then the field vectors D, E, B and H are computed from A and α . The steps necessary to obtain Maxwell's and Poynting's equations in terms of electromagnetic potentials is presented in reference 49.

Expressed in terms of these potentials and in tensor notation

$$\int_V (E_i \dot{D}_i + H_i \dot{B}_i) dV = - \oint n_i [\gamma (\dot{D}_i + J_i) - e_{ijk} \dot{A} H_k] dS - \int_V E_i J_i dV \quad (\text{A-16})$$

with the Poynting vector defined as

$$h = \gamma (\dot{D}_i + J_i) - e_{ijk} \dot{A} H_k \quad (\text{A-17})$$

First Law of Piezoelectricity

Since the net change in charge within the body of an insulator is zero (charge resides on the outside of the body),

$$\rho_e = 0$$

Furthermore, because there is no current flow in an insulator,

$$J_i = 0$$

Finally since the materials considered in this thesis are polarized and nonmagnetized dielectrics

$$M_i = 0$$

From the above conditions Maxwell's equations for the piezoelectric material are

$$e_{ijk} H_{k,j} = \dot{D}_i \quad (A-18)$$

$$e_{ijk} E_{k,j} = -B_i \quad (A-19)$$

$$B_{i,i} = 0 \quad (A-20)$$

$$D_{i,i} = 0 \quad (A-21)$$

with

$$D_i = \epsilon_0 E_i + P_i \quad (A-22)$$

$$H_i = \mu_0 B_i \quad (A-23)$$

Likewise from Poynting's theorem the electromagnetic energy flow out of the surface enclosing the volume of interest is

$$h = \gamma \dot{D}_i - e_{ijk} \dot{A}_j H_k \equiv \gamma \dot{D}_i \quad (\text{A-24})$$

Using the quasistatic electric approximation Equation (A-16) reduces to ⁶⁴

$$-\oint_S n_i h_i dS = \int_V (E_i \dot{D}_i + H_i \dot{B}_i) dV \quad (\text{A-25})$$

Using the principle of conservation of energy and equation (A-25) the equations of motion for a piezoelectric body are derived.

For a piezoelectric body bounded by a surface S with a unit outward normal n , the rate of increase of energy (kinetic and internal) is equal to the work done by the surface tractions and the flux of electric energy outward across S assuming no body forces.

$$\frac{\partial}{\partial t} \int_V (1/2 \dot{u}_j \dot{u}_j + U) dV = \oint (t_j \dot{u}_j - n_j \gamma \dot{D}_j) \quad (\text{A-26})$$

where

ρ = density of the material

u = internal strain energy

t_j = applied tractions

γ = scalar potential

D_j = rate of charge developed per unit area

Using the following relations

$$T_{ij,j} = \ddot{u}_j \quad \text{Equilibrium}$$

$$D_{i,i} = 0 \quad \text{Equation A-21 for the dielectric body}$$

$$E_k = -\gamma_{,k} \quad \text{Definition}$$

$$S_{ij} = \frac{1}{2}(u_{i,j} + u_{j,i}) \quad \text{Kinematics}$$

where T_{ij} is the stress tensor and S_{ij} is the strain tensor.

From the above relations and equation (A-26)⁸

$$\dot{U} = T_{ij} \dot{S}_{ij} + E_i \dot{D}_i \quad (\text{A-27})$$

Equation (A-28) represents the first law of thermodynamics for a piezoelectric medium, which states that for an adiabatic process, the change in the internal energy of the piezoelectric material is equal to the rate of mechanical and electrical work done per unit volume.

Piezoceramic Constitutive Equations

Starting with equation (A-28) an electric enthalpy⁸ can be defined as

$$\bar{H} = U - E_i D_i \quad [\text{N m}] \quad (\text{A-28})$$

differentiating equation (A-28) with respect to time and combining it with equation (A-27) yields

$$\dot{H} = T_{ij} \dot{S}_{ij} - D_i \dot{E}_i \quad (A-29)$$

which implies that H is a function of the strain and the electric field. Since

$$H = \frac{\partial H}{\partial S_{ij}} S_{ij} + \frac{\partial H}{\partial E_i} E_i \quad (A-30)$$

subtracting equations (A-30) from (A-29) results in

$$T_{ij} - \frac{\partial H}{\partial S_{ij}} S_{ij} - D_i + \frac{\partial H}{\partial E_i} E_i = 0 \quad (A-31)$$

S_{ij} and E_i are arbitrary therefore

$$T_{ij} = \frac{\partial H}{\partial S_{ij}}, \quad D_i = - \frac{\partial H}{\partial E_i} \quad (A-32)$$

for equation (A-32) to be satisfied.

Linear piezoelectric theory⁸, results in specifying a homogeneous quadratic form for H;

$$H = \frac{1}{2} C_{ijk}^E S_{ij} S_k - e_{ijk} E_i S_{jk} - \frac{1}{2} \epsilon_{ij}^S E_i E_j \quad (A-33)$$

where

C_{ijk}^E = elastic coefficients for a constant electric field.

e_{ijk} = piezoelectric coefficients

ϵ_{ij} = dielectric coefficients

From equation (A-32) the stress and the electric displacement are specified as

$$T_{ij} = C_{ijkl}^E S_{kl} - e_{kij} E_k = \frac{\partial H}{\partial S_{ij}} \quad (A-34)$$

$$D_i = e_{ikl} S_{kl} + \epsilon_{ik} E_k = \frac{\partial H}{\partial E_i} \quad (A-35)$$

Substituting equations (A-34) and (A-28) into (A-33) yields in

$$U = \frac{1}{2} C_{ijkl}^E S_{ij} S_{kl} + \frac{1}{2} \epsilon_{ij} E_i E_j \quad (A-36)$$

where there is no piezoelectric interaction term in the positive definite stored energy function U .

Equations (A-33) and (A-34) represent the constitutive equations for an unbounded piezoelectric medium. The other forms noted in the literature (6) are:

$$S_{ij} = S_{ijkl}^E T_{kl} + d_{kij} E_k \quad (A-37)$$

$$D_i = d_{ikl} T_{kl} + \epsilon_{ik}^T E_k \quad (A-38)$$

and

$$S_{ij} = S_{ijkl}^D T_{kl} + g_{kij} D_k \quad (A-39)$$

$$E_i = -g_{ikl} T_{kl} + \beta_{ik}^T D_k \quad (A-40)$$

and

$$T_{ij} = C_{ijkl}^D S_{kl} - h_{kij} D_k \quad (A-41)$$

$$E_i = -h_{ikl} S_{kl} + \beta_{ik}^S D_k \quad (A-42)$$

Note, the superscripts designate the following condition:

T = constant stress

E = constant electric field

S = constant strain

D = constant electric displacement

The matrix relationship between the coefficients in equations (A-34) to (A-42) are expressed in the following matrix form as²⁸:

$$[\beta^T] = [\epsilon^T]^{-1}$$

$$[g] = [\beta^T][d]$$

$$[S^D] = [S^E] - \text{trans}([d])[\beta^T][e]$$

$$[e] = [d][C^E]$$

$$[h] = [\beta^S][e]$$

$$[C^D] = [C^E] + \text{trans}([e])[\beta^S][e]$$

$$[\beta^S] = [\beta^T] + [h][S^D] \text{trans}([h])$$

$$[\epsilon^S] = [\epsilon^T] - [d][C^E] \text{trans}([d])$$

To use equations (A-33) to (A-42) for analysis of the electromechanical coupling of unimorph piezoceramic sensors and actuators to elastic bodies requires knowledge of the piezoceramic mechanical, dielectric and piezoelectric coefficients. The piezoceramic used is a ferroelectric material.

To obtain the necessary coefficients, for the particular ferroelectric used requires a review of crystallography⁸ and its application to this class of materials.

Ferroelectric ceramics consist primarily of a single crystal type structure of polycrystalline material. When this material is poled by the application of an intense external electric field at elevated temperatures it is made piezoelectric and rendered a single crystal symmetry on a macroscopic scale.

Crystals are grouped into seven systems depending on their symmetry. These systems are further divided into classes according to their symmetry to a point. In all, there are 32 classes of which are considered to be piezoelectric⁸.

The lead zirconate titanate (PZT) type of ferroelectric is a hexagonal crystal system and identified using the international crystallographic system as 6mm which is distinguished by an axis of sixfold symmetry.

To relate the constitutive parameters to the different crystalline systems an elasto-electric matrix description is used⁸. This method of description relates the coupling between the elastic

and dielectric properties (equation A-33 and A-34) by an arrangement of the dielectric and elastic coefficients. The elasto-electric matrix consists of a nine by nine matrix where in each column is related to the independent variable such as stress or electric field component and each row to a dependent variable such as strain or electric displacement.

For example, the triclinic crystalline system or the one possessing neither symmetry axes or symmetric planes has 45 different coefficients as shown below:

	S_{11}	S_{22}	S_{33}	S_{23}	S_{31}	S_{12}	E_1	E_2	E_3
T_{11}	C_{11}	C_{12}	C_{13}	C_{14}	C_{15}	C_{16}	e_{11}	e_{21}	e_{31}
T_{22}	C_{21}	C_{22}	C_{23}	C_{24}	C_{25}	C_{26}	e_{12}	e_{22}	e_{32}
T_{33}	C_{31}	C_{32}	C_{33}	C_{34}	C_{35}	C_{36}	e_{13}	e_{23}	e_{33}
T_{23}	C_{41}	C_{42}	C_{43}	C_{44}	C_{45}	C_{46}	e_{14}	e_{24}	e_{34}
T_{31}	C_{51}	C_{52}	C_{53}	C_{54}	C_{55}	C_{56}	e_{15}	e_{25}	e_{35}
T_{12}	C_{61}	C_{62}	C_{63}	C_{64}	C_{65}	C_{66}	e_{16}	e_{26}	e_{36}
D_1	e_{11}	e_{12}	e_{13}	e_{14}	e_{15}	e_{16}	ϵ_{11}	ϵ_{12}	ϵ_{13}
D_2	e_{21}	e_{22}	e_{23}	e_{24}	e_{25}	e_{26}	ϵ_{21}	ϵ_{22}	ϵ_{23}
D_3	e_{31}	e_{32}	e_{33}	e_{34}	e_{35}	e_{36}	ϵ_{31}	ϵ_{32}	ϵ_{33}

where the following use of compressed notation is applicable:

ij or kl	p or q
11	1
22	2
33	3
23 or 32	4
31 or 13	5

Note:

$$S_{ij} = S_{pq, i} = j, p, q = 1, 2, 3$$

$$2S_{ij} = S_{pq, i} = j, p, q = 4, 5, 6$$

For a 6mm hexagonal crystal the elasto-electric matrix becomes

	S_{11}	S_{22}	S_{33}	S_{23}	S_{31}	S_{12}	E_1	E_2	E_3
T_{11}	C_{11}	C_{12}	C_{13}	0	0	0	0	0	e_{31}
T_{22}	C_{21}	C_{11}	C_{13}	0	0	0	0	0	e_{31}
T_{33}	C_{31}	C_{31}	C_{33}	0	0	0	0	0	e_{33}
T_{23}	0	0	0	C_{44}	0	0	0	e_{15}	0
T_{31}	0	0	0	0	C_{44}	0	e_{15}	0	0
T_{12}	0	0	0	0	0	C_{66}	0	0	0
D_1	0	0	0	0	e_{15}	0	ϵ_{11}	0	0
D_2	0	0	0	e_{15}	0	0	0	ϵ_{11}	0
D_3	e_{31}	e_{31}	e_{33}	0	0	0	0	0	ϵ_{33}

with ten different coefficients.

Note, that $C_{66} = (C_{11} - C_{12})/2$.

The piezoelectricity of the 6mm crystalline material is now classed by three independent piezoelectric constants, e_{31} , e_{33} and e_{15} or as noted previously d_{31} , d_{33} and d_{15} . The data available on the piezoceramic materials is usually given in the later form.

Equations (A-33) and (A-34) are expanded for example (ref. 74) to obtain the following constitutive equations for an unbounded 6mm piezoceramic medium.

$$T_{11} = C_{11}u_{1,1} + C_{12}u_{2,2} + C_{13}u_{3,3} + e_{31}E_3$$

$$T_{22} = C_{21}u_{1,1} + C_{11}u_{2,2} + C_{13}u_{3,3} + e_{31}E_3$$

$$T_{33} = C_{31}u_{1,1} + C_{13}u_{2,2} + C_{33}u_{3,3} + e_{33}E_3$$

$$T_{23} = C_{44}(u_{3,2} + u_{2,3}) + e_{15}E_2$$

$$T_{31} = C_{44}(u_{3,1} + u_{1,3}) + e_{15}E_1$$

$$T_{12} = C_{66}(u_{1,2} + u_{2,1})$$

$$D_1 = e_{15}u_{3,1} + e_{15}u_{1,3} - \epsilon_{11}E_1$$

$$D_2 = e_{15}(u_{3,2} + u_{2,3}) - \epsilon_{11}E_2$$

$$D_3 = e_{31}u_{1,1} + e_{31}u_{2,2} + e_{33}u_{3,3} - \epsilon_{33}E_3$$

List of Piezoelectric Coefficients and Their Units

C_{ijkl}, C_{pq}	Elastic Stiffness Constant	N/M^2
d_{ijk}, d_{ip}	Piezoelectric Constant	M/V or C/N
e_{ijk}, e_{ip}	Piezoelectric Constant	C/M^2
E_i	Electric Field Component	V/M
g_{ijk}, g_{ip}	Piezoelectric Constant	$V-M/N$ or M^2/C
h_{ijk}, h_{ip}	Elect. Enthalpy Density	J/M^3
D_i	Electric Disp. Component	C/M^2
C	Capacitance	Farad
S_{ijkl}, S_{pq}	Elastic Compliance Constant	M^2/N
β_{ij}	Impermittivity Constant	$M/Farad$
ϵ_0	Perm. of free space ($8.85e-12$)	$Farad/M$
ϵ_{ij}	Perm. component	$Farad/M^5$

APPENDIX B

FINITE ELEMENT ACTIVE BEAM MODEL

This appendix contains the following:

- a) The derivation of the element matrices of a beam finite element model with a piezoceramic driver.
- b) The derivation of the element matrices of a beam element with a piezoceramic sensor and actuator.
- c) Investigation of the effects of Guyan condensation on the active structural damping matrix.

BEAM ELEMENT WITH AN ACTUATOR

The finite element model ⁴⁸ of a beam element shown in figure B-1 with a perfectly bonded unimorph piezoceramic driver and subjected only to bending is derived follows: Fixing node i-1.

$$w_{i-1} = 0, \theta_{i-1} = 0$$

Equilibrium for the beam is

$$\frac{d^2 w}{dx^2} = \frac{1}{EI} [-M_i + V_i(L-x) + K_D V_D] \quad (B-1)$$

where V_D is the DC voltage applied to the driver.

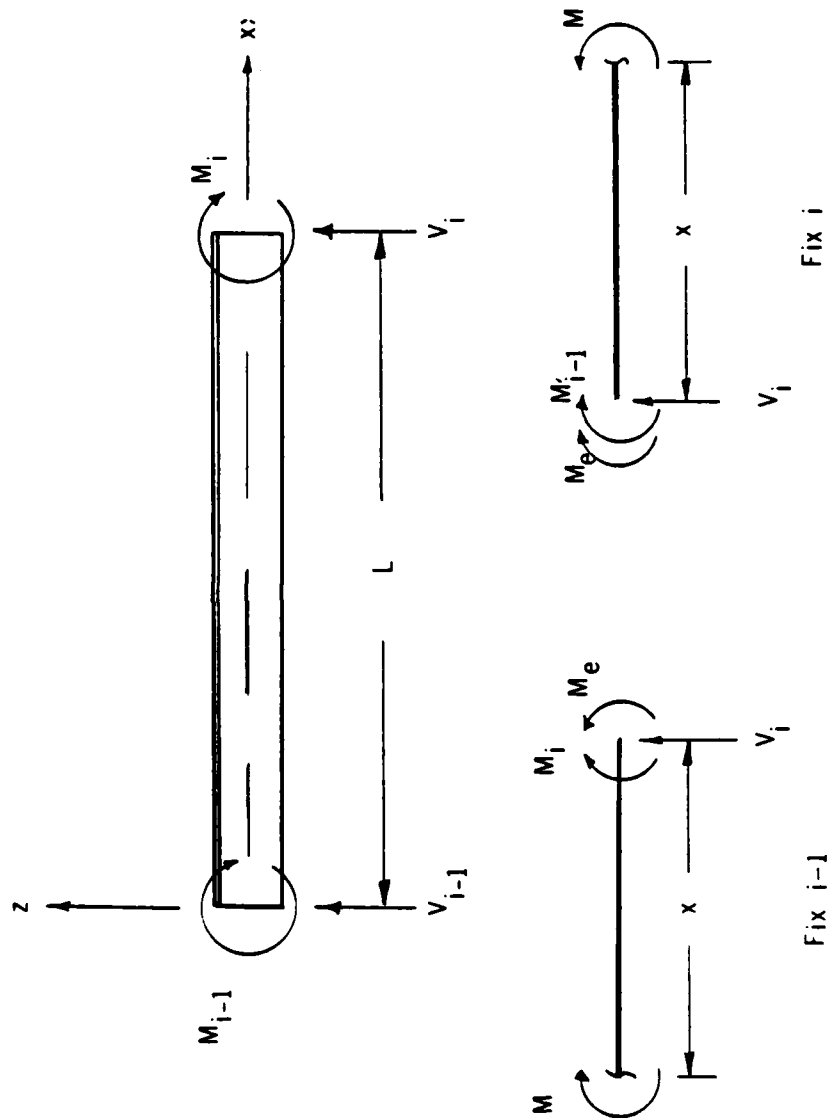


Figure B-1 Actuator Element With Free Body Diagrams

Integrating once gives

$$\frac{dw}{dx} = \frac{1}{EI} [-M_i x + V_i (Lx + \frac{x^2}{2}) + K_D V_D x] + c_1 \quad (B-2)$$

$$x = 0, \quad \frac{dw}{dx} = 0 \quad c_1 = 0$$

$$x = L, \quad \frac{dw}{dx} = -\theta_i$$

Solving for the rotation at node i gives

$$\theta_i = \frac{1}{EI} [-M_i L + \frac{V_i L^2}{2} - K_D V_D L] \quad (B-3)$$

Integrating equation (B-2) gives

$$w = \frac{1}{EI} \left[\frac{-M_i x^2}{2} + V_i \left(\frac{Lx^2}{2} + \frac{x^3}{6} \right) + \frac{K_D V_D x^2}{2} + c_2 \right] \quad (B-4)$$

$$x = 0, \quad w = 0 \quad c_2 = 0$$

$$x = L, \quad w = w_i$$

Solving for the displacement at node i gives

$$w_i = \frac{1}{EI} \left[-\frac{M_i L^2}{2} + \frac{V_i L^3}{3} + \frac{K_D V_D L^2}{2} \right] \quad (B-5)$$

Combining equations (B-3) and (B-5) in matrix form and taking the inverse of the flexibility matrix gives

$$\begin{Bmatrix} V_i \\ (M_i - K_D V_D)/L \end{Bmatrix} = [K_{BB}] \begin{Bmatrix} W_i \\ \theta_i L \end{Bmatrix} \quad (\text{B-6})$$

where

$$[K_{BB}] = \frac{EI}{L^3} \begin{bmatrix} 12 & 6 \\ 6 & 4 \end{bmatrix}$$

Fixing node i results in the following free body diagram shown in figure B-2. Equilibrium for the beam is now with $W_i = 0$ and $\theta_i = 0$.

$$\frac{d^2 w}{dx^2} = \frac{1}{EI} [V_{i-1}x + M_{i-1} + K_D V_D] \quad (\text{B-7})$$

where V_D is again the DC voltage applied to the driver. Integrating once gives

$$\frac{dw}{dx} = \frac{1}{EI} \left[M_{i-1}x + \frac{V_{i-1}x^2}{2} + K_D V_D x + c_1 \right] \quad (\text{B-8})$$

$$x = L, \frac{dw}{dx} = 0 \therefore c_1 = -\frac{1}{EI} \left[V_{i-1}L^2 + M_{i-1} + K_D V_D L \right]$$

$$x = 0, \frac{dw}{dx} = -\theta_1$$

Therefore solving for the rotation at node $i-1$ gives

$$\theta_1 = \frac{1}{EI} \left[M_{i-1}L + \frac{V_{i-1}L^2}{2} + K_D V_D L \right] \quad (\text{B-9})$$

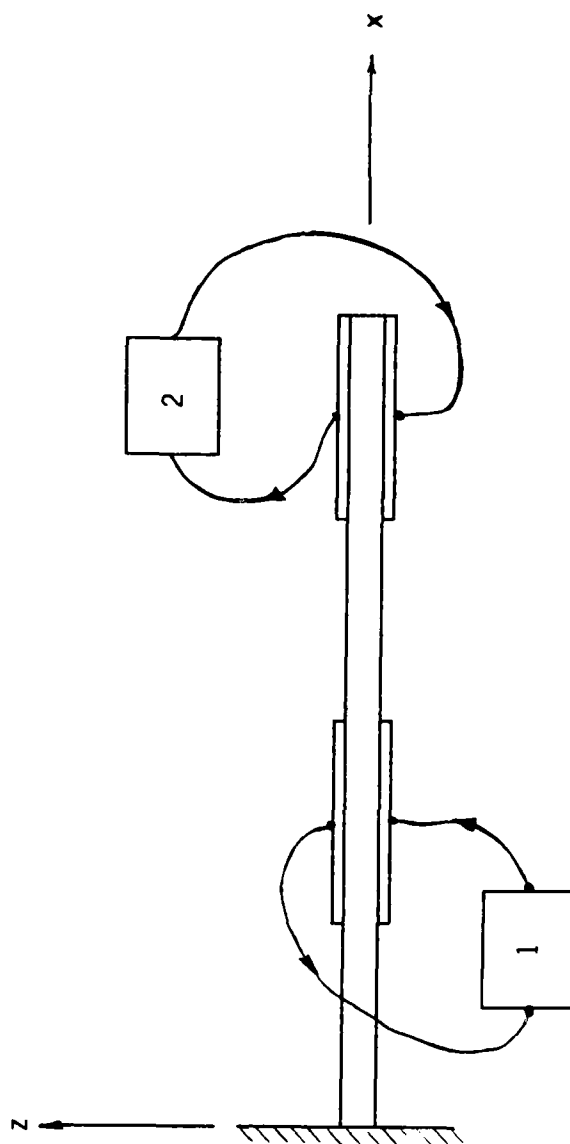


Figure B-2 Collocated Rate Control Example Configuration

Integrating equation (B-8) gives

$$w_1 = \frac{1}{EI} \left[\frac{M_{i-1}x^2}{2} + \frac{V_{i-1}x^3}{6} + \frac{K_D V_D x^2}{2} - \frac{V_{i-1}L^2 x}{2} - M_{i-1}Lx - K_D V_D Lx \right] + C_2 \quad (B-10)$$

$$\begin{aligned} x = L, w = 0 \quad C_2 &= \frac{1}{EI} \left[\frac{V_{i-1}L^3}{3} + \frac{M_{i-1}L^2}{2} + \frac{K_D V_D L^3}{2} \right] \\ x = 0, w = w \end{aligned}$$

Solving for the displacement at node $i-1$ gives

$$w_{i-1} = \frac{1}{EI} \left[\frac{V_{i-1}L^3}{3} + \frac{M_{i-1}L^2}{2} + \frac{K_D V_D L^2}{2} \right] \quad (B-11)$$

Combining equations (B-3) and (B-5) in matrix form and taking the inverse of the flexibility matrix gives

$$\begin{Bmatrix} V_{i-1} \\ (M_{i-1} + K_D V_D)/L \end{Bmatrix} = [K_{AA}] \begin{Bmatrix} w_{i-1} \\ \theta_{i-1} \end{Bmatrix} \quad (B-12)$$

$$[K_{AA}] = \begin{bmatrix} 12 & -6 \\ -6 & 4 \end{bmatrix}$$

To obtain K_{13} and K_{21} equilibrium at node $i-1$ can be written as

$$V_{i-1} + V_i = 0$$

$$-V_i L + M_{i-1} + M_i + K_D V_D - K_D V_D = 0$$

or in matrix form

$$\begin{Bmatrix} V_{i-1} \\ (M_{i-1} + K_D V_D)/L \end{Bmatrix} = \begin{bmatrix} -1 & 0 \\ 1 & -1 \end{bmatrix} \begin{Bmatrix} V_i \\ (M_i - K_D V_D)/L \end{Bmatrix} \quad (\text{B-13})$$

Substituting equation (B-6) into (B-13) yields

$$\begin{Bmatrix} V_{i-1} \\ (M_{i-1} + K_D V_D)/L \end{Bmatrix} = [K_{AB}] \begin{Bmatrix} W_i \\ \theta_i L \end{Bmatrix} \quad (\text{B-14})$$

where

$$[K_{AB}] = \frac{EI}{L^3} \begin{bmatrix} -12 & -6 \\ 6 & 2 \end{bmatrix}$$

Equilibrium at node i is

$$V_{i-1} + V_i = 0$$

$$M_i - K_D V_D + M_{i-1} + K_D V_D + V_{i-1} L = 0$$

or in matrix form

$$\begin{Bmatrix} V_i \\ (M_i - K_D V_D)/L \end{Bmatrix} = \begin{bmatrix} -1 & 0 \\ -1 & -1 \end{bmatrix} \begin{Bmatrix} V_{i-1} \\ (M_{i-1} + K_D V_D)/L \end{Bmatrix} \quad (\text{B-15})$$

Substituting equation (B-12) into (B-15) gives

$$\begin{Bmatrix} V_i \\ (M_i - K_D V_D)/L \end{Bmatrix} = [K_{BA}] \begin{Bmatrix} W_{i-1} \\ \Theta_{i-1} L \end{Bmatrix} \quad (\text{B-16})$$

where

$$[K_{BA}] = \frac{EI}{L^3} \begin{bmatrix} -12 & 6 \\ -6 & 2 \end{bmatrix}$$

Combining equations (B-6), (B-12), (B-14) and (B-16) gives the final result

$$\begin{Bmatrix} V_{i-1} \\ (M_{i-1} + K_D V_D)/L \\ V_i \\ (M_i - K_D V_D)/L \end{Bmatrix} = \frac{EI}{L^3} \begin{bmatrix} 12 & & & \\ -6 & 4 & \text{Sym} & \\ -12 & 6 & 12 & \\ -6 & 2 & 6 & 4 \end{bmatrix} \begin{Bmatrix} W_{i-1} \\ \Theta_{i-1} L \\ W_i \\ \Theta_i L \end{Bmatrix} \quad (\text{B-17})$$

or

$$\begin{Bmatrix} V_{i-1} \\ (M_{i-1} + K_D V_D)/L \\ V_i \\ (M_i - K_D V_D)/L \end{Bmatrix} = \frac{EI}{L^3} \begin{bmatrix} 12 & & & \\ -6L & 4L^2 & & \\ -12 & 6L & 12 & \\ -6L & 2L^2 & 6L & 4L^2 \end{bmatrix} \begin{Bmatrix} w_{i-1} \\ \theta_{i-1} \\ w_i \\ \theta_i \end{Bmatrix}$$

(B-18)

BEAM ELEMENT WITH PIEZOCERAMIC AN ACTUATOR AND SENSOR

Following the same procedure as before with the following additional assumptions

- a) The displacement and rotations are a function of both space and time.
- b) The motion is considered such that the inertial forces of the beam are neglected.
- c) The complete upper surface of the beam is covered by a sensor and the complete bottom surface by a driver.
- d) The polarity vector of the driver is positioned such that given a positive voltage, the applied moment will be of the same sign as in section 2.2. The free body diagrams in figure B1 and B2 are valid.

as in section 2.2. The free body diagrams in figure B1 and B2 are valid.

From equation (2.22) in chapter II, the equation for the voltage form the sensor is

$$V_S(t) = K_S \int_{x_{i-1}}^{x_i} \frac{\partial^3 w(x,t)}{\partial x^2 \partial t} dx \quad (B-19)$$

where

$$K_S = w_d h d_{31} c_{11}^E R_F$$

From chapter 11, rate feedback is defined as

$$V_D = V_S \quad (B-20)$$

Combining equation (B-20) with the integral (B-19) evaluated and substituting for V_D in equation (B-18) yields

$$\left\{ \begin{array}{c} V_{i-1} \\ M_{i-1} + K_D K_S [\dot{\theta} - \dot{\theta}_{i-1}] \\ V_i \\ M_i - K_D K_S [\dot{\theta} - \dot{\theta}_{i-1}] \end{array} \right\} = \frac{EI}{L^3} \underbrace{\left[\begin{array}{cccc} 12 & & & \\ -6L & 4L^2 & \text{Sym} & \\ -12 & 6L & 12 & \\ -6L & 2L^2 & 6L & 4L^2 \end{array} \right]}_{[K]} \left\{ \begin{array}{c} w_{i-1} \\ \theta_{i-1} \\ w_i \\ \theta_i \end{array} \right\} \quad (B-21)$$

Expanding the right hand side of equation (B-21) gives the final result

$$\begin{Bmatrix} V_{i-1} \\ M_{i-1} \\ V_i \\ M_i \end{Bmatrix} = \frac{EI}{L^3} [K] + K_D K_S \begin{bmatrix} 0 & 0 & 0 & 0 \\ 0 & 1 & 0 & -1 \\ 0 & 0 & 0 & 0 \\ 0 & -1 & 0 & 1 \end{bmatrix} \begin{Bmatrix} \dot{w}_{i-1} \\ \dot{\theta}_{i-1} \\ \dot{w}_i \\ \dot{\theta}_i \end{Bmatrix} \quad (B-22)$$

GUYAN CONDENSATION OF THE ACTIVE DAMPING MATRIX

Identification of the dynamic coupling of the active was presented in section chapter III. The five degree of freedom model consisted of only translational degrees of freedom with the rotational d.o.f. condensed out using Guyan condensation. Presented in this section is the results of condensation of the small four element of a beam shown on figure B-3 with two collocated sensor actuator pairs.

The structure considered was assumed not to have any internal damping. The mass and stiffness properties of the structure can be arranged as

$$\begin{bmatrix} M_{ww} & M_{w\theta} \\ M_{\theta w} & M_{\theta\theta} \end{bmatrix} \begin{Bmatrix} \ddot{w}_1 \\ \ddot{w}_n \\ \ddot{\theta}_1 \\ \ddot{\theta}_n \end{Bmatrix} + \begin{bmatrix} K_{ww} & K_{w\theta} \\ K_{\theta w} & K_{\theta\theta} \end{bmatrix} \begin{Bmatrix} w_1 \\ w_n \\ \theta_1 \\ \theta_n \end{Bmatrix} = \begin{Bmatrix} F_i \\ M_i \end{Bmatrix} \quad (B-23)$$

Given equation (B-23) a transformation matrix^{66,67} can be developed such that

$$\begin{matrix} 2n \times 1 \\ \left\{ \begin{array}{c} w_1 \\ \vdots \\ w_n \\ \theta_1 \\ \vdots \\ \theta_n \end{array} \right\} \end{matrix} = \begin{matrix} 2n \times n \\ \left[\begin{array}{c} [I] \\ [T] \end{array} \right] \end{matrix} \begin{matrix} n \times 1 \\ \left\{ \begin{array}{c} w \\ \vdots \\ w_n \end{array} \right\} \end{matrix} \quad (B-24)$$

where

$$[T] = - [K_{\theta\theta}]^{-1} [K_{\theta w}] \quad (B-25)$$

Using equation (B-25), equation (B-23) can be transformed to

$$[M] \left\{ \begin{array}{c} \ddot{w}_1 \\ \vdots \\ \ddot{w}_n \end{array} \right\} + [R] \left\{ \begin{array}{c} w_1 \\ \vdots \\ w_n \end{array} \right\} = \left\{ \begin{array}{c} F_1 \\ \vdots \\ F_n \end{array} \right\} \quad (B-26)$$

where

$$[M] = \left[\begin{array}{cc} [I] & [T]^T \end{array} \right] [M] \left[\begin{array}{c} [I] \\ [T] \end{array} \right] \text{ and } [\bar{K}] = \left[\begin{array}{cc} [I] & [T]^T \end{array} \right] [K] \left[\begin{array}{c} [I] \\ [T] \end{array} \right]$$

The assembled and rearranged structural damping matrix for the structure in figure (B-3) using equation (B-22) with $L = 1$ is

$$K_D K_S \underbrace{\begin{bmatrix} [0] & & & & [0] \\ & 1 & -1 & 0 & 0 \\ & -1 & 1 & 0 & 0 \\ [0] & 0 & 0 & 1 & -1 \\ & 0 & 0 & -1 & 1 \end{bmatrix}}_{[C_{ed}]} \begin{Bmatrix} \dot{w}_2 \\ \dot{w}_3 \\ \dot{w}_4 \\ \dot{w}_5 \\ \dot{\theta}_2 \\ \dot{\theta}_3 \\ \dot{\theta}_4 \\ \dot{\theta}_5 \end{Bmatrix} \quad (B-27)$$

with the stiffness matrix as

$$[K] = EI \begin{bmatrix} 24 & -12 & 0 & 0 & 0 & -6 & 0 & 0 \\ -12 & 24 & -12 & 0 & 6 & 0 & -6 & 0 \\ 0 & -12 & 24 & -12 & 0 & 6 & 0 & -6 \\ 0 & 0 & -12 & 12 & 0 & 0 & 6 & 6 \\ 0 & 6 & 0 & 0 & 8 & 2 & 0 & 0 \\ -6 & 0 & 6 & 0 & 2 & 8 & 2 & 0 \\ 0 & -6 & 0 & 6 & 0 & 2 & 8 & 2 \\ 0 & 0 & -6 & 6 & 0 & 0 & 2 & 4 \end{bmatrix} \begin{Bmatrix} w_2 \\ w_3 \\ w_4 \\ w_5 \\ \theta_2 \\ \theta_3 \\ \theta_4 \\ \theta_5 \end{Bmatrix} \quad (B-28)$$

With equation (B-28) partitioned as shown in equation (B-23) the transformation matrix can be computed according to equation (B-25)

$$[T] = \begin{bmatrix} -.2165 & -.7423 & .1856 & -.0309 \\ .8660 & -.0309 & -.7423 & .1237 \\ -.2474 & .8660 & -.2165 & -.4639 \\ .1237 & -.4330 & 1.6080 & -1.2680 \end{bmatrix} \quad (B-29)$$

To condense the structural electronic damping matrix to only displacement d.o.f. requires the following operation.

$$[C] = \begin{bmatrix} [I] & [T]^T \end{bmatrix} [C_{ED}] \begin{bmatrix} [I] \\ [T] \end{bmatrix} \quad (B-30)$$

The result of this operation is

$$[C] \begin{Bmatrix} \dot{w}_2 \\ \dot{w}_3 \\ \dot{w}_4 \\ \dot{w}_5 \end{Bmatrix} = K_D K_S \begin{bmatrix} 1.310 & & & \\ .2885 & 2.193 & \text{Sym} & \\ -.3278 & -3.030 & 4.191 & \\ -.1309 & 1.155 & -1.611 & .6705 \end{bmatrix} \begin{Bmatrix} \dot{w}_2 \\ \dot{w}_3 \\ \dot{w}_4 \\ \dot{w}_5 \end{Bmatrix} \quad (B-31)$$

The condensed form of the electronic damping matrix is fully populated and symmetric for collocated sensors and drivers.

APPENDIX C:

System Identification of Vibrating Structures

System identification is the process of using measured test data of a structure's response and usually some a priori information of the system's parameters to develop a mathematical model which simulates the system's behavior. System identification can be accomplished in the time or frequency domain employing either physical or modal data. Common approaches used are:

- a) The minimization of the error satisfying the system's equations with the measured response.
- b) The minimization of the differences between the measured and analytical response.
- c) Seeking a new set of system parameters that differ the least from a priori or specified values using the system equations as constraints.

Given the matrix description of a system as

$$[M] \{\ddot{x}_i\} + [C] \{\dot{x}_i\} + [K] \{x_i\} = \{f_i\} \quad (C-1)$$

where the matrix coefficients have been identified and represents the vector of the physical degrees of freedom and $\{f_i\}$ is the vector of the forcing functions, equation(C-1) becomes the baseline analytical model.

This model can be used for example to study changes in the physical system as well as changes in the boundary conditions.

The system can also be characterized by

$$[Z(\omega)] \{x_i(\omega)\} = \{f_i(\omega)\} \quad (C-2)$$

where the inverse of

$$[Z(\omega)]^{-1} = [-\omega^2[M] + j\omega[C] + [K]]^{-1} = [Y(\omega)] \quad (C-3)$$

is the mobility matrix and each element is a transfer function. The identification of $[Y(\omega)]$ can be used to study the effects of various forces on the structure or for a component synthesis analysis⁶⁵.

The system can also be characterized by

$$\lambda_i^2 [M] \{\phi_i\} + \lambda_i [C] \{\phi_i\} + [K] \{\phi_i\} = \{0\} \quad (C-4)$$

where λ_i and ϕ_i are the eigenparameters. In this form the general validation of an existing analytical model can be obtained. This particular characterization was used in an algorithm developed to identify the baseline system matrices without active control. A brief outline of this procedure is given next for completeness.

The system matrices of a dynamic system, such as the one described by equation (C-1), satisfy the eigenvalue problem

$$\lambda_i^2 M\phi_i + L_i C\phi_i + K\phi_i = 0 \quad (i = 1, 2, \dots, 2n) \quad (C-5)$$

where

λ_i = i th complex eigenvalue

If one uses arbitrary matrices in place of the correct system matrices in Equation (C-5), it is not satisfied exactly. The norm of the resulting error matrix is then minimized over all the modes with respect to the matrix elements subject to symmetry constraints. This process results in a set of homogeneous simultaneous equations given by

$$ML_1 + L_1M + CL_2 + L_2^T C + KL_3 + L_3^T K = 0 \quad (C-6)$$

$$ML_2^T + L_2M + CL_4 + L_4C + KL_5 + L_5^T K = 0 \quad (C-7)$$

$$ML_3^T + L_3M + CL_5^T + L_5C + KL_6 + L_6 K = 0 \quad (C-8)$$

where

$$L = ZF^2(F^T)^2 Z^T, \quad L = ZF(F^T)^2 Z^T$$

$$L = Z(F^T)^2 Z, \quad L = ZFF^T Z^T$$

$$L = ZF^T Z^T, \quad L = ZZ^T$$

$$Z = [\text{Re}(\phi_i) \dots \text{Re}(\phi_i) \quad \text{Im}(\phi_i) \dots \text{Im}(\phi_i)]$$

and

$$F = \begin{bmatrix} \Lambda_R & \Lambda_I \\ -\Lambda_I & \Lambda_R \end{bmatrix}$$

with

$$\Lambda_R = \text{diag}[\text{Re}(\phi_i) \dots \text{Re}(\phi_i)]$$

$$\Lambda_I = \text{diag}[\text{Im}(\phi_i) \dots \text{Im}(\phi_i)]$$

If some of the matrix coefficients are known a priori, the remaining unknown coefficients can be determined from these equations.

If the identified matrices are such that they satisfy the eigenvalue problem with respect to the measured modal parameters exactly, the orthogonality conditions are also satisfied. If the error in the eigenvalue problem is not zero, orthogonality is satisfied approximately. However, even in this case, orthogonality is satisfied exactly with respect to the identified modal parameters, which in turn are approximately equal to the measured modal parameters.

The identification procedure used to compute the mass, damping and stiffness matrices required that some of the mass or stiffness elements to be known a priori. To provide this information, models for the various test cantilevered beams were developed using the GTSTRU DL⁶⁷ finite element code.

The finite element model consisted of plane frame XZ type elements. The mass of the accelerometer located at the tip of the test beams was included as a lumped mass at the tip node point of the model. The mass of the piezoceramic transducers and wires was considered negligible and therefore not included. Finally, depending

on the model, a reduced set of modes were usually of interest. This required reduction in the number of degrees of freedom using Guyan condensation⁶⁶.

APPENDIX D:

ACTIVE CONTROL EXPERIMENTS

Experimental Setup and Equipment

Structural dynamic control experiments were undertaken to evaluate the performance of the active control of simple structures. Three cantilever beam were selected which had the following dimensions:

- #1) Steel Beam 24x2x.5 inch.
- #2) Aluminum Beam 24x2x.25 inch.
- #3) Aluminum Beam 9x.651x.172 inch

Beam #3 was used for the identification of the dynamic coupling coefficients. All three beams were welded to a thick metal plate which was bolted a support frame. Figure D-1 is a drawing of a typical beam experimental setup.

Piezoceramin unimorph transducers were used to sense and dynamically control the cantilevered beams. The transducer locations for the three beams are shown in figure D-2. The transducers were supplied by Piezoelectric Corp. and were made out of G1195 material which is a lead zirconate titanate (PZT) type compound. Depending on the transducer, it consisted of either $3/4 \times 3/4 \times .010$ in. or a $1.5 \times .655 \times .010$ thin sheet of piezoceramic sandwiched by two nickel

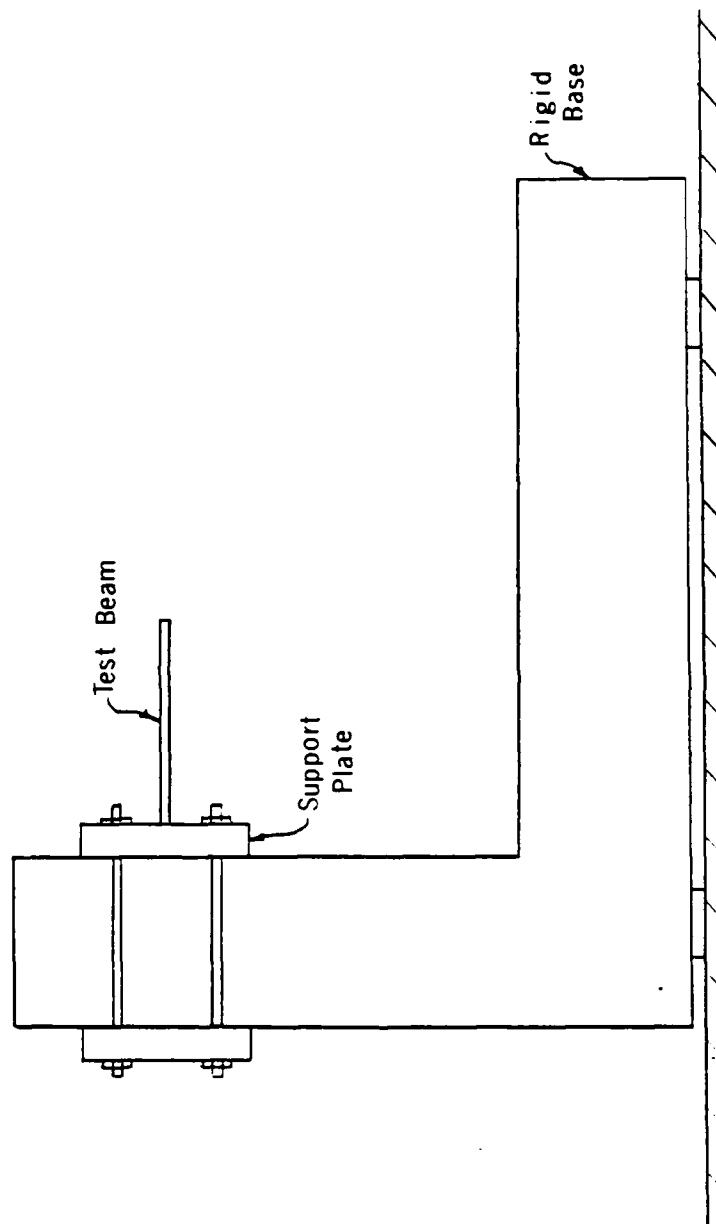


Figure D-1 Experimental Beam Mechanical Support

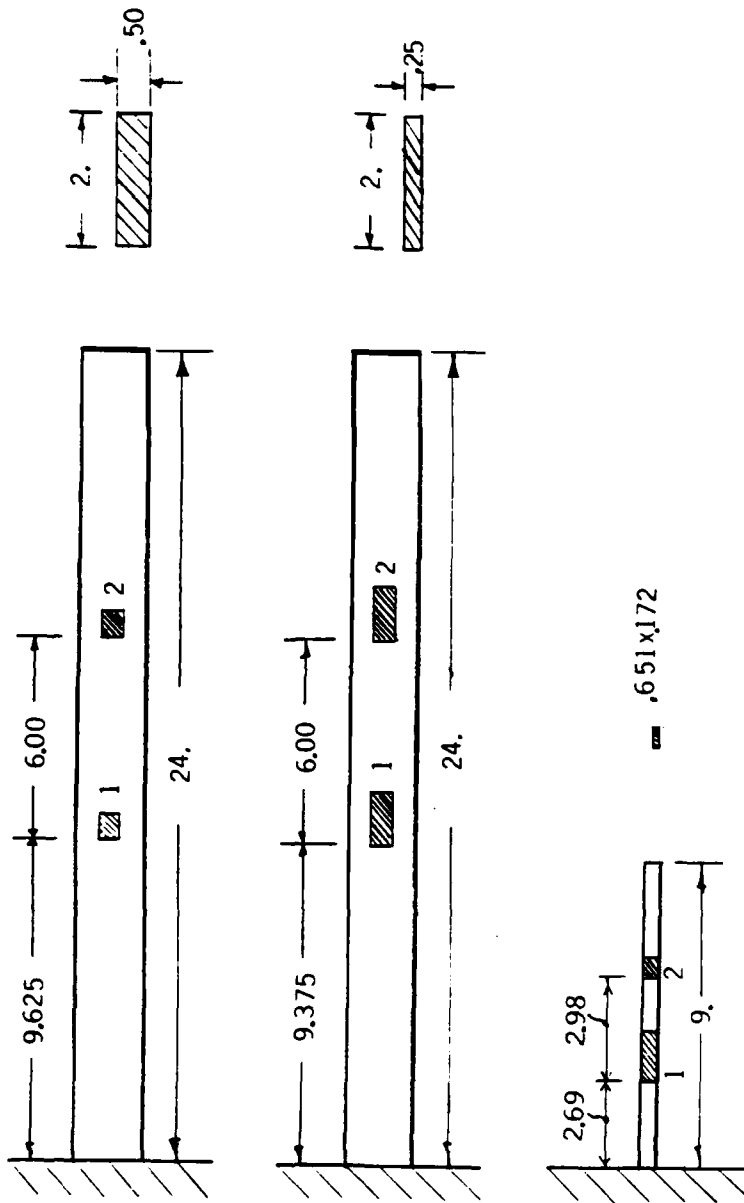


Figure D-2 Test Beams Collocated Sensor/Actuator Locations

electrodes that cover the entire surfaces. Shielded leads were soldered to the electrodes at the corners of the transducers. Table D-1 lists the material and piezoelectric specification for the PZT material.

For each configuration, the transducers were bonded to the beam at the desired locations with a thin layer of epoxy. A small amount of micro bubbles were mixed in the epoxy to keep the bottom of the electrodes insulated from the beam surface and to maintain an even layer of adhesive. The epoxy consisted of a two part mix which required five^{min.} to cure at room temperature.

In general, the response measurements of the beams were made using accelerometers (BBN model 507 Sn 1346, PCB model 303A SN 7384). The accelerometers were usually fixed at a single location (tip) and an impact hammer with a force transducer (PCB model 208A03 SN 4417 and PCB 086B80 Sn1284) was moved along the beam to the different locations to apply impact excitation.

For each collocated transducer pair, one transducer was selected as the sensor and the other as an actuator. The current output of the sensor was conditioned by an active feedback control system which provided high voltage output to the actuator.

Two prototype active feedback control units were provided by Dr. R.L. Forward from Hughes Research, Malibu CA. These units were designed for the sole purpose of demonstrating the potential performance of active control using piezoceramic transducers. The units basically consist of a preamplifier, filter and high power

Table D-1. G-1195 Piezoceramic Coefficients.

Electrodes Nickel
Modulus = $6.3\text{E}+10$ N/M²
Capacitance (.75 x .75 x .01 in.) = $2.2\text{E}-08$ C/V
Capacitance (1.555 x .6086 x .01 in.) = $3.9\text{E}-08$ C/V
 g_{31} = $1.14\text{E}-02$ VM/N
 d_{31} = $1.79\text{E}-10$ M/V
 ϵ_{33} = $1.65\text{E}-08$ Farad/M
Curie Temp. = 360° C
Density = 7.6 gr/cc

output sections. The preamplifier section is simply a charge amplifier which converts the output of a piezoceramic thin sheet ceramic strain gage (current) to a voltage. The voltage is then filtered to a desired frequency, phase and frequency bandwidth (Q) prior to being amplified in the high power section for driving other piezoceramic strain gages. Figure D-3 is a drawing of the front panel of an active control unit. A detailed analysis of the active feedback and their calibration is covered later.

To measure and reduce the dynamic response data a 16 channel Computer Aided Test System (Genrad Model 2515 was used). This system provided a multitude of methods to evaluate the quality of the data as well as computing the change in modal damping upon the application of active control⁵¹. Figure D-4 shows a typical experimental setup with all of the primary signal conditioning equipment.

Test Procedure

Prior to each test, the gain, center frequency, bandwidth and phase of the active damping units was adjusted. The Q or bandwidth of the filter circuit was set at its narrowest setting which was 20. Using the output of the accelerometer or a sensor, the frequency at a particular gain setting was fine tuned until a minimum output was obtained for the given sinusoidal excitation applied by an piezoceramic actuator. The optimum phase setting was at 180 degrees for collocated sensors and was not optimized for the non collocated test.

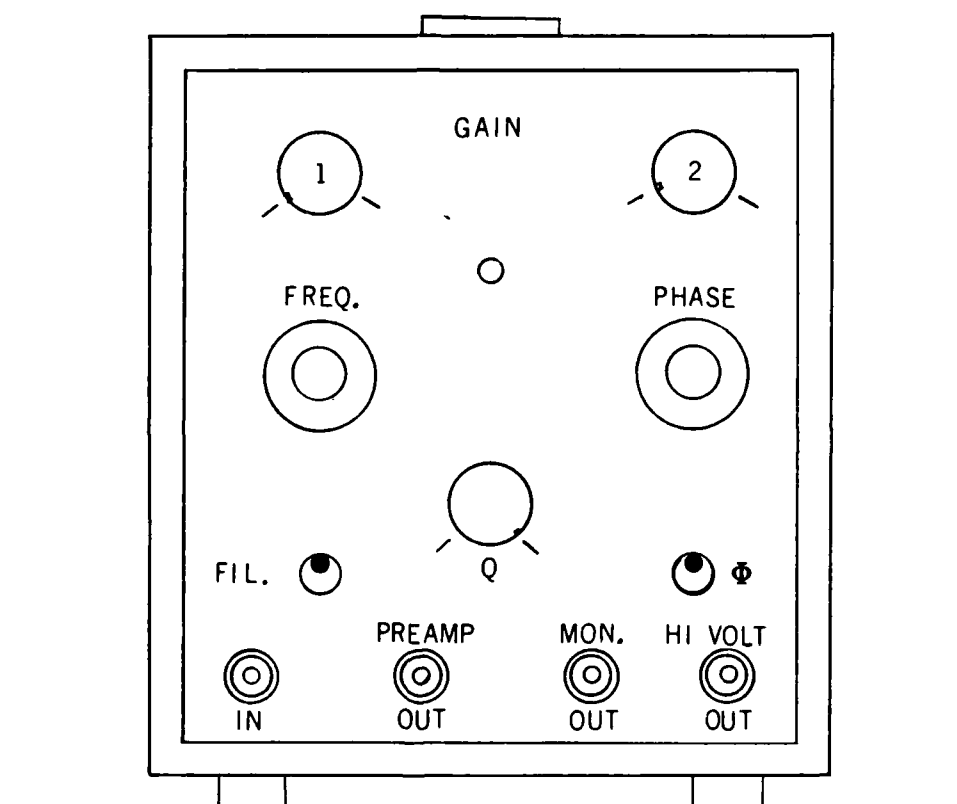


Figure D-3 Active Feedback Filter/Control Unit

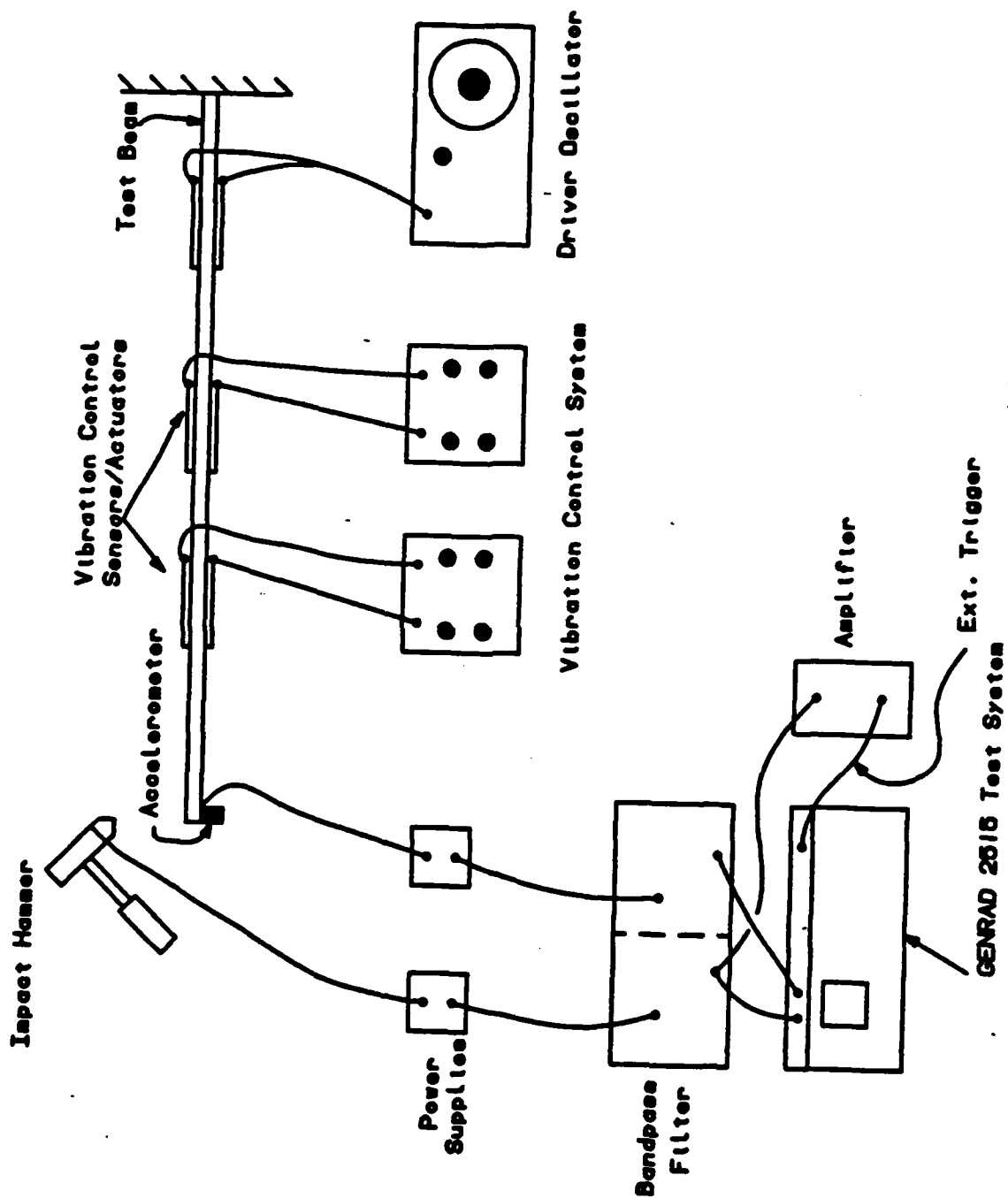


Figure D-4 Typical Test Configuration Setup

After the control units were set for a particular test configuration, impact response tests were undertaken. Both baseband and zoom⁵¹ frequency response analysis were used depending on the objective of the particular test.

The impact and response signals obtained for zoom analysis required filtering which was done by a pair of Krohn-Hite dual channel filters (models 3343 and 3342R). The filtering was necessary to maintain an acceptable signal to noise ratio. A wideband random signal was simultaneously applied to both channels and a transfer function was computed between them to measure any phase shift caused by the filters. No phase shift was detected in the frequency band of the experiments.

DATA PROCESSING AND REDUCTION

Using transfer function analysis techniques the modal parameters for the beams were determined. The impact/response measurements were averaged together together for each beam location and stored for later analysis. When a particular test condition was completed, the resulting transfer functions were processed using SDRC Modal Plus software⁵¹ to obtain complex modal parameters and mode shapes.

Various options available for modal analysis were explored and compared. Differences between the parameters identified on this single input output type system were slight and it was finally decided that the complex exponential technique⁵¹ was adequate to obtain the

complex pole and residue data. Finally, a circle fit routine was used to obtain the real and imaginary modal coefficients.

MODEL OF THE FEEDBACK ACTIVE CONTROL ELECTRONICS

Schematic drawings were supplied with the prototype electronics and are shown in figure D-5. Two tasks were undertaken to model the control units. The first task was to perform a detailed system analysis using the schematics. Secondly, since the possibility existed that components were altered from the original design, a series of calibration tests as well as physical examination of the internal components were performed. The test also served to further verify the differential equation model of the active control feedback filters.

As mentioned previously, each active control feedback filter consisted of a zero impedance preamplifier, bandpass filter, phase shifting circuit and high voltage output amplifier. Each subsection is identified on the schematic drawing in figure D-5.

The preamplifier subcircuit shown in figure D-6 can be appropriately modelled as shown in figure D-7. The input resistance is selectable from 10^6 to 10^{11} ohm with gain knob #1. The corner frequencies of the various parallel capacitor resistor networks were not within the 30 to 600 HZ experimental operating range and therefore their effect was considered negligible.

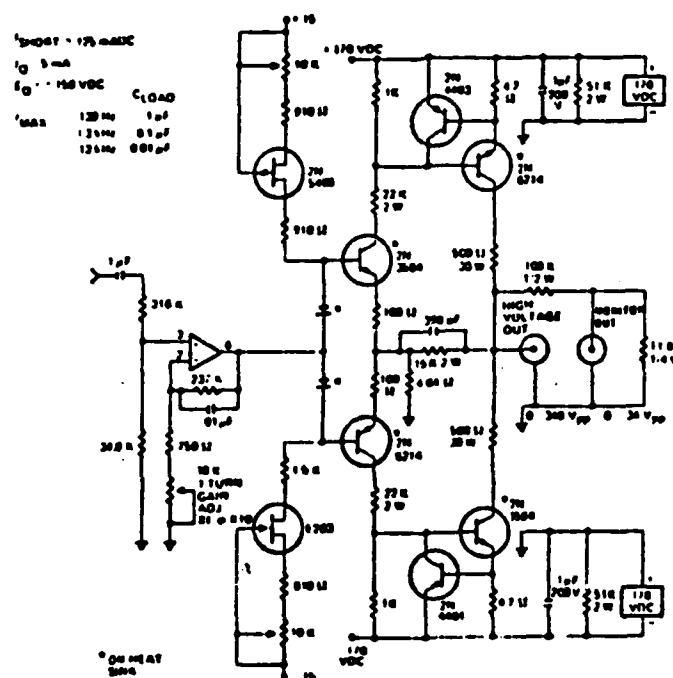
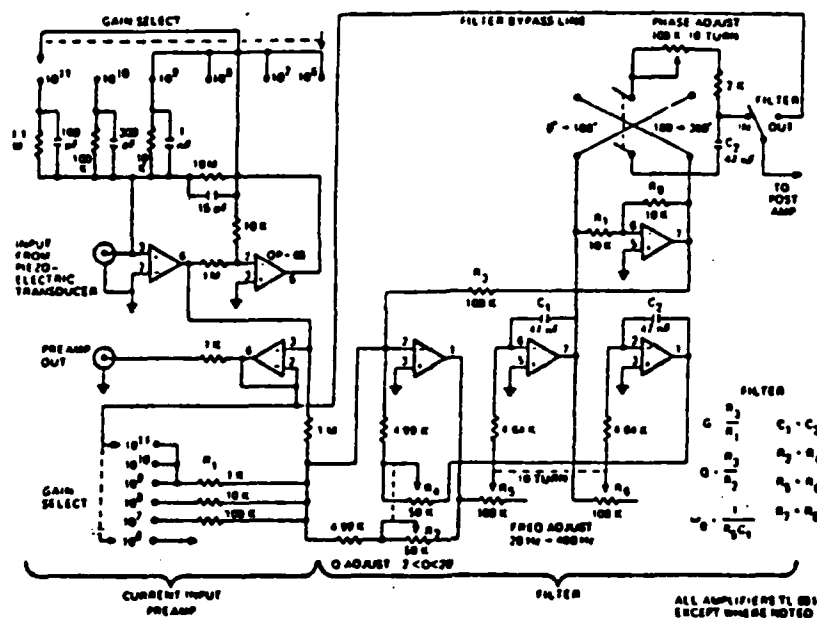


Figure D-5 Schematic Of The Active Feedback Filter Control Unit

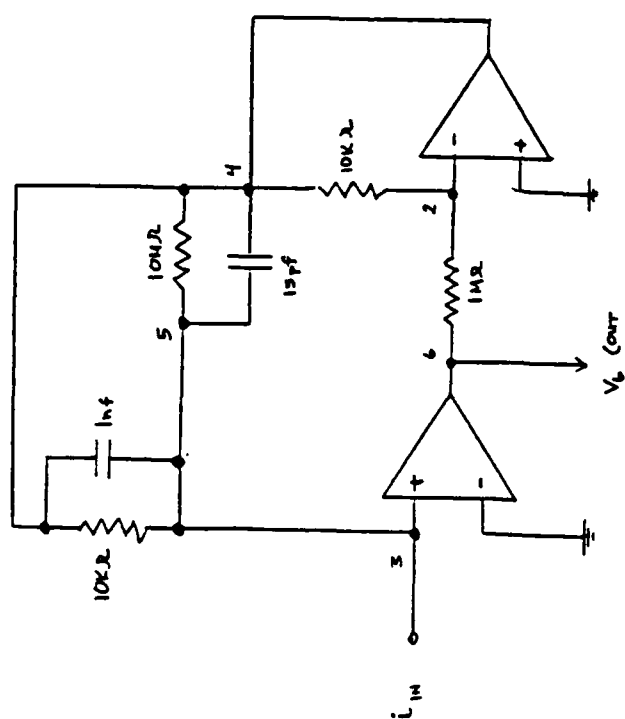


Figure D-6

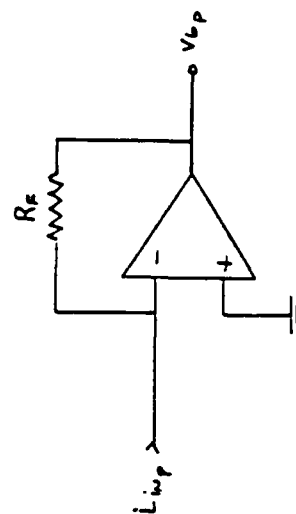


Figure D-7

Figures D-6 & D-7 Preamplifier Subcircuit And Equivalent Circuit

The equation modelling this portion of the control unit is

$$V_{6p}(\omega) = -R_F i_w(\omega) \quad (D-1)$$

The bandpass filter section is drawn in figure D-8. The filter center frequency and Q were adjustable. The filter Q was set at its maximum value of 20 for all experimental tests. Figure D-9 is a impedance block drawing of figure D-8 to assist in evaluating this part of the control unit. Using the principle of superposition, the solution for the voltage at node 3 is

$$V_3(\omega) = -\frac{Z_2(x_1)}{Z_1} V_1 - \frac{Z_2(x_1)}{Z_5(x_1)} V_7 - \frac{Z_2(x_1)}{X_8} V_8 \quad (D-2)$$

where x_1 represents the position of the Q adjustment knob. Solving for the voltage at nodes 5, 7 and 8 yields

$$V_5 = -(Z_4/Z_3(x_2))V_3 \quad (D-3)$$

$$V_7 = -(Z_7/Z_6(x_2))V_5 \quad (D-4)$$

$$V_8 = -(Z_9/Z_{10})V_5 \quad (D-5)$$

where x_2 represents the position of the center frequency adjustment knob.

Since $Z_9 = Z_{10}$ in equation (D-5)

$$V_8 = -V_5 \quad (D-6)$$

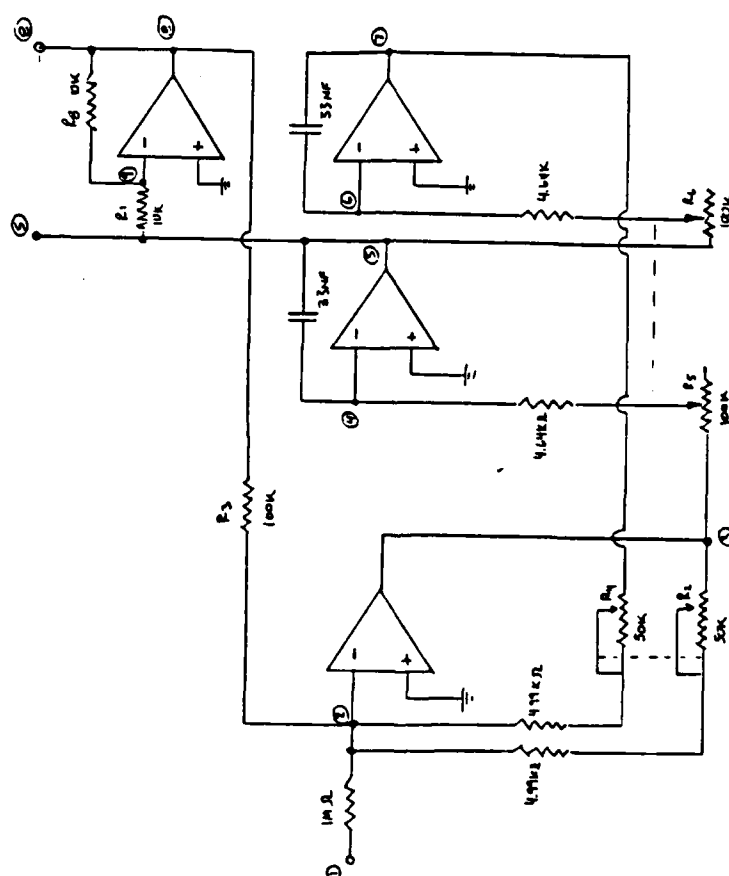
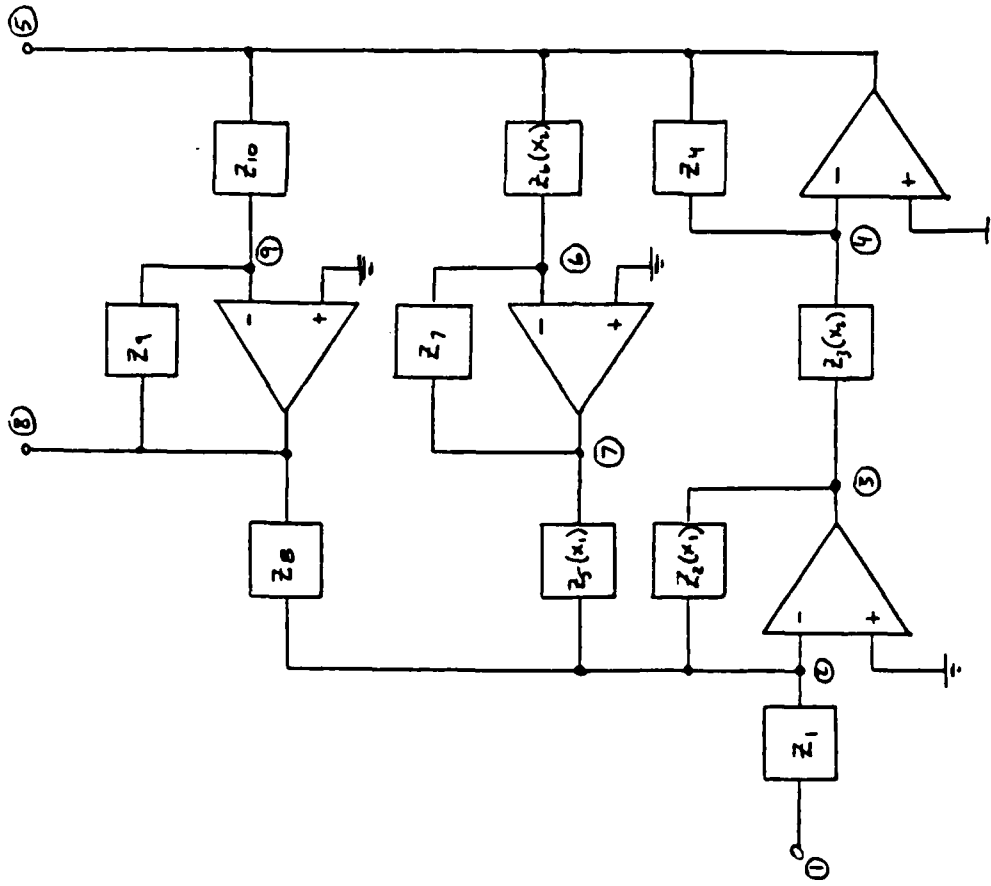


Figure D-8 Bandpass Filter Section



Z	VALUE
1	1 M Ω
2 & 5	4.99K Ω + 50K Ω (X_1)
3 & 6	4.64K Ω + 100K Ω (X_2)
4 & 7	1/(j ω 33 x 10 ⁻⁹)
8	100K Ω
9 & 10	10K Ω

Figure D-9 Impedance Block Diagram Of Bandpass Filter Circuit Section

Combining equations (D-3), (D-4) and (D-5) with (D-2) yields

$$V_5(\omega) = 0.1a \left(\frac{j\omega}{b - \omega^2 + j\omega a} \right) V_{6p}(\omega) \quad (D-7)$$

where

$$V_1(\omega) = V_{6p}(\omega)$$

$$a = \omega_0/Q, \quad b = \omega_0^2$$

$$\omega_0^2 = (1/Z_3^2)(x_2)c_1^2$$

$$Q = Z_8/Z_2(x_1)$$

The output from the bandpass filter is conditioned by the phase shifting network shown in figure D-10. The phase did not need adjustment a collocated sensor and actuator. The phase was set at zero and toggle switch which allowed a 180 degree shift was used to set the proper polarity for active feedback control.

The transfer function of the phase shifting network between nodes 5 and 10 is

$$V_{10}(\omega) = - [1/(1 + j(9.4 \times 10^{-5}\omega))] \quad (D-8)$$

The gain was computed for the transfer function in equation (D-8) for a frequency range of 1 to 5000 rad/sec. The results are plotted in figure D-11 and indicate a rolloff at about 2000 rad/sec.

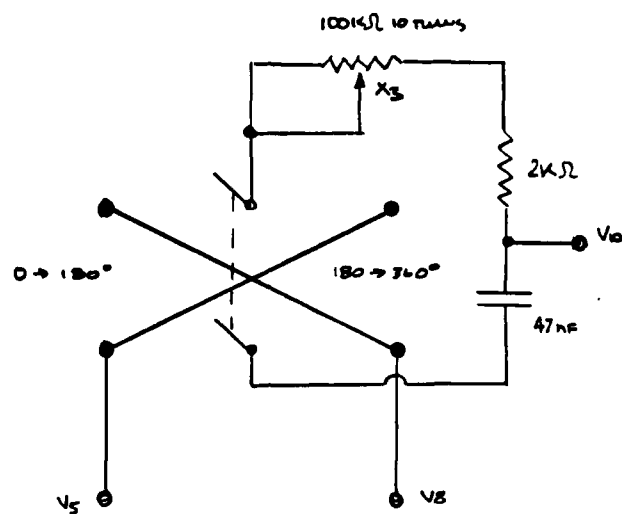


Figure D-10 Phase Adjustment Circuit Section

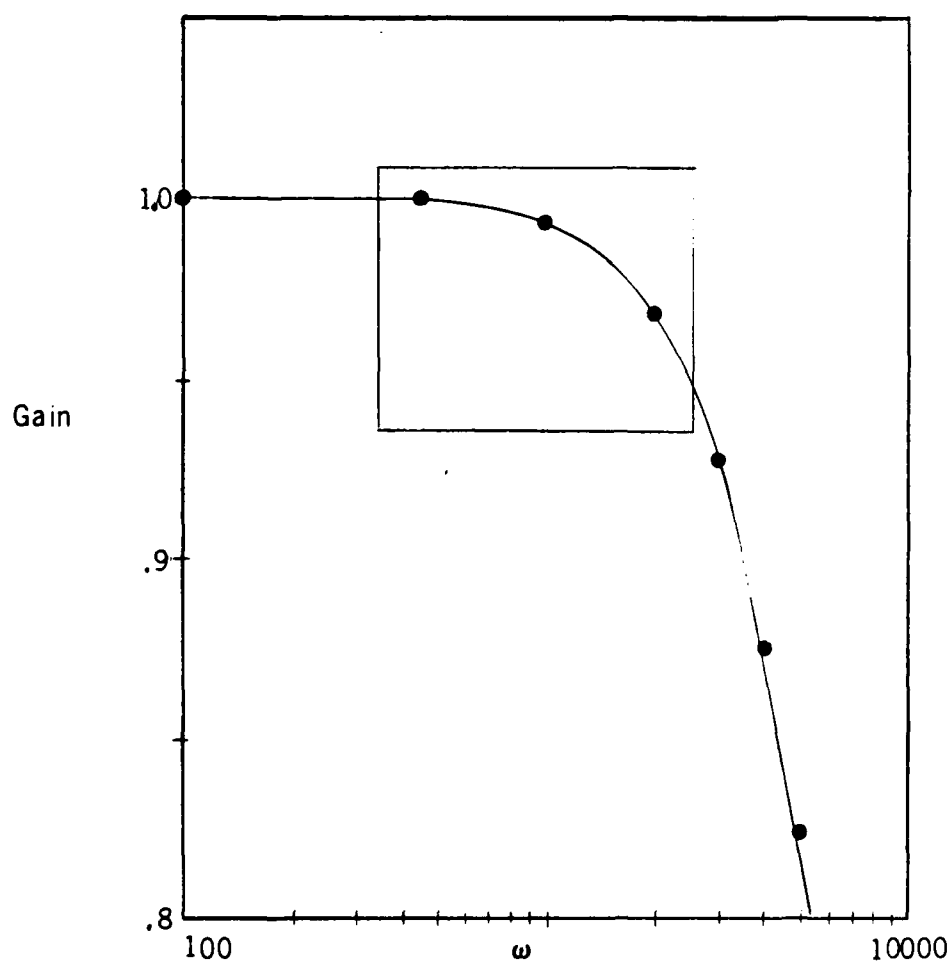


Figure D-11 Gain vs Freq. Phase Adjustment Circuit Section

After the phase network, the signal is further conditioned by a high gain voltage amplifier network shown in figure D-12. Analysis of this portion yielded

$$V_{11}(\omega) = .0992 \left(\frac{j\omega(a_n + j\omega)}{b - \omega^2 + j\omega a} \right) V_1(\omega) \quad (D-9)$$

The parameter a_n varies between 1.352×10^{45} to 1.375×10^5 as the gain adjustment knob #2 is adjusted from 1 to 10. Using the extreme values of a_n the gain was computed for a frequency range of 1 to 5000 rad/sec.

These results were presented in figures D-13 , and indicate a gain range of .3 to 3.3 through this section the final part of the amplifier had a gain of 30.

Combining equations (D-8), (D-9) and (D-10) and ignoring the poles and zeros out of the range of operation yields

$$V_{11}(\omega) = \frac{G\omega_0}{Q} \left(\frac{j\omega}{b - \omega^2 + j\omega a} \right) V_1(\omega) \quad (D-10)$$

where

G is the total gain through the system

$$V_1(\omega) = -R_F i_{IN}(\omega)$$

The range of the voltage gain from equation (D-8), (D-9) and (D-10) is approximately .9 to 9.9 when operating between 10 to 2000 rad/sec. To actually determine the gain for a control experiment

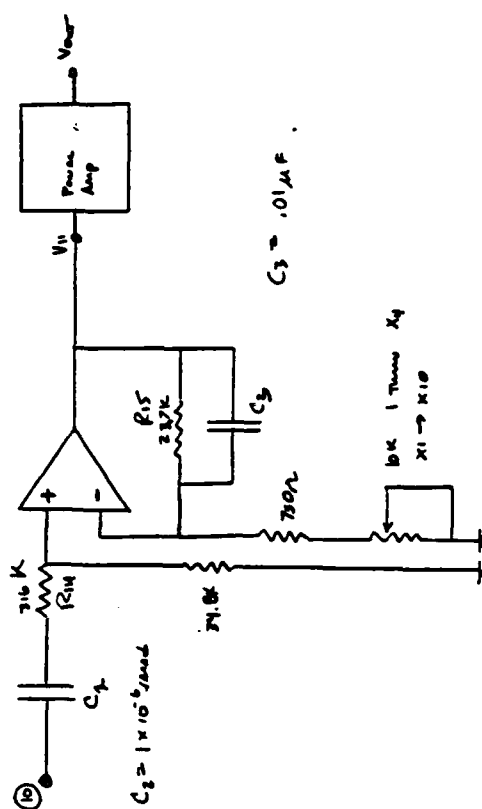


Figure D-12 Post Filter Circuit Section

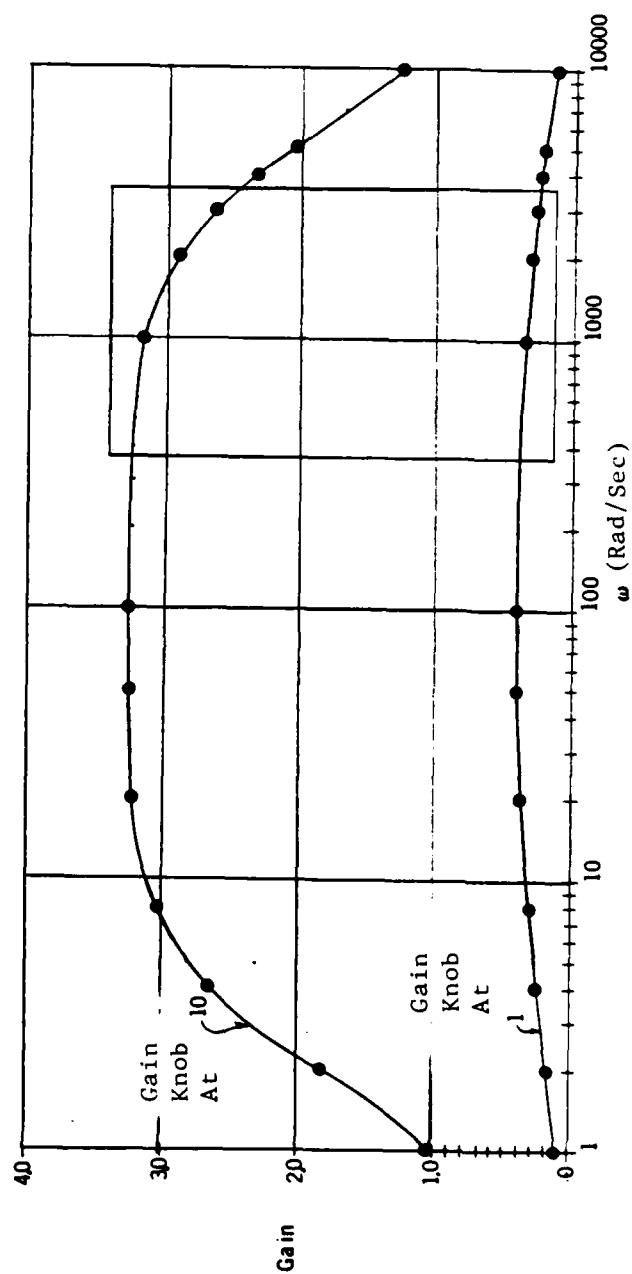


Figure D-13 Gain vs Freq. Post Filter Circuit Section

required that each control unit be calibrated after a particular test. Calibration was accomplished by providing a wideband current input to the preamplifier using a resistor in series with random voltage source. The transfer function between the preamplifier output voltage and the high voltage output provided the data for a least squares identification routine which identified the gain, Q and center frequency. This technique was presented in chapter III.

Table D-3 is the peak voltage at the center tuned frequency when a $1 V_{rms}$ random signal is passed through a 1×10^6 ohm resistor to the preamp input.

EXPERIMENTAL RESULTS

A variety of different tests were done to examine the active electronic damping performance using the G-1195 PZT type sensors/drivers on the cantilever beams and Table D-2 lists the major tests conducted.

Tests 1-23 were exploratory in nature and will not be discussed further. Test 25-26 were active control experiments applied to beam #3 and were used for the identification of the dynamic coupling coefficients.

Prior to each active control test, the baseline (no control) eigenvalues and eigenvectors were obtained for each configuration. Figures D-14a & D-14b are a typical sample of the transfer function data of the first and second modes. Table D-4 lists the complex eigenvalues for the first ten modes of beam #3 and the experimental eigenvectors for the first two bending modes. The eigenvectors were

Table D-2. Active Control Experiments

Test	Mode	Gain	Date Remarks
Beam #1			
1	---	---	11Dec84 No Active Control
2	2	9E6	11Dec84 S#2/A#2
3	2	4E7	11Dec84 S#2/A#2
4	3	1E6	11Dec84 S#1/A#1
5	3	9E6	12Dec84 S#1/A#1
6	2&3	9E6/1E6	13Dec84 S#1/A#1 & S#2/A#2
7	---	---	6Mar85 No Active Control
8	2	4E6	6Mar85 S#2/A#2
9	2	9E6	6Mar85 S#2/A#2
10	2	1E7	7Mar85 S#2/A#2
11	2	4E7	8Mar85 S#2/A#2
12	2	7E7	8Mar85 S#2/A#2
13	---	---	Jun85 No Active Control
14	2	4E6	Jun85 S#2/A#2
15	2	9E6	Jun85 S#2/A#2
16	3	4E6	Jun85 S#1/A#1
17	3	9E6	Jun85 S#1/A#1
18	2&3	4E6	Jun85 S#2/A#2&S#1/A#1
19	2&3	9E6	Jun85 S#2/A#2&S#1/A#1
20	2&3	4E6	Jun85 S#1/A#2&S#2/A#1
21	2&3	9E6	Jun85 S#1/A#2&S#2/A#1
Beam #2			
22	---	---	24Sep85 No Active Control
23	3	7.5E6	06Oct85 S#1,A#1
Beam #3			
24	---	---	16Jun86 No Active Control
25	1&2	1E6	26Jun86 S#1/A#2&S#2/A#2
26	1&2	8.5/7.5E6	29Jun86 S#1/A#2&S#2/A#2

Table D-3 Peak Voltage at Center Tuned Frequency of 232 Hz.

Control Unit ID.	Gain	Q	Volt
A	1E+06	2	.8862
	1E+06	20	.8021
	1E+07	20	8.095
B	1E+06	2	.9500
	1E+06	20	.7610
	1E+07	20	7.910

Notes: Wideband 1.0E-06 amp input DC-1024Hz. Phase shift 0.0

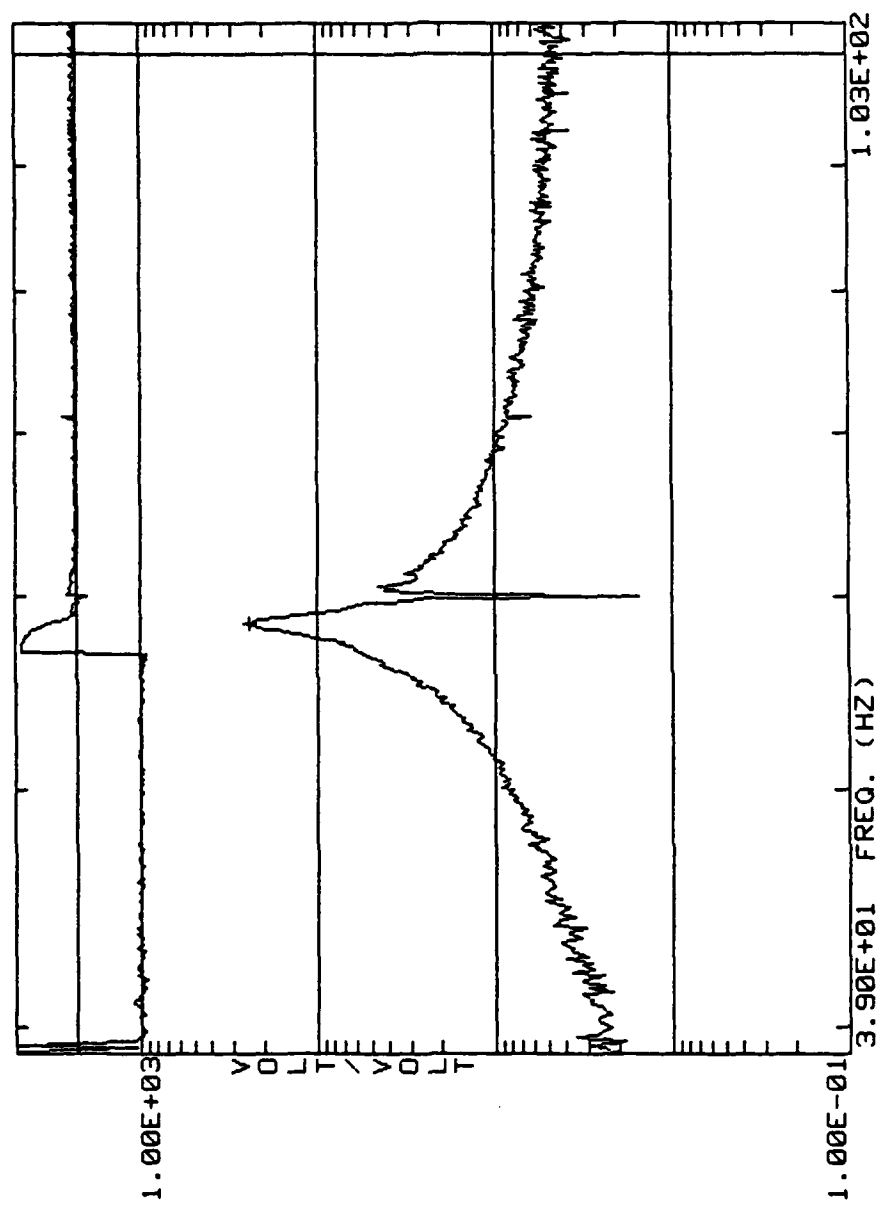


Figure D-14a First Mode Transfer Function - No Active Control

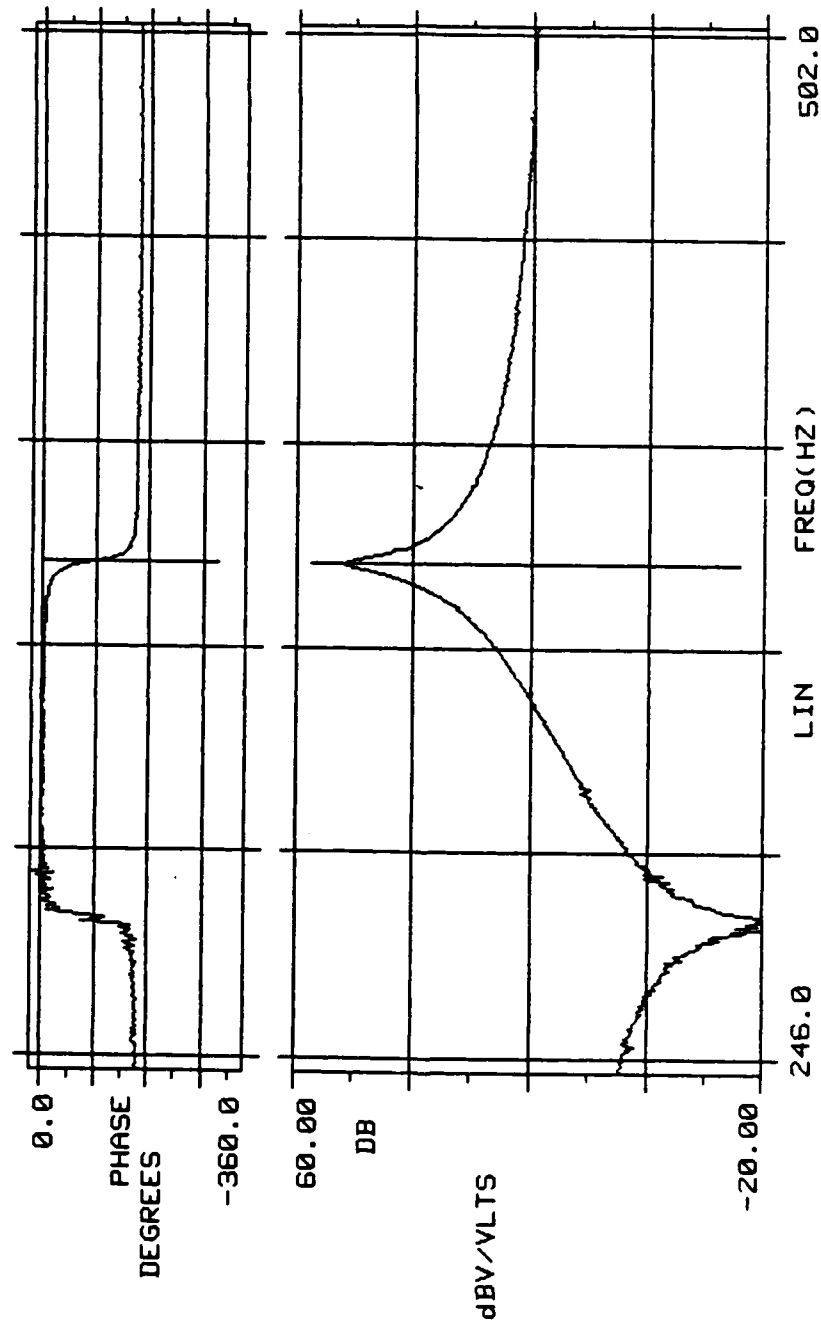


Figure D-14b Second Mode Transfer Function - No Active Control

Table D-4. Complex Eigenvalues and Real Eigenvectors Beam #3.

<u>Experimental</u>		
Mode	Freq. (Hz.)	Damping
1	58.301	.007
2	370.283	.00354
3	1040.00	.00390
4	2056.00	.00234
5	3304.00	.00234
<u>Analytical</u>		
6	7035.5	.005
7	10162.78	.005
8	15014.9	.005
9	24576.9	.005
10	50531.79	.005

<u>Experimental Real Eigenvectors</u>		
Location (x)	Mode 1	Mode 2
0.0	0.0	0.0
2.688	.1227	.6463
4.211	.3205	.9865
5.633	.4205	.8140
6.383	.5512	.3858
9.000	1.0	-1.0

computed for the first two modes using a circle fit routine and figures D-15a & D-15b are typical examples of the quality of the fit.

Two different levels of active control was applied in the experiments. Figure D-16 is an overlay of the baseline and the low and high gain tests. Table D-5 lists the actual gain values for each control circuit.

Figures D-17 and D-18 are a sample of the real and imaginary response comparisons for the baseline and active control tests. Numerical data from these control tests were transferred to the cyber for use by the dynamic coupling identification scheme.

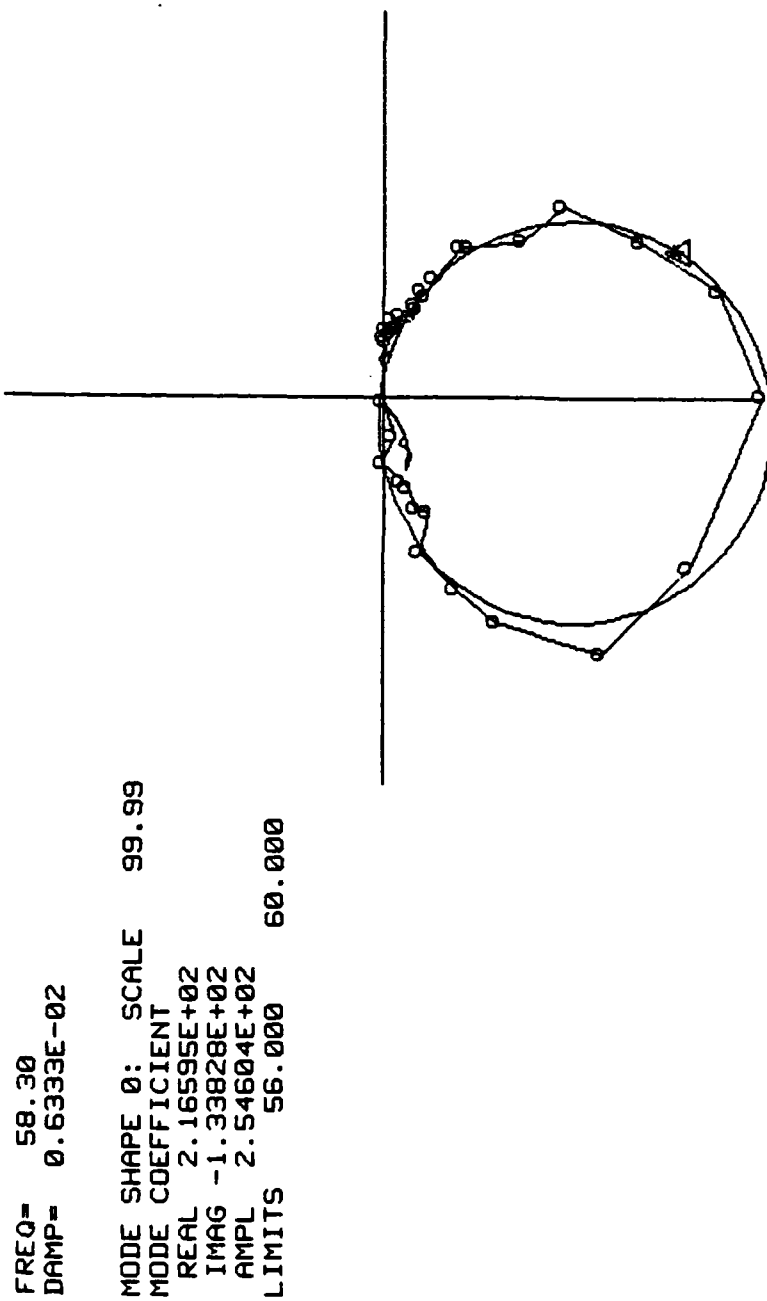


Figure D-15a Circle Fit First Mode - No Active Control

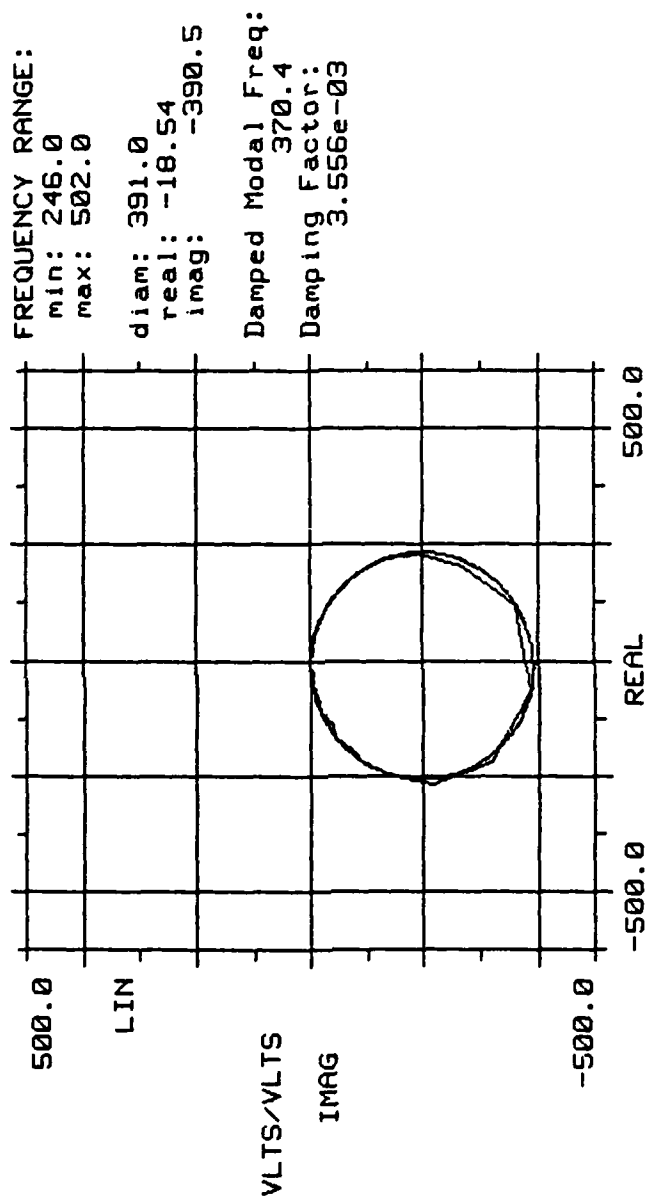


Figure D-15b Circle Fit Second Mode - No Active Control

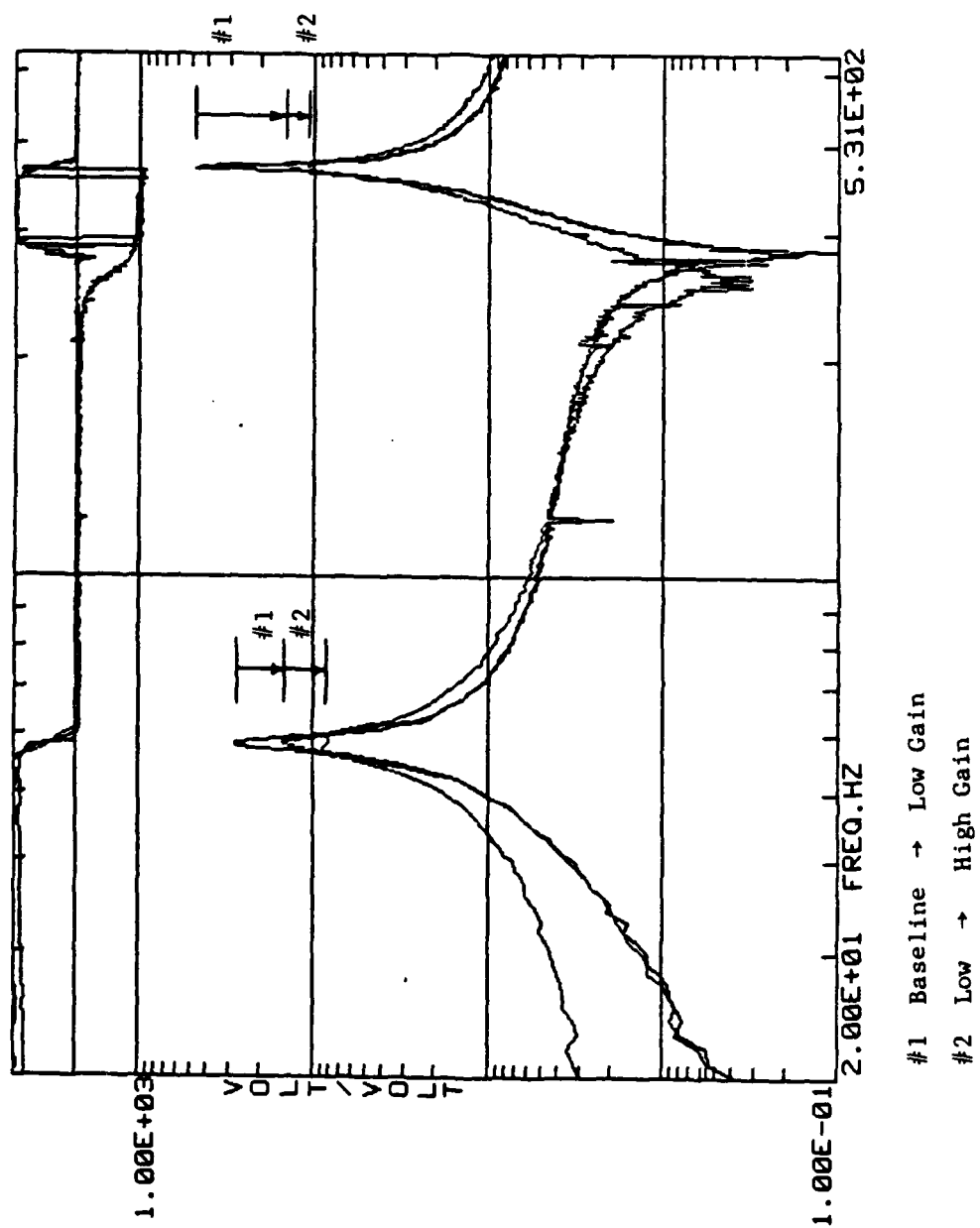


Figure D-16 Baseline, Low And High Gain Comparisons

Table D-5 Experimental Gain Values for Beam #3 Modal
Control Tests

Test	Mode	Gain.*
#1	1	1.0E+06
	2	1.0E+06
#2	1	8.5E+06
	2	7.0E+06

* Note: Gain Represents Total Gain From Sensor to Actuator
Including Preamplifier and Voltage Gain.

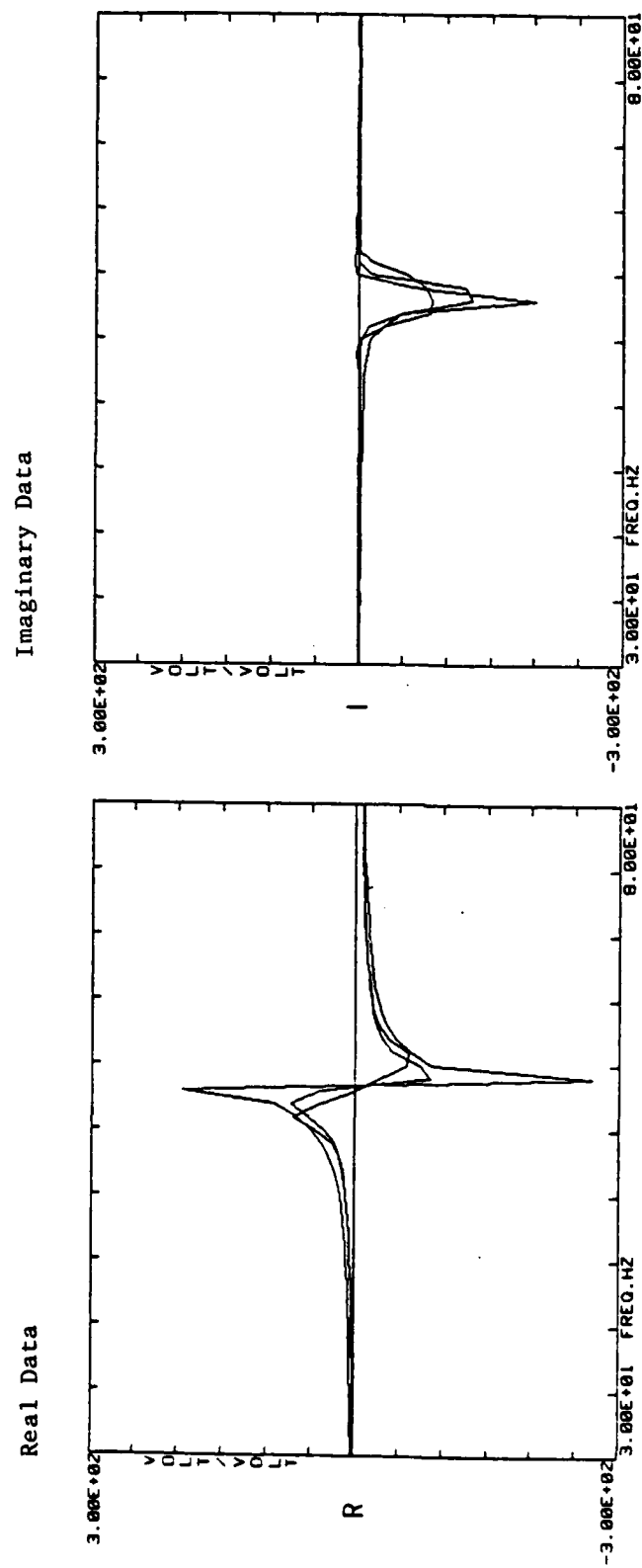


Figure D-17 Real And Imaginary Data Comparisons - Mode 1 Control

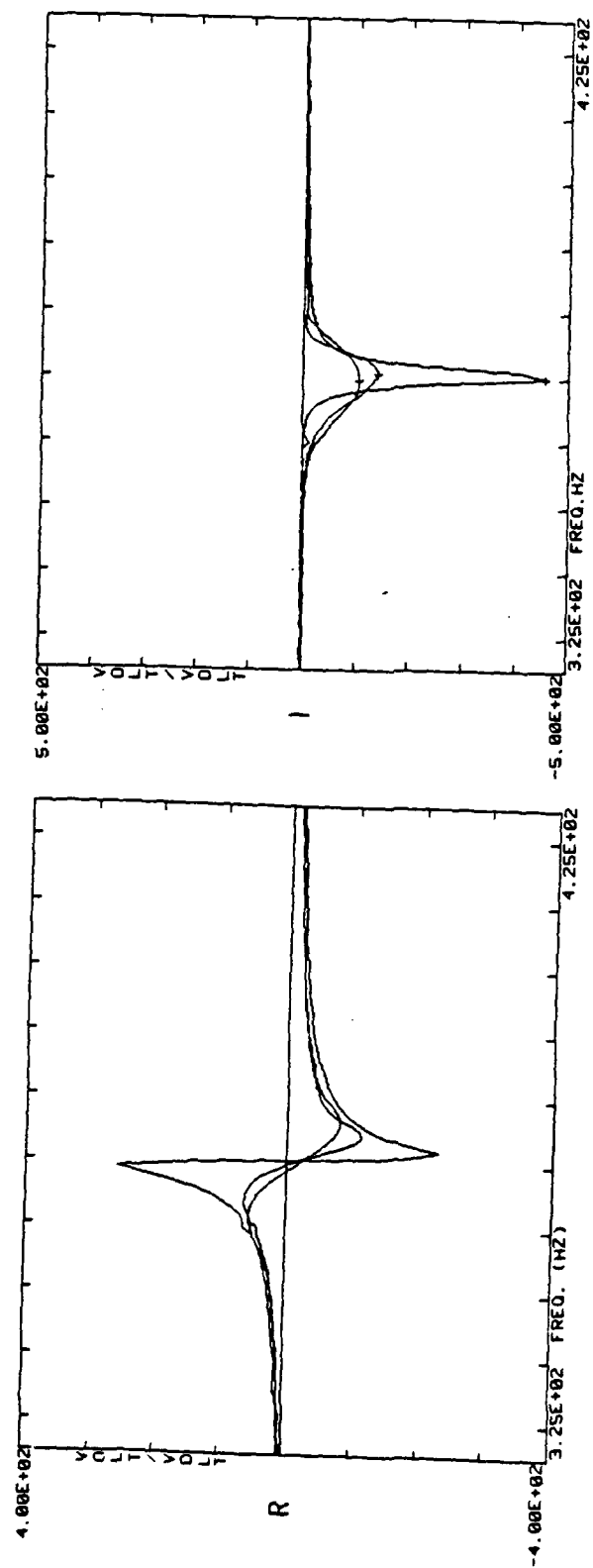


Figure D-18 Real And Imaginary Data Comparisons - Mode 2 Control

REFERENCES.

1. H.F. Olsen, "Electronic Control of Mechanical Noise, Vibration and Reverberation, "Journal of the Acoustical Society of America, pp. 966, 972, 1956.
2. R.L. Forward, "Electronic Damping of Vibration in Optical Structures", Applied Optics, pp. 690, 697, March 1979.
3. R.L. Forward, C.P. Liu, "Electronic Damping of Resonances in Gimbal Structures," AIAA paper No. 81-0556, Proceedings AIAA/ASME/ASCE/AIS 22nd Structures, Structural Dynamics, and Materials Conference, Atlanta, GA., 6-8 April 1981.
4. R.L. Forward, C.J. Swigert, "Electronic Damping of Orthogonal Bending Modes in a Cylindrical Mast", AIAA 81-4017/4018, J. Spacecraft and Rockets, Jan-Feb. 1981.
5. R.L. Forward, C.J. Swigert, M.W. Obal, "Electronic Damping of a Large Optical Bench", Shock and Vibration Bulletin, No. 53, pp. 51-61, May 1983.
6. W.P. Mason, "Piezoelectricity, its History and Applications", J. Acous. Soc. Am. Vol. 70 pp. 1561-1566, Dec. 1981
7. J. Van Randerat, R.E. Settrington, "Piezoelectric Ceramics", Mullard Limited Pub. Co. London, c 1974.
8. "IEEE Standard on Piezoelectricity", IEEE Std. 176-1978, Institute of Electrical and Electronics Engineers Inc., 1978.
9. "American Standard Method of Measurement of Piezoelectric Ceramics", Electronic Industries and American Standards Association, 1962.
10. D. Berlincourt, "Piezoelectric Ceramics" Characteristics and Applications", J. Acous. Soc. Am. Vol. 70 pp. 1586-1595, Dec. 1981.
11. G.M. Sessler, "Piezoelectricity in Polyvinylidene fluoride", J. Acou. Soc. Am. Vol. 70(6), pp. 1596-1608, Dec. 1981.
12. Takuso Sato, Hiroyuki Ishidi, Osamu Ideda, "Adaptive PVDF Piezoelectric Deformable Mirror System", Applied Optics, Vol. 19, No. 9, pp. 1430-1434, 1980.

13. Takuso Sato, Hiromi Ishikawa, Osamu Ikeda, "Multilayered Deformable Mirror Using PVDF Film", Applied Optics, Vol. 21, No. 9, pp. 3664-3668, 1982.
14. J. Plump, J.E. Hubbard Jr., T. Bailey, "Nonlinear Control of a Distributed System: Simulation and Experimental Results", Internal Report MIT Draper Labs, Sept. 1985.
15. T. Bailey, J.E. Hubbard, "Distributed Piezoelectric Polymer Active Vibration Control of a Cantilever Beam", J. Guidance and Control, Sept-Oct 1985, pp. 605-611.
16. W.P. Mason, "Electrostrictive Effect in Barium Titanate Ceramics", Physical Review, Vol. 74, No. 9, pp. 1134-1147, 1 Nov. 1948.
17. K. Uchino, Y. Tsuchiya, et. al., "Deformable Mirror Using the PMN Electrostrictor", Applied Optics, Vol. 20 No. 17 pp. 3077-3080, 1 Sept. 1981.
18. J.W. Hardy, "Active Optics: A New Technology for the Control of Light", Proceedings of the IEEE, Vol. 66, pp. 651-697, June 1978.
19. N.T. Adelman, "Spherical Mirror with Piezoelectrically Controlled Curvature", Applied Optics, Vol. 16, No. 12 pp. 3075, Dec. 1977.
20. N.T. Alderman, Y. Stavsky, "Flexural-Extensional Behavior of Composite Piezoelectric Circular Plates", J. Acous. Soc. Am. Vol. 67, pp. 819-822, Mar. 1980.
21. S.A. Kokorowski, "Analysis of Adaptive Optical Elements Made From Piezoelectric Bimorphs", J. Opt. Soc. Am. Vol. 69, No. 1, pp. 18u1-18i7, Jan 1979
22. E. Steinhaus, S.G. Lipson, "Bimorph Piezoelectric Flexible Mirror", J. Acous. Soc. Am. Vol. 69, No. 3, pp. 478-481, Mar. 1979.
23. P. Halevi, "Bimorph Piezoelectric Flexible Mirror: Graphical Solution and Comparison with Experiment", J. Opt. Soc. of Am. Vol. 73, pp. 110-113, Jan. 1983.
24. R.M. Scott, "New Technique for Controlling Optical Mirror Shapes", Opt. Engr., Vol. 14, No. 2, pp. 112-115, Mar-Apr. 1975.
25. M.R. Steele, F. Harrison, P.G. Harper, "The Piezoelectric Bimorph: An Experimental and Theoretical Study of its Quasistatic Response", J. Phys. D: Appl. Phys. Vol. 11, pp. 979-989, 1978.
26. R.M. White, "Surface Elastic Waves", Proc. IEEE Vol. 58, No. *, pp. 1238-12786, Aug 1970.

27. R. Holland, E.P. EerNisse, "Design of Resonant Piezoelectric Devices", Research Monograph No. 56, MIT Press, Cambridge Mass. c 1969.
28. E.P. EerNisse, "Resonances of One Dimensional Composite Piezoelectric and Elastic Structures", IEEE Trans. on Sonics and Ultrasonics, Vol. 14, No. 2, pp. 59-67, Apr. 1967.
29. W.J. Denkmann, "Analysis of Structural-Acoustic Interactions in Metal Ceramic Transducers", IEEE Trans. on Audio and Electroacoustics, Vol. 21, No. 4, pp. 317-324, Aug 1973.
30. N.V. Kinh, W. Pajewski, "Generation of Acousto-Electrical Waves using a Source of Transverse Vibrations", Polish Acoustic Society, Vol. 5, pp. 261-274, 1980.
31. B.A. Auld, "Wave Propagation and Resonance in Piezoelectric Materials", J. Acou. Soc. Am. Vol. 70, pp. 1578-1585, Dec 1981.
32. R.E. Mckechnie, "A Method of Damping the Piezoelectric Accelerometer", Instr. Soc. of Am. Vol. 11, pp. 45-51, c. 1972.
33. E.F. Crawley, J. de Luis, "Use of Piezoceramics as Distributed Actuators in Large Space Structures", AIAA No. 85-0626, 26th SDM AIAA/ASME/ASCE/AHS Conf. Proc. 15-17, April 1985.
34. S. Senturia, B.D. Wedlock, "Electronic Circuits and Applications", John Wiley and Sons Inc. NY, pp. 94-105, c 1975.
35. Y. Kagawa, G.M.L. Gladwell, "Finite Element Analysis of Flexure-Type Vibrators with Electrostrictive Transducers", IEEE Trans. on Sonic and Ultrasonics, Vol. SU-17, No. 1, pp. 41-49, Jan 1970.
36. E.P. EerNisse, "Coupled Mode Approach to Elastic Vibration Analysis", J. Acous. Soc. Am., Vol. 40, No. 5, pp. 1045-1050, Mar 1966.
37. G.S. Nurre, R.S. Ryan, H.N. Scofield and J.L. Sims, "Dynamics and Control of Large Space Structures", J. of Guidance and Control, Vol. 7, No. 5, pp. 514-526, Sept-Oct 1984.
38. M.J. Balas, "Feedback Control of Flexible Systems", IEEE Trans. on Automatic Control, Vol. AC23, No. 4, pp. 673-679, Aug 1978.
39. L. Meirovitch, H. Baruh, H. Oz, "A Comparison of Control Techniques for Large Flexible Systems", J. of Guidance and Control, Vol. 6, No. 4, pp. 302-310, July-Aug 1983.
40. J.D. Simon, S.K. Mitter, "A Theory of Modal Control", Information and Control, Vol. 13, pp. 316-353, 1968.

41. D.G. Luenberger, "An Introduction to Observers", IEEE Trans. On Auto. Control, Vol. AC-16, No. 6., pp. 586-602, Dec 1971.
42. R.L. Forward, "Picostrain Measurement with Piezoelectric Transducers", J. Appl. Phys. Vol. 51(11), pp. 5601-5603, Nov 1980.
43. W.L. Hallauer, Jr., G.R. Skidmore, R.N. Gehling, "Modal-Space Active Damping of a Plane Grid: Experiment and Theory", J. of Guidance and Control, Vol. 8, No. 3, May - June 1985.
44. W.L. Hallauer, Jr., J.F.M. Barthelemy, "Sensitivity of Modal Space Control to Nonideal Conditions", AIAA 81-4246, J. Guidance and Control, Vol. 4, No. 5, pp. 564-566, Sept-Oct 1981.
45. S. Hanagud, M. Meyyappa, Y.P. Cheng and J.I. Craig, "Identification of Structural Dynamic Systems with Nonproportional Damping, "Presented at the 25th AIAA/ASME/ASCE/AHS SDM Conference, 1984.
46. L. Meirovitch, "Computational Methods in Structural Dynamics", Sijthoof and Noordhoff Inter. Pub. Netherlands c 1980.
47. R.H. Cannon, Jr., D.E. Rosenthal, "Experiments in Control of Flexible Structures with Non Collocated Sensors and Actuators", J. Guidance and Control, Vol. 7, No. 5, pp. 546-553, Sept-Oct 1984.
48. "H.C. Martin, Introduction to Matrix Methods of Structural Analysis", McGraw Hill Book Co., c 1966, pp. 69-76.
49. D.T. Paris, F.K. Hurd, "Basic Electromagnetic Theory", McGraw Hill Book Co. NY. NY. c 1969.
50. H. Hablani, S. Shrivastava, "A Real Transformation for Modal Analysis of Flexible Damped Spacecraft", Acta Astronautica, Vol. 6, pp. 615-630, 1979.
51. User and Reference Manual for Modal-Plus 8.0, General Electric CAE International, Structural Dynamics research Corp. c. 1983.
52. R.H. Cannon Jr., E. Schmitz, "Precise Control of Flexible Manipulators", (Need to get ref. Info.), pp. 841-861.
53. R. Potter, "A General Theory of Modal Analysis for Linear Systems", Shock and Vibration Digest, Vol. 7 Pu. Shock and Vibr. Info. Center, Naval Research Lab. Wash. D.C., pp. 3-11, Nov 1975.
54. D.G. Schultz, J.L. Melsa, "State Functions and Linear Control System", McGraw-Hill Book Co., N.Y., N.Y. c 1967.
55. W.F. Ames, "Numerical Methods for Partial Differential Equations", Academic Press, pp. 47-49, c 1977.

56. G.J. Balas, R. Shepherd, "Dynamics and Control of a Large Deployable Reflector", AIAA/ASME/ASCE/AHS 26th SDM Conference, Vol. 2, pp. 729,734, April 15-17, 1985.
57. L. Meirovitch, H. Baruh, "Effect of Damping on Observation Spillover Instability", J. of Optimization Theory and Application, Vol. 35, No. 1, pp. 31-44, Sep 1981.
58. T.F. Elbert, "Estimation and Control of Systems", Van Nostrand Reinhold Co., c 1984.
59. W.S. Levine, M. Athans, "On the Determination of the Optimal Constant Output Feedback Gains for Linear Multivariable Systems", IEEE Trans. Auto Control Vol. AC-15, No. 1, pp. 44-48, Feb 1970.
60. J.M. Mendel, "A Concise Derivation of Optimal Constant Limited State Feedback Gains", IEEE Trans. Auto. Control, Vol, AC-19, pp. 447-448, Aug. 1974.
61. K. Ogata, "Modern Control Engineering", Prentice Hall Inc., Englewood Cliffs, N.J. Chaps. 14-16, c 1970.
62. W.P. Mason, R.N. Thurston, "Physical Acoustics", Vol. 1 Part A and Vol. 9, Academic Press, N.Y., c 1964.
63. D.D. Moerder, A.J. Calise, "Convergence of a Numerical Algorithm for Calculating Optimal Output Feedback Gains", IEEE Trans. Auto. Control Vol., AC-30, No. 9, pp. 900-903, Sept. 1985.
64. H.F. Tiersten, "Electroelastic Interactions and the Piezoelectric Equations", J. Acous. Soc. Am. Vol. 70, pp. 1567-1575, Dec. 1981.
65. A. Berman, "Parameter Identification Techniques for Vibrating Structures", The Shock and Vibration Digest Naval Research Lab. Wash. D.C., Vol 11, No. 1, pp. 13-16, Jan 1979.
66. R.J. Guyan, "Reduction of Stiffness and Mass Matrices", AIAA Journal, Vol. 3, No. 2, pp. 380, Jan. 1965.
67. GTSTRU DL User's Manual, Vol. 1-3, Georgia Institute of Technology, GTICS Sys. Lab., School of Civil Engineering, Atlanta, GA. (Need to get ref. info).
68. E.O. Doebelin, "Measurement Systems: Application and Design", McGraw Hill Book Col. N.Y., N.Y., pp. 256-263, c 1966.
69. H.V. Malmstadt, C.G. Enke, S.R. Crouch, "Electronics and Instrumentation for Scientists", The Benjamin/Cummings Pub. Co., pp. 115-119, c 1981.

70. V. Komkov, "Optimal Control Theory for the Damping of Vibration of Simple Elastic Systems", Lecture notes in Mathematics, No. 253, Springer-Verlag, N.Y., 1972.
71. M.C. Dokmeci, "Dynamic Applications of Piezoelectric Crystals Part I-III", The Shock and Vibration Digest, Naval Research Lab. Wash. D.C., Vol. 15, No. 1 Jan. 1983.
72. L. Meirovitch, "Analytical Methods in Vibrations", MacMillan Co. N.Y., N.Y. c 1967.
73. G. Schulz, G. Heimbold, "Dislocated Actuator/Sensor Positioning and Feedback Design for Flexible Structures", J. of Guidance and Control, pp. 361-367, Sept-Oct. 1983.
74. H.F. Tiersten, "Linear Piezoelectric Plate Vibrations", Plenum Press N.Y., pp. 277, 293 c 1969.
75. S.V. Hanagud, M. Meyyappa, J.I. Craig, "Method of Multiple Scales and Identification of Nonlinear Structural Dynamics Systems",
76. Y. Bard, "Nonlinear Parameter Estimation", Academic Press, N.Y., N.Y., c 1974.
77. S.V. Hanagud, M.W. Obal, M. Meyyappa, "Electronic Damping Techniques and Active Vibration Control", AIAA/ASME/ASCE/AHS 25th SDM Conference, April 15-17, 1985.
78. A.E. Bryson, Yu-Chi Ho, "Applied Optimal Control", Ohemisphere Publishing Co. c 1975, pp. 148-152.

VITA

Michael Walter Obal was born on December 9th 1952 in Ft. Monmouth, New Jersey. In 1970 he entered Stevens Institute of Technology in Hoboken, New Jersey and received a Bachelor of Engineering (Mechanical) in 1974 and a Master of Engineering (Mechanical) in 1975. In October 1975, he began military service for the United States as an Air Force Officer. In 1979 he received a Master of Business Administration from Wright State University in Dayton, Ohio. After completing a tour of duty at the Air Force Flight Dynamics Laboratory, he was selected to the Air Force Test Pilot School as a Flight Test Engineer Candidate. Completing this program he was assigned to the Air Force Weapons Laboratory as a crew member on the Airborne Laser Laboratory. In 1982 he entered the Air Force Institute of Technology Civilian Institution Program and upon acceptance by Georgia Institute of Technology began his Ph.d. studies.

END

12-86

DTIC